

8-2016

CIRCUMVENTING CISPLATIN RESISTANCE IN OVARIAN CANCERS THROUGH REACTIVATION OF p53 BY NON-CROSS-RESISTANT PLATINUM ANALOGS

Michelle Martinez-Rivera

Follow this and additional works at: http://digitalcommons.library.tmc.edu/utgsbs_dissertations

 Part of the [Inorganic Chemicals Commons](#), [Molecular Biology Commons](#), and the [Therapeutics Commons](#)

Recommended Citation

Martinez-Rivera, Michelle, "CIRCUMVENTING CISPLATIN RESISTANCE IN OVARIAN CANCERS THROUGH REACTIVATION OF p53 BY NON-CROSS-RESISTANT PLATINUM ANALOGS" (2016). *UT GSBS Dissertations and Theses (Open Access)*. 694.

http://digitalcommons.library.tmc.edu/utgsbs_dissertations/694

This Dissertation (PhD) is brought to you for free and open access by the Graduate School of Biomedical Sciences at DigitalCommons@TMC. It has been accepted for inclusion in UT GSBS Dissertations and Theses (Open Access) by an authorized administrator of DigitalCommons@TMC. For more information, please contact laurel.sanders@library.tmc.edu.

**CIRCUMVENTING CISPLATIN RESISTANCE IN OVARIAN CANCERS THROUGH
REACTIVATION OF p53 BY NON-CROSS-RESISTANT PLATINUM ANALOGS**

by

Michelle Martinez-Rivera, B.S.

APPROVED:

Zahid H. Siddik, Ph.D.
Advisory Professor

Gary Gallick, Ph.D.

Peng Huang, MD, Ph.D.

Shuxing Zhang, Ph.D.

Bulent Ozpolat, MD, Ph.D.

Sonal Gupta, Ph.D.

APPROVED:

**Dean, The University of Texas
Graduate School of Biomedical Sciences at Houston**

**CIRCUMVENTING CISPLATIN RESISTANCE IN OVARIAN CANCERS THROUGH
REACTIVATION OF p53 BY NON-CROSS-RESISTANT PLATINUM ANALOGS**

**A
DISSERTATION**

**Presented to the Faculty of
The University of Texas
Health Science Center at Houston
Graduate School of Biomedical Sciences
and
The University of Texas
M. D. Anderson Cancer Center
Graduate School of Biomedical Sciences
in Partial Fulfillment
of the Requirements
for the Degree of
DOCTOR OF PHILOSOPHY**

by

**Michelle Martinez-Rivera, B.S.
Houston, Texas**

August, 2016

Dedication

This dissertation is dedicated to:

- The Almighty for His is all honor and glory forever and ever:

“I am a little pencil in God's hands. He does the thinking. He does the writing. He does everything and sometimes it is really hard because it is a broken pencil and He has to sharpen it a little more.” - Mother Teresa

- The many women afflicted with ovarian cancer:

It is my hope that these studies provide a foundation to better fight this disease.

- My family and friends, especially my husband Tarak Bhatt, son Agustin Bhatt and parents Jose Martinez-Rivera and Damaris Rivera-Ortiz:

Your unconditional support and love made it possible!

Acknowledgements

I would really like to thank my mentor, Dr. Zahid H. Siddik for allowing me to pursue my degree in his laboratory and for his dedicated mentorship throughout these years. I would like to express my sincere gratitude to my committee members: Dr. Gary E. Gallick, Dr. John S. McMurray, Dr. Peng Huang, Dr. Shuxing Zhang and Dr. Bulent Ozpolat for their continued guidance and insightful recommendations which contributed for the development of my studies. I would like to thank Dr. George M. Stancel for having believed in me and giving me the opportunity to pursue my studies at GSBS. I am very grateful to all the past and present members in the Siddik lab. I would like to thank Dr. Guangan He for taking the time to teach me standard lab protocols. I would like to thank Dr. Xiaolei Xie for his help with the kinase assay. I would like to thank Dr. Marcia Ogasawara for her insightful recommendations. I would also like to thank the summer students, Nicole Martinez-Rivera, Gustavo Rivera-Alvarez and Mohammad Sadath. It was a great honor to have served as their mentor. I would also like to thank our collaborator Dr. Cristina Ivan for gathering the TCGA patient data and RPPA analysis. I am very grateful to the UTHealth Student InterCouncil (SIC) for allowing me to develop my leadership skills and to serve for the needs of UTHealth students. Finally, I would like to thank my husband Tarak Bhatt and son Agustin Bhatt, your unconditional love lightened this journey; my parents Jose Martinez-Rivera and Damaris Rivera-Ortiz, your sacrifice and teachings gave the tools I needed to be able to walk through this journey; my family, friends, specially my best friend Dr. Wilfredo Garcia-Beltran, and the beautiful St. Vincent de Paul community, your company during this journey made it fun!

Abstract

CIRCUMVENTING CISPLATIN RESISTANCE IN OVARIAN CANCERS THROUGH REACTIVATION OF P53 BY NON-CROSS-RESISTANT PLATINUM ANALOGS

Michelle Martinez-Rivera, B.S.

Advisory Professor: Zahid H. Siddik, Ph.D.

Cisplatin (cis-Pt), an anticancer platinum (Pt) drug, is used widely in the treatment of several malignancies, such as ovarian cancer. This Pt compound induces DNA damage, which results in p53 activation through post-translational modifications, mainly phosphorylation, culminating in execution of programmed cell-death. However, despite initial therapeutic response to cis-Pt, clinical resistance to this drug emerges leading to disease progression. Pt-resistance phenotypes have been associated with dysfunction in the p53 signaling pathway. Therefore, an effort to understand molecular mechanisms that prevent p53 activity and induce cis-Pt resistance becomes vital for designing Pt-based drugs able to re-activate p53 and improve clinical management of ovarian cancer patients. To investigate the mechanism responsible for p53 inactivation, an ovarian tumor panel composed of cis-Pt sensitive (A2780) and resistant (2780CP/CI-16, OVCAR-10, HEY and OVCA 433) cell lines was established, with two (2780CP/CI-16 and OVCAR-10) harboring missense mutant p53. The data obtained from these cancer cell lines have identified a correlation between cis-Pt resistance, regardless of p53 status (wild-type vs. mutant), and lack of phosphorylation of p53 at Ser20 after cis-Pt treatment. Cis-Pt resistant cell lines expressed low levels of Chk2, a kinase responsible to phosphorylate p53 at Ser20, as a common feature. It was confirmed, through the

generation of Chk2 knock-out clones from A2780 cells using the CRISPR/Cas9 system, that Chk2 is essential for cis-Pt to mediate phosphorylation of p53 at Ser20 and induce p53 transcriptional activity. As validation of its critical role, Chk2 knock-out in these cells leads to cis-Pt resistance. However, cis-Pt resistance was circumvented by a number of cis-Pt analogs. In this regard, oxaliplatin (oxali-Pt), a non-cross-resistant Pt analog currently used in colon cancer but not ovarian cancer, was the most effective. Interestingly, the mechanism for oxali-Pt involved restoration of p53 phosphorylation at Ser20 through a Chk2 independent pathway. RPPA analysis has identified the MAPK pathway as a possible target of activation by oxali-Pt to phosphorylate p53 at Ser20. Systematic studies using targeted inhibitors have identified MEK1/2, but not ERK1/2, as a novel biomarker important to mediate p53-Ser20 phosphorylation by oxali-Pt. Overall, the findings gathered in this research project have revealed Ser20 of p53 as a key site that induces cis-Pt resistance when its phosphorylation is not induced by cis-Pt due to loss of Chk2, whereas its phosphorylation by oxali-Pt via MEK1/2 leads to circumvention of this resistance. This knowledge may lead to repurposing oxali-Pt in ovarian cancer and improve survival of cancer patients.

Table of Contents

Dedication.....	iii
Acknowledgements.....	iv
Abstract.....	v
Table of Contents.....	vii
List of Illustrations.....	xiv
List of Tables.....	xvii
List of Appendices.....	xix
Abbreviations.....	xx
Chapter 1.....	1
1.1. Ovarian Cancer.....	2
1.2. Cisplatin.....	5
1.2.1. Discovery of cisplatin.....	5
1.2.2. Mode of action of cisplatin.....	6
1.3. Role of p53 in cancer and therapeutics.....	10
1.3.1. Induction of apoptosis.....	13
1.3.2. Induction of checkpoint response and cell cycle arrest.....	14
1.3.3. Induction of senescence.....	15

1.4. Mechanisms leading to cisplatin resistance from failure of p53 activity.....	17
1.4.1. Significance of phosphorylation in post-translational modifications of p53.....	19
1.4.2. Mutant p53.....	22
1.5. The role of <i>TP53</i> gene status in response to platinum treatment in ovarian cancer.....	23
1.6. Other mechanisms inducing resistance to cisplatin.....	28
1.7. Platinum analogs non-cross-resistant to cisplatin.....	34
1.8. Hypothesis and Specific Aims.....	39
Chapter 2.....	42
2.1. Synthesis of trans-[Pt(Py) ₂ Cl ₂].....	43
2.2. FAAS parameters.....	44
2.3. Preparation of stock platinum drug solutions.....	45
2.4. Cell culture.....	45
2.5. Cytotoxic evaluations.....	46
2.6. Cellular Pt drug uptake.....	47
2.7. DNA extraction and purification.....	49
2.8. DNA Pt adducts.....	49
2.9. Partition coefficient.....	49
2.10. DNA interstrand crosslinks.....	50

2.11. Platination of FBS proteins.....	51
2.12. <i>TP53</i> sequencing.....	52
2.13. Generation of stable knock-out clones.....	52
2.14. Knock-in transfections.....	53
2.15. Western blot analysis.....	55
2.16. Chk2 expression in cisplatin-resistant ovarian tumor cell lines.....	55
2.17. Chk2 knock-down.....	56
2.18. Proteasomal regulation of Chk2.....	56
2.19. Chk2 half-life determination.....	57
2.20. Quantification of <i>CHEK2</i> transcripts.....	57
2.21. <i>CHEK2</i> gene methylation.....	58
2.22. miRNA TaqMan assays.....	59
2.23. MicroRNA expression.....	60
2.24. RPPA analysis.....	60
2.25. Platinum treatment for Western analysis.....	61
2.26. MEK/ERK inhibitor exposure.....	61
2.27. Effect of MEK inhibitor U0126 on platinum cytotoxicity.....	62
2.28. Ability of MEK1/2 to phosphorylate p53 at Ser20.....	62
2.29. Antibodies.....	63

2.30. Ovarian cancer patient survival analysis.....	63
2.31. Statistical Analysis.....	64
Chapter 3.....	65
3.1. Rationale and Background.....	66
3.2. Results.....	69
3.2.1. Determination of the structure and purity of trans-PyPt.....	69
3.2.2. Cytotoxic evaluations of DMF and pyridine.....	72
3.2.3. Activity of structurally-distinct Pt analogs in ovarian cancer cell lines.....	75
3.2.4. Pt uptake and DNA-Pt adducts formation of structurally-distinct Pt analog.....	78
3.2.5. Partition coefficient of structurally-distinct platinum analogs.....	81
3.2.6. DNA interstrand crosslinks index of structurally-distinct platinum analog.....	84
3.2.7. Studies to determine reactivity of structurally-distinct platinum analog.....	88
3.3. Conclusions.....	91
Chapter 4.....	94
4.1. Rationale and Background.....	95

4.2. Results.....	97
4.2.1. <i>TP53</i> sequencing in the ovarian tumor panel.....	97
4.2.2. Generation of stable p53 knock-out clones in ovarian cancer cell lines.....	99
4.2.3. Cytotoxicity of platinum drugs in p53 ^{-/-} ovarian cancer cell lines...	101
4.2.4. Oxali-Pt treatment results in greater p53 expression and functional activity than cis-Pt at equimolar concentrations in the ovarian tumor panel.....	104
4.2.5. Comparison of activation and phosphorylation of p53 between cis-Pt and oxali-Pt.....	106
4.2.6. p53-Ser20 phosphorylation strongly enhances expression of p21.....	109
4.2.7. Activation of p53 by cis-Pt and oxali-Pt at equitoxic concentrations in the ovarian tumor panel.....	111
4.2.8. Cis-Pt resistant ovarian tumor cell lines exhibit substantial downregulation of Chk2 as a common feature.....	115
4.2.9. Chk2 knock-out or knock-down in A2780 cells inhibits cis-Pt mediated phosphorylation of p53-Ser20 and p53 transcriptional activity.....	117
4.2.10. Chk2 expression directly correlates with cytotoxic and therapeutic response to platinum.....	120

4.2.11. Chk2 knock-in restores the capacity of cis-Pt to induce p53 transcriptional activation and increase cytotoxicity in A2780 Chk2 ^{-/-} cells.....	123
4.2.12. Examination of mechanism of Chk2 downregulation in cis-Pt resistant cells.....	125
4.2.13. Analysis of CpG island methylation of <i>CHEK2</i> in the ovarian tumor panel.....	128
4.2.14. Expression levels of microRNAs predicted to target <i>CHEK2</i>	130
4.2.15. Examination of Chk2 expression by miR-340 and miR-425.....	132
4.3. Conclusions.....	134
Chapter 5.....	137
5.1. Rationale and Background.....	138
5.2. Results.....	139
5.2.1. Time-dependent activation of p53 in A2780 and 2780CP/CI-16 by cis-Pt and oxali-Pt.....	139
5.2.2. Analysis of differences in the mechanism of action of cis-Pt vs. oxali-Pt in A2780 and 2780CP/CI-16.....	142
5.2.3. Analysis of RPPA data to identify the unknown kinase responsible for p53 phosphorylation at Ser20 and p53 transcriptional activation by oxali-Pt.....	144

5.2.4. Involvement of ERK1/2 in mediating p53 phosphorylation at Ser20 and p53 transcriptional activation by oxali-Pt.....	147
5.2.5. Involvement of MEK1/2 in p53 phosphorylation at Ser20 and p53 transcriptional activation by oxali-Pt.....	150
5.2.6. MEK1/2 expression positively correlates with cell survival and therapeutic response to Pt.....	153
5.2.7. MEK1/2 phosphorylate p53 at Ser20 in vitro.....	155
5.3. Conclusions.....	157
Chapter 6 Discussion.....	160
Chapter 7 Future Directions.....	181
Appendix.....	191
References.....	233
Vita.....	266

List of Illustrations:

Figure 1. Cisplatin mode of action.....	9
Figure 2. p53 transcriptional activity regulation.....	12
Figure 3. Mechanisms leading to failure of p53 activity.....	18
Figure 4. p53 post-translational modifications.....	21
Figure 5. Effect of p53 status on survival curves for ovarian cancer patients.....	27
Figure 6. Ras/MAPK pathway.....	33
Figure 7. Research goals.....	41
Figure 8. Chemical structure of platinum analogs investigated.....	68
Figure 9. Nuclear magnetic resonance studies of trans-PyPt.....	70
Figure 10. Cytotoxic evaluations of DMF and pyridine.....	74
Figure 11. Activity of structurally-distinct Pt analogs in ovarian cancer cell lines.....	76
Figure 12. Pt uptake and DNA-Pt adducts formation of structurally-distinct Pt analogs.....	79
Figure 13. Partition coefficient of structurally-distinct platinum analogs.....	82
Figure 14. DNA interstrand crosslink index of structurally-distinct platinum analogs.....	85
Figure 15. Reactivity of structurally-distinct platinum analogs.....	89
Figure 16. Conclusions Chapter 3.....	93

Figure 17. Generation of p53 knock-out clones in ovarian cancer cell lines.....	100
Figure 18. Cytotoxicity of platinum drugs in p53 ^{-/-} ovarian cancer cell lines.....	102
Figure 19. Dose-response relationship for p53 expression and p21 upregulation with cis-Pt and oxali-Pt in the ovarian tumor panel.....	105
Figure 20. Induction of p21 and p53 phosphorylation at Ser15 and Ser20 by cis-Pt and oxali-Pt.....	108
Figure 21. p53-Ser20 phosphorylation strongly enhances expression of p21	110
Figure 22. Expression and activation of p53 after cis-Pt or oxali-Pt treatment at equitoxic concentrations in the ovarian tumor panel.....	113
Figure 23. Cis-Pt resistant ovarian tumor cell lines exhibit substantial downregulation of Chk2 as a common feature.....	116
Figure 24. Downregulation of Chk2 in A2780 cells inhibits cis-Pt mediated phosphorylation of p53-Ser20 and p53 transcriptional activity.....	119
Figure 25. Chk2 expression directly correlates with cytotoxic and therapeutic response to platinum.....	121
Figure 26. Chk2 knock-in restores the capacity of cis-Pt to induce p53 transcriptional activation and increase cytotoxicity in A2780 Chk2 ^{-/-} cells.....	124
Figure 27. Examination of Chk2 downregulation in cis-Pt resistant cells.....	127
Figure 28. Analysis of CpG island methylation of <i>CHEK2</i> in the ovarian tumor panel.....	129

Figure 29. Expression levels of microRNAs predicted to interact with <i>CHEK2</i>	131
Figure 30. Examination of Chk2 regulation by miR-340 and miR-425.....	133
Figure 31. Conclusions Chapter 4.....	136
Figure 32. Time-dependent activation of p53 in A2780 and 2780CP/CI-16 by cis-Pt and oxali-Pt.....	141
Figure 33. Differences in the mechanism of action of cis-Pt vs. oxali-Pt in A2780 and 2780CP/CI-16.....	143
Figure 34. Analysis of RPPA data to identify the unknown kinase responsible for p53 phosphorylation at Ser20 and p53 transcriptional activation by oxali-Pt.....	146
Figure 35. Involvement of ERK1/2 in p53 phosphorylation at Ser20 and p53 transcriptional activation by oxali-Pt.....	149
Figure 36. Involvement of MEK1/2 in mediating p53 phosphorylation at Ser20 and p53 transcriptional activation by oxali-Pt.....	152
Figure 37. MEK1/2 expression positively correlates with cytotoxic and therapeutic response to Pt.....	154
Figure 38. MEK1/2 phosphorylate p53 at Ser20 in vitro.....	156
Figure 39. Conclusions Chapter 5.....	159
Figure 40. Targeted Pt chemotherapy in ovarian cancer patients.....	180

List of Tables:

Table 1. Staging System for Ovarian Carcinoma.....	4
Table 2. FAAS parameters used to measure Pt metal.....	44
Table 3. Range of concentrations (μM) of Pt drugs and geometric factor used to assess cytotoxicity in the ovarian panel by MTT assay.....	47
Table 4. Range of concentrations of Pt drugs (μM) and geometric factor used in concentration increases to assess cytotoxicity in $p53^{-/-}$ and $\text{Chk}2^{-/-}$ clones.....	53
Table 5. Concentration range (μM) for Pt drugs and geometric factor used in concentration increases for cytotoxic evaluations after Chk2-ki in A2780- $\text{Chk}2^{-/-}$	54
Table 6. Values for elemental and NMR analysis of trans-PyPt.....	71
Table 7. IC_{50} values (μM) of structurally-distinct Pt analogs in ovarian cancer cell lines.....	77
Table 8. Resistance factor values relative to A2780 of structurally-distinct Pt analogs in ovarian cancer cell lines.....	77
Table 9. Cellular platinum uptake ($\times 10^3$ ng Pt/ mg Protein/ hr) values for structurally-distinct platinum analogs in A2780 and 2780CP/CI-16 tumor models.....	80
Table 10. DNA platinum adducts (ng Pt/ mg DNA/ hr) values of structurally-distinct platinum analogs in A2780 and 2780CP/CI-16 tumor models.....	80
Table 11. Partition coefficient values of structurally-distinct platinum analogs.....	83

Table 12. Excitation values for ethidium bromide at a given wavelength.....	86
Table 13. Emission values for ethidium bromide at a given wavelength.....	87
Table 14. DNA interstrand crosslink (ICLs) index of structurally-distinct platinum analogs.....	87
Table 15. Half-life ($t_{1/2}$) and rate constant (k) values of structurally-distinct platinum analogs.....	90
Table 16. Analysis of p53 status in ovarian cancer cell lines.....	98
Table 17. IC ₅₀ values (μ M) of Pt drugs in CRISPR engineered p53 ^{-/-} ovarian cancer cell lines.....	103
Table 18. Multiples of IC ₅₀ (X1, X3 and X5) concentrations of cis-Pt and oxali-Pt used for treating the ovarian tumor panel.....	114
Table 19. IC ₅₀ values (μ M) of Pt drugs in A2780 Chk2 ^{-/-} cells.....	122
Table 20. IC ₅₀ values (μ M) of Pt drugs in A2780 Chk2 ^{-/-} cells after Chk2 knock-in...	124
Table 21. miRNAs predicted to target <i>CHEK2</i> using miRBase: the microRNA database.....	131

List of Appendices:

Appendix 1: RPPA values for heatmap for A2780 and 2780CP/CI-16 treated with cis-Pt and oxali-Pt.....	191
Appendix 2: Analysis of protein changes from RPPA data generated for A2780 and 2780CP/CI-16 treated with cis-Pt and oxali-Pt.....	212
Appendix 3: RPPA data intersections.....	220
Appendix 4: Analysis of the functionality of p53 missense mutations in ovarian cancer patients and cell lines.....	229

Abbreviations

AIF	Apoptosis-inducing factor
APAF-1	Apoptotic protease-activating factor 1
ATR	Ataxia telangiectasia and Rad3-related
Bad	Bcl-2-associated death promoter
BLAST	Basic local alignment search tool
C	Carbon
Cdk	Cyclin-dependent kinase
CHK1	Checkpoint kinase 1
CHK2	Checkpoint kinase 2
Cis-Pt	Cisplatin
Cis-PyPt	Cis-[Pt(Py) ₂ Cl ₂]
Cl	Chloride
CTR	Cooper-transporting
Cu	Copper
DACH	1,2-diaminocyclohexane
DAP	1R,2R-diaminocyclohexane (trans-diacetato)(dichloro)platinum(IV)
DISC	Death-inducing signaling complex
DMF	N-N-Dimethylformamide-D7
FAAS	Flameless atomic absorption spectrometry
FADD	Fas-associated death domain
FBS	Fetal bovine serum
E. coli	Escherichia coli
ERCC	Excision repair cross-complementation
ERK	Extracellular signal-regulated kinases
EtBr	Ethidium bromide
FDA	Food and Drug Administration
FIGO	Federation of Gynecology and Obstetrics

GOF	Gain-of-function
GSH	Glutathione
H	Hydrogen
HER-2	Human epidermal growth factor receptor 2
HGSOC	High grade serous ovarian carcinoma
HMG1	High-mobility group 1
HMG2	High-mobility group 2
hMLH1	Human mutL homolog 1
hMSH2	Human mutS homolog 2
ICLs	Interstrand crosslinks
IHC	Immunohistochemistry
JNK	c-Jun N-terminal kinases
l	Liquid
LOF	Loss-of-function
MAPK	Mitogen-activated protein kinase
MAPKK	MAP kinase kinase
MAPKKK	MAP kinase kinase kinase
MMR	Mismatch repair
MSP	Methylation-specific PCR
N	Nitrogen
NCI	National Cancer Institute
NER	Nucleotide excision repair
Oxali-Pt	Oxaliplatin
PBS	Phosphate buffered saline
PI3K	Phosphatidylinositol-4,5-bisphosphate 3-kinase
Pt	Platinum
PUMA	p53 upregulated modulator of apoptosis
s	Solid

SLC	Solute carrier
RPPA	Reverse phase protein lysate
TBP	TATA binding protein
TCGA	The Cancer Genome Atlas
TGCT	Testicular germ cell tumors
TNFR	Tumor necrosis factor receptor
Trans-Pt	Transplatin
Trans-PyPt	Trans-[Pt(Py) ₂ Cl ₂]
UBTF	Upstream binding transcription factor
XP	Xeroderma Pigmentosum
FASAY	Yeast functional assay

Chapter 1

Introduction

Note: With the permission of Elsevier journal, parts of this Chapter were taken from my review publication Martinez-Rivera M and Siddik ZH, Resistance and gain-of-resistance phenotypes in cancers harboring wild-type p53. Biochem.Pharmacol. 83: 1049-1062, 2012.

1.1. Ovarian Cancer:

Ovarian cancer is a heterogeneous disease consisting of a variety of tumor types with different biological and clinical profiles that have been classified into three broad categories: epithelial cells, germ cells and stromal cells. Epithelial ovarian cancer constitutes over 90% of cases of ovarian cancer and it is further divided into five subtypes: serous (which is the most frequent subtype and comprises 70% of cases), endometrioid, clear cell, mucinous, Brenner tumors and undifferentiated tumors [1-3].

The International Federation of Gynecology and Obstetrics (FIGO) has defined the stages of ovarian cancer into stages I, II, III and IV (**Table 1**). In early stage cancer, the tumor is confined to the ovaries (stage I) or is limited to one or both ovaries with pelvic extension (stage II). Ovarian cancer patients within these stages exhibit a satisfactory 5-year survival rate of over 90%. Unfortunately, about 80% of ovarian cancer patients are diagnosed at an advanced stage, stages III and IV, where the tumor has metastasized outside the pelvis. Thus, the 5-year survival rate drops below 30% [4]. As a consequence, ovarian cancer has become the leading cause of death from gynecological cancers among American women. In fact, statistical studies performed in

the United States reported that in 2014 about 21,980 women were afflicted with ovarian cancer from which 14,270 cases resulted in death [5].

The current treatment for advanced ovarian carcinoma involves cytoreductive surgery in order to remove the bulk of the tumor. Since most patients cannot be cured by surgery alone due to residual microscopic and macroscopic peritoneal malignant cells, ovarian cancer patients following surgery are administered a combination of platinum (Pt) chemotherapy, involving primarily cisplatin (cis-Pt) or carboplatin, with taxanes. At the beginning of treatment, patients exhibit a satisfactory response, however, about 80% of patients eventually develop resistance to treatment leading to the death of the patient [6;7].

Pt chemotherapy has remained the first-line treatment in the fight against ovarian cancer for almost 40 years, yet, the survival rate of women with ovarian cancer has not improved due to the development of resistance. Therefore, to advance Pt-based therapy and enhance ovarian cancer patient responses in the clinic, studies that identify novel therapeutic targets which contribute to Pt resistance and the development of new and effective non-cross-resistant Pt analogs are pertinent [8].

Table 1. Staging System for Ovarian Carcinoma

Stage	Description
I	Growth limited to the ovaries
A	One ovary; no ascites; capsule intact; no tumor on external surface
B	Two ovaries; no ascites; capsule intact; no tumor on external surface
C	One or both ovaries with: surface tumor; ruptured capsule; or ascites or peritoneal washings with malignant cells
II	Pelvic extension
A	Involvement of uterus and/or tubes
B	Involvement of other pelvic tissues
C	IIA or IIB with factors as in IC
III	Peritoneal implants outside pelvis and/or positive retroperitoneal or inguinal nodes
A	Grossly limited to true pelvis; negative nodes; microscopic seeding of abdominal peritoneum
B	Implants of abdominal peritoneum 2 cm or less; nodes negative
C	Abdominal implants greater than 2 cm and/or positive retroperitoneal or inguinal nodes
IV	Distant metastasis

Table is taken with permission from Bukowski RM, Ozols RF, and Markman M, The management of recurrent ovarian cancer. Seminars in Oncology 34: S1-S15, 2007.

License number: 3794370291161

1.2. Cisplatin:

1.2.1. Discovery of cisplatin:

Cis-Pt has been used consistently in the treatment of ovarian cancer. It was discovered accidentally by Dr. Barnett Rosenberg in the 1960s, while investigating the role of electrical currents on *Escherichia coli* (*E. coli*) bacterial cell growth. He observed that the shape of *E. coli* cells, growing in a buffer of ammonium chloride under administered current through Pt electrodes immersed in the buffer, changed from its classical sausage or rod shape to an elongated filamentous shape. It was eventually determined that the change in shapes was due to inhibition of cellular division triggered by Pt leached from the Pt electrodes. After much investigation, one of the Pt species was identified as *cis*-[PtCl₂(NH₃)₂] (*cis*-Pt) [9-11]. These findings led to the hypothesis that *cis*-Pt could inhibit the proliferation of rapidly dividing cancer cells. Therefore, the anticancer activity of *cis*-Pt was tested in mice where its potent activity promoted large solid tumors to disappear and even after 6 months the recurrence of tumors was not seen [12;13]. Thus, almost 40 years ago *cis*-Pt entered clinical trials and in 1978 it was approved by the Food and Drug Administration (FDA); becoming the first Pt drug to be used in the treatment against cancer. *Cis*-Pt has been used as first-line therapy for several cancers, including testicular, ovarian, cervical, head and neck, small-cell lung, bladder, melanoma and lymphoma cancers [14].

1.2.2. Mode of action of cisplatin:

Cis-Pt is a neutral, square planar molecule that exists primarily in its inactive state as $\text{cis-}[\text{Pt}(\text{Cl})_2(\text{NH}_3)_2]$. For activity, it must undergo aquation reaction by displacement of chloride (Cl) ligands bound to Pt with water molecules, which impart a positive charge to make the molecule reactive toward negatively charged centers and form irreversible covalent links. When administered intravenously to the patient, cis-Pt encounters a high Cl concentration (~100 mM) in the blood plasma. This high Cl concentration limits aquation reaction and maintains cis-Pt primarily in its inactive state [15]. Even then, studies indicate that after one day of cis-Pt administration, 65-98% of the Pt drug is bound to plasma proteins [16;17]. Once the remaining inactive cis-Pt has reached tumor cells, it can cross the cell membrane either by passive diffusion or active transport via copper (Cu)-transporting (CTR) transmembrane proteins. Inside the cell, the Cl concentration decreases substantially (~2-30 mM), allowing displacement of Cl ligand by water molecule to yield the activated form of cis-Pt (**Figure 1**) [15].

The positively charged reactive cis-Pt, $[\text{PtCl}(\text{H}_2\text{O})(\text{NH}_3)_2]^+$, can be subjected to a variety of attacks by nucleophilic centers in nucleic acids and proteins. Studies have identified DNA to be the primary biological target of the activated cis-Pt, which mainly reacts with the N7 position of guanine (G) and adenine (A) purine bases to form the monoadduct complex $[\text{PtCl}(\text{G/A-DNA})(\text{NH}_3)_2]^+$ [18]. The subsequent dissociation of the second Cl ligand allows the conversion of cis-Pt monoadducts to bifunctional interstrand and intrastrand DNA crosslinks. DNA damage produced by cis-Pt is present as monoadducts (9%), intrastrand cross-links (60% on dGG and 30% on dAG) and

interstrand cross-links (1%). These lesions can cause local distortions (unwinding and bending) in the DNA, which is capable of blocking DNA replication and transcription and leads to the activation of signaling events that lead to apoptosis [19].

The signaling pathway cascade triggered by cis-Pt-induced DNA damage initiates with the recognition of distortions from DNA adducts by distortion-specific DNA damage sensor proteins, which include the mismatch repair (MMR) proteins human mutL homolog 1 (hMLH1) and human mutS homolog 2 (hMSH2), the high-mobility group HMG1 and HMG2 proteins, the upstream binding transcription factor RNA polymerase I (UBTF) and the TATA binding protein (TBP). These DNA damage sensor proteins play a crucial role to activate transducer kinases. Some of the most relevant kinases implicated in this process are the ataxia telangiectasia and Rad3-related protein (ATR), the checkpoint kinase 1 and 2 (CHK1 and CHK2) and the mitogen-activated protein kinase (MAPK) family. Transducer kinases in turn drive the stabilization and activation of the most critical effector protein, the transcription factor p53, which is responsible to execute cis-Pt's anticancer effects by inducing programmed cell death (apoptosis) [20].

The dependency of cis-Pt on the p53 pathway is best illustrated in testicular germ cell tumors (TGCT). TGCT is one of the few solid tumors in which the incidence of wild-type p53 is nearly 100% and treatment of patients with cis-Pt in advanced stages is highly curative, as indicated by the 5-year survival rate of 90% [21]. The importance of p53 in mediating cis-Pt cytotoxicity is illustrated by the significant loss in sensitivity

towards cis-Pt treatment after siRNA-mediated silencing of p53 in TGCT cells [22]. In addition, gene-expression array profiling studies in TGCT cells identified 54% of the upregulated genes in response to cis-Pt treatment as p53 pro-apoptotic downstream targets and upregulation of such genes is prevented after p53 knock-down [23].

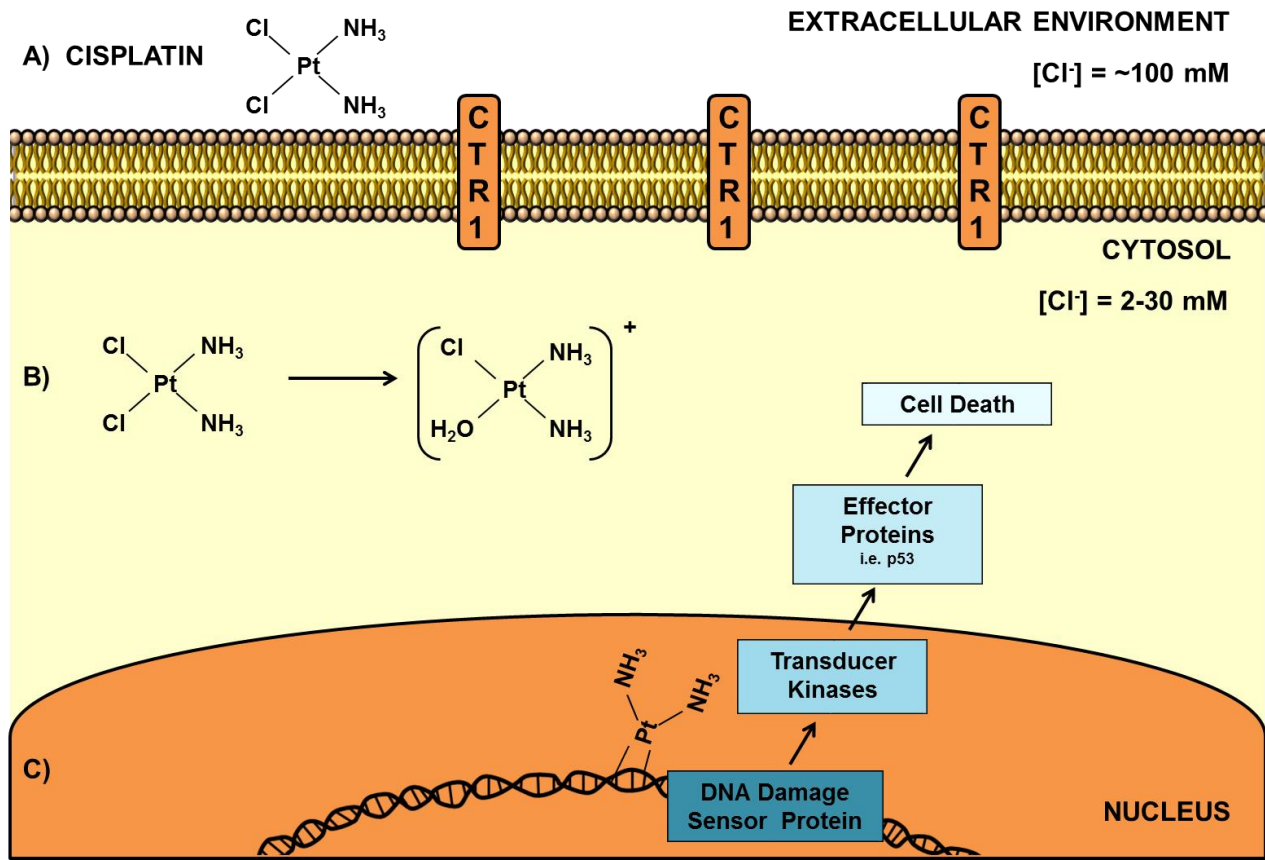


Figure 1. Cisplatin mode of action

A) Cis-Pt remains in its inactive state in the blood plasma due to the high Cl concentration (~100 mM). Once cis-Pt has reached its target cell, it can cross the cell membrane by passive diffusion or active transport via CTR1. **B)** Inside the cell, the low Cl concentration (~2-30 mM) allows the activation of cis-Pt by the replacement of the Cl ligand by water, creating a positively charged reactive cis-Pt species, [PtCl(H₂O)(NH₃)₂]⁺. **C)** The activated form of cis-Pt reacts with the N7 position of purine bases in chromosomal DNA. Cis-Pt-induced DNA damage triggers a signaling cascade leading to the activation of DNA damage sensor proteins, transducer kinases and effector proteins with the ultimate goal of inducing cell death.

1.3. Role of p53 in cancer and therapeutics:

The tumor suppressor p53 protein, was first identified as an oncogene in 1989 [24], is encoded by the *TP53* gene located on chromosome 17p13.1 and is composed of several domains: (i) a DNA-binding domain, (ii) a transactivation domain, (iii) an oligomerization domain, (iv) a proline-rich domain and v) a C-terminal regulatory domain [25]. The p53 protein functions mainly as a transcriptional activator by binding to specific DNA sequences of target genes involved in a broad range of biological functions such as: cell cycle arrest, DNA repair, senescence, apoptosis and inhibition of angiogenesis [26]. Cellular levels of p53 are usually kept low because of its short half-life of ~20 minutes. Degradation of p53 occurs mainly by binding to Mdm2, an E3 ligase that catalyzes monoubiquitination of p53 in the C-terminal domain and thereby targets it for proteasomal degradation [27;28]. A close homolog, Mdm4, can also regulate p53 function by binding to its transactivation domain, but unlike Mdm2 it cannot directly ubiquitinate p53 [29]. However, Mdm2 and Mdm4 work together to promote p53 degradation.

Pt agents elicit a therapeutic response in part, through activation of p53 (**Figure 2**). Activation of p53 is accomplished by post-translational modifications, including phosphorylation and dephosphorylation at ~23 distinct sites by a network of kinases [30;31]. Thus, under stress conditions, as may ensue after cis-Pt-induced DNA damage, specific kinases, such as ATM, ATR, Chk1 and Chk2, become activated. These kinases induce p53 phosphorylation, which allows p53 to dissociate from the Mdm2-Mdm4-p53 complex. The resulting stabilization of p53 and its translocation to the nucleus enable

p53 to bind as a tetramer to specific DNA sequences and transactivate target genes [28;31;32]. This transactivation by p53 is critical for its cellular functions, which include arresting the cell cycle to permit DNA repair and, if the damage is too severe to be repaired, activating cell death pathways [33]. Although the p53 tumor suppressive signaling cascade paradoxically fails to prevent cancer from developing in the first place, it can still be activated in many cancer cells with DNA damaging drugs to induce an antitumor response [34;35]. However, the eventual failure of p53 to become activated in tumor cells during the course of chemotherapy is the most significant mechanism of drug resistance. This failure results from the loss of three of the most significant cellular pathways involved in antitumor response during chemotherapy: (i) induction of programmed cell death, (ii) induction of checkpoint response and cell cycle arrest and (iii) induction of permanent cell cycle arrest (senescence); these pathways normally contribute independently or collectively to final therapeutic outcomes in patients. A brief discussion of these processes is warranted to better appreciate p53-dependent resistance mechanisms.

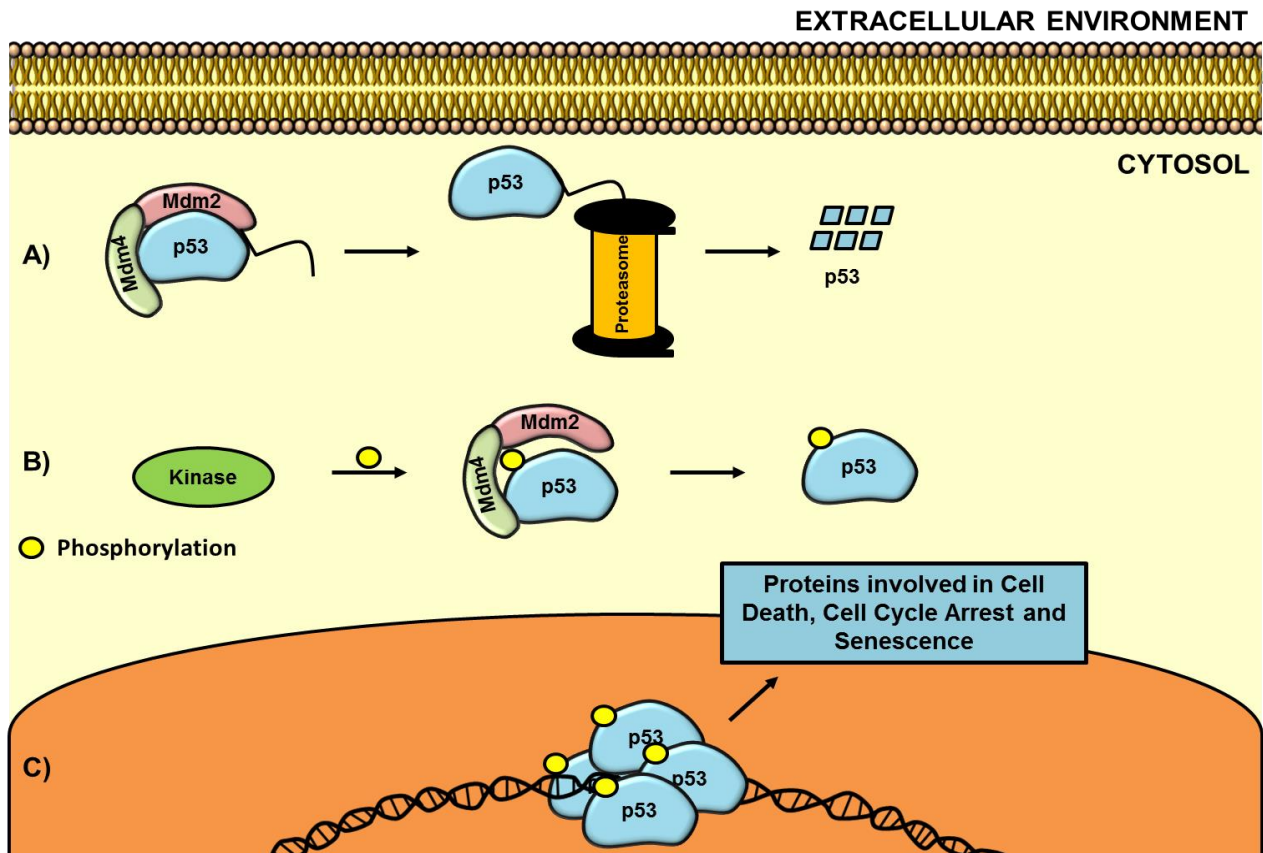


Figure 2. p53 transcriptional activity regulation

A) Cellular levels of p53 are kept low due to its regulation by Mdm2/Mdm4. Degradation of p53 occurs mainly by binding to Mdm2. Mdm2 is responsible for p53 ubiquitination in the C-terminal domain, targeting p53 for proteasomal degradation. **B)** When cells undergo stress, as mediated by cis-Pt-induced DNA damage, specific kinases phosphorylate p53, allowing p53 stabilization and activation. **C)** Activated p53 translocates to the nucleus, where it functions as a transcriptional factor by binding as a tetramer to specific DNA sequences and inducing the transcription of genes involved in apoptosis, cell cycle arrest and senescence.

1.3.1. Induction of apoptosis:

Although p53 can mediate apoptosis in a transcription-dependent manner, it is also involved in transcription-independent apoptosis. In the transcription-dependent process, two distinct signaling pathways are involved: extrinsic and intrinsic pathways. In the extrinsic pathway, p53 induces the transcription of death receptors of the tumor necrosis factor receptor (TNFR) family: Fas, APO-1, CD95, DR5 and PERP. After a ligand binds to its specific receptor, the formation of the death-inducing signaling complex (DISC) is accomplished by recruitment of the Fas-associated death domain (FADD) and caspase-8 and -10, leading to the activation of the effector caspases (e.g. caspase-3 and -7) and resultant DNA fragmentation as a hallmark of apoptosis [36].

In contrast, the intrinsic pathway is activated through a DNA damage mechanism that involves mitochondrial apoptotic events, which are regulated largely by the Bcl-2 family of proteins. Upon stabilization and activation, p53 translocates to the nucleus where it transactivates the pro-apoptotic genes *Bax*, *Noxa*, *PUMA* and *Bid* [37]. Of these, *Bax* is the most important pro-apoptotic gene to be induced by p53, but its translocation and functional multimerization depend on other proapoptotic family members [38]. Bax can either homo-multimerize or hetero-multimerize with Bak in the outer mitochondrial membrane and thereby induce the release of cytochrome c, Smac/DIABLO and apoptosis-inducing factor (AIF) from the mitochondrial intermembrane space to the cytosol. The apoptosome complex, formed by cytochrome c, apoptotic protease-activating factor 1 (APAF-1), and pre-cleaved caspase-9, activates effector caspase-3, -6, and -7 to induce DNA fragmentation as the final stage

of apoptosis [39]. Interestingly, the intrinsic and extrinsic pathways are connected via Bid, which upon cleavage to t-Bid by caspase-8 translocates to the mitochondria and activates the proapoptotic proteins Bax and Bak [37].

In the transcription-independent mechanism of apoptosis, some of the induced p53 translocates to the mitochondria and physically interacts with the anti-apoptotic proteins Bcl-xL and Bcl-2 to promote the pro-apoptotic homo- or hetero-multimerization between Bak and Bax [40;41]. This occurs rapidly and before p53 exhibits its transcriptional activity. In addition, p53 disrupts the inhibitory Bak–Mcl1 complex by binding to Bak directly [42]. Taken together, these actions of p53 permeabilize the outer mitochondrial membrane and allow the release of pro-apoptotic factors into the cytoplasm. DNA damaging drugs may activate both membrane death receptors and the endogenous mitochondrial damage pathway; because these apoptotic mechanisms are deregulated in cancers, proteins involved in these pathways are molecular targets of great interest for cancer therapy [43]. Indeed, most of the anticancer agents that act through DNA damage or stress-inducing mechanisms require p53 to exhibit the apoptotic phenotype [44].

1.3.2. Induction of checkpoint response and cell cycle arrest:

DNA damage promoted by Pt agents can also result in the inhibition of cyclin-dependent kinase (Cdk) activities, thereby impacting cell cycle kinetics. More specifically, inhibition of distinct Cdk/cyclin complexes that are present throughout the cell cycle prevents or slows G1/S transition, S phase progression, G2/M transition, or all

three [45;46]. Although many of the Cdks can be inhibited by members of the Cip/Kip family members of Cdk inhibitors (p21, p27, and p57), p21 as a critical target of p53 is the most significant for inhibiting G1-phase Cdk4/cyclin D and Cdk2/cyclin E. This significance is reflected in the fact that p21 deletion alone can prevent G1-phase arrest [46-48], whereas other mechanisms exist to inhibit S- and G2-phase Cdk activities [47]. Indeed, DNA damaging agents can induce S- and G2-phase arrest even if p53 function is not present [49]. Cell cycle arrest is considered a critical step to allow DNA repair and cell survival, but if repair fails then apoptosis is induced. Whether persistent p21-dependent G1 arrest is actually a trigger for cell death is unclear. However, tumors retaining G1 checkpoint response appear to be more sensitive to therapeutic agents [50;51]. A strong positive correlation has been demonstrated between the ability of tumor cells to arrest in G1 and their sensitivity to Pt-based drugs in the National Cancer Institute (NCI) panel of 60 tumor cell lines [52]. This correlation is also consistent with the finding that mutant p53 tumor cells transfected with a p21 expression vector are sensitized to antitumor drugs [53;54]. In addition, small-molecule inhibitors of G1-phase Cdks not only arrest cells but also induce apoptosis [55;56]. Moreover, cells from p21 knockout mice lack G1 checkpoint response [57], and because such mice develop tumors [58], the tumor suppressive function of p53 may be mediated in part through the downstream effects of p21 in checkpoint response.

1.3.3. Induction of senescence:

Cellular senescence is defined as a permanent cell cycle arrest that prevents cell immortalization and transformation to a genetically unstable phenotype [59]. Therefore,

senescence is identified as an additional tumor suppressive mechanism in benign or premalignant cancer lesions [60]. Senescent cells remain metabolically active but acquire distinct changes in morphology and physiology characterized by enlarged cell size, chromatin condensation, changes in gene expression and high levels of senescence associated β -galactosidase. The senescence phenotype occurs as a result of various forms of stress stimuli such as telomerase shortening, oncogenic stimuli, ionizing radiation and DNA damaging agents [61]. Not surprisingly, p53 is the pivotal player in regulating replicative as well as premature (stress-induced) senescence. In line with this evidence, tumor cells containing wild-type p53 are more likely to undergo senescence in response to chemotherapy [62]. Stress-induced senescence is driven via the ATM/ATR-Chk2/Chk1-p53 pathway, with the involvement of several p53-dependent downstream molecular markers, such as p21, PML, PAI-1 and DEC1 [62]. Of these, p21 is the seminal controller of the senescence program. In this respect, p21-dependent G1 arrest in senescence is similar to that after checkpoint response, but the significant difference is that activation of the senescence program requires prolonged p53-dependent expression of p21, whereas the checkpoint response pathway requires a relatively transient transactivation of p21 by p53. Despite this difference, premature senescence, like apoptosis and G1 checkpoint response, can significantly contribute to the antitumor effects mediated by p53 with a variety of anticancer agents. Although apoptosis may have greater relevance in cancer chemotherapy, p53-dependent senescence may provide an important anti-proliferative option in cancer cells that have lost their ability to undergo p53-dependent apoptosis [63-67].

1.4. Mechanisms leading to cisplatin resistance from failure of p53 activity:

As previously discussed, induction of cell death by cis-Pt requires (i) the recognition of DNA damage, (ii) activation of transducer kinases, (iii) stabilization and activation of p53 via post-translational modifications, (iv) activation of downstream p53-dependent transcription of pro-apoptotic genes such as *Bax*, *Noxa*, *p53 upregulated modulator of apoptosis (PUMA)* and *Bid*, and finally (v) execution of cytotoxic programs. Studies have highlighted the importance of Bax in apoptosis and failure to increase Bax levels contributes to cis-Pt resistance. In addition, p53 transactivates target genes involved in cell cycle arrest and senescence, two processes that have an important role in mediating cis-Pt cytotoxicity. Therefore, p53 plays a pivotal role in mediating cis-Pt cell death, and thus, dysfunction in the p53 pathway has been associated with cis-Pt resistance [20]. Since p53 protein has a central role in facilitating the effects of cis-Pt by activating antiproliferative/pro-apoptotic pathways, it becomes a vulnerable target and tumor cells will select to attenuate p53 function leading to drug resistance and cell survival. The mechanisms that directly affect p53 function to induce drug resistance include failure of upstream pathways that stabilize and activate p53 through post-translational modifications, mutation in the p53 protein or a combination of both mechanisms (**Figure 3**) [68].

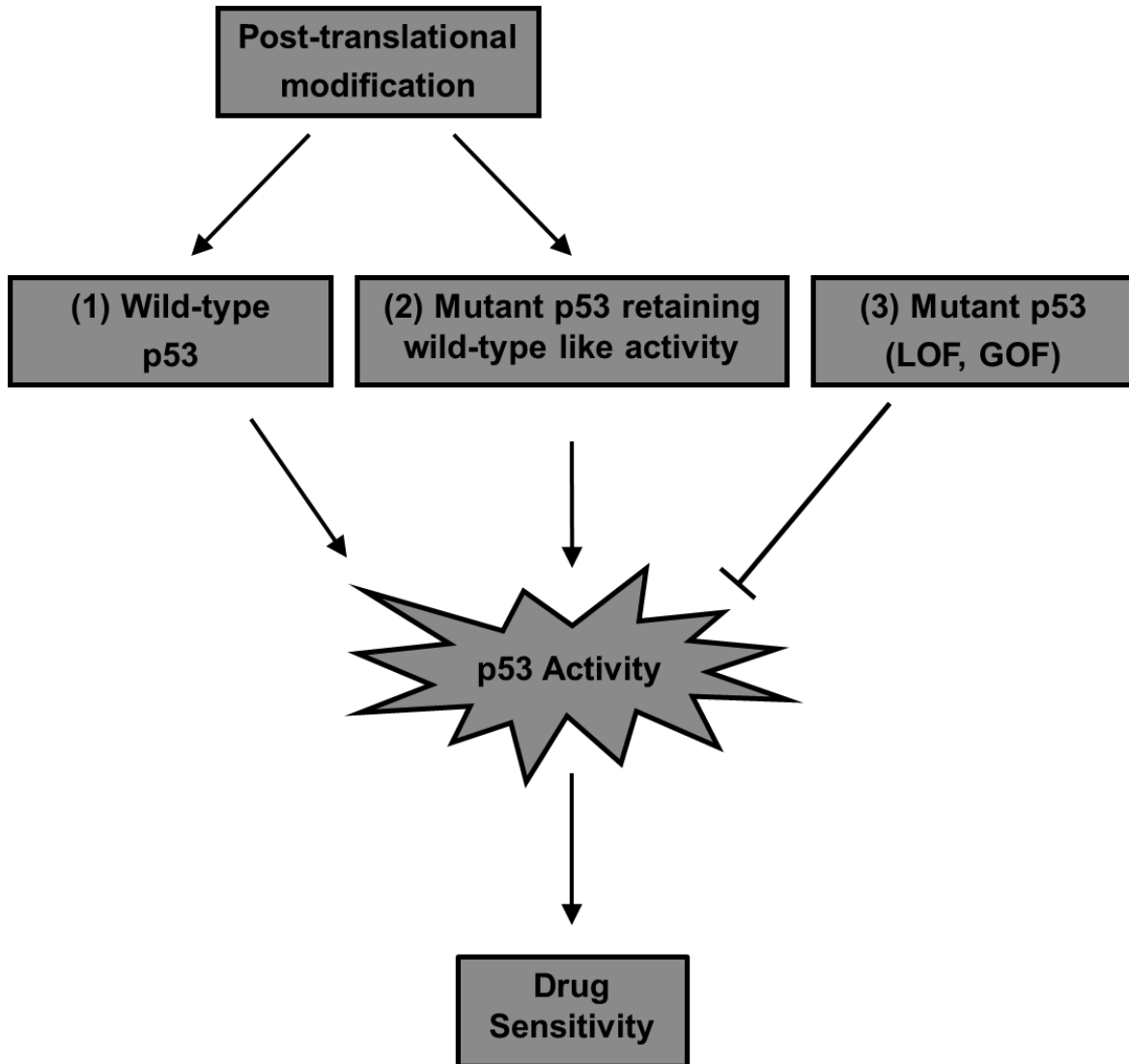


Figure 3. Mechanisms leading to failure of p53 activity

The mechanisms that directly affect p53 function to induce drug resistance include: failure of upstream pathways that stabilize and activate **(1)** wild-type and **(2)** mutant p53 (capable of retaining wild-type p53 function) through post-translational modifications, mainly phosphorylation, and **(3)** loss-of-function (LOF) and/or gain-of-function (GOF) mutation in the p53 protein.

1.4.1. Significance of phosphorylation in post-translational modifications of p53:

Stabilization and activation of p53 is governed by covalent post-translational modifications, such as phosphorylation, ubiquitination, acetylation, methylation, SUMOylation, neddylation, glycosylation and ribosylation [69;70]. A total of ~50 sites on p53 are now known to be subject to modifications after a stress stimulus [71]. The N-terminus is modified primarily by phosphorylation, whereas the C-terminus can be targeted by a variety of modifications, including phosphorylation [69]. Although an optimal combination of post-translational modifications is required for maximal p53 function, the antitumor effects of DNA damaging agents such as cis-Pt are dominantly governed by phosphorylation events [72;73]. There are ~23 possible sites on p53 that can be phosphorylated and each site can be targeted by multiple kinases, suggesting possible redundancy [31]. However, it is likely that a specific antitumor agent only activates an individual kinase for each of the several sites targeted for phosphorylation. As a result, a DNA damaging agent produces a unique signature of p53-phosphorylated sites that induces p53 to adopt a specific structural conformation and thereby transactivate a select set of downstream target genes specific for that agent. Therefore, deregulation of any critical kinase will alter the unique p53 phosphorylation signature, impede gene transactivation, and attenuate antitumor response.

Of the multiple p53 phosphorylation sites that have been associated with its antiproliferative and apoptotic functions, Ser15 and Ser20 in the DNA-binding domain at the N-terminus are recognized as the most critical and are therefore the most extensively studied (**Figure 4**) [31;74]. Studies demonstrate that phosphorylation at

these sites promote not only dissociation of p53 from Mdm2, as a prerequisite for p53 stabilization, but also its transcriptional activity [71;75-77]. Moreover, several studies suggest that the effects of phosphorylation at these sites may be cooperative, particularly because Ser20 phosphorylation is strongly dependent on the priming phosphorylation at Ser15 [78-80]. Indeed, dual phosphorylation at Ser20 with Ser15 is sufficient to induce apoptosis in glioma cells harboring wild-type p53 [81;82]. Further support is provided by studies in transgenic mice where mutations induced by replacing both Ser15 and Ser20 with alanine produced a more severe phenotype than a single mutation at either site, as evidenced by loss in apoptotic capacity, defects in replicative senescence, and latency in tumor appearance [69].

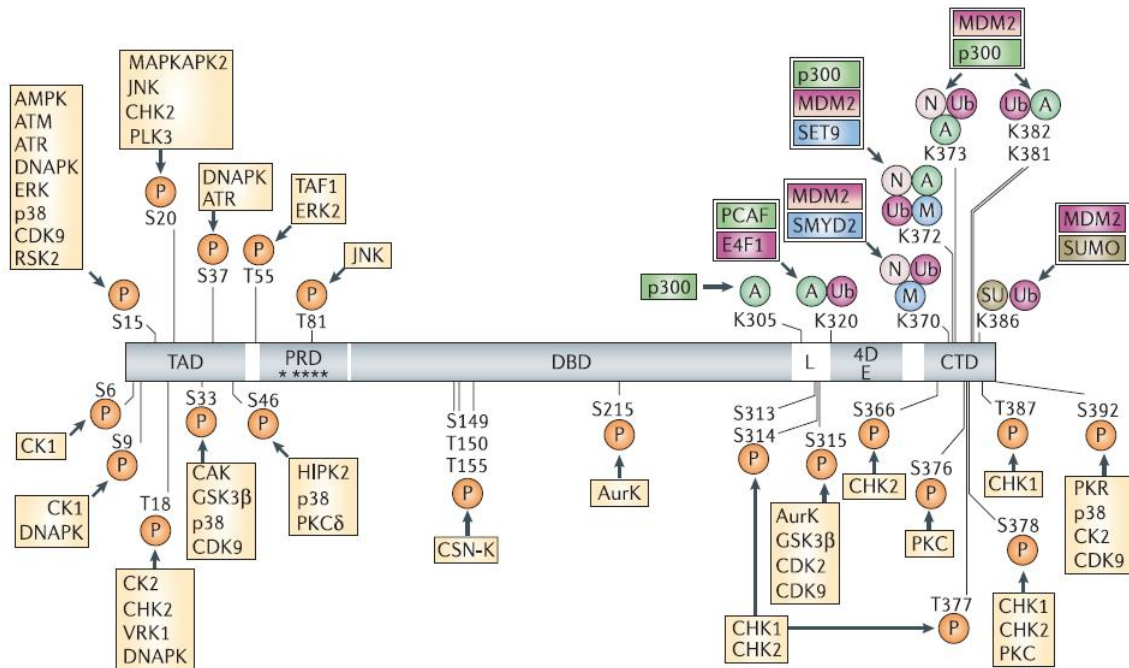


Figure 4. p53 post-translational modifications

Specific residues are modified as shown, with phosphorylation (P) in orange, acetylation (A) in green, ubiquitylation (Ub) in purple, neddylation (N) in pink, methylation (M) in blue and sumoylation (SU) in brown. Proteins responsible for these modifications are shown in matching colors. There are ~23 possible sites on p53 that can be phosphorylated. Each phosphorylation site can be targeted by multiple kinases and a single kinase can target multiple phosphorylation sites. From the therapeutic point of view, such redundancy may enable the phosphorylation of p53 at a common site by chemotherapeutic agents, with each agent activating the same or a different kinase targeting the common site.

Figure is taken with permission from Toledo F and Wahl GM, Regulating the p53 pathway: in vitro hypotheses, in vivo veritas. Nat.Rev.Cancer 6: 909-923, 2006.

License number: 3794361100557

1.4.2. Mutant p53:

One major mechanism acquired by cancer cells to inactivate p53 is through mutations, as occurs in ~50% of all human cancers. The majority of somatic p53 mutations are missense in nature, in which a point mutation is generated resulting in the expression of the full-length p53 protein with only a single amino acid substitution compared to its wild-type state. p53 missense mutations occur primarily in exons 4–9, which encode the DNA-binding domain [83]. Specific mutations in p53 are grouped into “contact” and “structural” classes, but both types impede the pro-apoptotic p53 transactivation functions by preventing binding of p53 with target promoter sites on DNA. Thus, “contact” mutations are located at amino acid positions in p53 that normally make direct contact with DNA and will disrupt promoter binding without necessarily altering p53 conformation. In contrast, “structural” mutations are located at amino acid positions in p53 that do not make direct contact with DNA and will induce a p53 configuration that is unable to bind to the specific DNA sites [84;85]. Nevertheless, both type of p53 mutations are sufficient to cause LOF of p53; altering the response of tumors to a wide range of clinical treatment regimens, including cis-Pt [29;86].

The spectrum of mutations in *TP53* is diverse. However, there are several frequent mutations in p53, denoted as “hotspot” mutations, such as R175, G245, R248, R249, R273 and R282. These “hotspot” mutations may not only confer loss of p53 functions but can also induce novel functions, leading to the so-called p53 GOF phenotype [95]. Evidence suggests that p53 GOF mutant activity includes 1) inactivation of transcriptional factors that have an important role in the cell death pathway (i.e. p63

and p73) and/or 2) transcriptional activation or repression of genes whose expression is not normally regulated by wild-type p53 (*BFGF*, *EGFR*, *HSP70* and *C-Myc*). In general, mutant p53 directly or indirectly impacts the transcriptional regulation of genes that mediate proliferation, metastasis and survival of tumor cells [87-90]. From the perspective of therapeutic response, it is clear that GOF mutations in p53 will inhibit both anti-proliferative and pro-apoptotic pathways, and, thus, induce resistance.

1.5. The role of *TP53* gene status in response to platinum treatment in ovarian cancer:

Several clinical studies have examined the role of *TP53* gene status in patient survival and the development of chemoresistance in ovarian cancer, and have concluded that the prognostic value of this tumor suppressor is somewhat conflicting. This conclusion stems from clinical observations in ovarian cancers in which therapeutic resistance in both mutant and wild-type p53 cancers is obtained. For instance, in a clinical study using cis-Pt treatment, it was found that cis-Pt induced a response in 46% of the patients in the wild-type p53 group and in a similar percentage (37%) of patients in the mutant p53 group [91]. Other studies with the Pt/paclitaxel combination have demonstrated that responses in the mutant p53 group are in fact significantly greater (wild-type, 47%; mutant, 86%) [92]. However, another similar clinical study with the Pt/paclitaxel combination demonstrated, in direct contrast, that responses in the wild-type p53 group were significantly greater (wild-type, 90.0%; mutant, 60.8%) [93]. Recently, The Cancer Genome Atlas (TCGA) project has identified *TP53* as the most commonly mutated gene in high grade serous ovarian carcinoma (HGSOC), exhibiting a

p53 mutation rate of 86% [94]. Furthermore, the survival curve in relation with *TP53* status in HGSOC patients generated from data extracted from TCGA indicates that there is no significant difference between patients stratified according to wild-type (34.4%) or mutant (39.9%) p53 (**Figure 5**). These reports provide evidence that *TP53* status is not a reliable marker to predict chemotherapeutic outcome in ovarian cancer patients.

The discrepancy seen in the role of *TP53* gene status in patient survival could be due to 1) inadequate methods to detect p53 gene status, 2) insufficient characterization of *TP53* mutations and/or 3) loss of p53 post-translational activation.

1) *Inadequate methods to detect p53 gene status :*

Some studies have determined *TP53* mutation by sequencing only partial segments of the gene, which may result in omitting the identification of possible mutations in the non-sequenced areas, thus, generating false negative results. Another method employed to detect mutant p53 is immunohistochemistry (IHC) staining. Mutant p53 status is indicated when IHC staining indicates high cellular levels of p53, since mutant p53 can escape proteasomal degradation by Mdm2/Mdm4 complex, resulting in an increased p53 half-life and hyper-stabilization. In contrast, identification of wild-type p53 is suggested when IHC staining shows low expression levels of p53 since it is tightly regulated by Mdm2/Mdm4 complex, as discussed in **Section 1.3**. However, mutant p53 in tumors may also exist at lower levels and, conversely, wild-type p53 may present at higher levels. Therefore, the IHC staining method has the potential to

produce both false negative and false positive results [95-97], indicating that this is not a good method to detect mutations.

2) *Insufficient characterization of TP53 mutations:*

A detailed study evaluating p53 transcriptional activity in 2,314 distinct p53 mutants, representing all possible p53 missense mutations, revealed that only 9.6% of p53 mutants exhibited no activity, 26.5% of p53 mutants had partial activity, whereas 63.9% of p53 mutants retained p53 activity comparable with that of wild-type p53 [98]. These results clearly demonstrate that not all p53 mutants are inactivating or dysfunctional and, therefore, classification of p53 status goes beyond the typical and simplistic categories of wild-type vs. mutant. Instead, *TP53* mutations should be categorized based on their functional activity: 1) functional, 2) LOF or 3) GOF. Thus, extensive research should be conducted to study the intrinsic biological behavior of each p53 mutant in order to predict patient response to chemotherapy, to identify common signaling pathways leading to chemoresistance and to better design anti-cancer drugs that can restore dysfunctional mutant p53 activity to one capable of promoting tumor drug response [83].

3) *Loss of p53 post-translational activation:*

One post-translational modification event playing an essential role in p53 response to chemotherapeutic treatment is phosphorylation of p53. It has been shown that wild-type p53 stabilization and activation, in response to DNA damaging agents, is regulated by a series of phosphorylation events of numerous serine and threonine

residues within its N- and C-terminal regions [31]. Ser15 and Ser20 are two of the most critical phosphorylation sites at the N-terminus region on p53 that are associated with enhancing wild-type p53 stabilization, transcriptional activity, anti-proliferative and apoptotic functions. Therefore, deregulation in the ability of Pt compounds to induce p53 phosphorylation may jeopardize p53 transcriptional activity and lead to a resistant phenotype. Indeed, studies have shown that downregulation of Chk2, a kinase reported to phosphorylate p53 at Ser20 after cis-Pt treatment, leads to resistance to some DNA damaging agents [99-101].

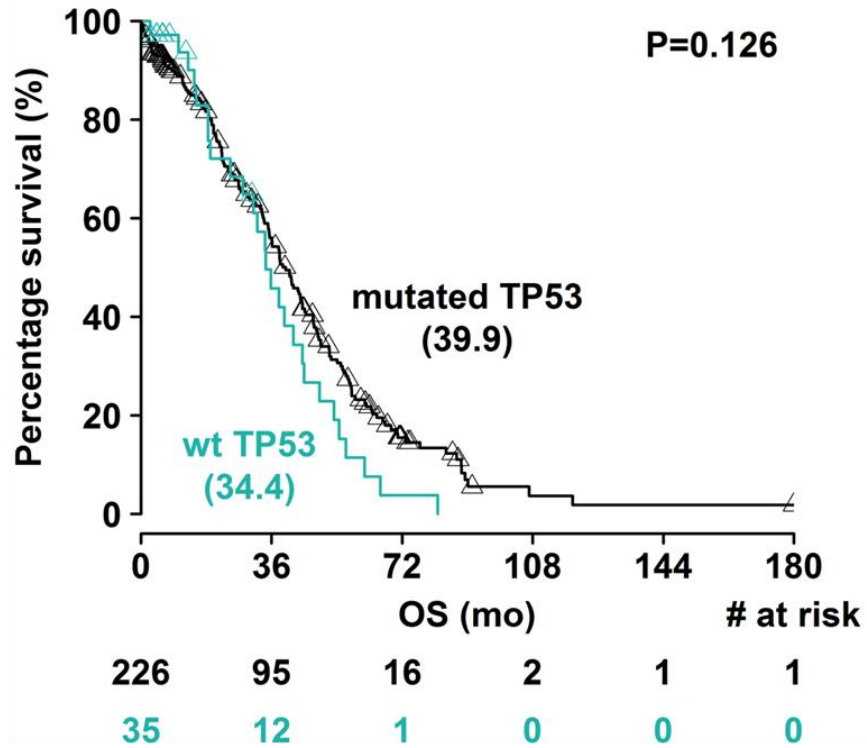


Figure 5. Effect of p53 status on survival curves for ovarian cancer patients

In HGSOC patients the rate of p53 mutation is ~86%. However, the 5-year survival curve of ovarian cancer patients shows that there is no significant improvement in the therapeutic outcome of patients containing wild-type (34.4 months) vs. mutant p53 (39.9 months).

1.6. Other mechanisms inducing resistance to cisplatin:

Tumors cells express multiple mechanisms of resistance that may include p53 dysfunction, as discussed above. The combined mechanisms can severely limit the clinical anticancer activity of cis-Pt. Resistance of tumor cells towards cis-Pt can either be intrinsic or acquired over time after exposure to cis-Pt [102]. Even though the mechanisms of cis-Pt resistance are multifactorial, they can be classified into two major categories: 1) Mechanisms limiting the degree of cis-Pt-induced DNA damage and 2) Mechanisms that disrupt the cis-Pt-induced DNA damage signaling pathway that execute cell death. A brief discussion of the most relevant mechanisms involved in these two major categories that may coexist with the p53 dysfunctional state is provided in the following paragraphs.

Mechanisms limiting the degree of cis-Pt-induced DNA damage:

1) *Decreased intracellular drug accumulation:*

This mechanism of cis-Pt resistance includes decreased uptake and/or increased efflux of cis-Pt. As previously discussed, cis-Pt can be actively transported inside the cell through several transmembrane transporters, including the Na⁺/K⁺-ATPase [103] and members of solute carrier (SLC) transporters (e.g., CTR) [104]. Therefore, any alteration in these transporters will reduce the intracellular uptake of cis-Pt. On the other hand, efflux of cis-Pt is mainly achieved through the ATP-dependent glutathione (GSH)-conjugated efflux pump upon reaction of cis-Pt with GSH, a protein rich in sulfhydryl groups [105].

In ovarian cancer, it has been shown that the P-type ATPase membrane proteins play an important role in mediating cis-Pt resistance. The Cu transporters ATP7A and ATP7B have been found to be highly expressed in cis-Pt resistant ovarian cancer cells when compared with cis-Pt sensitive cells and have been shown to be involved in intracellular cis-Pt trafficking and export [106-109]. In vivo combinational therapy experiments of ATP7B siRNA with cis-Pt effectively reduced tumor growth [110]. In addition, knock-down of ATP7B resulted in cis-Pt sensitivity and increased DNA-Pt adducts formation in cis-Pt-resistant cells [110]. The mechanism by which ATP7B inactivates cis-Pt is by directly interacting with cis-Pt through its Cu-binding domain at the NH₂-terminal, which is rich in methionine [110]. Such interaction leads to cis-Pt resistance. Similarly, another P-type ATPase member, ATP11B, has been associated with cis-Pt resistance in ovarian cancer cells [111]. It has been shown that ATP11B expression correlates with higher tumor grade in human ovarian cancer samples and with cis-Pt resistance in human ovarian cancer cell lines. Furthermore, knock-down of ATP11B through siRNA in cis-Pt sensitive and resistant ovarian cancer cells in vitro and in mice leads to sensitivity towards cis-Pt [111]. In contrast, overexpression of ATP11B in ovarian cancer cells leads to cis-Pt resistance [111]. ATP11B shares a high homology in protein structure with ATP7A and ATP7B; however, unlike ATP7A and ATP7B, ATP11B does not contain a metal-binding motif at the amino terminus, which is required for Pt binding. Therefore, ATP11B does not inactivate cis-Pt through direct interaction. ATP11B major role is to translocate phospholipids from the outer and inner leaflet of membrane bilayers [112]. This major function of ATP11B along with cellular Pt content and cis-Pt efflux kinetics studies strongly suggest that ATP11B enhances the export of

cis-Pt from cells via the vesicular secretory pathway [111]. Taken together, these findings have identified ATP family proteins as important targets for overcoming cis-Pt resistance.

2) Increased inactivation by thiol-containing molecules:

Even though the primary mode of action of cis-Pt is to react with chromosomal DNA in order to induce DNA damage, cis-Pt can also react with thiol groups found in cysteine and methionine amino acids from sulfur donating proteins. GSH and metallothionein are rich in thiol groups whereby, an increase in GSH and metallothionein will decrease the availability of activated cis-Pt to react with DNA; thus, contributing to cis-Pt resistance [12;113].

3) Increased DNA repair of cis-Pt-induced DNA damage:

The first response from tumor cells towards cis-Pt-induced DNA damage is to attempt to repair such damage. The most abundant form of DNA crosslinks produced by cis-Pt are the intrastrand crosslinks, which are primarily repaired by the nucleotide excision repair (NER) pathway. Thus, upregulation of proteins involved in the NER pathway, such as Xeroderma Pigmentosum (XP) and excision repair cross-complementation (ERCC) proteins, will enhance repair and prevent the capacity of cis-Pt to induce persistent DNA damage and, thereby, cause cis-Pt resistance [102].

Mechanisms that disrupt cis-Pt-induced DNA damage signaling:

1) *Overexpression of human epidermal growth factor receptor 2 (HER-2) and the phosphatidylinositol-4,5-bisphosphate 3-kinase (PI3K)/Akt pathway:*

Activation of the tyrosine kinase transmembrane receptor HER-2 leads to activation of the PI3K/Akt pathway. Akt activity leads to several antiapoptotic features by promoting phosphorylation of p21, which sequesters p21 in the cytoplasm and reduces its level in the nucleus [114], induces translocation of Mdm2 into the nucleus leading to degradation of the p53 tumor-suppressor protein [115;116] and inactivate the proapoptotic proteins Bcl-2-associated death promoter (Bad) and procaspase-9 [117;118].

2) *Role of Ras and MAPK pathway:*

Binding of extracellular stimuli, such as cytokines, growth factors or mitogens, to their respective receptors at the cell membrane leads to the formation of the coupling complex Shc/Grb2/SOS. The Shc/Grb2/SOS complex promotes a GDP to GTP exchange in Ras, thus, activating Ras [119]. The GTP-bound active Ras can then initiate a series of sequential phosphorylation events in the MAPK family comprised of three protein kinases [120]. First, RAS phosphorylates MAP kinase kinase kinase (MAPKKK), which phosphorylates MAP kinase kinase (MAPKK), which in turn phosphorylates MAP kinase (MAPK). Mammalian cells possess three well characterized MAPK subfamily members: the extracellular signal-regulated kinases (ERK), the c-Jun N-terminal kinases (JNK) and the p38 kinases [121]. These activated MAPKs target many other substrates, such as transcription factors, regulating cell proliferation,

differentiation, cell survival and apoptosis (**Figure 6**) [122]. In the ERK1/2 MAPK module, Raf phosphorylates MEK1/2 and MEK1/2 phosphorylates ERK1/2. This phospho-ERK1/2 phosphorylates other proteins in the cytoplasm (e.g. p53) or nucleus (e.g. Elk1) [123].

All three MAPKs have been shown to become activated in tumor cells by cis-Pt treatment [124]. Activation of MAPKs can lead to either resistance or sensitivity towards cis-Pt. This cis-Pt driven sensitivity or resistance by MAPKs could depend on cell context or the extent of DNA damage promoted by cis-Pt. MAPK pathway leads to cis-Pt resistance by activating transcription factors, such as c-Myc, c-Fos and c-Jun, which promote the induction of genes that increase thiol-containing molecules and/or upregulate DNA adduct repair pathways [125]. Alternatively, MAPK pathway leads to cis-Pt sensitivity by inducing post-translational modifications of p53 which are necessary for p53 to exert its transcriptional activity and induce cell death [126]. Indeed, it has been shown that ERK, JNK and p38 are able to phosphorylate p53 and some of these phosphorylation sites are depicted in **Figure 4** [31]. However, it has been suggested that ERK activation plays the most critical role in inducing apoptosis after cis-Pt treatment [127]. Studies have shown that the RAF/MEK/ERK pathway drives apoptosis in a p53 dependent manner [128] and activation of ERK upon cis-Pt treatment has been shown to contribute to p53 phosphorylation at Serine-15 (Ser-15) in ovarian cancer [129]. In addition, inhibition of the MEK/ERK pathway leads to cis-Pt resistance in human cervical carcinoma cells [130].

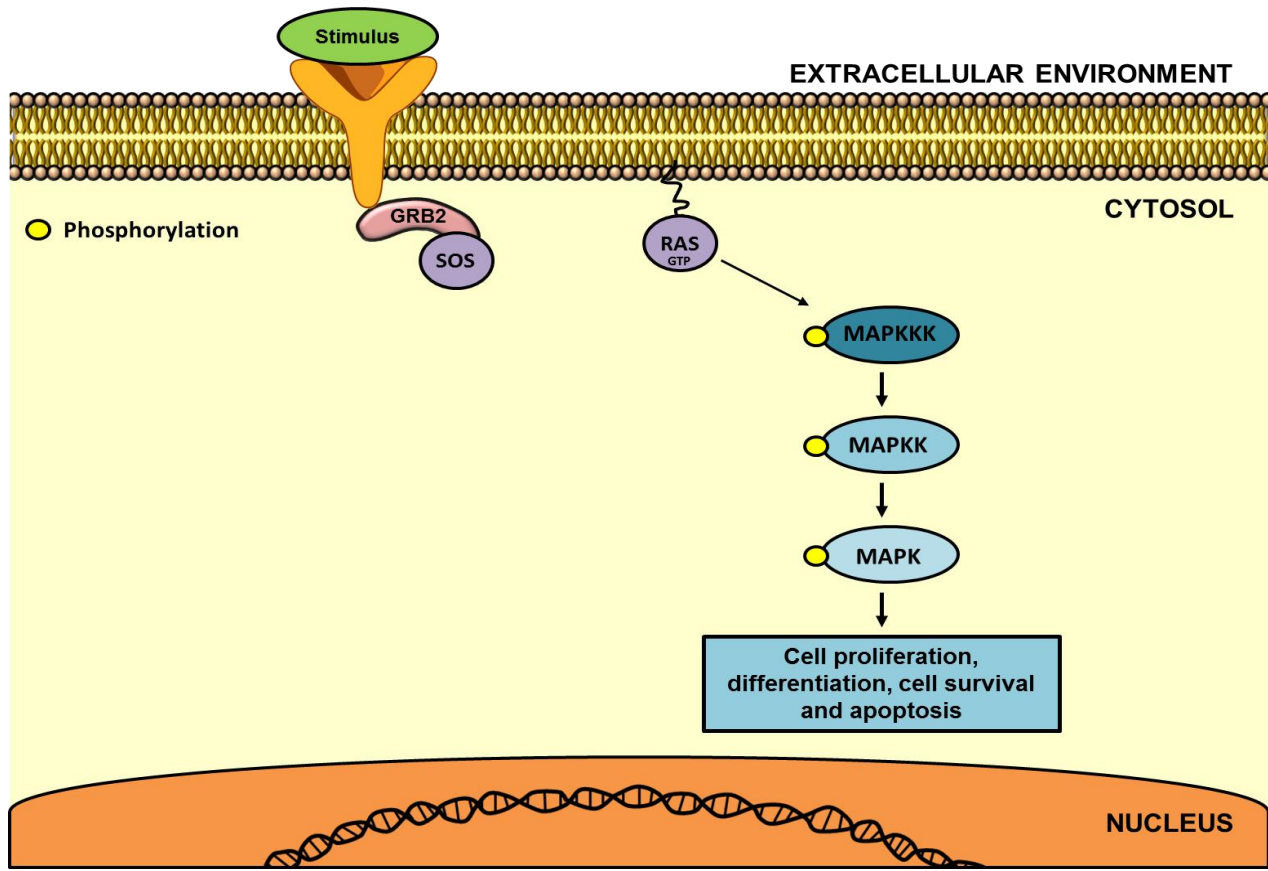


Figure 6. Ras/MAPK pathway

Ras/MAPK signaling pathway originates by activation of Ras through GDP to GTP exchange promoted by the Shc/Grb2/SOS complex. Active Ras phosphorylates the MAPKKK, which phosphorylates MAPKK, which in turn phosphorylates MAPK. Activated MAPKs target many other substrates in the cytoplasm or nucleus leading to the regulation of cell proliferation, differentiation, cell survival and apoptosis.

1.7. Platinum analogs non-cross-resistant to cisplatin:

Since the discovery of cis-Pt, Pt drugs have been used in the clinic for the treatment of a wide range of solid tumors. However, intrinsic and acquired resistance against approved Pt compounds remain a major obstacle for their effectiveness in cancer treatment. Therefore, extensive research has been employed in developing new Pt analogs that may circumvent such resistance and improve therapeutic outcome of patients. In order to achieve this goal, it is essential to take a close look at the basic structure of Pt compounds. Pt compounds have a square planar configuration with a general chemical structure of $[\text{Pt}(\text{X})_2(\text{L})_2]$, in which X is an equatorial leaving (labile) group, L is an equatorial (stable) carrier amine ligand and the central metal atom is in a bivalent Pt (II) oxidation state [15]. Thus, cis-Pt is a simple structure with $\text{L} = \text{NH}_3$ and $\text{X} = \text{Cl}$ [131]. There are some modifications that can be performed, individually or as a group, for the synthesis of new promising Pt compounds: 1) substitution of X, L or both with alternate chemical groups, 2) creation of different Pt isomers (cis vs. trans) and 3) increasing the oxidation state of the Pt atom to tetravalent Pt(IV) [132]. A more detailed explanation of each group with their respective examples will be provided in the following paragraphs.

1) Substitution of X, L or both with alternate chemical groups:

Oxaliplatin (oxali-Pt), a third generation Pt derivative, is an excellent example where modifications to the basic structure of cis-Pt yields a different activity profile. The chemical structure of oxali-Pt has $\text{L} =$ bidentate 1,2-diaminocyclohexane (DACH) and $\text{X} =$ oxalate [131]. Even though oxali-Pt forms similar DNA damage as cis-Pt (described in

Section 1.2.2), oxali-Pt DNA damage reflects different distortion angle and degree of local unwinding in the formation of DNA-adducts due to its different carrier ligand. DACH-Pt-DNA adducts formed by oxali-Pt are bulkier, more hydrophobic, more effective at inhibiting DNA synthesis and more cytotoxic than cis-diammine-Pt-DNA adducts formed by cis-Pt. Moreover, due to differences in unwinding and bending angles of DNA between cis-Pt and oxali-Pt-DNA adducts, the specialized proteins recognizing these drug-specific adducts are different. For instance, it has been shown that the DNA damage induced by oxali-Pt is not recognized by HMGB and MMR proteins, whereas cis-Pt adduct recognition is highly dependent on these proteins. Thus, loss of these proteins result in resistance to cis-Pt but not to oxali-Pt [133]. As a consequence, DNA adducts formed by cis-Pt and oxali-Pt induce the activation of independent DNA damage signaling pathways, but which converge on p53-dependent apoptosis.

In 2002, oxali-Pt, was approved by the FDA in the United States for the treatment of advanced colorectal cancer, a disease in which cis-Pt treatment has proven to be ineffective. In advanced ovarian cancer, oxali-Pt entered Phase II and Phase III clinical trials in patients that do not respond to the current first-line treatment [133]. Clinical results from these trials have shown synergistic effect of oxali-Pt cytotoxicity in combination with other chemotherapeutic agents, thus, making oxali-Pt an attractive compound to be considered for the treatment against ovarian cancer. In addition, oxali-Pt has shown favorable cytotoxic and antitumor activity against tumor models that

demonstrate intrinsic and/or acquired cis-Pt resistance, such as in leukemia, colon, ovarian cancer, breast, melanoma, bladder and glioma cancers [134].

2) Creation of different Pt isomers (*cis* vs. *trans*):

Pt compounds with *trans* geometry (that is, where X or L in $[\text{Pt}(\text{X})_2(\text{L})_2]$ is in a *trans* configuration) were initially proven to be inactive [135]. Pharmacokinetic studies have shown that transplatin (*trans*-Pt) is highly reactive, with 70% of the drug inactivated by conjugation with GSH after 4 hours incubation with red blood cells, whereas only 35% of *cis*-Pt-GSH conjugate was formed in the same time [136]. The rapid inactivation of *trans*-Pt by blood plasma components decreases the amount of *trans*-Pt available to react with DNA and induce programmed cell death. As a consequence, the anticancer activity of *trans*-Pt is low. Recently, a new class of modified *trans*-platinum (II) compounds, with chemical structure $\text{trans}-[\text{Pt}(\text{X})_2(\text{L})_2]$ where L = planar heterocyclic amine, have been reported to have novel activity profile against different cancer cell lines. In addition, a group of *trans*-planar heterocyclic amine Pt (II) compounds from the NCI were identified to be active against *cis*-Pt resistant cell lines, suggesting that these compounds may be able to overcome *cis*-Pt mechanisms of resistance [137]. One possible explanation could be in the difference of DNA adducts formed by these Pt compounds. While *cis*-Pt and oxali-Pt mainly generate DNA damage in the form of intrastrand crosslinks, *trans*-Pt compounds generate DNA interstrand cross-links between the N7-Guanine and N3-Cytosine bases. These two types of crosslinks are likely to activate intrinsic signaling pathway cascades, each leading to different biological outcomes [138]. However, further pharmacological and biological

characterization of these novel compounds should be conducted in order to identify their potential for clinical development.

3) Changes on the oxidation state of the Pt atom:

Modification of Pt (II) to Pt (IV) compounds is achieved by increasing the oxidation state of the Pt atom through the addition of two axial ligand groups, enabling the formation of the tetrahedral chemical structure: $[\text{Pt}(\text{AL})_2(\text{X})_2(\text{L})_2]$, where AL= axial ligand. Axial ligands have been shown to play an essential role in the stability and lipophilicity of Pt compounds [139]. In terms of stability, addition of axial ligands significantly decrease the rate of reduction of Pt compounds in the bloodstream, thus, promoting a decrease in the participation of the Pt compound in unwanted side reactions, which leads to lower toxicity. Likewise, there will be an increase in the intact levels of the activated Pt compound reaching its target site at the DNA; enabling a higher cytotoxic activity. In addition, studies have revealed that different axial ligands have different reduction potentials. For example, the reduction potential for the most utilized axial ligands decreases as follows: chloro > carboxylate > hydroxyl. Incorporation of axial ligands may also lead to higher lipophilicity of some Pt (IV) complexes, which may improve the ability of the compound to cross the cell membrane through passive diffusion, leading to an increase in cellular uptake [140]. Finally, the activity of the Pt (IV) compound relies on its reduction to Pt (II), since it is the Pt (II) complex which confers the cytotoxic mechanism of action [141]. The rational design of Pt (IV) compounds from already proven active Pt (II) compounds may improve the compound's stability, lipophilicity, enhancing its ability to circumvent cis-Pt resistance.

Indeed, the promising potential of Pt (IV) compounds can be appreciated by iproplatin, tetraplatin, and JM216, which are Pt (IV) compounds that have entered clinical trials [15;142].

1.8. Hypothesis and Specific Aims:

Cis-Pt is used as the first-line treatment in ovarian cancer patients. Even though patients exhibit initial therapeutic response to this drug, they eventually develop clinical resistance to therapy, leading to disease progression, a 5-year survival rate below 30% and patient death. Therefore, in order to improve Pt-based therapy it is pertinent to identify novel mechanisms of Pt resistance that could then be used as rational therapeutic targets. Dysfunction of tumor-suppressor p53 has been identified to play a fundamental role in the development of Pt-resistant phenotypes. Attenuation of p53 function is affected by failure of upstream pathways that induce p53 post-translational modifications, by mutation in the p53 protein or a combination of both. Recent data from TCGA in the form of survival curves for ovarian cancer patients show that status of p53 does not impact response to Pt treatment. That is, wild-type p53 does not present a survival advantage to the patients. Therefore, I **hypothesize** that cisplatin fails to activate p53 in Pt resistance, but which can be overcome by structurally-distinct platinum analogs.

The following **specific aims**, with the intended goals (**Figure 7**), were designed to test this hypothesis:

Aim 1: To characterize the cytotoxic and biochemical/molecular pharmacologic properties of structurally-distinct platinum analogs in cisplatin-resistant ovarian tumor models

Aim 2: To determine the failure in p53 post-translational modifications as a causative factor in cisplatin resistance

Aim 3: To define the novel mechanism of action of the structurally-distinct lead analog that circumvents cisplatin resistance

The findings gathered in this research project will help reveal possible approaches for circumventing cis-Pt resistance and, thus, may lead to improvements in the survival of ovarian cancer patients, and perhaps also in other types of cancers relying on Pt therapy.

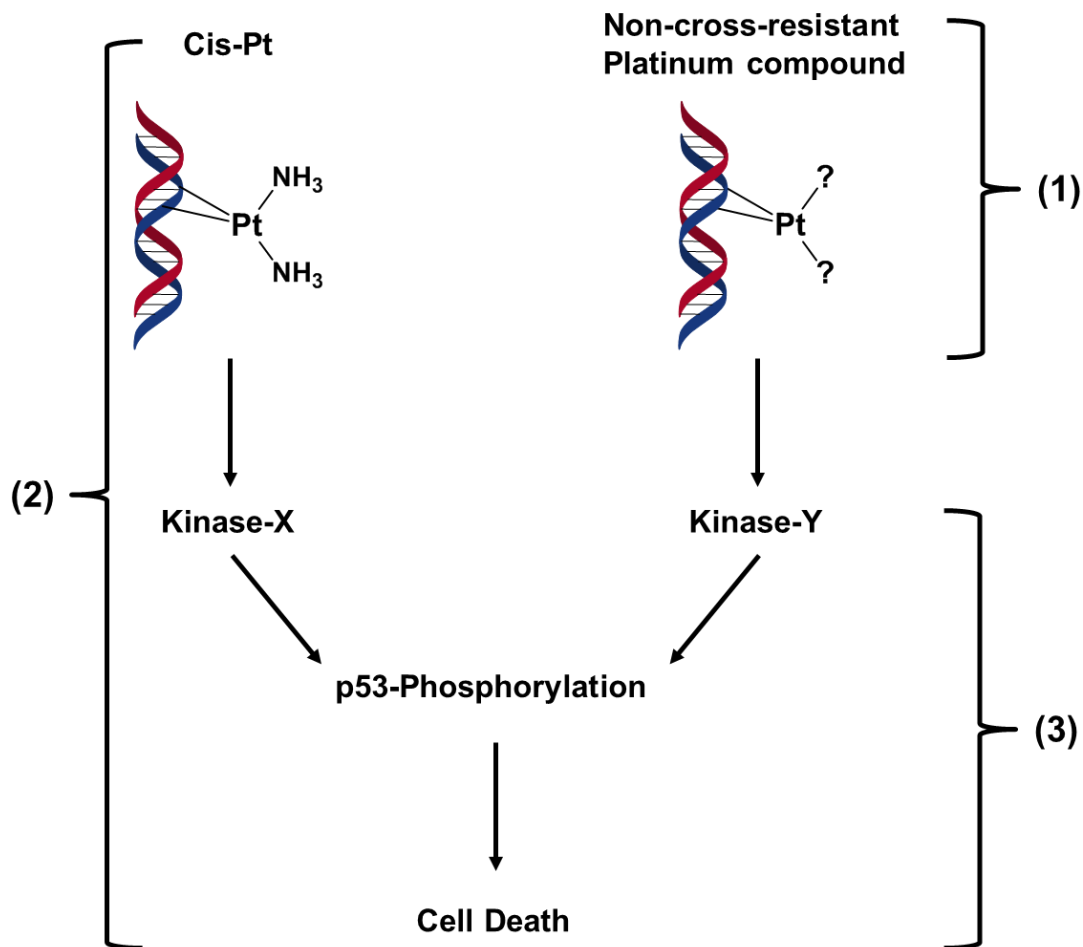


Figure 7. Research goals

(1) Aim 1: To characterize the cytotoxic and biochemical/molecular pharmacologic properties of structurally-distinct platinum analogs in cis-Pt-resistant ovarian tumor models **(2)** Aim 2: To determine the failure in p53 post-translational modifications as a causative factor in cis-Pt resistance **(3)** Aim 3: To define the novel mechanism of action of the structurally-distinct lead analog that circumvents cis-Pt resistance

Chapter 2

Materials and Methods

2.1. Synthesis of trans-[Pt(Py)₂Cl₂]:

The procedure employed for the synthesis of trans-[Pt(Py)₂Cl₂] (trans-PyPt) was adapted from [143]. In a 50 mL round bottle, a magnetic stir bar, 500 mg of K₂PtCl₄ (s) (GFS Chemicals, Columbus, OH, USA) and 5 mL of water were added. The mixture was stirred at room temperature using a hot plate until K₂PtCl₄ (s) completely dissolved in water and became K₂PtCl₄ (l). In a separate 10 mL beaker, 700 μL of pyridine (0.978 g/mL) (Sigma-Aldrich, St. Louis, MO, USA) were mixed with 5 mL of EtOH (Pharmco-AAPER, Brookfield, CT, USA). The pyridine/EtOH mixture was added to the K₂PtCl₄ (l) solution and the reaction was stirred at 85°C for 20 min. After 5 min, a ready precipitate corresponding to cis-[Pt(Py)₂Cl₂] (s) (cis-PyPt) was observed. At the end of the reaction, the solution turned clear, which indicated the formation of [Pt(Py)₄Cl₂] (l). The temperature of the reaction was then increased to 100°C. The volume of the reaction was reduced through evaporation to 1 mL, at which point a bright yellow precipitate corresponding to trans-PyPt (s) began to form. In order to ensure maximal trans-PyPt precipitation, small aliquots of 500 μL of acetone (Fisher Chemical, Fair Lawn, NJ, USA) were added. Trans-PyPt was filtrated using a Büchner funnel, washed with water, EtOH and acetone three times and left drying under vacuum overnight. The percent yield achieved for trans-PyPt was 88.4%. 10 mg of trans-PyPt was submitted for independent elemental analysis (Galbraith Laboratories, Inc., Knoxville, TN, USA). A separate 25 mg of trans-PyPt was dissolved in 0.6 mL of N-N-Dimethylformamide-D7 (DMF) (Cambridge Isotope Laboratories, Inc., Andover, MA, USA) and was characterized by NMR (Nuclear Magnetic Resonance Facility, The University of Texas MD Anderson Cancer Center, Houston, TX, USA).

2.2. FAAS parameters:

Pt content was measured by flameless atomic absorption spectrometry (FAAS) using the GTA 120 Graphite Tube Atomizer (Agilent Technologies, Mulgrave, Victoria, Australia). FAAS was set up with the following detection parameters: wavelength of 265.9 nm, slit width of 0.5 nm, lamp current of 10.0 mA, graphite furnace tubes, argon as the inert gas to prevent oxidation of furnace tubes, and the ramp temperatures and time durations listed in **Table 2**.

Table 2. FAAS parameters used to measure Pt metal

Step	Temperature (°C)	Time (s)	Ar Flow (L/min)	Pt Signal Read	Signal Storage
1	75	5.0	0.3	No	No
2	120	60.0	0.3	No	No
3	300	20.0	0.3	No	No
4	750	25.0	0.3	No	No
5	1200	25.0	0.3	No	No
6	1200	10.0	0.3	No	No
7	1200	2.0	0.0	No	Yes
8	2700	0.7	0.0	Yes	Yes
9	2700	3.0	0.0	Yes	Yes
10	2700	1.0	0.3	No	Yes

Calibration curve preparation: A calibration curve was generated using the following working standards: 100 µg/L, 200 µg/L, 400 µg/L, 800 µg/L, 1600 µg/L. Working standards were generated from the certified Pt standard stock solution containing 1,000 µg/mL Pt in 5% HCl (Sigma-Aldrich, St. Louis, MO, USA). Serial dilutions from the Pt stock solution were made using 0.1 N HCl as follows: 1,000 µg/mL Pt → 10 µg/mL Pt → 0.2 µg/mL Pt.

2.3. Preparation of stock platinum drug solutions:

Cis-Pt, oxali-Pt, 1R,2R-diaminocyclohexane (trans-diacetato)(dichloro)platinum(IV) (DAP) [144] and trans-PyPt (present study) were synthesized in our lab. Trans-Pt and cis-PyPt were purchased from Sigma-Aldrich (St. Louis, MO, USA). Solutions were made with the following solvents: 0.9% sodium chloride (Baxter, Deerfield, IL, USA) for cis-Pt, water for oxali-Pt and DAP and 100% DMF (OmniSolv, Gibbstown, NJ, USA) for trans-Pt, cis-PyPt and trans-PyPt. The general procedure for preparing the stock drug solutions was as follows: In a liquid scintillation vial, 10 mg of the Pt compound and 10 mL of the corresponding solvent were added. The mixture was sonicated in a water bath for 15 min in order to facilitate dissolution of the Pt compound. Undissolved particles were removed by filtration using a 25 mm syringe filter with membrane pore size of 0.2 μm (Fisher Scientific, Fair Lawn, NJ, USA). Pt concentration was measured using FAAS (**Section 2.2**).

2.4. Cell culture:

A2780 cell line was derived from patient before treatment and is considered to be sensitive towards cis-Pt [145]. 2780CP/CI-16 cell line was derived as a clone from A2780/C30 cells, which were made cis-Pt-resistant by intermittent exposure to cis-Pt [146]. A2780 and A2780/C30 cell lines were kindly provided by Dr. Thomas Hamilton (Fox Chase Cancer Center, Philadelphia, PA, USA). OVCAR-10, HEY and OVCA-433 were established from cis-Pt resistant patients [49] and were obtained from Dr. Robert Bast (The University of Texas MD Anderson Cancer Center, Houston, TX, USA).

A2780, 2780CP/CI-16, OVCAR-10 and HEY were maintained in RPMI 1640 (Sigma-Aldrich, St. Louis, MO, USA) supplemented with 10% fetal bovine serum (FBS) (Sigma-Aldrich, St. Louis, MO, USA) and antibiotics (100 µg/mL streptomycin and 100 units/mL penicillin). OVCA-433 was maintained in Minimum Essential Medium Eagle (MEM) with Earle's salts and L-glutamine (Corning Cellgro, Manassas, VA, USA) containing 10% FBS, 1 mM sodium pyruvate (HyClone Laboratories, Inc., South Logan, UT), 1 mM nonessential amino acids (Corning Cellgro, Manassas, VA, USA) and antibiotics (100 µg/mL streptomycin and 100 units/mL penicillin). All cell lines were grown in an atmosphere of 37°C and 5% CO₂.

2.5. Cytotoxic evaluations:

The procedure employed for cytotoxic evaluations was adapted from [49]. Ovarian cancer cells growing in tissue culture dishes were trypsinized, diluted to appropriate concentrations and plated in 96-well plates in aliquots of 100 µL/well to achieve the following densities: A2780, 200 cells/well; 2780CP/CI-16 and OVCAR-10, 500 cells/well; HEY, 150 cells/well; and OVCA-433, 300 cells/well. Plates were incubated overnight at 37°C. Aliquots of 100 µL/well from serial dilutions of Pt drugs in medium (**Table 3**) were added to cells. Plates were further incubated at 37°C for 5 days. The final DMF concentration in wells containing trans-Pt, cis-PyPt and trans-PyPt, was 0.125% (v/v). After drug exposure for 5 days, 50 µL of an MTT solution (3 mg/mL) (Acros Organics, Morris Plains, NJ, USA) was added to each well and plates were incubated for 4 hr. The medium was removed and purple MTT formazan crystals were dissolved in 100 µL of 100% DMSO (Fisher Scientific, Fair Lawn, NJ, USA). Plates were

shaken for 5-10 min and absorbance values were measured at 570 nm with a multiwell scanning spectrophotometer (Molecular Devices, Sunnyvale, CA, USA). IC₅₀ values were determined from the sigmoidal plot of % cell survival vs. log of drug concentration using the Prism software (GraphPad v.6, La Jolla, CA, USA).

Table 3. Range of concentrations (μM) of Pt drugs and geometric factor used to assess cytotoxicity in the ovarian panel by MTT assay

A2780	cis-Pt	trans-Pt	cis-PyPt	trans-PyPt	oxali-Pt	DAP
Geometric factor	2	3	3	3	2.5	2
Treatment (μM)	0.031-8.0	0.026-57.5	0.009-20.0	0.008-17.0	0.0005-0.80	0.006-1.60
2780CP/CI-16	cis-Pt	trans-Pt	cis-PyPt	trans-PyPt	oxali-Pt	DAP
Geometric factor	2	3	3	3	2	2
Treatment (μM)	0.5-128	0.026-57.5	0.009-20.0	0.008-17.0	0.031-8.0	0.031-8.0
OVCAR-10	cis-Pt	trans-Pt	cis-PyPt	trans-PyPt	oxali-Pt	DAP
Geometric factor	2	3	3	3	2	2
Treatment (μM)	1.0-256	0.026-57.5	0.009-20.0	0.008-17.0	0.013-3.2	0.013-3.2
HEY	cis-Pt	trans-Pt	cis-PyPt	trans-PyPt	oxali-Pt	DAP
Geometric factor	2	3	3	3	2	2
Treatment (μM)	0.25-64.0	0.026-57.5	0.009-20.0	0.008-17.0	0.05-12.8	0.05-12.8
OVCA-433	cis-Pt	trans-Pt	cis-PyPt	trans-PyPt	oxali-Pt	DAP
Geometric factor	2	3	3	3	2.5	2.5
Treatment (μM)	0.60-160	0.026-57.5	0.009-20.0	0.008-17.0	0.026-39.2	0.025-38.5

2.6. Cellular Pt drug uptake:

Cellular Pt drug uptake measurement were made using the procedure from [147]. 2 x 10⁶ A2780 or 2 x 10⁶ 2780CP/CI-16 cells were plated and incubated in 10-cm dishes at 37°C overnight. A final concentration of 200 μM of the Pt drug was added to the cells,

and dishes were further incubated at 37°C for 2 hr. Cells were then washed with ice cold phosphate buffered saline (PBS) three times, scraped with a rubber policeman and pelleted by centrifugation at 2,000 rpm at 4°C for 3 min in 15 mL Falcon tubes. The pellet was washed twice with 10 mL of ice cold PBS, resuspended in a final PBS volume of 300 μ L and transferred to a 1.5 mL microfuge tube. For protein measurements, cell lysate was generated by taking 1/3 of the final PBS suspension (100 μ L) and adding 25 μ L of ice-cold extraction buffer (composed of 50 mM Tris HCl; pH 7.4) (Fisher Scientific, Fair Lawn, NJ, USA), 10 mM NaF (Sigma-Aldrich, St. Louis, MO, USA), 2 mM EDTA (Sigma-Aldrich, St. Louis, MO, USA), 150 mM NaCl (Fisher Scientific, Fair Lawn, NJ, USA)) with 0.5% NP-40 (Sigma-Aldrich, St. Louis, MO, USA), and 2 mM phosphatase inhibitors (Thermo Fisher Scientific, Rockford, IL). Cell lysates were centrifuged at 15,000 rpm at 4°C for 10 min and protein concentration was quantified by bicinchoninic acid (BCA) assay (Bio-Rad, Hercules, CA, USA). The remaining pellet, corresponding to 2/3 of the final PBS volume (200 μ L), was digested with 25 μ L of benzethonium hydroxide (Sigma-Aldrich, St. Louis, MO, USA) in a water bath at 55°C overnight. Finally, to the samples were added 100 μ L of 0.3 N HCl (Sigma-Aldrich, St. Louis, MO, USA). Samples were vortexed for 15 s and the Pt content determined by FAAS using the parameters described in **Section 2.2**. The Pt concentrations were normalized to protein levels, and drug uptake was expressed as ng Pt/mg protein/hr.

2.7. DNA extraction and purification:

A pellet corresponding to 1×10^6 cells was washed with ice cold PBS. DNA from these pellets was extracted using the QIAamp® DNA Mini Kit (QIAGEN, Valencia, CA, USA) following the manufacturer's protocol. Extracted DNA was quantified using the NanoDrop (Thermo Fisher Scientific, Wilmington, DE, USA).

2.8. DNA Pt adducts:

Measurements of DNA Pt adducts were made using the procedure previously reported [147]. 2×10^6 A2780 or 2×10^6 2780CP/CI-16 cells were plated and incubated in 10-cm dishes at 37°C overnight. A final concentration of 200 μ M of the Pt drug was added to the cells and dishes were further incubated at 37°C for 2 hr. Cells were washed with ice cold PBS three times, scrapped and pellet was obtained by centrifugation at 2,000 rpm at 4°C for 3 min in 15 mL Falcon tubes. The pellet was washed twice with 10 mL of ice cold PBS. DNA extraction, purification and quantification were performed as described in **Section 2.7** and the Pt content determined by FAAS using the parameters described in **Section 2.2**. The Pt concentrations were normalized to DNA concentration, and Pt adducts were expressed as ng Pt/mg DNA/hr.

2.9. Partition coefficient:

The reported procedure [148] was followed to assess partition coefficient. Pt drug was diluted in 500 μ L of water to a final concentration of 50 μ M in 1.5 mL microfuge

tube. 500 μL of n-octanol (0.824 g/mL) (Acros Organics, Morris Plains, NJ, USA) were added to the drug solution and tubes were shaken mechanically for 15 min. Samples were then centrifuged at 15,000 rpm for 5 min. After centrifugation, two phases were obtained. The top phase corresponded to the organic phase (n-octanol) and the phase in the bottom to the aqueous phase (water). The phases were separated by transferring the organic phase into a new 1.5 mL microfuge tube. Pt content in each phase was analyzed by FAAS using the parameters described in **Section 2.2**. Partition coefficients were expressed as $\log(\text{Partition Ratio})$, where $\text{Partition Ratio} = \frac{P_{t_{n\text{-octanol}}}}{P_{t_{\text{water}}}}$.

2.10. DNA interstrand crosslinks:

The procedure for measurements of DNA interstrand crosslinks (ICLs) has been previously validated [149]. Briefly, to 13 x 100 mm borosilicate tubes containing 200 μL of Calf thymus DNA (70 $\mu\text{g/mL}$) (Sigma-Aldrich, St. Louis, MO, USA) a final concentration of 25 μM of Pt drug was added. For control calf thymus DNA was used with no Pt treatment. The reaction was allowed to take place at 37°C for 30 min. Samples were divided in aliquots of equal volumes into two 13 x 100 mm borosilicate tubes. 400 μL of EB Buffer (20 mM potassium phosphate (Sigma-Aldrich, St. Louis, MO, USA), 2 mM EDTA (Sigma-Aldrich, St. Louis, MO, USA), pH 11.8) were added to all samples. One of the sample pairs was heated in a heating block at 100°C for 10 min to denature the DNA and the other pair was left at room temperature. Both sample pairs were then placed in a water bath at 13°C for 3 min, followed by the addition of 1 mL of EB buffer. The water bath temperature was increased to 15°C and samples were further

incubated for 3 min. Finally, 1.5 mL of EtBr from a working stock of 2 µg/mL in EB Buffer was added to both samples. Fluorescence was measured at $\lambda_{\text{excitation}}=305$ nm and $\lambda_{\text{emission}}=590$ nm using a fluorimeter (Perkin Elmer Norwalk, CT, USA). ICLs index was calculated using the following formula: $ICLs\ index = (-\ln x_{\text{treated}}) - (-\ln x_{\text{control}})$;

where $x = \frac{(\text{fluorescence}_{\text{non-heated}}) - (\text{fluorescence}_{\text{heated}})}{(\text{fluorescence}_{\text{non-heated}})}$.

2.11. Platination of FBS proteins:

Reactivity of the Pt drug to FBS proteins was assessed as described previously [147]. A final concentration of 25 µM of Pt drug was added to 3 mL of 100% FBS in a 15 mL Falcon tubes. The reaction was incubated at 37°C for 0, 5 min, 15 min, 30 min, 1 hr, 2 hr, 4 hr and 6 hr. At each time point, a reaction tube (FBS + Pt drug) was taken and an aliquot of 200 µL was added to 800 µL of ice cold methanol (Fisher Chemical, Fair Lawn, NJ, USA) in a 1.5 mL microfuge tube. Samples were vortexed and left on ice for 5 min in order to ensure maximal FBS precipitation. Precipitated FBS was removed by centrifugation at 15,000 rpm at 4°C for 5 min. The content of free (unreacted) Pt in the supernatant was analyzed by FAAS using the parameters described in **Section 2.2**. Pt drug half-lives were determined from the first order reaction equation, $\ln[A] = \ln[A]_0 - kt$, where $t_{1/2} = \frac{0.693}{k}$, using the GraphPad Prism software.

2.12. TP53 sequencing:

DNA samples extracted from ovarian cancer cell lines following the procedure described in **Section 2.7** were sent for *TP53* sequencing to the Sequencing and Microarray Core Facility at The University of Texas MD Anderson Cancer Center, Houston, TX.

2.13. Generation of stable knock-out clones:

CRISPR/Cas-GFP vectors were purchased from Sigma-Aldrich, St. Louis, MO, USA and the gRNA designs were obtained from Sigma webpage: <http://crispr.sigmainformatics.com/CrisprSearch>. The selected designs to generate control (ctrl), *TP53* ($p53^{-/-}$) and *CHEK2* ($Chk2^{-/-}$) knock-out are as follow: *TP53* (HS0000019748, NM_001126117), *CHEK2* (HS0000041294, NM_001005735) and universal negative control (CRISPR08). $p53^{-/-}$ was generated in A2780, 2780CP/CI-16, OVCAR-10 and HEY cell lines. $Chk2^{-/-}$ was carried out in A2780 cells.

A2780, 2780CP/CI-16, OVCAR-10 and HEY cell lines at 70% confluence were transfected with 25 μ g of CRISPR/Cas9-GFP plasmid using Lipofectamine 2000 (Life Technologies, Carlsbad, CA, USA) following the manufacturer's recommended protocol. After 48 hr of transfection, GFP positive cells were sorted using the BD FACSAria™ cell sorter (BD Biosciences, Franklin Lakes, NJ, USA). GFP positive cells were collected and grown in T75 flask. At 80% confluence, cells were trypsinized and dilutions of aliquots of 100, 200, 300, 400 and 500 cells were grown in 10-cm dishes. Single clones

from the 10-cm dishes were selected, grown in 12-well plates and characterized through Western blot analysis (**Section 2.15**). Clones expressing the knock-out phenotype were selected for further experiments including cytotoxic evaluations (**Section 2.5**). The concentration range and the geometric constant used for concentration increments used in cytotoxic evaluations are listed in **Table 4**.

Table 4. Range of concentrations of Pt drugs (μM) and geometric factor used in concentration increases to assess cytotoxicity in $p53^{-/-}$ and $\text{Chk2}^{-/-}$ clones

Clones: A2780-ctrl; A2780- $p53^{-/-}$; A2780- $\text{Chk2}^{-/-}$		
	cis-Pt	oxali-Pt
Geometric factor	2	2
Treatment (μM)	0.078-20.0	0.039-10.0
Clones: 2780CP/CI-16-ctrl; 2780CP/CI-16- $p53^{-/-}$ OVCAR-10-ctrl; OVCAR-10- $p53^{-/-}$		
	cis-Pt	oxali-Pt
Geometric factor	2	2
Treatment (μM)	0.586-150	0.078-20.0
Clones: HEY-ctrl; HEY- $p53^{-/-}$		
	cis-Pt	oxali-Pt
Geometric factor	2	2
Treatment (μM)	0.313-20.0	0.039-2.5

2.14. Knock-in transfections:

p53 Plasmids: 6×10^5 A2780- $p53^{-/-}$ cells were seeded into 6-well plates and were incubated overnight at 37°C. Cells were transfected with pcDNA3 control (1 μg), p53 wild-type (0.5 μg) or p53 mutant (1 μg p53-S20A or 0.5 μg p53-S20D) expression vectors. The reagent Lipofectamine 2000 was used for the transfection process following the manufacturer's recommended protocol. After 48 hr of transfection, cells

were collected and processed for Western blot analysis (**Section 2.15**). p53 plasmids were kindly provided by Dr. Mickey C.-T. Hu (Stanford University School of Medicine, Stanford, CA, USA) [150].

Chk2 Plasmid: 5×10^5 A2780-Chk2^{-/-} cells were seeded into 6-well plates and incubated overnight at 37°C. A2780-Chk2^{-/-} cells were transfected with 2 µg of pEGFP-C1 control or Chk2 expression vectors using Lipofectamine 2000 following the manufacturer's recommended protocol. After 48 hr of transfection, cells were untreated or treated with Pt drugs (cis-Pt: 1µM; oxali-Pt 0.6 µM) for 24 hr, collected and processed for Western blot analysis (**Section 2.15**). For IC₅₀ determinations, transfected cells were trypsinized after 24 hr of transfection, diluted to appropriate concentrations and aliquots of 100 µL/well containing 1200 cells were plated to 96-well plates. The previously described cytotoxic evaluations procedure in **Section 2.5** was followed. Cells were exposed to the range of final Pt drug concentrations, shown in **Table 5** for 3 days. Chk2 plasmid was a gift from Dr. Junjie Chen and Dr. Kathy McGowan (The University of Texas MD Anderson Cancer Center, Houston, TX, USA).

Table 5. Concentration range (µM) for Pt drugs and geometric factor used in concentration increases for cytotoxic evaluations after Chk2-ki in A2780-Chk2^{-/-}

Clones: A2780-Chk2 ^{-/-} -pEGFP-C1; A2780-Chk2 ^{-/-} -pEGFP-C1 Chk2		
	cis-Pt	oxali-Pt
Geometric factor	2	2
Treatment (µM)	0.078-20.0	0.039-10.0

2.15. Western blot analysis:

Ovarian cancer cells exposed to vehicle or Pt drugs were scraped and pelleted by centrifugation at 3,000 rpm and 4°C for 1 min. Cell pellets were resuspended in 50-100 µL ice-cold extraction buffer (**Section 2.6**) containing 0.5% NP-40 and 2 mM phosphatase inhibitors, and sonicated. Cell lysates were centrifuged at 15,000 rpm at 4°C for 10 min. Supernatants were isolated, quantified by BCA assay and processed for immunoblotting. 50 µg of protein extracts were run in a 4-15% gradient SDS-PAGE ready gel (Bio-Rad, Hercules, CA, USA), electrophoretically transferred for 1 hr at 300 mA to a nitrocellulose membrane, blocked with 5% milk for 1 hr, probed with primary antibody overnight and secondary antibody for 1 hr (**Section 2.29**). Finally, blots were developed using the chemiluminescence detection kit Clarity™ Western ECL Substrate (Bio-Rad, Hercules, CA, USA). For densitometric analysis of the band, the X-ray films were scanned and the signals were analyzed using ImageJ software.

2.16. Chk2 expression in cisplatin-resistant ovarian tumor cell lines:

7×10^5 A2780 cells, 8×10^5 2780CP/CI-16 cells, 8×10^5 OVCAR-10 cells, 6×10^5 HEY cells and 7×10^5 OVCA-433 cells were seeded into 6-well plates and were incubated overnight at 37°C. After 24 hr of incubation, Western blot analysis, as described in **Section 2.15**, was performed.

2.17. Chk2 knock-down:

5 x 10⁵ A2780 cells were seeded into 6-well plates and were incubated overnight at 37°C. A2780 cells were transfected with 100 nM of control siRNA (siCtrl) or Chk2 siRNA (siChk2) using RNAimax (Life Technologies, Carlsbad, CA, USA) following the manufacturer's recommended protocol. After 48 hr of transfection, cells were treated with Pt drugs (1 µM cis-Pt; 0.6 µM oxali-Pt) for 24 hr, then collected and processed for Western blot analysis (**Section 2.15**).

Primers used for siRNA were as follows: *siCtrl*: Forward-

CUUACGCUGAGUACUUCGAdTdT; Reverse-UCGAAGUACUCAGCGUAAGdTdT

(Sigma Life Science, The Woodlands, TX)

siChk2: Forward-GAACAGAUAAAUACCGAACTt; Reverse-

GUUCGGUAUUUAUCUGUUCt (Sigma Life Science, The Woodlands, TX).

2.18. Proteasomal regulation of Chk2:

7 x 10⁵ A2780 cells, 8 x 10⁵ 2780CP/CI-16 cells, 8 x 10⁵ OVCAR-10 cells, 6 x 10⁵ HEY cells and 7 x 10⁵ OVCA-433 cells were seeded into 6-well plates and were incubated overnight at 37°C. Cells were treated with DMSO or 1 µM of MG132 (Sigma-Aldrich, St. Louis, MO, USA) for 6 hr at 37°C, collected and processed for Western blot analysis (**Section 2.15**).

2.19. Chk2 half-life determination:

7 x 10⁵ A2780 cells were seeded into 6-well plates and were incubated overnight at 37°C. Cells were treated with DMSO or 4 µM of Cycloheximide (Sigma-Aldrich, St. Louis, MO, USA) at 37°C for 0.5 hr, 2 hr, 4 hr and 8 hr. At each time point, cells were collected and processed for Western blot analysis (**Section 2.15**). Chk2 and p53 bands at each time-point were quantified by densitometry and half-lives were determined by generating a plot of Normalized densitometric readings (%) vs Time (hr) using Prism software.

2.20. Quantification of *CHEK2* transcripts:

7 x 10⁵ A2780 cells, 8 x 10⁵ 2780CP/CI-16 cells, 8 x 10⁵ OVCAR-10 cells, 6 x 10⁵ HEY cells and 7 x 10⁵ OVCA-433 cells were seeded into 6-well plates and were incubated overnight at 37°C. RNA was isolated from ovarian cancer cells using the AurumTM Total RNA Mini kit (Bio-Rad, Hercules, CA, USA) following the manufacturer's protocol. Extracted RNA was quantified using NanoDrop and normalized to the same concentration. Expression levels of *CHEK2* and the internal control *GAPDH* were evaluated using the quantitative real-time PCR (RT-PCR) method. RT-PCR was performed using 1 µg of RNA, the iTaqTM Universal SYBR Green One-Step Kit (Bio-Rad, Hercules, CA, USA) and CFX384TM Real-Time System (Bio-Rad, Hercules, CA, USA) following the manufacturer's protocol. Primers for *CHEK2* and *GAPDH* were purchased from Bio-Rad and have been previously validated against the desired target by the manufacturer. Relative expression levels were calculated using the 2^{-ΔCt} method.

2.21. *CHEK2* gene methylation:

DNA was extracted from A2780, 2780CP/CI-16, OVCAR-10, HEY and OVCA-433 cells following the procedure described in **Section 2.7**. DNA samples were sent to the DNA Methylation Analysis Core at The University of Texas MD Anderson Cancer Center, Houston, TX, USA, where the Bisulfite Pyrosequencing and Methylation-Specific PCR (MSP) procedures were employed in order to assess *CHEK2* methylation levels [151-153]. Primers used for *CHEK2* methylation studies were purchased from Sigma Life Science, The Woodlands, TX and their sequences are as follows:

1) **Bisulfite Pyrosequencing**: Near exon 1: *CHEK2-P1*: Forward 1-
GAGGGGAATTAGGGTTTTAAGTTT, Reverse 1-
CTCCCCAACCTCAACCAACAAAATAAC; *CHEK2-P1*: Forward 2-
GTTATATGGGGAATTTTTGTTGGGTGTTT, Reverse 2-
CCCCCTTCAACTCAAACTACA; Near exon 2: *CHEK2-P2*: Reverse 3-
AAACCAAAAATATACTAATACAATCAACAC, Forward 3-
TTTTTAAAGTGAGGGATTATAGGAGTGAA

2) **MSP**: Near exon 1: P1 (Methylation): Forward-TTACGTTTGTTTTTTAGATTTTCGT,
P1 (Methylation): Reverse-AAATTCTTCTACCCACAATACCG, P2 (Unmethylation):
Forward-TTATGTTTGTTTTTTAGATTTTGT, P2 (Unmethylation): Reverse-
CAAATTCTTCTACCCACAATACCA; Near exon 2: P3 (Methylation): Forward-
TTTTTCGGGTTTAAGCGATTTTTTTGTTT, P3 (Methylation): Reverse-

ACGCGAAAATTCACCTCCTATAATCCCGCA, P4 (Unmethylation): Forward-
TTTTTTGGGTTTAAGTGATTTTTTTGTTT, P4 (Unmethylation): Reverse-
ACACAAAAATTCACCTCCTATAATCCCACA.

2.22. miRNA TaqMan assays:

An *in silico* assay to predict microRNAs interacting with *CHEK2* mRNA levels was performed using the miRBase: the microRNA database (<http://www.mirbase.org/>). Total RNA samples were prepared from A2780, 2780CP/CI-16, OVCAR-10, HEY and OVCA-433 tumor cells using TRIzol LS Reagent (Invitrogen, Carlsbad, CA, USA). RNA extraction was performed according to manufacturer's instructions. RNA quantity was assessed with NanoDrop and RNA integrity was analyzed by gel electrophoresis. MicroRNA expression was tested using TaqMan microRNA assays (Applied Biosystems, Foster City, CA, USA) following the manufacturer's protocol. The cDNA was synthesized using TaqMan Reverse Transcription Reagents kit (Applied Biosystems, Foster City, CA, USA) and employed for quantitative RT-PCR analysis together with TaqMan probes (hsa-miR-134, -300, -340, -381, -425) (Applied Biosystems, Foster City, CA, USA), internal control U6 snRNA (Applied Biosystems, Foster City, CA, USA) and SsoFast Supermix (Bio-Rad, Hercules, CA, USA) following the manufacture's protocol. Relative expression levels were calculated using the $2^{-\Delta Ct}$ method.

2.23. MicroRNA expression

6×10^5 A2780 cells were seeded into 6-well plates and were incubated overnight at 37°C. Cells were transfected with 100 nM of pre-miR-Ctrl, pre-miR-340 or pre-miR-425 (Applied Biosystems, Foster City, CA, USA) using Lipofectamine 2000 following the manufacturer's recommended protocol. After 48 hr and 72 hr of transfection, cells were collected, lysed and microRNA TaqMan assay (**Section 2.22**) and Western blot analysis (**Section 2.15**) were performed.

2.24. RPPA analysis:

1×10^6 A2780 or 2780CP/CI-16 cells were plated and incubated in 10-cm dishes at 37°C overnight. A2780 cells were untreated or treated with 1 μ M cis-Pt or 0.6 μ M oxali-Pt and, similarly, 2780CP/CI-16 cells were untreated or treated with 5 μ M cis-Pt or 3 μ M oxali-Pt for 24 hr. Cells were washed with ice cold PBS three times, scraped and pelleted by centrifugation at 2,000 rpm at 4°C for 3 min in 15 mL Falcon tubes. The resultant pellet was sent for reverse phase protein lysate (RPPA) analysis to the RPPA Core Facility-Functional Proteomics at The University of Texas MD Anderson Cancer Center, Houston, TX, USA. The core provided normalized values for 217 antibodies. A description of the procedure for the core facility can be found at <https://www.mdanderson.org/education-and-research/resources-for-professionals/scientific-resources/core-facilities-and-services/functional-proteomics-rppa-core/rppa-process/index.html>

A $\log_2(x+1)$ transformation to the normalized data was applied and further analyses using the functions of LIMMA library was performed. A linear model was fitted

to each protein and empirical Bayes methods were used to obtain the statistics. Protein differentially expressed ($p < 0.005$) between different types of samples were thus identified. The protein of interest for this thesis were the ones exhibiting significant upregulation by A2780 treated with cis-Pt or oxali-Pt and 2780CP/CI-16 treated with oxali-Pt only. Statistical analysis and set intersections were performed in R (version 3.2.2).

2.25. Platinum treatment for Western analysis:

6×10^5 A2780 cells, 7×10^5 2780CP/CI-16 cells, 7×10^5 OVCAR-10 cells, 5×10^5 HEY and 6×10^5 OVCA-433 cells were seeded into 6-well plates and were incubated overnight at 37°C. Cells were exposed to Pt drugs for 24 hr, collected and processed for Western blot analysis (**Section 2.15**).

2.26. MEK/ERK inhibitor exposure:

7×10^5 2780CP/CI-16 cells were seeded into 6-well plates and were incubated overnight at 37°C. Cells were treated for 1 hr with DMSO, 1.5 μM of ERK1/2 inhibitor SCH772984 (Selleckchem, Houston, TX, USA), 100 μM of MEK1/2 inhibitor PD98059 (Cell Signaling, Danvers, MA, USA) or 10 μM of the MEK1/2 inhibitor U0126-EtOH (Selleckchem, Houston, TX, USA). After 1 hr, 2780CP/CI-16 cells were treated with 5 μM cis-Pt or 3 μM oxali-Pt for 24 hr. Cells were collected and processed for Western blot analysis (**Section 2.15**).

2.27. Effect of MEK inhibitor U0126 on platinum cytotoxicity:

A2780CP/CI-16 were trypsinized, diluted to appropriate concentrations and 1200 cells/well were plated to 96-well plates in aliquots of 100 μ L/well. Plates were incubated overnight at 37°C. Similar to the procedure reported [154], cells were treated for 1 hr with aliquots of 50 μ L/well of 10 μ M of U0126-EtOH inhibitor, followed by addition of aliquots of 50 μ L/well of cis-Pt 5 μ M or oxali-Pt 3 μ M for 3 days. At this time, aliquots of 50 μ L/well of an MTT solution (3 mg/ml) were added to the plates and cells were further incubated at 37°C for 4 hr. The medium was removed and 100 μ L of 100% DMSO was added in order to dissolve MTT formazan crystals. Plates were shaken for 5-10 min, absorbance values were measured at 570 nm with a multiwell scanning spectrophotometer and % cell survival determined.

2.28. Ability of MEK1/2 to phosphorylate p53 at Ser20:

The procedure was similar to that reported [155;156]. 25 μ M of ATP (Sigma-Aldrich, St. Louis, MO, USA), 12.5 ng/ μ L of recombinant p53 (Santa Cruz Biotechnology, Dallas, TX, USA) and 20 ng/ μ L of recombinant MEK-1 or MEK-2 (SignalChem, Richmond, BC, Canada) were added in a 1.5 mL microfuge tube. Chk2 plasmid (**Section 2.14**) was immunoprecipitated from A2780 cells treated with cis-Pt 1 μ M and used as a control. Immunoprecipitated Chk2 was mixed with 25 μ M of ATP and 12.5 ng/ μ L of recombinant p53. Reaction Buffer (150 mM NaCl, 4 mM MnCl₂ (Sigma-Aldrich, St. Louis, MO, USA), 6 mM MgCl₂ (Sigma-Aldrich, St. Louis, MO, USA), 10% (v/v) glycerol (Sigma-Aldrich, St. Louis, MO, USA), 1 mM dithiothreitol (Sigma-Aldrich,

St. Louis, MO, USA), 100 μ M Na₃VO₄ (Sigma-Aldrich, St. Louis, MO, USA), 50 mM HEPES (pH 7.5) (Sigma-Aldrich, St. Louis, MO, USA)) was then added to complete a final volume reaction of 25 μ L. The reaction was incubated at 30°C for 20 min. At the end of the reaction, samples were processed for Western blot analysis (**Section 2.15**).

2.29. Antibodies:

Antibodies specific to p53 (1:2000) (sc-126 and sc-6243), p21 (1:500) (sc-6246), β -actin (1:4000) (sc-47778), Ser20-p53 (1:500) (sc-18079-R), Chk2 (1:500) (sc-9064), Ser217/221-MEK (1:1000) (sc-81503), Mdm2 (1:1000) (sc-13161) and Mdm4 (1:500) (sc-374147) were purchased from Santa Cruz Biotechnology, Dallas, TX, USA. Antibodies against Ser15-p53 (1:1000) (9284), Thr68-Chk2 (1:1000) (2197), ERK1/2 (1:1000) (4695), T202/Y204-ERK (1:1000) (4376), MEK1/2 (9122), MEK1 (2352), MEK2 (9125) and Ser217/221-MEK (9154) were purchased from Cell Signaling, Danvers, MA, USA. Secondary ECL Anti-Mouse IgG, Horseradish (1:4000) (from sheep) (NA931) and ECL Anti-Rabbit IgG, Horseradish (1:4000) (from sheep) (NA934) were purchased from GE Healthcare, Houston, TX, USA.

2.30. Ovarian cancer patient survival analysis:

We downloaded RPPA Level3 data publicly available from the Cancer Genome Atlas Project (TCGA; <http://tcga-data.nci.nih.gov/>) for Chk2 and MEK1/2 in patients with ovarian serous cystadenocarcinoma (OV). Patient overall survival information, Pt status and *TP53* mutation status were retrieved for OV patients from cBioPortal

(<http://www.cbioportal.org/>). The analyses were carried out in R (version 3.2.2). All the tests were two-sided and considered statistically significant at the 0.05 level. The Log-rank test was employed to determine the association between *TP53* mutation status (wild-type vs. mutant) and overall survival and the Kaplan-Meier method was used to generate survival curves. For Chk2 and MEK1/2, the tumor samples were dichotomized into high and low RPPA level groups at percentile cutoffs between 0.25 and 0.75 with a step of 0.01. We tested whether a log-rank test applied at any cut-point would yield a nominal P value <0.05. The optimal cutoff percentile (as determined by the lowest P value) was thus identified for Chk2 and MEK1/2. Proteins levels were stratified by low and high groups according to Pt status. The Kaplan-Meier plots were generated for high and low Chk2 and MEK1/2 groups stratified according to Pt status. The numbers of patients at risk in each group at different time points are presented at the bottom of the graphs.

2.31. Statistical Analysis:

Experiments were repeated three independent times and mean values with standard error of mean were calculated and presented. A two tailed unpaired Student's t test or ANOVA test was used to compare two groups or multiple groups, respectively, in an experiment. A p value <0.05 was considered statistically significant.

Chapter 3

To characterize the cytotoxic and biochemical/molecular pharmacologic properties of structurally-distinct platinum analogs in cisplatin-resistant ovarian tumor models

3.1. Rationale and Background:

Despite efforts to develop better therapeutic options for the treatment of ovarian cancer, cis-Pt still remains one of the most effective chemotherapeutic agents available against this disease. Indeed, for almost four decades cis-Pt has been the first-line treatment for ovarian cancer patients. However, one of the major challenges that ovarian cancer patients face is intrinsic or acquired resistance of tumor cells towards cis-Pt. Therefore, the search for novel Pt drugs able to circumvent cis-Pt resistance continues. In this regard, studies performed by Tito Fojo and colleagues led to the classification of 107 Pt compounds into 12 groups based on their chemical structures and distinctive activity profiles against 60 diverse NCI human cancer cell lines. Interestingly, further structure-activity studies of 38 Pt compounds from 4 groups against cis-Pt resistant cells led to the identification of novel Pt compounds able to retain cytotoxic activity in these cells [137]. However, the biochemical and molecular pharmacologic properties of such Pt compounds are poorly understood. Such information is important in defining the mode of action of novel compounds and/or the specific mechanism targeted in tumor cells to circumvent cis-Pt resistance. Therefore, the aim of this study is to select structurally-distinct Pt analogs that exhibit a potential to circumvent cis-Pt resistance in ovarian cancer cell lines and characterize their cytotoxic and pharmacological properties. The analogs selected were trans-PyPt and oxali-Pt, together with cis-Pt. These compounds are clustered in three different groups based on their ligand “L” in the chemical structure: A) Amine (cis-Pt), B) Pyridine (trans-PyPt) and C) DACH (oxali-Pt) ligand groups (**Figure 8**). The cis-PyPt and trans-Pt analogs were included to test the specificity of the trans-PyPt compound and the generality of trans-

structures to circumvent cis-Pt resistance. DAP was also included as a DACH-Pt(IV) analog to assess the effect of the tetravalent Pt(IV) state by comparison to the analogous divalent Pt(II) structure in oxali-Pt. These Pt drugs were evaluated in an ovarian tumor panel consisting of a sensitive model (A2780) and four cis-Pt-resistant models (2780CP/CI-16, OVCAR-10, HEY and OVCA-433). The intent of this study is to identify a lead Pt analog, which exhibits the desirable pharmacologic characteristics and circumvents cis-Pt resistance, for mechanistic evaluation.

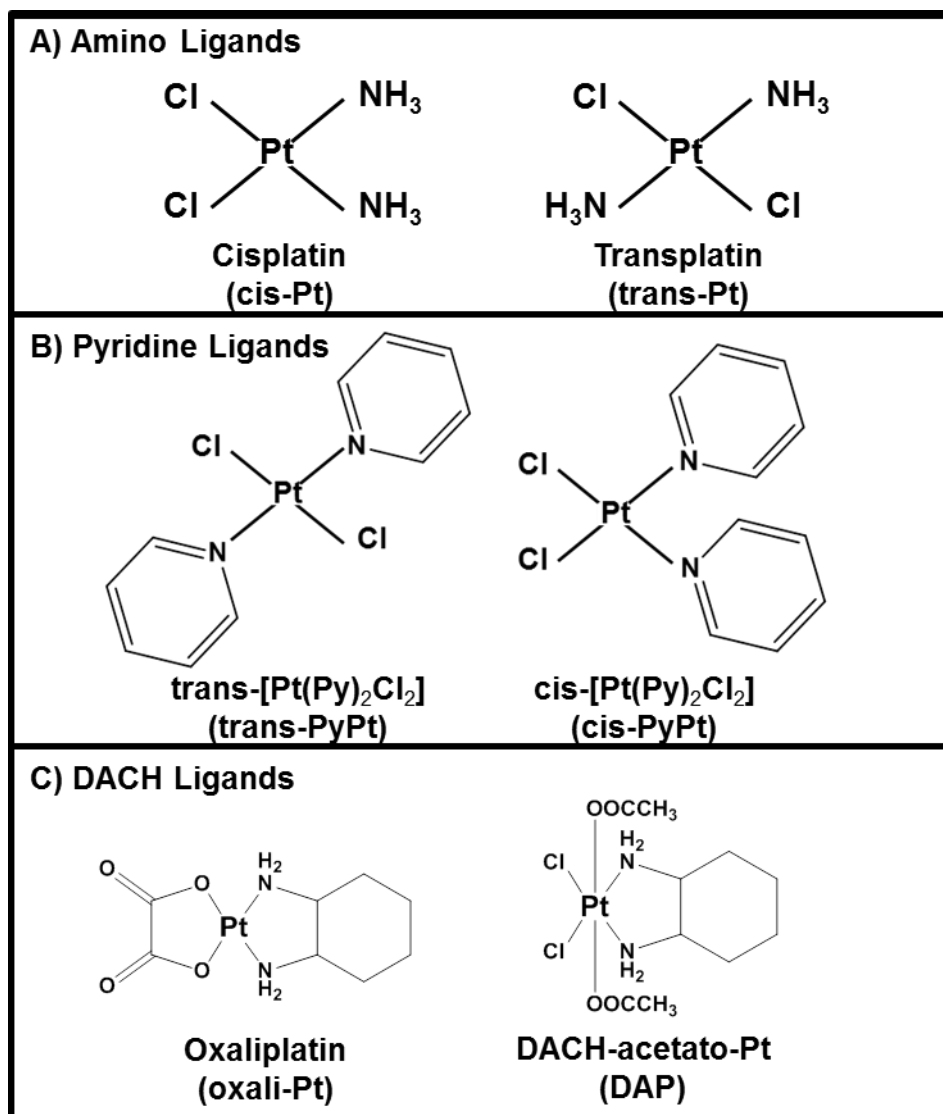


Figure 8. Chemical structure of platinum analogs investigated

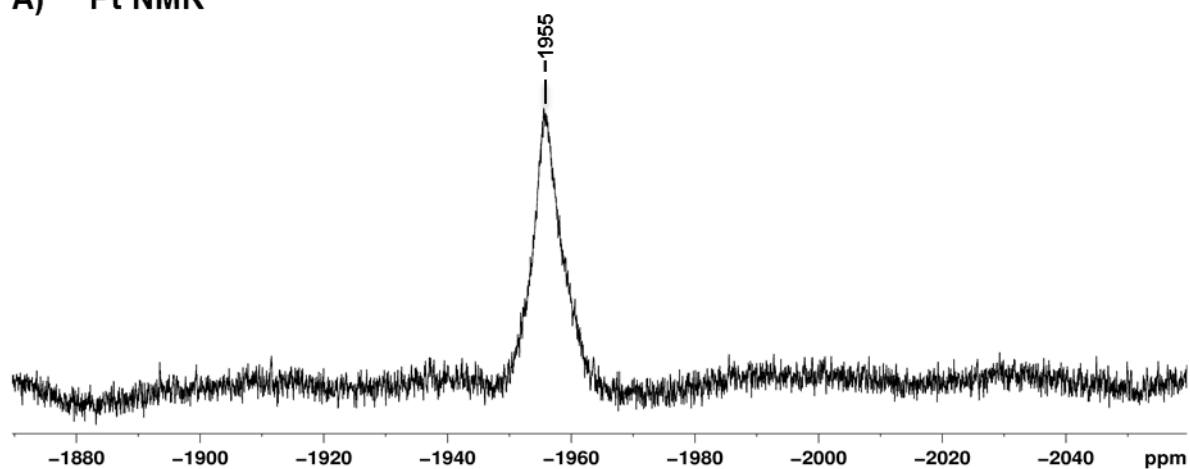
Pt compounds containing **A)** Amine, **B)** Pyridine or **C)** DACH ligand selected to explore their capacity to circumvent cis-Pt resistance.

3.2. Results:

3.2.1. Determination of the structure and purity of trans-PyPt:

The majority of the Pt compounds were available in the lab or purchased, except for the trans-PyPt, which was synthesized. The chemical structure of trans-PyPt was characterized through ^{195}Pt NMR (**Figure 9A**) and ^1H NMR spectroscopy (**Figure 9B**). The ^{195}Pt NMR spectrum showed a clear peak at -1955 ppm, which indicates the presence of the Pt atom with the pyridine ligands in a trans configuration. Presence of any cis impurity would have been indicated by a peak at -2002 ppm [143], but this was absent to indicate that the synthesized compound was exclusively in the trans state. The ^1H NMR spectrum exhibited three different peaks corresponding to three protons in unique chemical environment in the pyridine molecule: H_1 at 8.94 ppm, H_2 at 7.35 ppm and H_3 at 7.82 ppm. The error in the values obtained from NMR analysis ranged between 0.15%-0.34% (**Table 6**), demonstrating that the synthesized trans-PyPt was indeed the correct structure. In addition, values obtained from elemental analysis of carbon, hydrogen and nitrogen (CHN) reflected percentage of errors of $<10\%$ (**Table 6**), establishing that the trans-PyPt compound was obtained with high purity.

A) ^{195}Pt NMR



B) ^1H NMR

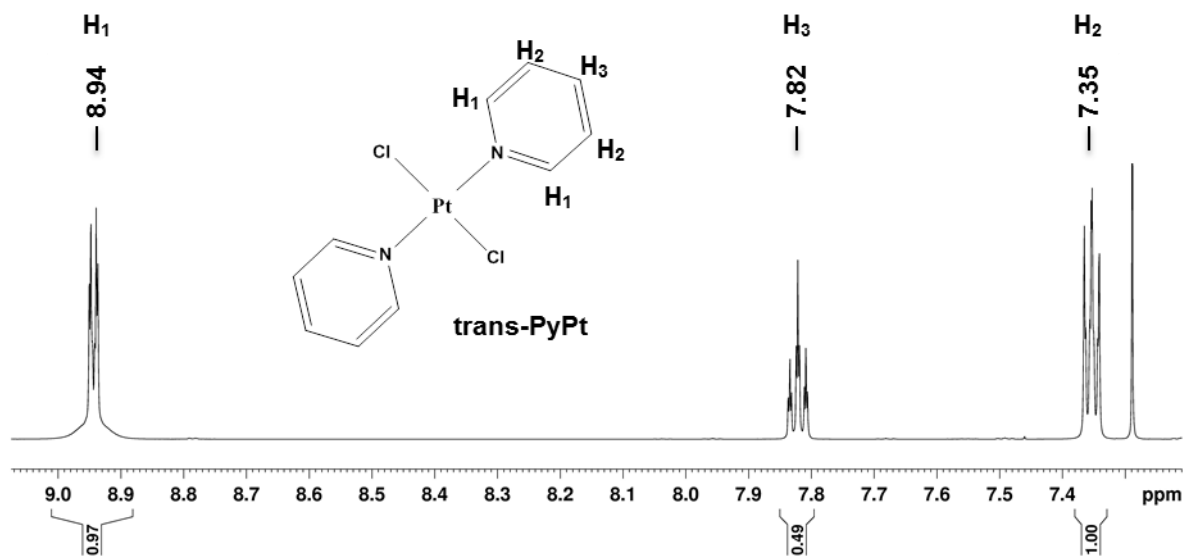


Figure 9. Nuclear magnetic resonance studies of trans-PyPt

Spectra were obtained by ^{195}Pt NMR (A) and ^1H NMR (B) spectroscopy.

Table 6. Values for elemental and NMR analysis of trans-PyPt

	NMR (ppm)				Elemental analysis (%)		
	H₁	H₂	H₃	Pt	C	H	N
Experimental Value	8.94	7.35	7.82	-1955	28.2	2.19	6.49
Theoretical Value	8.91	7.33	7.8	-1952	28.3	2.38	6.6
Percentage Error (%)	0.34	0.27	0.26	0.15	0.35	7.98	1.67

3.2.2. Cytotoxic evaluations of DMF and pyridine:

Several of the Pt analogs are insoluble in aqueous solvents and require solubilization in an organic solvent. However, solvents such as DMSO were avoided to prevent inactivation of the Pt drug. Due to its inertness towards Pt, DMF was selected as the optimal solvent, but it can be cytotoxic. Also, interaction of the two PyPt analogs with macromolecules in tissue culture media and in cells could release the potentially cytotoxic pyridine ligand into the environment. Therefore, it was first necessary to 1) set the maximal % (v/v) DMF concentration permissible in media containing the trans-Pt, cis-PyPt and trans-PyPt compounds that induces only moderate cytotoxicity and avoids significant impact on the determination of IC₅₀ values for these compounds, and 2) determine the cytotoxic potency, if any, of the pyridine ligand alone. Dose-response curves for DMF (% v/v) against sensitive A2780 and isogenic cis-Pt-resistant 2780CP/CI-16 cells are sigmoidal and demonstrate that cell survival ranges from 90-100% at 0.02-0.16% DMF, but drop close to 0% at 0.63-5% DMF (**Figure 10A**). The IC₅₀ values obtained for DMF in A2780 and 2780CP/CI-16 tumor models were 0.23% ± 0.013% and 0.33% ± 0.012%, respectively (**Figure 10B**), and demonstrate a 1.5-fold cross-resistance of 2780CP/CI-16 cells to DMF. As a consequence, a final concentration of 0.125% DMF (v/v) was selected in the measurement of IC₅₀ values of trans-Pt, cis-PyPt and trans-PyPt compounds. Finally, dose-response curves of the pyridine ligand in five ovarian tumor cell lines (A2780, 2780CP/CI-16, OVCAR-10, HEY and OVCA-433) demonstrate that cell survival is maintained between 80-100% at all treatment concentrations (0.04-27 μM) (**Figure 10C**). Thus, the pyridine compound

alone did not exhibit significant cytotoxic effects in the ovarian tumor panel in the concentration range examined.

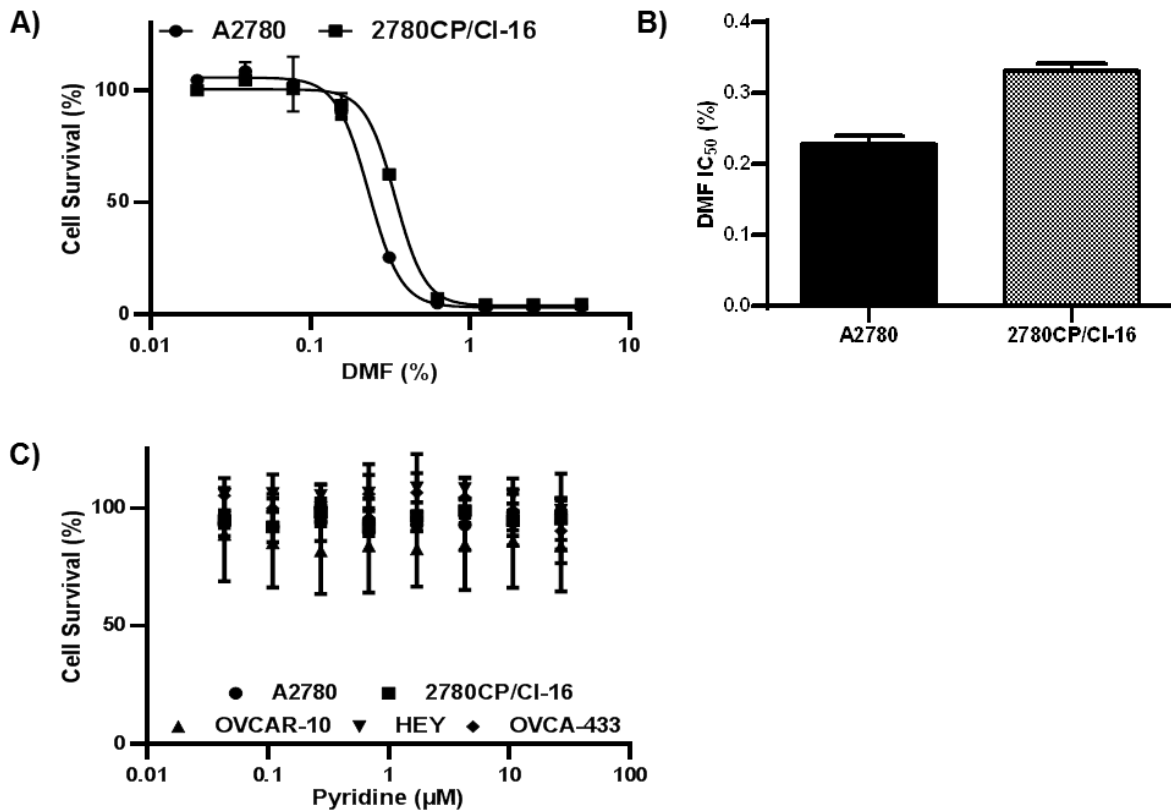


Figure 10. Cytotoxic evaluations of DMF and pyridine

A) Dose-response curve for DMF in A2780 and 2780CP/CI-16 tumor models using final dilutions of DMF from 0.02%-5% (v/v). **B)** IC₅₀ values of DMF (% v/v) in A2780 and 2780CP/CI-16 tumor models. **C)** Dose-response relationship for pyridine in A2780, 2780CP/CI-16, OVCAR-10, HEY and OVCA-433 cell lines using final concentrations of pyridine ranging from 0.04-27 μM in 0.125% DMF. N=3; Mean ± SD

3.2.3. Activity of structurally-distinct Pt analogs in ovarian cancer cell lines:

The activity of Pt compounds was determined using the MTT assay 5 days after initiating drug exposure. Cytotoxicity studies show that IC₅₀ values for cis-Pt are low for A2780 cells (0.298 μM). In contrast, 2780CP/CI-16, OVCAR-10, HEY and OVCA-433 cell lines exhibited high IC₅₀ values for cis-Pt (3.289-8.89 μM) (**Figure 11A** and **Table 7**). Therefore, the resistance factors calculated for cis-Pt in 2780CP/CI-16, OVCAR-10, HEY and OVCA-433 cell lines relative to A2780 are high (>10) in all four cell lines (**Figure 11B** and **Table 8**). These data clearly establish that the ovarian tumor panel selected for this study is composed of a sensitive cell line (A2780) and 4 resistant cell lines (2780CP/CI-16, OVCAR-10, HEY and OVCA-433) toward cis-Pt. In addition, the data demonstrate that the Pt compounds investigated had variable potencies in comparison to cis-Pt, with the trans-PyPt, oxali-Pt and DAP having greater potencies (lower IC₅₀ values when compared to cis-Pt) in each cell line (**Figure 11A** and **Table 7**). However, all Pt analogs gave lower resistance factors in cis-Pt resistant cell lines, but trans-PyPt, oxali-Pt and DAP compounds exhibited the lowest resistance factors ranging from 1.36-4.89 (**Figure 11B** and **Table 8**).

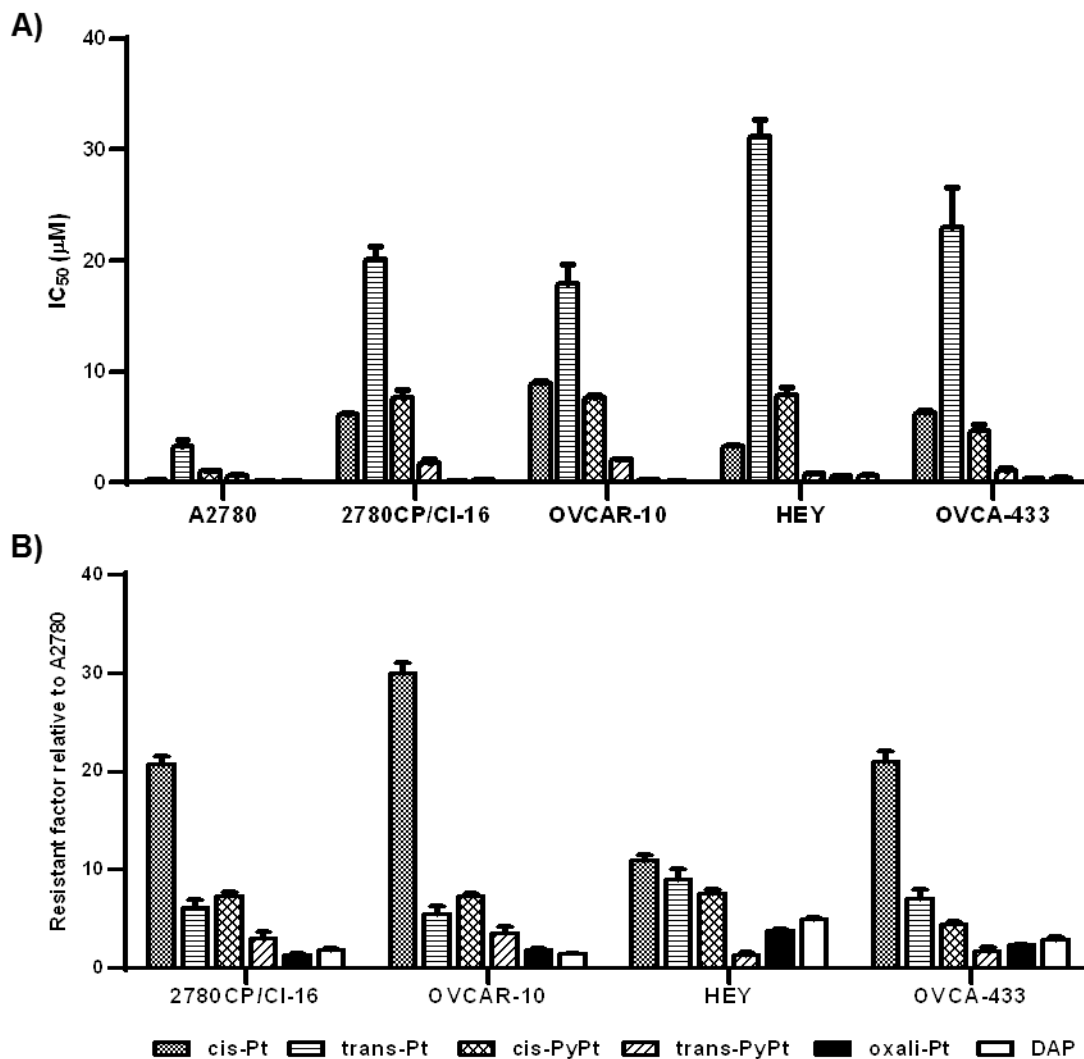


Figure 11. Activity of structurally-distinct Pt analogs in ovarian cancer cell lines

A) IC₅₀ values for Pt compounds were determined using a 5-day continuous Pt exposure MTT protocol in A2780, 2780CP/CI-16, OVCAR-10, HEY and OVCA-433.

B) Resistance factor (RF) values relative to A2780 cells for 2780CP/CI-16, OVCAR-

10, HEY and OVCA-433 were calculated from the formula $RF = \frac{IC_{50-Resistant\ Cell\ Line}}{IC_{50-Sensitive\ Cell\ Line}}$.

N=3; Mean ± SD

Table 7. IC₅₀ values (μM) of structurally-distinct Pt analogs in ovarian cancer cell lines

Pt-Compound	A2780	2780CP/CI-16	OVCAR-10	HEY	OVCA-433
cis-Pt	0.298 ± 0.010	6.217 ± 0.076	8.89 ± 0.29	3.289 ± 0.068	6.34 ± 0.21
trans-Pt	3.26 ± 0.38	20.16 ± 0.64	17.9 ± 1.0	31.21 ± 0.85	23.0 ± 2.0
cis-PyPt	1.064 ± 0.027	7.65 ± 0.43	7.68 ± 0.15	7.95 ± 0.40	4.69 ± 0.30
trans-PyPt	0.60 ± 0.11	1.77 ± 0.20	2.116 ± 0.043	0.793 ± 0.031	1.04 ± 0.15
oxali-Pt	0.1540 ± 0.0040	0.2090 ± 0.0040	0.282 ± 0.024	0.589 ± 0.013	0.354 ± 0.016
DAP	0.1370 ± 0.0040	0.236 ± 0.014	0.1930 ± 0.0040	0.666 ± 0.026	0.401 ± 0.026

Table 8. Resistance factor values relative to A2780 of structurally-distinct Pt analogs in ovarian cancer cell lines

Pt-Compound	A2780	2780CP/CI-16	OVCAR-10	HEY	OVCA-433
cis-Pt	1.000 ± 0.054	20.73 ± 0.82	29.7 ± 1.5	10.97 ± 0.46	21.0 ± 1.1
trans-Pt	1.00 ± 0.17	6.12 ± 0.77	5.45 ± 0.75	9.5 ± 1.2	7.0 ± 1.1
cis-PyPt	1.000 ± 0.039	7.26 ± 0.43	7.26 ± 0.26	7.45 ± 0.43	4.43 ± 0.30
trans-PyPt	1.00 ± 0.27	3.00 ± 0.64	3.53 ± 0.68	1.32 ± 0.26	1.67 ± 0.43
oxali-Pt	1.000 ± 0.037	1.357 ± 0.044	1.82 ± 0.16	3.83 ± 0.12	2.27 ± 0.13
DAP	1.000 ± 0.042	1.752 ± 0.099	1.409 ± 0.051	4.89 ± 0.22	2.92 ± 0.19

3.2.4. Pt uptake and DNA-Pt adducts formation of structurally-distinct Pt analogs:

Circumvention of cis-Pt resistance by structurally-distinct Pt compounds may be due to greater uptake into the cell and formation of higher levels of DNA adducts. Therefore, Pt uptake and DNA-Pt adducts formation from each Pt analog was studied in A2780 and its isogenic cell line 2780CP/CI-16 (**Figure 12**). Results demonstrate a reduction of cis-Pt uptake (**Figure 12A** and **Table 9**) and DNA-Pt adducts (**Figure 12B** and **Table 10**) in the resistant 2780CP/CI-16 cells when compared to A2780, and such behavior is also seen with all other Pt compounds. Oxali-Pt and DAP exhibited lower levels of Pt uptake and DNA-Pt adducts when compared to cis-Pt in both cell lines. Therefore, circumvention of cis-Pt resistance with these two analogs is not due to enhanced capacity for Pt uptake and to form DNA-Pt adducts. In contrast, trans-PyPt accumulated at high levels (**Figure 12A** and **Table 9**) as well as substantially greater levels of DNA-Pt adducts (**Figure 12B** and **Table 10**) in both cell lines, which indicates that this analog, unlike oxali-Pt and DAP, may depend on its favorable biochemical pharmacologic property to circumvent cis-Pt resistance. This may also apply to trans-Pt as the data demonstrate that trans analogs are accumulated in both cell lines to a greater extent and form greater level of DNA adducts than the corresponding cis compounds. It is also worth noting that the higher uptake correlates with higher DNA adducts.

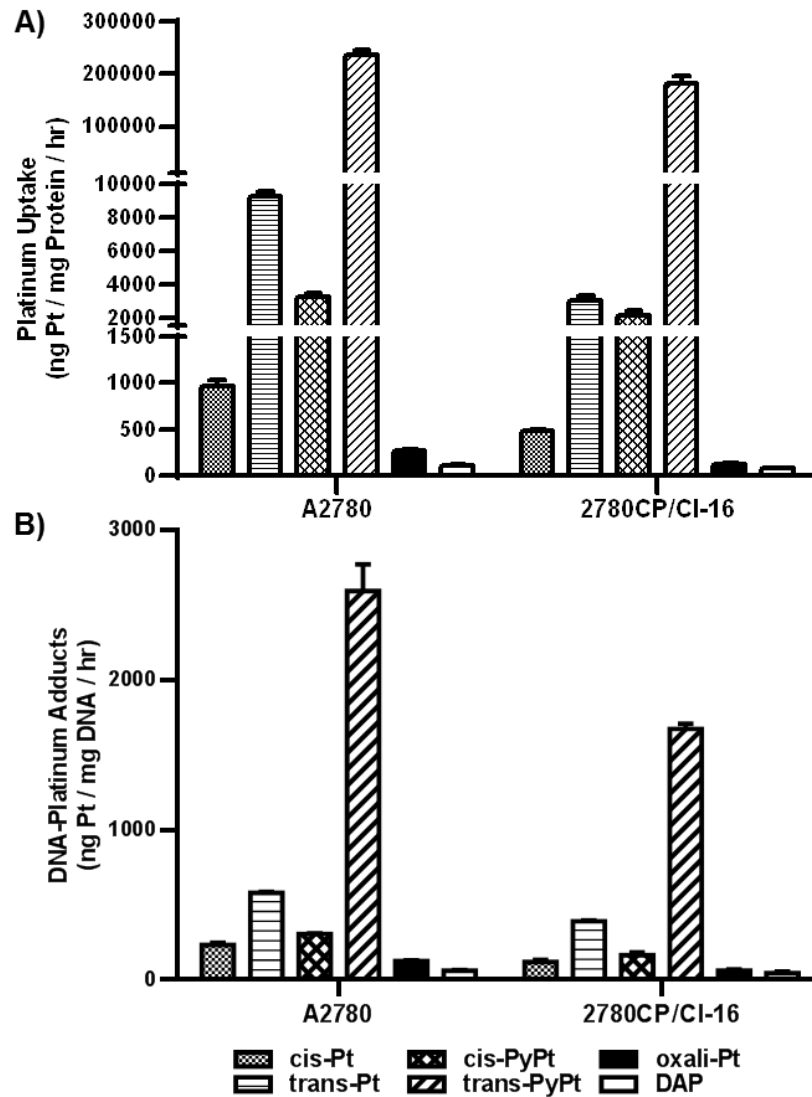


Figure 12. Pt uptake and DNA-Pt adducts formation of structurally-distinct Pt analogs

A) Pt uptake after exposing A2780 and 2780CP/CI-16 cell lines to 200 μ M of Pt compound for 2 hr at 37°C. **B)** DNA-Pt adducts formation after exposing A2780 and 2780CP/CI-16 cell lines to 200 μ M of Pt compound for 2 hr at 37°C. N=3; Mean \pm SD

Table 9. Cellular platinum uptake ($\times 10^3$ ng Pt/ mg Protein/ hr) values for structurally-distinct platinum analogs in A2780 and 2780CP/CI-16 tumor models

Pt Compound	A2780	2780CP/CI-16
cis-Pt	0.962 \pm 0.070	0.4830 \pm 0.0070
trans-Pt	9.30 \pm 0.33	3.01 \pm 0.27
cis-PyPt	3.22 \pm 0.22	2.12 \pm 0.30
trans-PyPt	235.4 \pm 8.9	182.4 \pm 12.6
oxali-Pt	0.267 \pm 0.015	0.127 \pm 0.011
DAP	0.108 \pm 0.016	0.0770 \pm 0.0060

Table 10. DNA platinum adducts (ng Pt/ mg DNA/ hr) values of structurally-distinct platinum analogs in A2780 and 2780CP/CI-16 tumor models

Pt Compound	A2780	2780CP/CI-16
cis-Pt	232.4 \pm 14.7	118.7 \pm 13.4
trans-Pt	579.8 \pm 7.8	391.4 \pm 5.5
cis-PyPt	306.8 \pm 2.0	163.3 \pm 20.1
trans-PyPt	2595.9 \pm 177.1	1673.4 \pm 34.3
oxali-Pt	125.2 \pm 4.0	61.2 \pm 8.8
DAP	59.6 \pm 4.6	44.6 \pm 10.1

3.2.5. Partition coefficient of structurally-distinct platinum analogs:

The greater cellular uptake and DNA adduct formation with trans Pt analogs and the relatively lower uptake and adducts with oxali-Pt and DAP, together with the knowledge that the trans Pt analogs and cis-PyPt require DMF for dissolution, suggests that lipophilicity may be a factor contributing to biochemical and molecular pharmacologic characteristics of the Pt analogs. Therefore, it was important to investigate the lipophilicity of Pt compounds by measuring their partition ratio and partition coefficient in a hydrophobic vs. hydrophilic phase using n-octanol and water as solvents, respectively. Partition coefficient values were as follows: trans-PyPt > cis-PyPt > DAP > trans-Pt > oxali-Pt > cis-Pt (**Figure 13** and **Table 11**). In addition, the partition ratio is less than 1 for cis-Pt, trans-Pt, cis-PyPt, oxali-Pt and DAP, thus, the majority of the concentration of these compounds is retained in the hydrophilic aqueous phase (**Table 11**). In contrast, the partition ratio is greater than 1 only for trans-PyPt, indicating that most of the trans-PyPt is found in the hydrophobic n-octanol phase (**Table 11**). Therefore, the lipophilicity of trans-PyPt more likely contributes to increased uptake and, thereby, increased DNA adduct formation. However, the relationship between uptake and partition coefficient is not readily apparent for the diverse Pt structures involved. On the other hand, comparing structures within a given class indicates a positive correlation. Thus, the greater uptake of trans-Pt vs. cis-Pt and of trans-PyPt vs. cis-PyPt can be explained by difference in partition coefficients between the isomeric pairs.

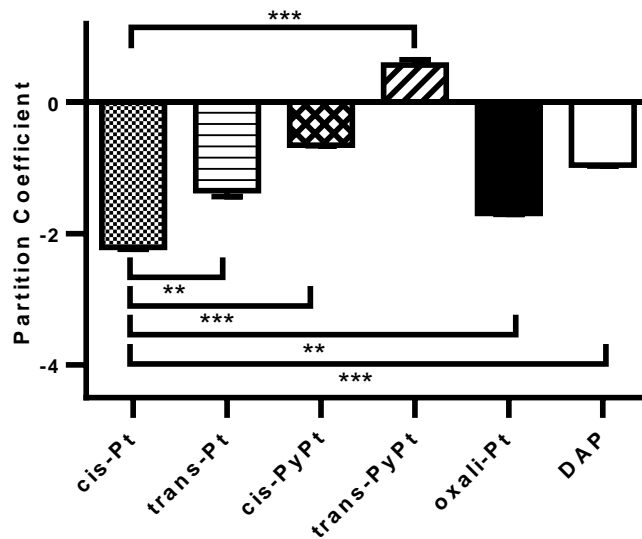


Figure 13. Partition coefficient of structurally-distinct platinum analogs

Partition coefficient (PC) of Pt compounds (25 μ M) after allowing 15 min for distribution between an n-octanol/water phase, where $PC = \log P$ and $P = \frac{Pt_{n-octanol}}{Pt_{water}}$. Student's t test was used to determine statistical significance, which was indicated by p value ≤ 0.05 . N=3; Mean \pm SD

Table 11. Partition coefficient values of structurally-distinct platinum analogs

Pt-Compounds	Partition Ratio (P)	Partition Coefficient (log P)
cis-Pt	0.00620 ± 0.00020	-2.206 ± 0.017
trans-Pt	0.0457 ± 0.0054	-1.346 ± 0.050
cis-PyPt	0.2240 ± 0.0036	-0.6500 ± 0.0070
trans-PyPt	3.76 ± 0.38	0.571 ± 0.045
oxali-Pt	0.02030 ± 0.00030	-1.6920 ± 0.0060
DAP	0.1115 ± 0.0021	-0.9530 ± 0.0080

3.2.6. DNA interstrand crosslinks index of structurally-distinct platinum analogs:

Cis-Pt forms both interstrand and intrastrand DNA crosslinks, with interstrand constituting about 5-8% of adducts and intrastrand about 82-95% [157;158]. The nature of crosslinks determines which DNA damage signaling pathways may become activated. Thus, the potential ability of Pt analogs to induce greater levels of ICLs was investigated as this may provide a general understanding of how the Pt analogs may circumvent cis-Pt resistance. The ICLs assay relies on completely denaturing DNA, with presence of ICLs preventing local DNA denaturation, and this is detected by the intercalating agent ethidium bromide (EtBr). The spectra for EtBr was first generated to confirm that the reported excitation and emission wavelengths are acceptable (**Figure 14A**). Based on these data, it was acceptable to measure the relative light unit (RLU) for fluorescence intensity using the reported wavelengths, $\lambda_{\text{excitation}}=305$ nm and $\lambda_{\text{emission}}=590$ nm [149], as these wavelengths were close to their respective λ_{max} found in the present study (**Table 12** and **Table 13**). DNA ICLs data with Pt compounds shows that cis-Pt has an ICLs index of 0.106, with trans-Pt, cis-PyPt and trans-PyPt demonstrating a 2- to 6-fold higher index and oxali-Pt and DAP giving a 2- to 3-fold lower value (**Figure 14B** and **Table 14**). Interestingly, there appears to be a correlation between ICLs index in a cell-free system and DNA-Pt adducts formed intracellularly (**Table 14** vs. **Table 10**).

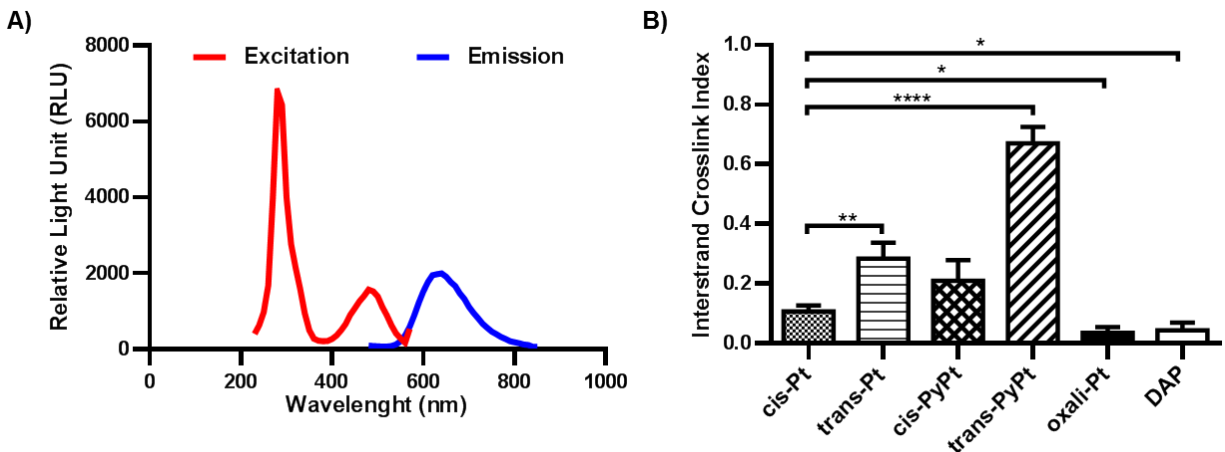


Figure 14. DNA interstrand crosslink index of structurally-distinct platinum analogs

A) Emission and excitation spectrum of ethidium bromide. **B)** Interstrand crosslink index from the reaction of 25 μM of Pt compounds with 7 μg of calf thymus DNA for 30 min at 37°C, where $\text{ICLs index} = [-\ln(x_{\text{treated}})] - [-\ln(x_{\text{control}})]$ and $x = \frac{\text{fluorescence}_{\text{non-heated}} - \text{fluorescence}_{\text{heated}}}{\text{fluorescence}_{\text{non-heated}}}$. Student's t-test was used to determine statistical significance, p value ≤ 0.05 . N=3; Mean \pm SD

Table 12. Excitation values for ethidium bromide at a given wavelength

Wavelength (nm)	Excitation (RLU)	Wavelength (nm)	Excitation (RLU)
230	401	410	366
240	628	420	503
250	978	430	669
260	1682	440	908
270	3998	450	1080
280	6792	460	1261
290	6438	470	1402
300	3996	480	1568
310	2771	490	1525
320	2144	500	1388
330	1585	510	1117
340	944	520	887
350	499	530	629
360	275	540	416
370	226	550	285
380	207	560	169
390	219	570	538
400	270		

Table 13. Emission values for ethidium bromide at a given wavelength

Wavelength (nm)	Emission (RLU)	Wavelength (nm)	Emission (RLU)
520	71	690	1323
530	81	700	1118
540	123	710	955
550	210	720	814
560	364	730	672
570	591	740	561
580	891	750	463
590	1223	760	397
600	1524	770	320
610	1772	780	270
620	1947	790	211
630	1976	800	185
640	1994	810	159
650	1909	820	126
660	1768	830	112
670	1666	840	62
680	1469	850	61

Table 14. DNA interstrand crosslink (ICLs) index of structurally-distinct platinum analogs

Pt-Compounds	ICLs index
cis-Pt	0.106 ± 0.011
trans-Pt	0.283 ± 0.031
cis-PyPt	0.208 ± 0.040
trans-PyPt	0.670 ± 0.032
oxali-Pt	0.034 ± 0.011
DAP	0.043 ± 0.015

3.2.7. Studies to determine reactivity of structurally-distinct platinum analogs:

Trans-Pt has been shown to be inactive due to its high reactivity [159]. Therefore, the reactivity of Pt compounds was assessed by measuring their reactivity rate by mixing 25 μM of each compound in FBS, analyzing unreacted (free) Pt at 0, 5 min, 15 min, 30 min, 1 hr, 2 hr, 4 hr and 6 hr, and determining the half-life by fitting the data to a monoexponential decay equation. The decay curves for the compounds are shown in **Figure 15A** and the half-lives in **Figure 15B**. The data show that cis-Pt, cis-PyPt and oxali-Pt have similar reaction rates with $t_{1/2}$ of 4.0, 3.4 and 2.4 hr, respectively (**Table 15**). However, trans-PyPt was found to be highly reactive exhibiting a substantially low $t_{1/2}$ (<1 min), with the corresponding trans-Pt also demonstrating a high reactivity with a $t_{1/2}$ of about 10 min (**Table 15**), thus most of the compound is expected to become inactivated by side reactions before interacting with DNA. In contrast, DAP, the only Pt (IV) compound in the group, was the most stable compound with a relatively longer $t_{1/2}$ of 12 hrs, which may preserve the compound in its inactivated state and enhance the concentration of the compound reacting with DNA.

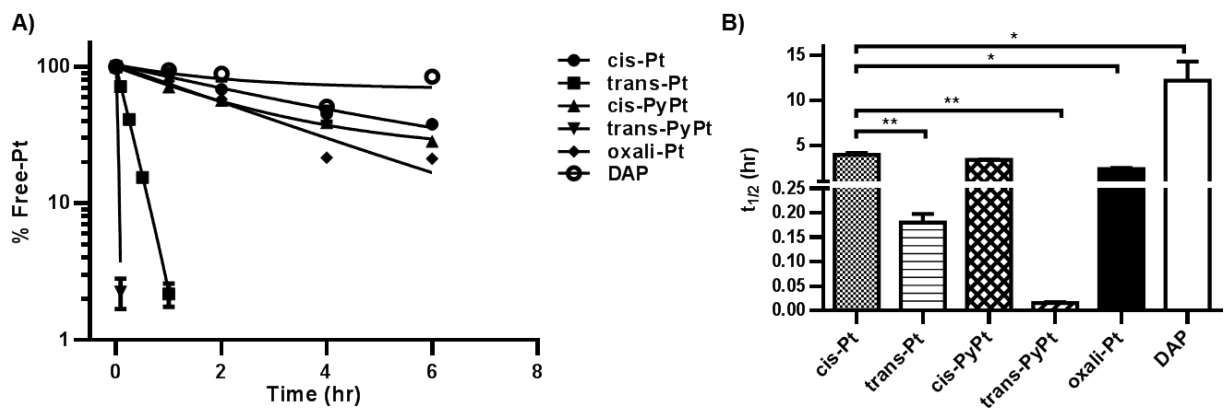


Figure 15. Reactivity of structurally-distinct platinum analogs

A) Reaction rate of 25 μ M of Pt compound with FBS at 37°C for 0, 5 min, 15 min, 30 min, 1 hr, 2 hr, 4 hr and 6 hr. **B)** Half-life ($t_{1/2}$) of Pt drugs calculated using $\ln[A] = \ln[A]_0 - kt$ and $t_{1/2} = \frac{0.693}{k}$. Student's t test was used to determine statistical significance, p value ≤ 0.05 . N=3; Mean \pm SD

Table 15. Half-life ($t_{1/2}$) and rate constant (k) values of structurally-distinct platinum analogs

Pt-Compound	k (1/hr)	$t_{1/2}$ (hr)
cis-Pt	0.1740 ± 0.0050	3.99 ± 0.34
trans-Pt	3.87 ± 0.12	0.1790 ± 0.0060
cis-PyPt	0.2030 ± 0.0020	3.42 ± 0.14
trans-PyPt	46.5 ± 3.6	0.0150 ± 0.0010
oxali-Pt	0.2890 ± 0.0080	2.40 ± 0.22
DAP	0.0580 ± 0.0050	12.0 ± 5.9

3.3. Conclusions:

This Chapter has demonstrated the successful synthesis of trans-PyPt with high purity, as demonstrated by the low errors (<10%) in NMR and CHN analysis. Cytotoxicity studies performed with structurally-distinct Pt analogs showed that among the Pt compounds investigated, oxali-Pt, DAP and trans-PyPt exhibited greater potencies compared to cis-Pt in both sensitive and cis-Pt-resistant cell lines. Moreover, these Pt compounds were able to circumvent cis-Pt resistance. The mechanism by which oxali-Pt, DAP and trans-PyPt circumvented cis-Pt resistance was further investigated by examining Pt uptake and DNA-Pt adducts formation with each Pt analog in cis-Pt sensitive A2780 and its isogenic cis-Pt resistant 2780CP/CI-16 cell lines. Generally, a reduction in Pt uptake and DNA-Pt adducts with all Pt analogs was observed in 2780CP/CI-16 cells when compared to A2780 cells. Interestingly, circumvention of cis-Pt resistance by oxali-Pt and DAP was observed even though these two compounds exhibited lower levels of Pt uptake and DNA-Pt adducts when compared to cis-Pt in both cell lines. Unlike oxali-Pt and DAP, trans-PyPt was accumulated at high levels and it formed substantially greater levels of DNA-Pt adducts in both cell lines. Thus, its capacity to circumvent cis-Pt resistance could be triggered by multiple mechanisms, including those that may be independent of the DNA damage signaling pathway. The greater cellular uptake and DNA adduct formation by trans-PyPt was shown to be due to its greater lipophilicity, as noted by a partition ratio greater than 1, indicating that most of the compound is found in the hydrophobic phase. Therefore, it is likely that the lipophilicity of trans-PyPt favors its transport through the cell membrane allowing this compound to accumulate in high concentrations inside the cell. Since Pt

compounds can also form links between the two DNA strands, the potential of Pt analogs to induce ICLs was examined as a possible mechanism used by Pt analogs to circumvent cis-Pt resistance. Results for DNA ICLs again show that oxali-Pt and DAP had a lower cross-link index value and trans-PyPt had a higher value when compared to cis-Pt. Finally, it was important to investigate the reactivity of Pt compounds since past studies have demonstrated that trans-Pt is a very reactive molecule, which results in its clinical inactivity. Indeed, trans-Pt and trans-PyPt were found to be highly reactive with $t_{1/2}$ less than 10 min. In contrast, DAP, the only Pt (IV) compound in the group, was the most stable compound with a relatively longer $t_{1/2}$ of 12 hrs. Cis-Pt, cis-PyPt and oxali-Pt had similar reaction rates. In conclusion, the results in this Chapter suggest that oxali-Pt and DAP were able to circumvent cis-Pt resistance more efficiently. Nevertheless, trans-PyPt also exhibited intrinsic molecular pharmacologic characteristics, thus, efforts by researchers in modifying and optimizing its chemical structure to increase its stability could enhance its clinical potential. Perhaps increasing trans-PyPt oxidation state to (IV) by addition of axial ligands could result in a more stable compound as observed for DAP. Oxali-Pt was selected as the lead structurally-distinct analog for further studies since it is an already FDA approved compound, but so far only for the treatment of colon cancer. Oxali-Pt induced DNA damage is different from cis-Pt induced DNA damage due to the difference in their carrier ligand, DACH vs NH_3 , respectively. This difference in DNA damage result in the activation of an intrinsic signaling pathway (**Figure 16**).

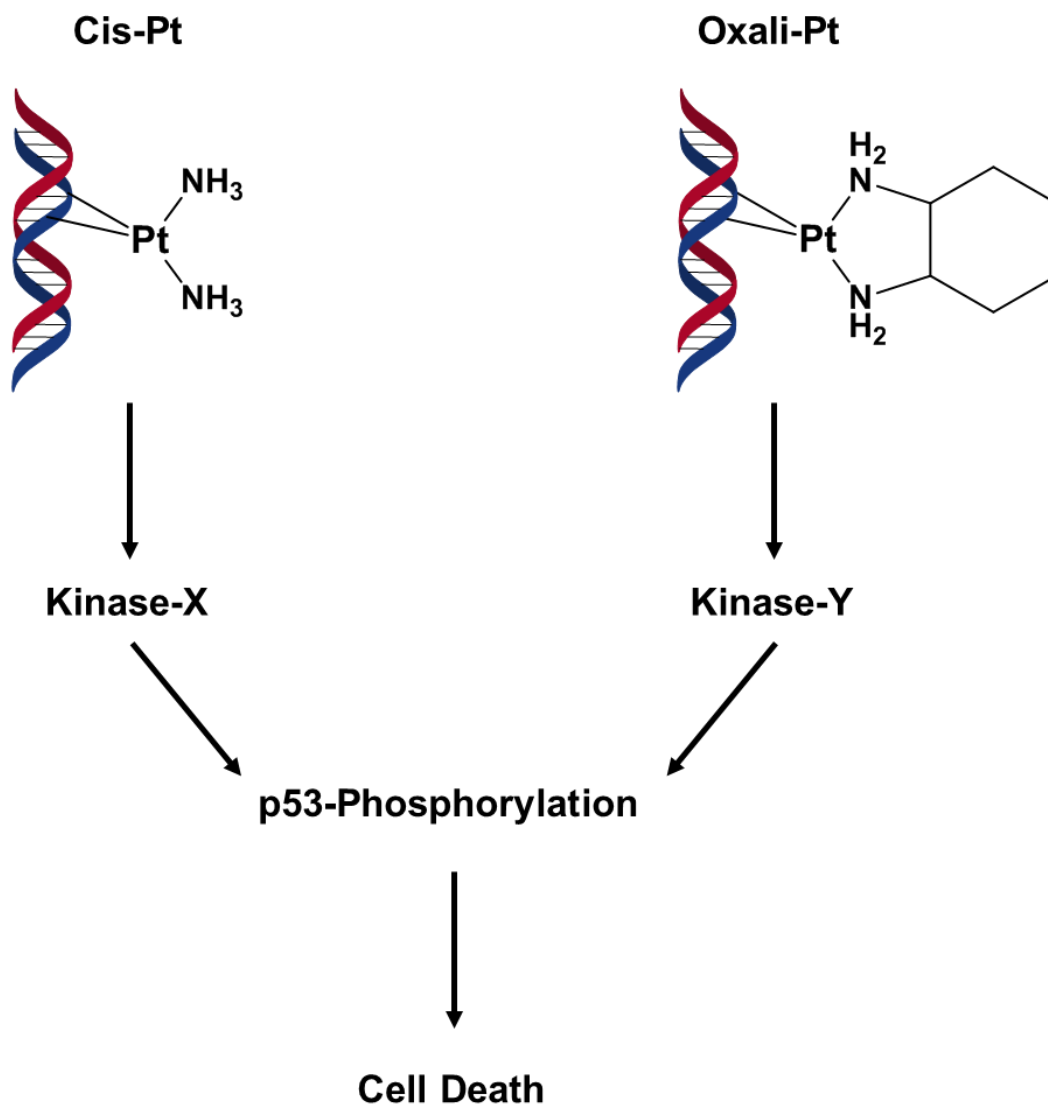


Figure 16. Conclusions Chapter 3

Oxali-Pt was selected as the lead structurally-distinct analog for studies performed in Chapter 4 and Chapter 5. It forms distinctly different adducts by virtue of the “L” ligand; specifically NH₃ vs. DACH. These distinct adducts likely transduce DNA damage signals along independent pathways.

Chapter 4

To determine the failure in p53 post-translational modifications as a causative factor in cisplatin resistance

4.1. Rationale and Background:

The tumor suppressor p53 has been shown to play an important role in mediating cis-Pt cytotoxicity, driving cancer cells to death. Conversely, loss of p53 activity has been associated with cis-Pt resistance [22;23]. The two main ways in which p53 loss of function is seen are through mutations and loss of post-translational modifications (e.g. phosphorylation events) in the p53 molecule. Furthermore, the data on the prognostic value of p53 status for therapeutic outcome in clinical studies with ovarian cancer patients has been highly variable [91-93]. More specifically, wild-type p53 can lead to a better, worse or similar response to treatment when compared to mutant p53, with the similar response best demonstrated by the TCGA survival curves shown in **Figure 5** [94]. Such studies make it questionable to use p53 status as a molecular marker in ovarian cancer patients to predict response to treatment. This is likely due to such use of p53 status, without considering p53 functional status. For instance, mutation of p53 may not necessarily lead to loss of function, as has been demonstrated for about 64% of all potential p53 mutants [98]. Similarly, regulation of p53 stability and/or transcriptional activity is dependent on p53 phosphorylation, especially on the critical Ser15 and Ser20 residues [68]. Hence, intrinsic p53 phosphorylation events promoted by Pt compounds could activate the function of the p53 molecule and the resultant potent cytotoxicity of the Pt drug. Conversely, absence of post-translational modification could result in failure of p53 activation and Pt-drug resistance. This is exemplified by loss of wild-type p53 function and resistance to fludarabine in chronic lymphocytic leukemia that lack ATM kinase activity, which is important for post-translational modification of p53 [160]. Therefore, the aim of this study is to determine the potential

failure of p53 post-translational modifications in promoting cis-Pt resistance. To investigate this premise, special focus will be given to Ser15 and Ser20 phosphorylation of p53 and p53 molecular pathway and their response to cis-Pt. In Chapter 3, oxali-Pt has been demonstrated to be a lead non-cross-resistant Pt to cis-Pt ovarian cancer cell lines. Hence, oxali-Pt was selected to examine whether circumvention of cis-Pt resistance is associated with an opposite effect to cis-Pt on phosphorylation at the two critical sites of p53. For consistency, the studies will be conducted in cis-Pt-resistant ovarian cancer cell lines used in Chapter 3. The results obtained in this chapter will give a better understanding in how cis-Pt resistance arises based on p53 function and how oxali-Pt may be able to circumvent this resistance in cis-Pt resistant ovarian cancer cell lines.

4.2. Results:

4.2.1. *TP53* sequencing in the ovarian tumor panel:

Given that mutation may lead to inactivation of p53 as a major mechanism leading to cis-Pt resistance, *TP53* gene status in the ovarian tumor panel was determined by DNA sequencing. The results demonstrate that the cis-Pt-sensitive A2780 cell line has wild-type p53. In contrast, 2780CP/CI-16, OVCAR-10, HEY and OVCA-433 cells were demonstrated to have p53 missense mutations (**Table 16**). Specifically, 2780CP/CI-16 harbored heterozygous V172F mutation, OVCAR-10 expressed V172F and G266R heterozygous mutations, and HEY and OVCA-433 were found to have the same P72R homozygous mutation. Whether these mutations are the primary cause of cis-Pt resistance needs to be addressed. The P72R mutation is an extensively studied polymorphism, but evidence does not support a role for this mutation in cancer susceptibility, including ovarian cancer susceptibility [161;162]. In fact, this mutation has been shown to promote apoptosis [161]. Based on the transcriptional activity in a yeast functional assay (FASAY), this P72R mutant appears to behave like wild-type p53 (**Table 16**). As regards V172F and G266R mutations, both induce a loss of p53 function in the FASAY. However, a previous report has demonstrated that the mutant p53^{V172F} in 2780CP/CI-16 cells responds normally to ionizing radiation by becoming stabilized and then transactivating the target p21 gene [146]. Thus, mutation in p53 may not necessarily prevent normal p53 function in cells challenged with DNA damaging agents, and this is possible with non-cross-resistant Pt analogs such as oxali-Pt.

Table 16. Analysis of p53 status in ovarian cancer cell lines

Cell Line	Base Change	Type	Effect	Gene Status	p53 transcriptional activity
A2780	None	None	None	Wild-type	+
2780CP/CI-16	139G>K	Heterozygous	V172F	Mutant	-
OVCAR-10	139G>K	Heterozygous	V172F	Mutant	-
	14G>R	Heterozygous	G266R	Mutant	-
HEY	119C>G	Homozygous	P72R	Mutant	+
OVCA-433	119C>G	Homozygous	P72R	Mutant	+

The p53 transcriptional activity (or p53 function) is predicted using a database of p53 mutants assessed in a yeast functional assay (http://p53.fr/TP53Mutload/database_access/search.php).

+, functional; -, inactive.

4.2.2. Generation of stable p53 knock-out clones in ovarian cancer cell lines:

To further characterize the relationship between p53 and Pt resistance, several p53^{-/-} from A2780, 2780CP/CI-16, OVCAR-10 and HEY cells using the novel CRISPR/Cas9 technique were generated. Selected stable p53^{-/-} clones were confirmed as lacking p53 expression by immunoblots, whereas control clones expressed p53 (**Figure 17A-D**). Absence of p53 also caused loss of expression of the target p21. To further test lack of p53 expression, knock-out clones were exposed to the Pt drugs. Immunoblots indicated continued absence of p53 by a lack of p53 and p21 inductions, even after 24 hr of cis-Pt or oxali-Pt treatment. Control clones exposed to cis-Pt either had no effect or modestly induced p53, with little or no upregulation of p21, in all four cell lines. These studies were not designed to examine the relative expression of p53 and p21 after cis-Pt treatment in sensitive A2780 clones vs. clones from resistant cells, as this would have required immunoblot development on the same gel for direct comparison. However, it is apparent that oxali-Pt robustly induced p53 and p21 in clones from both cis-Pt sensitive and resistant cell lines (**Figure 17A-D**). This is noteworthy for another reason: the data with oxali-Pt indicate that p53 is functional in all control clones from the four cell lines, irrespective of the specific p53 mutation present, as shown in **Table 16**, and that p21 upregulation by cis-Pt and oxali-Pt is p53-dependent.

Note: Repeated efforts to generate p53^{-/-} clones from OVCA-433 cells failed, and the cause of this is not known.

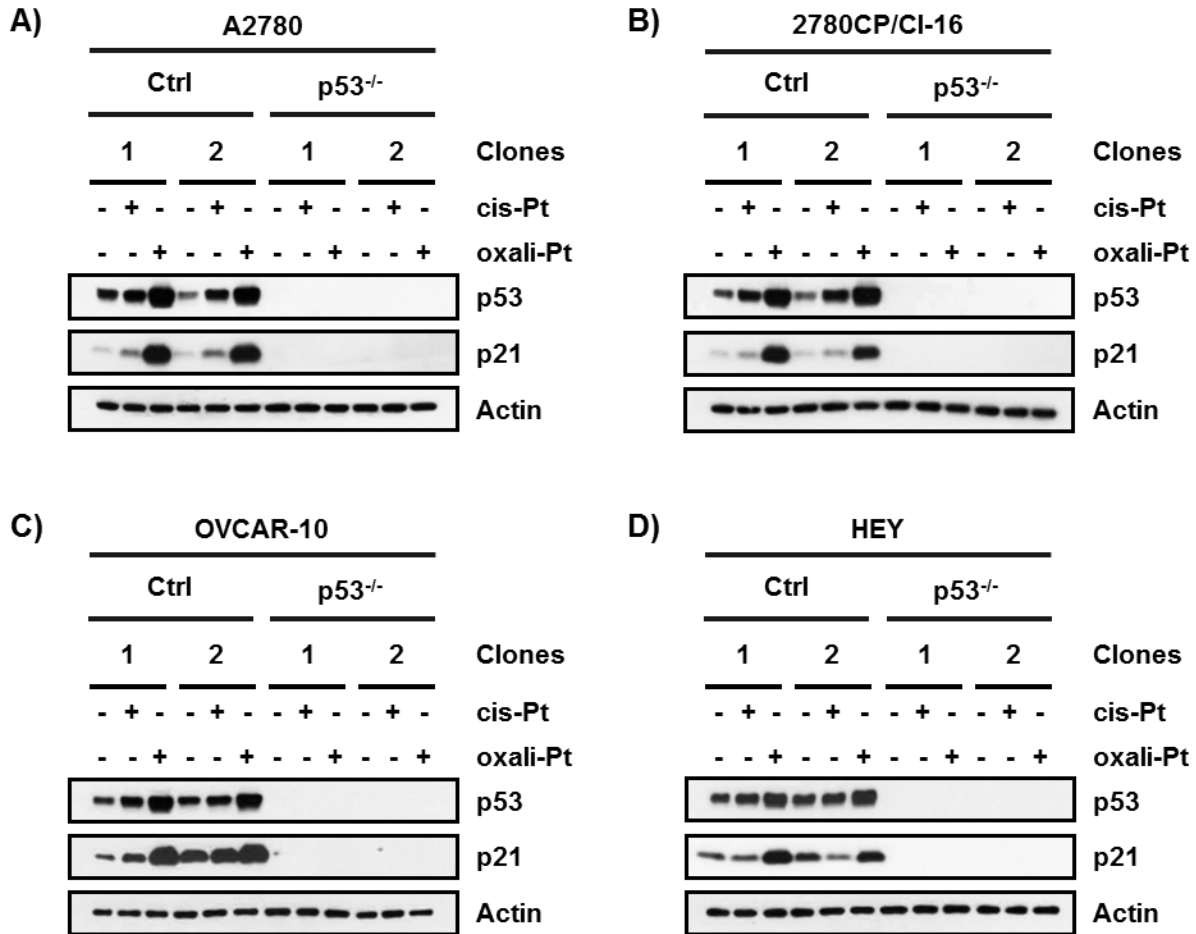


Figure 17. Generation of p53 knock-out clones in ovarian cancer cell lines

A) A2780, B) 2780CP/CI-16, C) OVCAR-10 and D) HEY cell lines were transfected with 25 μ g of CRISPR/Cas-GFP plasmid. After 48 hr of transfection, GFP positive cells were collected and expanded. Clones were selected and characterized through Western blot. A2780 clones were exposed to cis-Pt (1 μ M) or oxali-Pt (0.6 μ M) for 24 hr. 2780CP/CI-16, OVCAR-10 and HEY clones were similarly exposed to cis-Pt (5 μ M) or oxali-Pt (3 μ M) for 24 hr. Levels of p53 and p21 were examined by Western blot.

4.2.3. Cytotoxicity of platinum drugs in p53^{-/-} ovarian cancer cell lines:

Dependence of cis-Pt and oxali-Pt on p53, as indicated in the preceding section, was examined using cytotoxicity as the end-point in p53^{-/-} clones (**Figure 18**). Control clones from 2780CP/CI-16, OVCAR-10 and HEY cells displayed resistance to cis-Pt, which was consistent with results in Chapter 3. Knock-out of p53 in clones from A2780 and 2780CP/CI-16 cells led to a significant increase in cis-Pt IC₅₀ values (**Figure 18A** and **Table 17**); thus, presence of p53 is essential for cis-Pt cytotoxicity in these cell lines. On the other hand, p53 knock-out in OVCAR-10 and HEY clones led to a significant decrease in cis-Pt IC₅₀ values (**Figure 18A** and **Table 17**), indicating that the presence of potentially functional p53 in these cell lines is associated with cis-Pt resistance. Interestingly, oxali-Pt was less active in each p53^{-/-} clone, but the effect was more pronounced in A2780 and HEY clones (**Figure 18B** and **Table 17**). Thus, the cytotoxicity of oxali-Pt relies on the presence of p53 in all four cell lines (A2780, 2780CP/CI-16, OVCAR-10 and HEY), and that the p53 in these cells is functional, as indicated by the significant increase in oxali-Pt IC₅₀ values in p53 knock-out cell lines (**Figure 18B** and **Table 17**). Moreover, the data clearly demonstrates how the cytotoxicity is impacted differently between cis-Pt and oxali-Pt by the loss of p53 in some resistant cells.

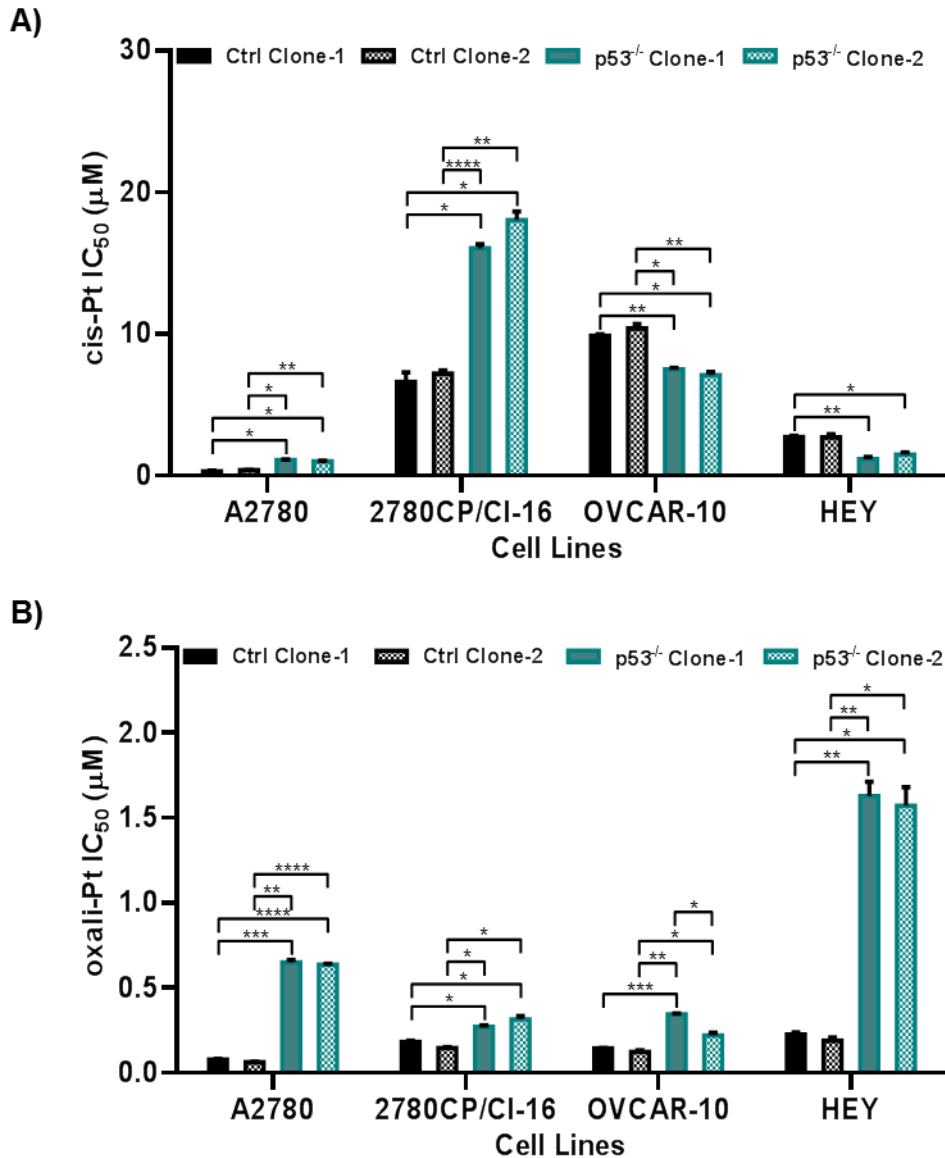


Figure 18. Cytotoxicity of platinum drugs in p53^{-/-} ovarian cancer cell lines

Cytotoxicity of **A)** cis-Pt or **B)** oxali-Pt was measured in two p53^{-/-} clones derived from A2780, 2780CP/CI-16, OVCAR-10 and HEY tumor cells. Clones were continuously exposed to Pt drug for 5 days at 37°C. MTT was used to assess IC₅₀ values, which were determined by sigmoidal fit of data using GraphPad Prism software. ANOVA test was used to determine statistical significance, p value ≤0.05. N=3; Mean ± SD

Table 17. IC₅₀ values (μM) of Pt drugs in CRISPR engineered p53^{-/-} ovarian cancer cell lines

Pt-Drug	Clones	A2780	2780CP/CI-16	OVCAR-10	HEY
cis-Pt	Ctrl-1	0.305 ± 0.030	6.61 ± 0.67	9.87 ± 0.11	2.722 ± 0.092
	Ctrl-2	0.379 ± 0.017	7.19 ± 0.24	10.38 ± 0.32	2.68 ± 0.23
	p53 ^{-/-} -1	1.083 ± 0.046	16.03 ± 0.30	7.49 ± 0.11	1.15 ± 0.16
	p53 ^{-/-} -2	0.998 ± 0.036	18.03 ± 0.60	7.08 ± 0.22	1.47 ± 0.16
oxali-Pt	Ctrl-1	0.0780 ± 0.0040	0.1810 ± 0.0080	0.1450 ± 0.0010	0.223 ± 0.014
	Ctrl-2	0.0620 ± 0.0030	0.1460 ± 0.0040	0.1220 ± 0.0090	0.188 ± 0.019
	p53 ^{-/-} -1	0.649 ± 0.016	0.2700 ± 0.0080	0.3430 ± 0.0060	1.627 ± 0.084
	p53 ^{-/-} -2	0.6360 ± 0.0060	0.314 ± 0.019	0.219 ± 0.017	1.57 ± 0.11

4.2.4. Oxali-Pt treatment results in greater p53 expression and functional activity than cis-Pt at equimolar concentrations in the ovarian tumor panel:

Since cis-Pt and oxali-Pt cytotoxicity in p53^{-/-} cells exhibited different cytotoxic sensitivity, p53 expression and p53 activity, as indicated by p21 upregulation in immunoblots, following exposure to increasing equimolar concentrations of cis-Pt or oxali-Pt for 24 hr was examined (**Figure 19**). In cis-Pt sensitive A2780 cells, low concentrations of cis-Pt and oxali-Pt (starting at 1 μ M) are able to increase levels of p53 and p21. In addition, the two Pt-drugs increased p53 levels in a dose-dependent manner in A2780 cells (**Figure 19A**). Cells appeared to demonstrate a saturation of p53 activity in response to cis-Pt and oxali-Pt treatment above 5 μ M, as indicated by little or no increase in p21. However, in cis-Pt resistant 2780CP/CI-16, OVCAR-10 and HEY cell lines, oxali-Pt promoted a more robust induction of levels of p53 at all concentrations when compared to cis-Pt (**Figure 19B-D**). In addition, p21 levels after oxali-Pt treatment remain fairly constant over the concentration range (**Figure 19B-D**). Therefore, at equimolar concentrations, oxali-Pt is able to trigger a more robust p53 response and this leads to greater transcriptional activity compared to cis-Pt in resistant cell lines.

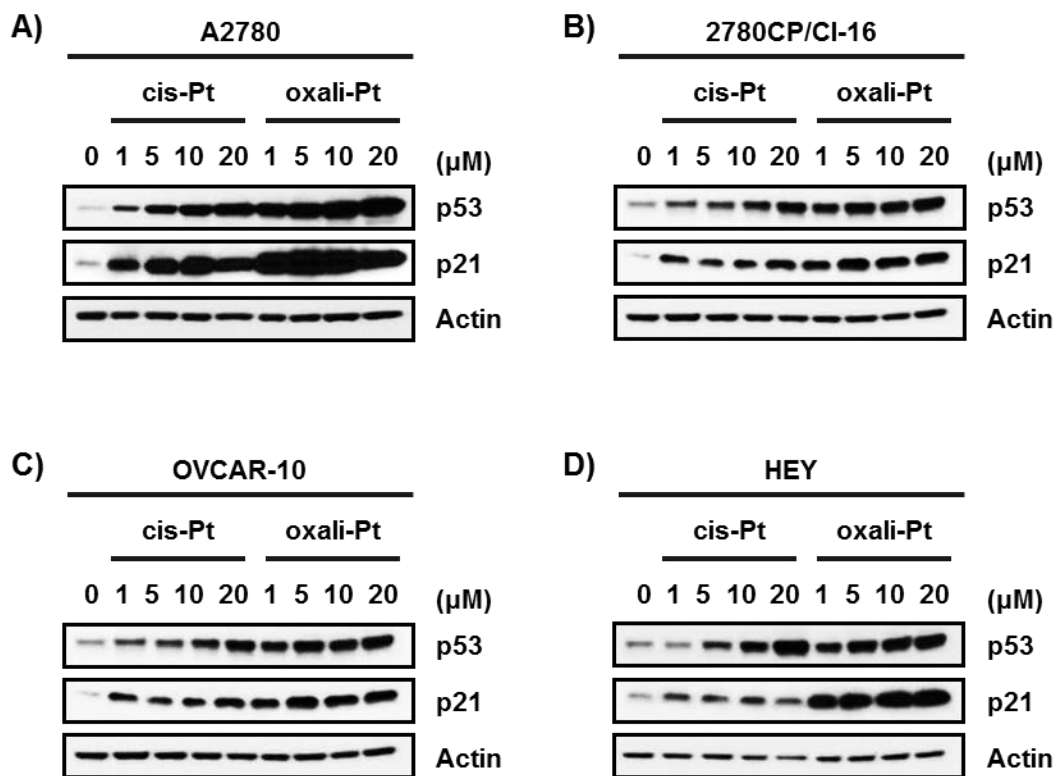


Figure 19. Dose-response relationship for p53 expression and p21 upregulation with cis-Pt and oxali-Pt in the ovarian tumor panel

Examination of p53 and p21 levels in **A)** A2780, **B)** 2780CP/CI-16, **C)** OVCAR-10 and **D)** HEY cell lines 24 hr after treatment with 1, 5, 10 and 20 μ M of cis-Pt or oxali-Pt.

4.2.5. Comparison of activation and phosphorylation of p53 between cis-Pt and oxali-Pt:

The preceding section provided immunoblots that allowed direct comparison between cis-Pt and oxali-Pt in a dose-dependent manner for their effects on p53 or p21 in each cell line. For comparison between cell lines, it is necessary to examine the changes in the same immunoblot. Given the dose-response effects for cis-Pt and oxali-Pt on p53 transcriptional activity using p21 as a biomarker, the 5 μ M drug concentration was selected to compare the effects as higher drug exposures in the cis-Pt sensitive A2780 cells did not result in further increases in p21. Using this concentration in cis-Pt resistant cell lines (2780CP/CI-16, OVCAR-10 and HEY), the potential of these two Pt compounds to phosphorylate the two sites on p53 that have been reported as most critical for its anti-proliferative and apoptotic functions, Ser15 and Ser20, was studied [68]. After 24 hr of cis-Pt treatment increased p53 levels were seen in all cell lines (**Figure 20A**). However, p53 increases in cis-Pt resistant 2780CP/CI-16, OVCAR-10 and HEY cells were lower than in cis-Pt sensitive A2780 cells. Similarly, p21 increases in these cis-Pt resistant cells were lower as compared to A2780 cells. In contrast, oxali-Pt increased greater levels of p53 and p21 than cis-Pt in all cell lines (**Figure 20A**). In terms of phosphorylation events, increases in p53-Ser15 phosphorylation promoted by cis-Pt or oxali-Pt were observed in all cell lines, but the relative increases by the two drugs were not consistent with increases in p53 or p21. Specifically, in the HEY cell line cis-Pt induces greater p53-Ser15 phosphorylation than oxali-Pt, whereas increases in p53 and p21 by cis-Pt were much lower than by oxali-Pt (**Figure 20A and 20B**). On the other hand, cis-Pt and oxali-Pt are both able to induce p53-Ser20 phosphorylation in

sensitive A2780 and cis-Pt resistant 2780CP/CI-16, OVCAR-10 and HEY cells and its relative induction correlates with relative increases in p53 and p21 (**Figure 20A** and **20B**). Based on the data presented, phosphorylation at Ser20 is a good correlate for p53 stabilization and activation by the Pt drugs.

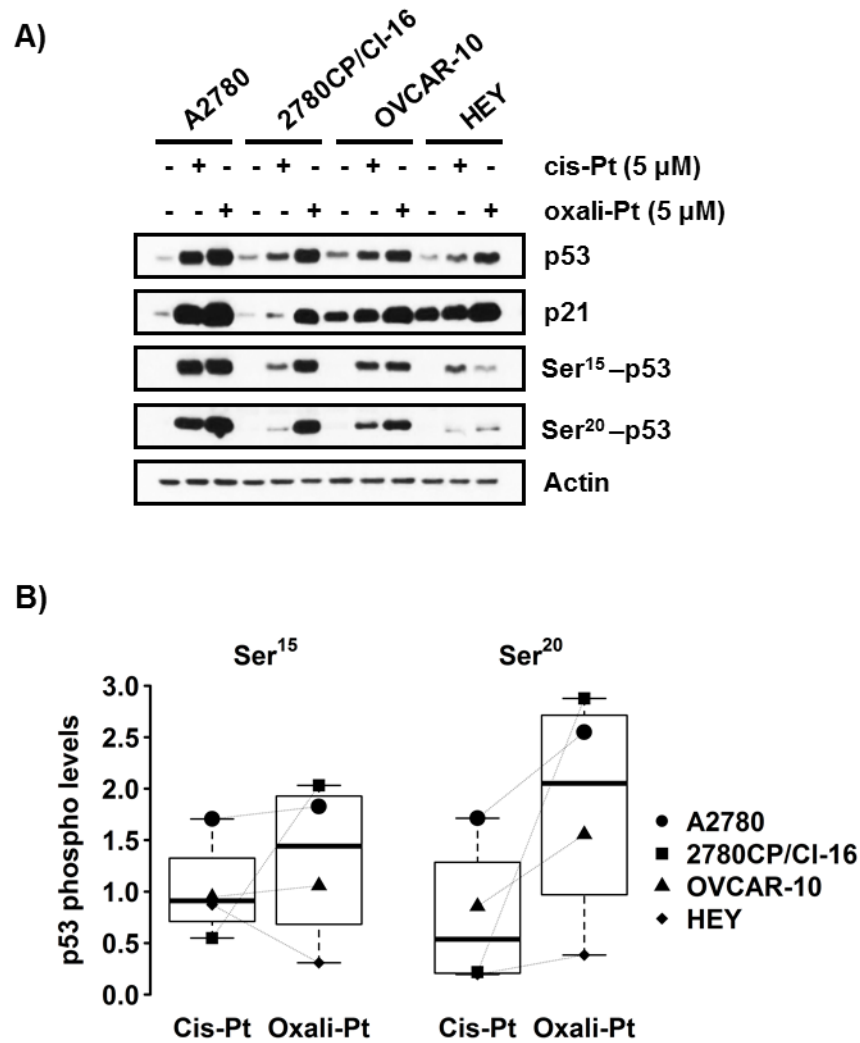


Figure 20. Induction of p21 and p53 phosphorylation at Ser15 and Ser20 by cis-Pt and oxali-Pt

A) Examination of p53, p21, p53-Ser15 and p53-Ser20 levels in A2780, 2780CP/CI-16, OVCAR-10 and HEY cell lines treated with 5 μ M of cis-Pt or oxali-Pt for 24 hr. **B)** Densitometric analysis of p53 phosphorylation at Ser15 and Ser20 in A2780, 2780CP/CI-16, OVCAR-10 and HEY cell lines treated with 5 μ M of cis-Pt or oxali-Pt for 24 hr.

4.2.6. p53-Ser20 phosphorylation strongly enhances expression of p21:

Since a strong correlation after Pt treatment was established between p53-Ser20 phosphorylation and p21 expression in cis-Pt resistant cell lines, the importance of p53-Ser20 phosphorylation in promoting p53 transcriptional activity was investigated. Therefore, p21 levels were measured in p53-deficient A2780 p53^{-/-} cells transfected with plasmids expressing: 1) wild-type p53, 2) mutant p53-S20A (constitutively dephosphorylated mimic) or 3) mutant p53-S20D (constitutively phosphorylated mimic). Transfections were titrated to provide similar levels of total p53 expression at 48 hr, as shown in **Figure 21A**. As anticipated, p53-Ser 20 phosphorylation was detected only in the phosphomimetic S20D mutant. All three forms of p53 demonstrated activity by their ability to transactivate p21. However, the immunoblot and densitometric data for p21 expression show that there was no difference between wild-type p53 and mutant p53-S20A, but the p53-S20D is able to increase p21 to significantly greater levels compared to wild-type p53 or mutant p53-S20A (**Figure 21A** and **21B**). These results validate the significance of Ser20 phosphorylation for p53 activation.

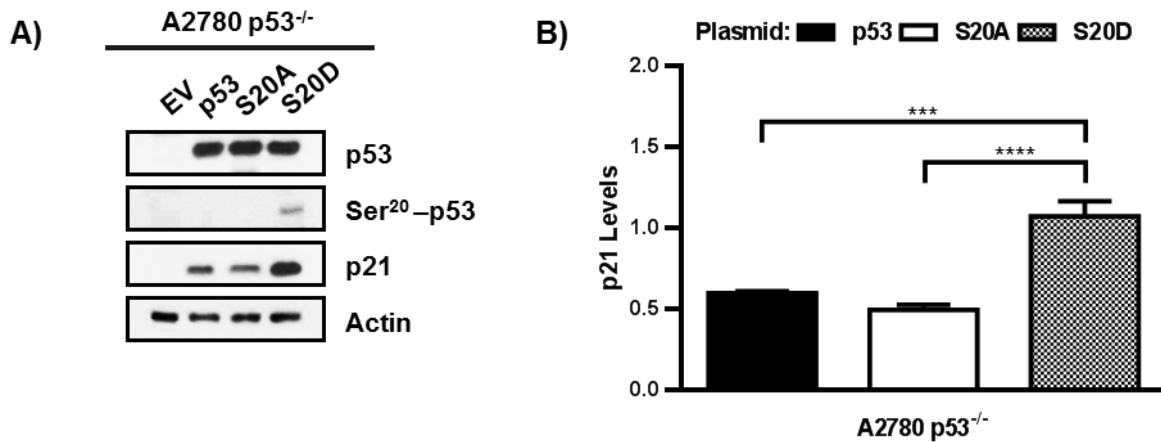


Figure 21. p53-Ser20 phosphorylation strongly enhances expression of p21

A) Evaluation of basal levels of p53, p53-Ser20 and p21 in A2780 p53^{-/-} cells transfected with pcDNA3 control (1 µg), wild-type p53 (0.5 µg), mutant p53-S20A (1 µg) or p53-S20D (0.5 µg) expression vectors for 48 hr. **B)** Densitometric analysis of p21 levels induced by wild-type p53, p53-S20A or p53-S20D in A2780 p53^{-/-} cells. Student's t test was used to determine statistical significance, p value ≤0.05. N=3; Mean ± SD

4.2.7. Activation of p53 by cis-Pt and oxali-Pt at equitoxic concentrations in the ovarian tumor panel:

Preceding studies were conducted at equimolar drug concentrations. However, each cell line expresses different sensitivity to each drug, as defined by the IC₅₀ value, which is a composite of all resistance mechanisms, including reduced drug uptake and enhanced DNA repair. Thus, it is possible that differences in p53 expression and activation between cis-Pt and oxali-Pt may become minimal using concentrations based on IC₅₀ values. Therefore, to further characterize the different capacity of cis-Pt and oxali-Pt in promoting p53 phosphorylation and transcriptional activity, p53 response at equitoxic Pt drug concentrations (IC₅₀ X1, X3 and X5) (**Table 18**) in A2780, 2780CP/CI-16, OVCAR-10 and HEY cell lines was examined (**Figure 22**). The immunoblots developed from cell lysates prepared 24 hr after drug exposure show in general that cis-Pt and oxali-Pt increase p53 levels with increasing drug concentrations in all four cell lines (**Figure 22A-D**). Furthermore, in cis-Pt sensitive A2780 cells, both Pt compounds are able to promote an increase in p53-Ser20 phosphorylation and levels of p53 transcriptional targets p21 and Mdm2 in a concentration-dependent manner, with oxali-Pt demonstrating a greater effect at each equitoxic concentration (**Figure 22A**). Similarly, in cis-Pt resistant 2780CP/CI-16, OVCAR-10 and HEY cell lines, the low equitoxic concentration of cis-Pt was as effective or less effective than oxali-Pt at inducing p53-Ser20 phosphorylation, p21 and Mdm2 levels. However, higher equitoxic concentrations of cis-Pt were more effective than oxali-Pt at inducing Ser20 phosphorylation in resistant cell lines, but this greater Ser20 phosphorylation by cis-Pt did not necessarily translate into comparably greater expression of p53 transcription

factors, p21 or Mdm2 (**Figure 22B-D**). One explanation is that cis-Pt in general is not as efficient as an equitoxic concentration of oxali-Pt at Mdm2-dependent reduction in Mdm4, which is also a prerequisite in the transactivation function of p53.

Although equitoxic concentrations were effective as anticipated in eliminating differences between cis-Pt and oxali-Pt for p53-dependent induction of p21 in 2780CP/CI-16 and OVCAR-10 cells, this was not the case in A2780 and HEY where oxali-Pt still demonstrated a greater effect (**Figure 22A-D**). Nevertheless, the data obtained are useful in correlating p53 activation, using p21 expression as a marker, with drug sensitivity and resistance. For this exercise, actual concentrations were used in defining this correlation, which is shown in **Figure 22E**. It is readily apparent from this figure that cis-Pt increased p21 at lower concentrations in A2780, whereas higher concentrations of this drug are needed for this increase in cis-Pt resistant cells. In contrast, increases in p21 with oxali-Pt clustered at lower concentrations, similar to that for cis-Pt in A2780 cells. Thus, high cytotoxicity of cis-Pt in A2780 cells and of oxali-Pt in all four cell lines correlates with p53-dependent p21 expression at low drug concentrations and, conversely, low cytotoxicity of cis-Pt in 2780CP/CI-16, OVCAR-10 and HEY cell lines was associated with p21 expression occurring at high drug concentrations. In other words, higher cis-Pt concentrations were needed to overcome the factor preventing p53 activation by cis-Pt in resistant cells.

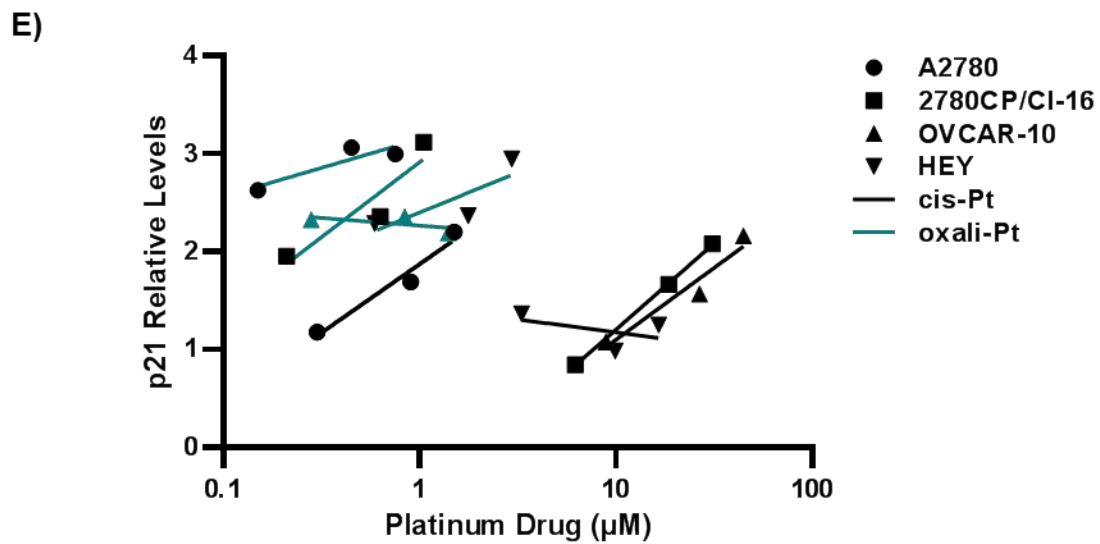
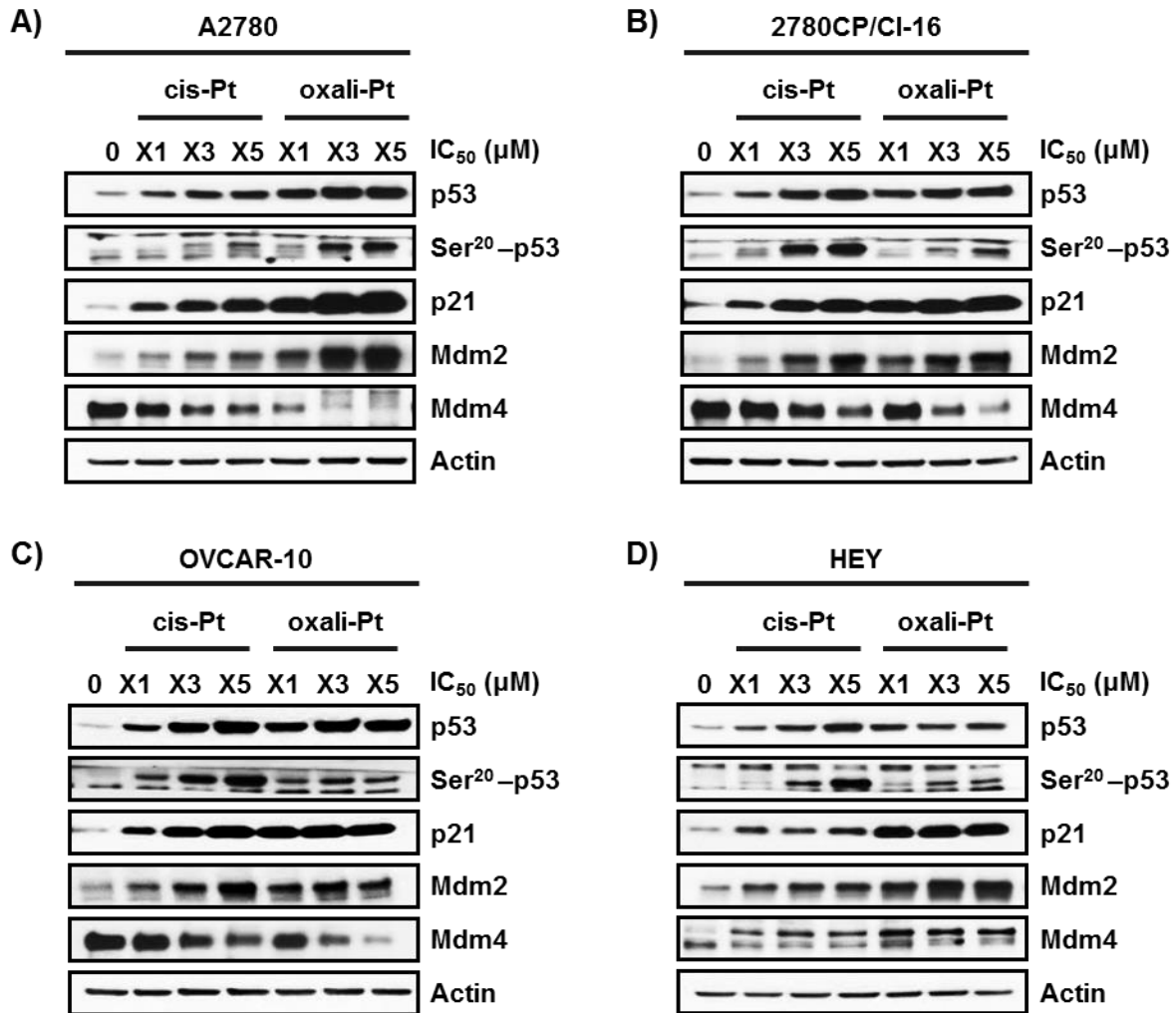


Figure 22. Expression and activation of p53 after cis-Pt or oxali-Pt treatment at equitoxic concentrations in the ovarian tumor panel

A) A2780, **B)** 2780CP/CI-16, **C)** OVCAR-10 and **D)** HEY cell lines treated with cis-Pt or oxali-Pt at equitoxic concentrations based on multiples of IC₅₀ (X1, X3 and X5) for 24 hr. Cell lines were collected and the immunoblot developed with the indicated antibody. **E)** Densitometric analysis of p21 bands in immunoblots shown in Figures A-D.

Table 18. Multiples of IC₅₀ (X1, X3 and X5) concentrations of cis-Pt and oxali-Pt used for treating the ovarian tumor panel

Pt-Compound	IC₅₀ (μM)	A2780	2780CP/CI-16	OVCAR-10	HEY
cis-Pt	X1	0.30	6.2	8.9	3.3
	X3	0.90	18.6	26.7	9.9
	X5	1.5	31.0	44.5	16.5
oxali-Pt	X1	0.15	0.20	0.28	0.60
	X3	0.45	0.60	0.84	1.8
	X5	0.75	1.0	1.4	3.0

4.2.8. Cis-Pt resistant ovarian tumor cell lines exhibit substantial downregulation of Chk2 as a common feature:

As suggested in the above section, resistance to cis-Pt in 2780CP/CI-16, OVCAR-10 and HEY may be due to mechanism(s) inhibiting facile activation of p53. One such mechanism may be related to Ser20 phosphorylation, which can regulate p21 transactivation, as seen in results obtained above with mutant p53-S20D plasmid. It has been reported that downregulation of Chk2, a kinase that phosphorylate p53 at Ser20 after cis-Pt treatment, leads to resistance [99;165]. In addition, our lab has previously reported that knock-down of Chk2 in A2780 cells reduced cis-Pt ability to induce p53 and p21 [180]. Therefore, it was reasonable to evaluate basal levels of Chk2 in the ovarian cancer panel, in order to assess if this kinase is downregulated in cis-Pt resistant cells. Indeed, the basal levels of Chk2 were substantially lower in all cis-Pt resistant cell lines (2780CP/CI-16, OVCAR-10, HEY and OVCA-433) than in A2780 cells (**Figure 23A** and **23B**). Thus, downregulation of Chk2 could account for failure of cis-Pt to induce p53-Ser20 phosphorylation, and provide an important mechanism in the development of cis-Pt resistance.

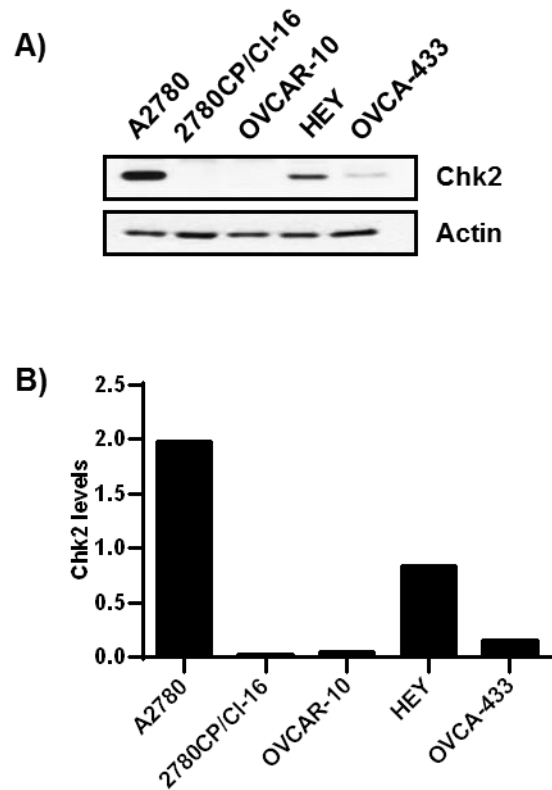


Figure 23. Cis-Pt resistant ovarian tumor cell lines exhibit substantial downregulation of Chk2 as a common feature

A) Evaluation of basal levels of Chk2 in A2780, 2780CP/CI-16, OVCAR-10, HEY and OVCA-433 cell lines. **B)** Densitometric analysis of immunoblots in Figure A.

4.2.9. Chk2 knock-out or knock-down in A2780 cells inhibits cis-Pt mediated phosphorylation of p53-Ser20 and p53 transcriptional activity:

To definitively test the inability of cis-Pt to induce p53-Ser20 phosphorylation and p53 transcriptional activity in absence of Chk2, Chk2^{-/-} clones were generated using the CRISPR technique. In addition, Chk2 silencing through siRNA transfection in cis-Pt sensitive A2780 cells was performed. In A2780 control clone, cis-Pt and oxali-Pt treatment after 24 hrs confirmed increases in total p53, p53-Ser15 phosphorylation, p53-Ser20 phosphorylation, p21 and Mdm2 levels and decreases in Mdm4 levels (**Figure 24A**). In addition, both drugs were shown to have no effect on total Chk2 but induce Chk2-Thr-68 phosphorylation. Similar results were also observed in A2780 cells transfected with control siRNA (**Figure 24B**). Immunoblots of A2780 Chk2^{-/-} clones and A2780 cells transfected with siRNA targeting Chk2 confirmed absence or substantial reduction of Chk2 (**Figure 24A and 24B**). Treatment of these Chk2 knock-out or knock-down cells with cis-Pt or oxali-Pt induced p53 and p53-Ser15 phosphorylation, but a slightly lower induction was noted with cis-Pt compared to control cells (**Figure 24A and 24B**). More importantly, the results show that p53-Ser20 phosphorylation and inductions of p21 and Mdm2 were severely diminished in Chk2 knock-out or knock-down cells after cis-Pt treatment in comparison to A2780 control cells (**Figure 24A and 24B**). In contrast, loss of Chk2 did not overtly affect the ability of oxali-Pt to induce p53-Ser20 phosphorylation, p21 and Mdm2. Finally, loss of Chk2 also impacted the ability of cis-Pt, but not oxali-Pt, to decrease levels of Mdm4 (**Figure 24A and 24B**). In conclusion, these results confirmed that Chk2 mediates cis-Pt-induced p53 phosphorylation at Ser20 and promote p53 transcriptional activity by increasing levels of p21 and Mdm2,

but that oxali-Pt induction of p53-Ser20 phosphorylation and p53 transcriptional activity occurs through a Chk2-independent pathway.

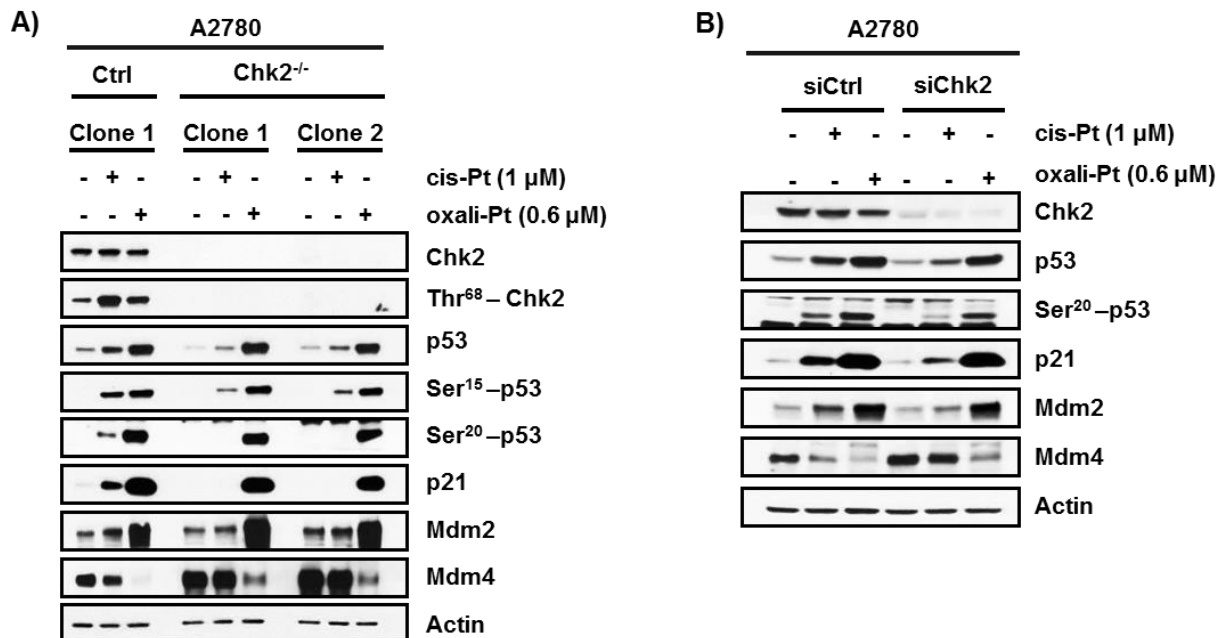


Figure 24. Downregulation of Chk2 in A2780 cells inhibits cis-Pt mediated phosphorylation of p53-Ser20 and p53 transcriptional activity

A) A2780 cell line was transfected with 25 μg of CRISPR/Cas-GFP plasmid. After 48 hr of transfection, GFP positive cells were collected and expanded. Chk2^{-/-} single clones were selected and characterized through Western blot. A2780 Chk2^{-/-} clones were exposed to cis-Pt 1 μM or oxali-Pt 0.6 μM for 24 hr. Proteins involved in the p53 pathway were examined through Western blot. **B)** A2780 cells were transfected with 100 nM of Control siRNA (siCtrl) or Chk2 siRNA (siChk2) for 48 hr. A2780 cells were treated with cis-Pt 1 μM or oxali-Pt 0.6 μM for 24 hr. Proteins involved in the p53 pathway were examined through Western blot.

4.2.10. Chk2 expression directly correlates with cytotoxic and therapeutic response to platinum:

The demonstration that cis-Pt is dependent on Chk2 for p53 stabilization and activation provided the rationale to investigate the involvement of Chk2 in Pt resistance in tumor models and ovarian cancer patients. Cytotoxicity experiments were conducted in A2780 control and Chk2^{-/-} clones using the standard 5-day MTT assay. The results demonstrate that IC₅₀ values of cis-Pt and oxali-Pt increased significantly (~2- to 3-fold) in A2780 Chk2^{-/-} clones when compared to controls (**Figure 25A** and **Table 19**). To demonstrate whether this increase in resistance after Chk2 knock-out was of clinical relevance, the TCGA data was mined to see the effect of Chk2 expression on survival of ovarian cancer patients in the clinic setting. Ovarian cancer patients were stratified as sensitive or resistant to Pt-therapy and further grouped according to Chk2 expression (high vs. low). In either sensitive or resistant patient group, high levels of Chk2 led to increased overall survival, whereas low levels of Chk2 was associated with reduced overall survival (**Figure 25B**). Thus, a low Chk2 expression inhibits cytotoxic response to cis-Pt not only in model systems, but also in patients.

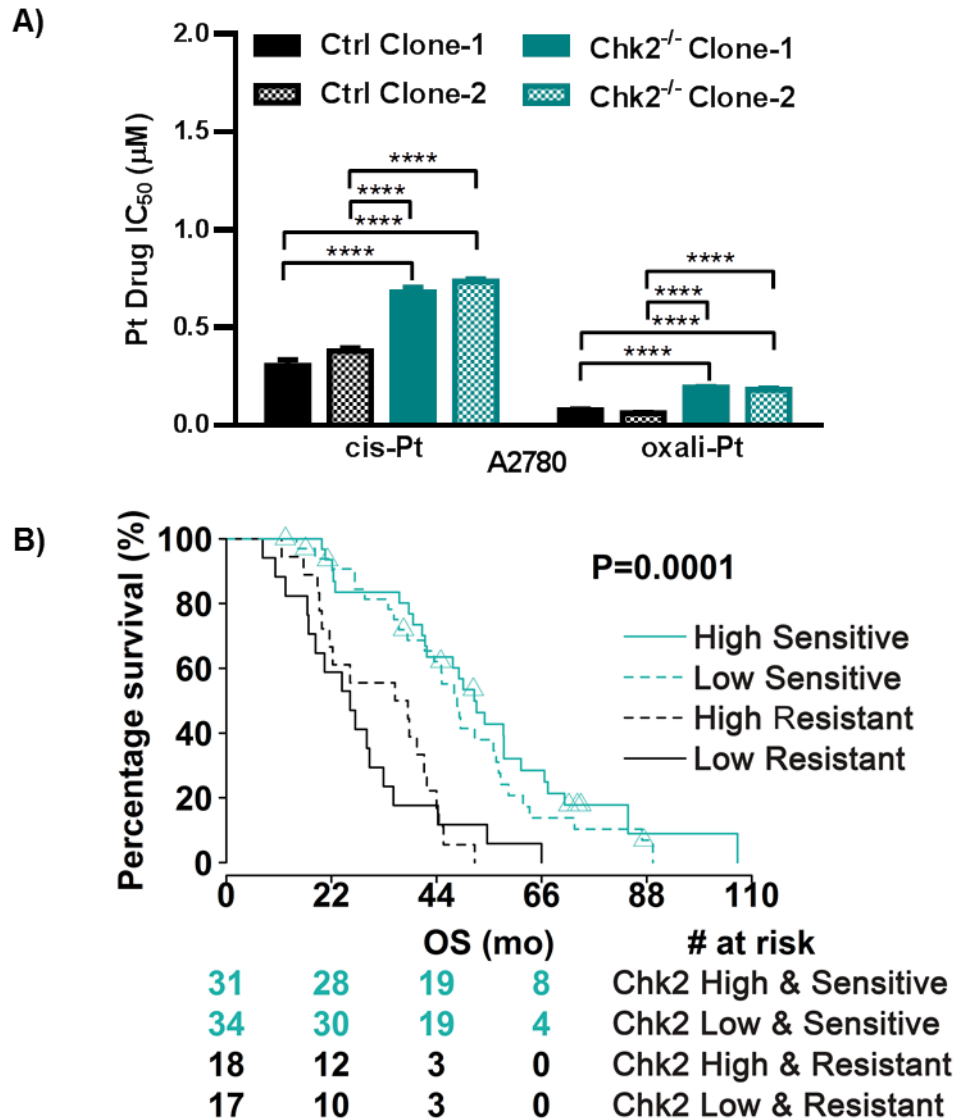


Figure 25. Chk2 expression directly correlates with cytotoxic and therapeutic response to platinum

A) Cytotoxicity of cis-Pt or oxali-Pt was assessed in A2780 Chk2^{-/-} clones. Cells were continuously exposed to a range of Pt concentrations for 5 days at 37°C. IC₅₀ values were determined using Prism. ANOVA test was used to determine statistical significance, p value ≤0.05. N=3; Mean ± SD **B)** Kaplan-Meier curves for ovarian cancer patients grouped into high and low levels of Chk2 and further stratified according to Pt status. The analysis was carried out in R (version 3.2.2). All the tests were two-sided and considered statistically significant at p value ≤0.05.

**Table 19. IC₅₀ values (μM) of Pt drugs in A2780
Chk2^{-/-} cells**

Pt-Drug	Clones	A2780
cis-Pt	Ctrl-1	0.305 ± 0.030
	Ctrl-2	0.379 ± 0.017
	Chk2^{-/-}-1	0.682 ± 0.024
	Chk2^{-/-}-2	0.736 ± 0.012
oxali-Pt	Ctrl-1	0.0780 ± 0.0040
	Ctrl-2	0.0620 ± 0.0030
	Chk2^{-/-}-1	0.1940 ± 0.0030
	Chk2^{-/-}-2	0.1820 ± 0.0070

4.2.11. Chk2 knock-in restores the capacity of cis-Pt to induce p53 transcriptional activation and increase cytotoxicity in A2780 Chk2^{-/-} cells:

Evidence has been provided that loss or low expression of Chk2 leads to cis-Pt resistance or poor survival of ovarian cancer patients treated with Pt-based therapy. In order to further validate Chk2 as a key kinase required for cis-Pt to induce p53 transcriptional activity and regulate Pt sensitivity, Chk2 knock-in experiments in A2780 Chk2^{-/-} cells were executed. The results in **Figure 26A** show that transfection of Chk2 plasmid led to good expression of Chk2. As expected, cis-Pt treatment in A2780 Chk2^{-/-} cells transfected with empty vector (EV) did not induce p21 expression. In contrast, oxali-Pt treatment in A2780 Chk2^{-/-} cells transfected with EV was able to promote p21 expression, which confirmed earlier data presented. However, cis-Pt treatment after Chk2 knock-in in A2780 Chk2^{-/-} restored the ability of cis-Pt to induce p21 expression, but no further increase in p21 expression was noted with oxali-Pt (**Figure 26A**). These studies were also extended to determine cytotoxicity of Pt drugs after Chk2 knock-in in A2780 Chk2^{-/-} cells by measuring IC₅₀ values using the MTT assay. In A2780 Chk2^{-/-} cells transfected with Chk2, a significant decrease in IC₅₀ values of cis-Pt and oxali-Pt was observed when compared to A2780 Chk2^{-/-} cells transfected with EV (**Figure 26B** and **Table 20**).

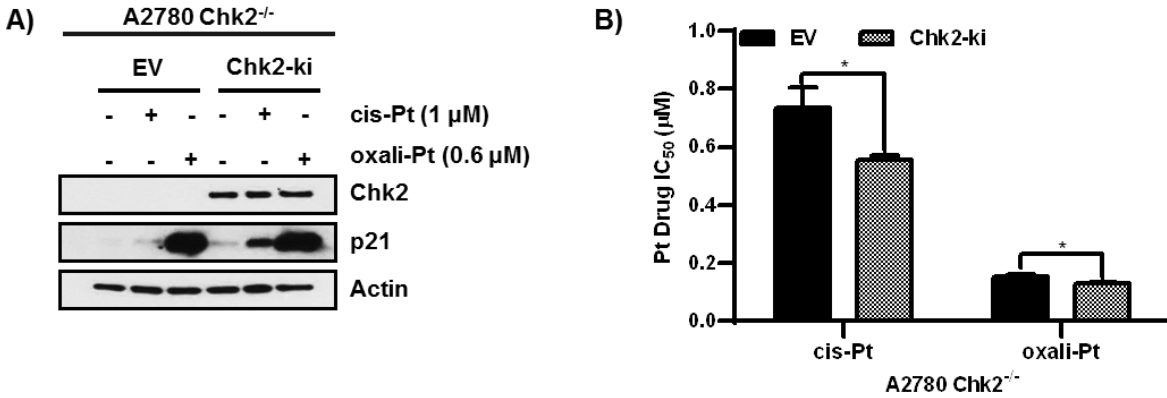


Figure 26. Chk2 knock-in restores the capacity of cis-Pt to induce p53 transcriptional activation and increase cytotoxicity in A2780 Chk2^{-/-} cells

A) A2780 Chk2^{-/-} cells were transfected with 2 μg of pEGFP-C1 control (EV) or Chk2 (Chk2-ki) expression vectors for 48 hr. Cells were treated with cis-Pt 1 μM or oxali-Pt 0.6 μM for 24 hr and processed for Western blot analysis. **B)** A2780 Chk2^{-/-} cells were transfected with 2 μg of pEGFP-C1 control (EV) or Chk2 (Chk2-ki) expression vectors for 24 hr. Cells were continuously exposed to a range of Pt concentrations for 3 days at 37°C. IC₅₀ values were determined using Prism. Student's t-test was used to determine statistical significance, p value ≤ 0.05. N=3; Mean ± SD

Table 20. IC₅₀ values (μM) of Pt drugs in A2780 Chk2^{-/-} cells after Chk2 knock-in

Pt-Drug	Plasmid	IC ₅₀ (μM)
cis-Pt	EV	0.735 ± 0.040
	Chk2	0.554 ± 0.010
oxali-Pt	EV	0.1520 ± 0.0050
	Chk2	0.1300 ± 0.0040

4.2.12. Examination of mechanism of Chk2 downregulation in cis-Pt resistant

cells:

The demonstration that Chk2 is important in cis-Pt mediated activation of p53 and greater cytotoxic response made it necessary to examine the mechanism of Chk2 downregulation in cis-Pt-resistant cells at the transcript and protein level. Relative expression levels of *CHEK2* transcripts were examined in A2780, 2780CP/CI-16, OVCAR-10, HEY and OVCA-433 cell lines by RT-PCR (**Figure 27A**). Results show that *CHEK2* transcript levels are significantly reduced in these cis-Pt resistant cell lines compared to cis-Pt sensitive A2780 cells. Therefore, transcriptional regulation of *CHEK2* transcripts plays a role in downregulation of Chk2 in cis-Pt resistant cells. To further examine if Chk2 downregulation is also regulated at the protein level, the involvement of enhanced proteasomal degradation was evaluated in A2780, 2780CP/CI-16, OVCAR-10, HEY and OVCA-433 cell lines using MG132 (**Figure 27B**). MG132 is a specific, potent, reversible and cell-permeable proteasome inhibitor, which results in inhibition of the degradation of ubiquitin-conjugated proteins. For this experiment p53 was used as an experimental control. Data shows that p53 levels increased in the ovarian tumor panel when treated with MG132, as a result inhibition of p53 proteasomal degradation was obtained. However, MG132 treatment did not increase levels of Chk2 compared to control in the ovarian tumor panel, which could be possible if the half-life of Chk2 was long. To test this possibility, the stability of Chk2 was examined in A2780 cells using cycloheximide, which serves as an inhibitor of protein biosynthesis. Using p53 as an experimental control, the results show that over time, p53 levels by immunoblot decrease (**Figure 27C**) with a p53 half-life of 0.43 hr (**Figure**

27D). In contrast, Chk2 levels did not change over time (**Figure 27C**) resulting in a long Chk2 half-life of ~29 hr (**Figure 27D**). This long half-life indicates that protein degradation may not be rapid enough to affect low levels of Chk2 in resistant cells. Hence, Chk2 downregulation in cis-Pt resistant cells occurs at the transcriptional level.

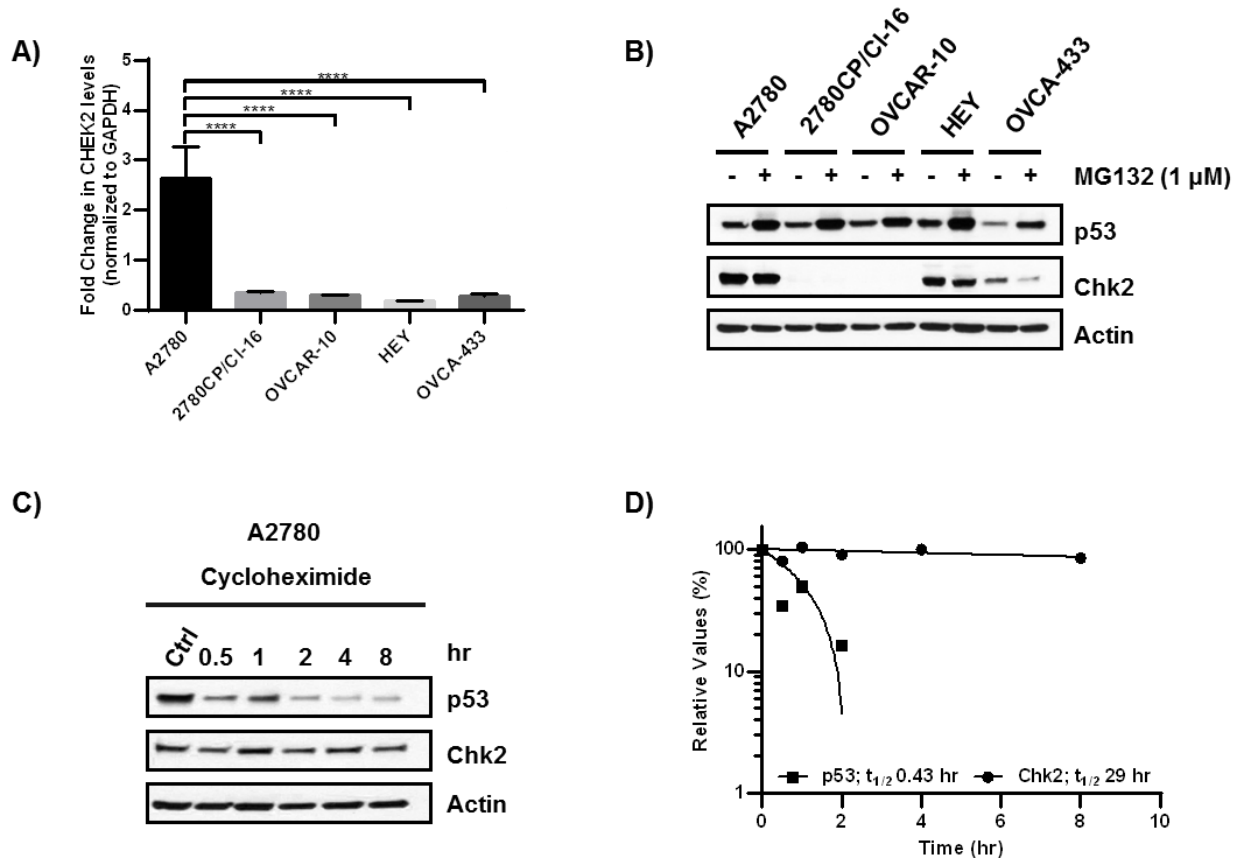


Figure 27. Examination of Chk2 downregulation in cis-Pt resistant cells

A) RT-PCR was performed using 1 μg of RNA from A2780, 2780CP/CI-16, OVCAR-10, HEY and OVCA-433 cell lines to examine expression levels of *CHEK2*, using the internal control *GAPDH*. Relative expression levels were calculated using the $2^{-\Delta Ct}$ method. **B)** A2780, 2780CP/CI-16, OVCAR-10, HEY and OVCA-433 cell lines were treated with DMSO or 1 μM of MG132 for 6 hr at 37°C and processed for Western blot analysis. **C)** A2780 cell line was treated with DMSO or 4 μM of cycloheximide for 0.5 hr, 1 hr, 2 hr, 4 hr and 8 hr at 37°C and processed for Western blot analysis. **D)** p53 and Chk2 half-lives determined from Relative Protein Values (%) vs Time (hr) using Prism software. Student's t test was used to determine statistical significance, p value ≤0.05. N=3; Mean ± SD

4.2.13. Analysis of CpG island methylation of *CHEK2* in the ovarian tumor panel:

It has been previously reported in gliomas and non-small cell lung cancer that Chk2 downregulation is due to promoter methylation [152;153]. Since cis-Pt resistant cells showed decreased levels of *CHEK2* transcripts, the presence of CpG island methylation in the *CHEK2* promoter regions in A2780, 2780CP/CI-16, OVCAR-10, HEY and OVCA-433 cell lines was determined. Basic Local Alignment Search Tool (BLAST) analysis of *CHEK2* identified two promoter regions of interest for this study (**Figure 28A**). S1 and S2 are primers that recognize exon 1 region and S3 is a primer targeting exon 2 region. Bisulfite pyrosequencing and methylation-specific PCR (MSP) analysis identified that *CHEK2* exon 1 is not methylated in A2780, 2780CP/CI-16, OVCAR-10, HEY and OVCA-433 cell lines. In contrast, these cell lines in general exhibited methylation at *CHEK2* exon 2 (**Figure 28B** and **28C**). Therefore, there was no difference in *CHEK2* methylation between cis-Pt sensitive and resistant cells and decrease in levels of *CHEK2* transcripts is not due to promoter methylation.

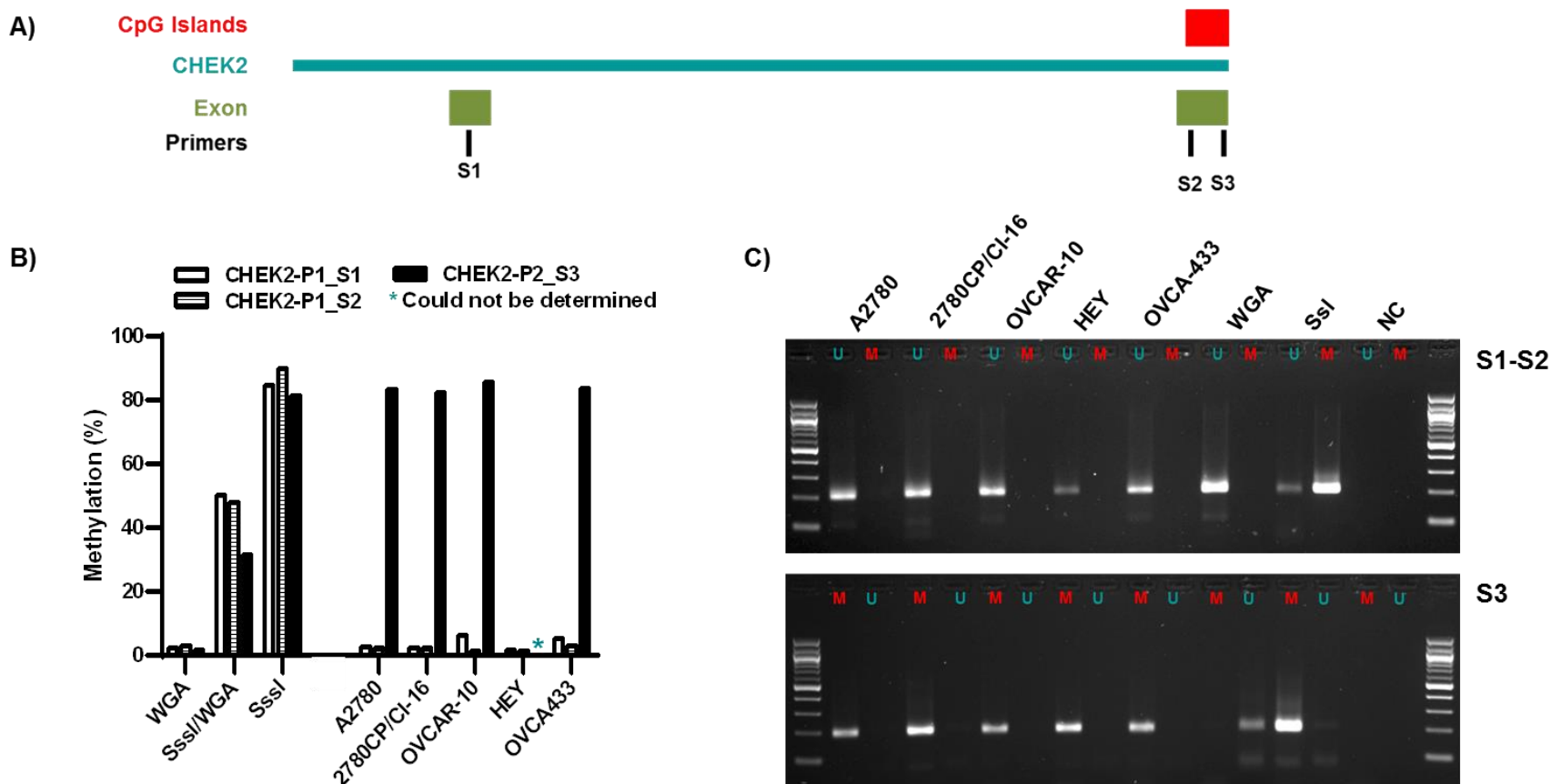


Figure 28. Analysis of CpG island methylation of *CHEK2* in the ovarian tumor panel

A) Schematic representation of CpG island analysis (•) in *CHEK2* gene (•). Exon 1 region is targeted by S1 and S2 primers and exon 2 region is targeted by S3 primer. **B)** Bisulfite pyrosequencing analysis in DNA samples from A2780, 2780CP/CI-16, OVCAR-10, HEY and OVCA-433 cell lines. **C)** Methylation-specific PCR (MSP) analysis in DNA samples from A2780, 2780CP/CI-16, OVCAR-10, HEY and OVCA-433 cell lines. Bisulfite pyrosequencing and MSP experiments were performed with experimental controls SssI (methyltransferase) and whole genome amplification (WGA).

4.2.14. Expression levels of microRNAs predicted to target *CHEK2*:

Since Chk2 is not regulated in cis-Pt resistant cells by promoter hypermethylation, it was appropriate to consider microRNA as a possible explanation. Regulation of *CHEK2* transcripts through microRNA was studied using the miRBase: the microRNA database (microRNA.org). Predicted microRNAs for *CHEK2* regulation were miR-134, -300, -340, -381 and -425 and their affinity predicted score values were 105, 67, 60, 67 and 28, respectively (**Figure 29A** and **Table 21**). Only significant expression of miR-340 and miR-425 were detected in A2780, 2780CP/CI-16, OVCAR-10, HEY and OVCA-433 by RT-PCR. There was no specific pattern observed in the expression levels of miR-340 and miR-425 between cis-Pt sensitive A2780 vs. cis-Pt resistant 2780CP/CI-16, OVCAR-10, HEY and OVCA-433 cell lines which could help explain the difference in levels of Chk2 between these two groups (**Figure 29B**). Therefore, it is possible that microRNA is not the mechanism suppressing *CHEK2* transcripts. On the other hand, in the isogenic pair of cell lines A2780 and 2780CP/CI-16, both microRNA-340 and -425 were upregulated in the cis-Pt resistant cell line (2780CP/CI-16) suggesting that there could be a relationship with *CHEK2* suppression when cell lines of the same genetic background are compared.

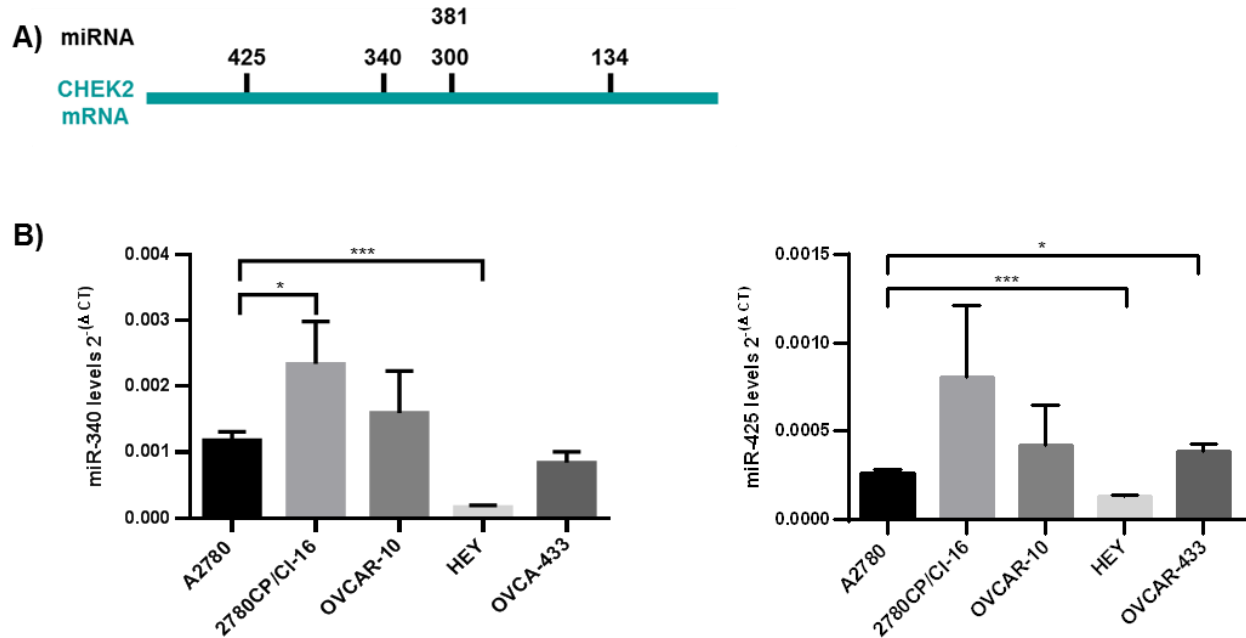


Figure 29. Expression levels of microRNAs predicted to interact with *CHEK2*:

A) Schematic representation of the expected interaction of microRNAs (•) with *CHEK2* (•). **B)** Levels of expression of microRNAs-340 and -425 in A2780, 2780CP/CI-16, OVCAR-10, HEY and OVCA-433 cell lines using RT-PCR. MicroRNAs-134, -300, -340, -381 and -425 were not detected. MicroRNAs -340 and -425 were expressed in all the cell lines tested and their levels of expression are reported as $2^{-\Delta Ct}$ values. Student's t test was used to determine statistical significance, p value ≤ 0.05 . N=3; Mean \pm SD

Table 21. miRNAs predicted to target *CHEK2* using miRBase: the microRNA database

miRNAs	Score Values
-134	105
-300	67
-340	60
-381	67
-425	28

4.2.15. Examination of Chk2 expression by miR-340 and miR-425:

Since levels of miR-340 and miR-425 appeared to be high in the cis-Pt resistant 2780CP/CI-16 vs. cis-Pt sensitive A2780 cell lines, the role of these microRNAs in regulating Chk2 expression by transfecting A2780 cells with pre-miR-340 and pre-miR-425 for 48 hr and 72 hr was examined. The excellent miR-340 and miR-425 transfection efficiency in A2780 at 48 hr and 72 hr was followed by RT-PCR (**Figure 30A**). However, high levels of miR-340 and miR-425, and even combinations of the two, were not able to completely abolish Chk2 expression (**Figure 30B** and **30C**). As a consequence, miR-340 and miR-425 are not implicated in the mechanism responsible for decreased levels of *CHEK2* transcripts.

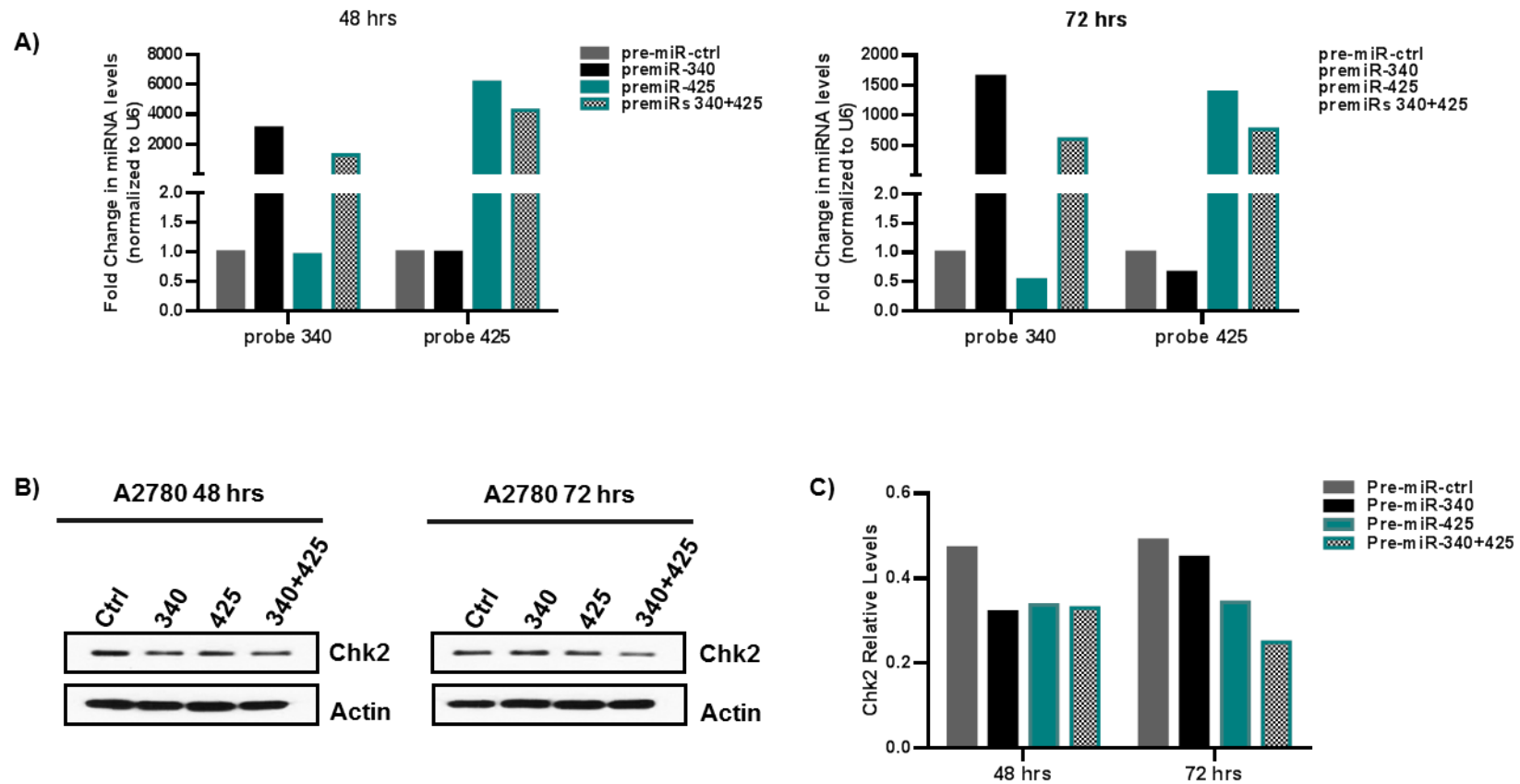


Figure 30. Examination of Chk2 regulation by miR-340 and miR-425

A) Expression levels of miR-340 and miR-425 in A2780 cells transfected with 100 nM of pre-miR-Ctrl, pre-miR-340 or pre-miR-425 for 48 hr and 72 hr using RT-PCR. **B)** Western blot analysis of Chk2 levels in A2780 cells transfected with 100 nM of pre-miR-Ctrl, pre-miR-340 or pre-miR-425 for 48 hr and 72 hr. **C)** Densitometric analysis of Chk2 relative levels in A2780 cells transfected with 100 nM of pre-miR-Ctrl, pre-miR-340 or pre-miR-425 for 48 hr and 72 hr.

4.3. Conclusions:

DNA sequencing has identified the cis-Pt-sensitive A2780 cell line as wild-type p53 and the cis-Pt resistant 2780CP/CI-16, OVCAR-10, HEY and OVCA-433 cells as containing p53 missense mutations. Although the dogma exists that p53 mutation leads to p53 inactivation and Pt resistance, the studies performed in this Chapter indicate that this is not always the case. It has been shown that mutation in p53 did not prevent normal p53 function in cis-Pt resistant cells challenged with the non-cross-resistant Pt analog oxali-Pt. In fact, p53^{-/-} clones responded differently to cis-Pt or oxali-Pt treatment. In the case of cis-Pt, knock-out of p53 led to increase in IC₅₀ values in A2780 and 2780CP/CI-16 clones but decrease in OVCAR-10 and HEY clones. Interestingly, oxali-Pt cytotoxicity relies on the presence and functionality of p53 in all four cell lines, as indicated by the significant increase in oxali-Pt IC₅₀ values in p53 knock-out cell clones. Further studies have indicated that these two Pt agents exert different post-translational modifications in p53 resulting in different ways to regulate p53 activity. Indeed, oxali-Pt is able to trigger a more robust p53 response and this leads to greater p53 transcriptional activity, as indicated by p21 and Mdm2 levels, compared to cis-Pt in the resistant cell lines. The capacity of each Pt compound to induce p53 expression and p53 transcriptional activity was shown to correlate with their potential to induce p53-Ser20 phosphorylation. It was also shown that p53-Ser20 phosphorylation strongly enhances p21 expression, thus, p53-Ser20 phosphorylation is a good marker to assess p53 transcriptional activation. In addition, cis-Pt resistant ovarian tumor cell lines exhibited substantial downregulation of Chk2, a kinase that has been shown to induce p53-Ser20 phosphorylation after cis-Pt treatment. Chk2 downregulation in cis-Pt

resistant cell lines occurs at the transcriptional level. Indeed, Chk2 knock-out or knock-down in A2780 cells inhibited cis-Pt mediated phosphorylation of p53-Ser20 and p53 transcriptional activity. In contrast, loss of Chk2 did not affect the ability of oxali-Pt to induce p53-Ser20 phosphorylation nor p53 transcriptional activity. Furthermore, Chk2 knock-out in A2780 cells led to cis-Pt and oxali-Pt resistance. Finally, in the clinic setting this Chapter also demonstrates that Pt sensitive or resistant ovarian cancer patients with high levels of Chk2 had increased overall survival when compared to corresponding patients expressing low levels of Chk2. In conclusion, cis-Pt mechanism of action has been elucidated (**Figure 31**). In essence, Chk2 is an important kinase that mediates cis-Pt response by phosphorylating p53 at Ser20 and promote p53 transcriptional activity. That is, presence of Chk2 is essential for cis-Pt cytotoxic response in tumor cells and in patients. However, parallel studies in this Chapter show that oxali-Pt induction of p53-Ser20 phosphorylation and p53 transcriptional activity occurs through a Chk2-independent pathway. Therefore, oxali-Pt mechanism of action will be investigated in Chapter 5.

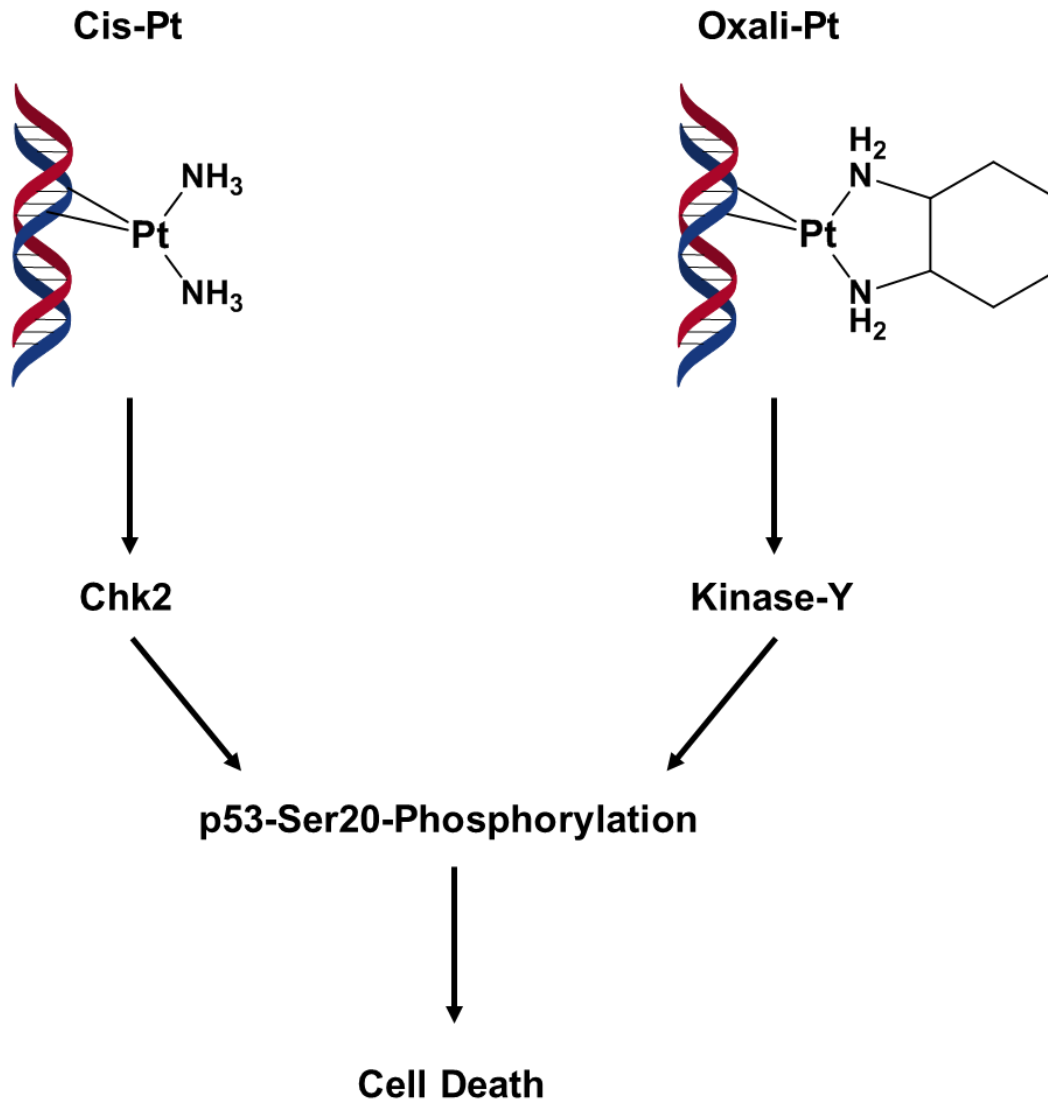


Figure 31. Conclusions Chapter 4

Chk2 is essential for cis-Pt to phosphorylate p53 at Ser20 and to promote p53 transcriptional activity. In contrast, oxali-Pt induction of p53-Ser20 phosphorylation and p53 transcriptional activity through a Chk2-independent pathway.

Chapter 5

To define the novel mechanism of action of the structurally-distinct lead analog that circumvents cisplatin resistance

5.1. Rationale and Background:

It has been shown that cis-Pt and oxali-Pt induce different DNA damage, due to their different carrier ligands, which leads to the activation of distinct signal transduction pathways. That is, the two drugs have different mechanisms of action. However, Pt-induced DNA damage signaling by both drugs converges to trigger phosphorylation of p53 by upstream activation of transducer kinases, and such phosphorylation of p53 is required for its transcriptional activation. There are multiple sites in p53 that can be phosphorylated, and each site can be targeted by multiple kinases, which suggests some redundancy [31]. The focus of attention in this chapter is the Ser20 site as the data in Chapter 4 demonstrates that cis-Pt fails to promote p53-Ser20 phosphorylation and p53 transcriptional activity due to downregulation of Chk2 in ovarian cancer cell lines resistant to cis-Pt. Whereas, it was observed that oxali-Pt is able to induce p53-Ser20 phosphorylation and p53 transcriptional activity in the same cell lines through a Chk2-independent pathway. Therefore, the aim of this study is to delineate the mechanism of action of oxali-Pt. More specifically, identification of the unknown novel kinase activated by oxali-Pt to promote p53-Ser20 phosphorylation and p53 transcriptional activity in ovarian cancer cell lines resistant to cis-Pt is a primary goal. To accomplish this goal, RPPA analysis will be conducted following exposure to cis-Pt and oxali-Pt of isogenic cis-Pt sensitive A2780 and cis-Pt resistant 2780CP/CI-16 cell lines. The RPPA array provides an opportunity to investigate a series of untested kinases for Ser20 phosphorylation of p53 that may enhance insights in the field of Pt treatment.

5.2. Results:

5.2.1. Time-dependent activation of p53 in A2780 and 2780CP/CI-16 by cis-Pt and oxali-Pt:

The results in Chapter 4 have demonstrated that cis-Pt lacks the ability to phosphorylate p53 at Ser20, but oxali-Pt has full capacity to modify this site. However, those studies examined immunoblots at 24 hr. Since it was possible that an earlier timepoint may be more desirable for additional investigations, it was appropriate to study the p53 pathway in response to cis-Pt and oxali-Pt in a time dependent manner in cis-Pt sensitive A2780 and cis-Pt resistant 2780CP/CI-16 cell lines. As uncovered in Chapter 4, expression of Chk2 was observed in A2780, but not in 2780CP/CI-16 cells (**Figure 32A-B**). Cis-Pt promoted Chk2-Thr68 phosphorylation, which was maximal in A2780 cells at 12 hr. In A2780 and 2780CP/CI-16 cell lines, cis-Pt treatment increased levels of total p53 and p53-Ser15 phosphorylated form in a time dependent manner, with maximal levels observed at 24 hr. Furthermore, cis-Pt treatment in A2780 was able to induce p53-Ser20 phosphorylation, p21 and Mdm2 at 12 hr and the levels at this time point were either maintained or further increased at 24 h (**Figure 32A**). Interestingly, in cis-Pt resistant 2780CP/CI-16 cells, cis-Pt treatment only promoted minimal increases in p53-Ser20 phosphorylation, p21 and Mdm2 levels when compared to the levels observed in A2780 (**Figure 32A**). However, p53-Ser15 phosphorylation by cis-Pt in resistant cells remained robust, although p53 induction was attenuated. This confirms that p53-Ser15 phosphorylation likely contributes to p53 stabilization, and does not appear to be associated in a significant way to transactivation of p21 or Mdm2. On the other hand, oxali-Pt treatment of A2780 and 2780CP/CI-16 cell lines leads to robust

induction in a time dependent manner of p53-Ser15 and p53-Ser20 phosphorylation, and p53, p21 and Mdm2 proteins (**Figure 32B**). Although Chk2-Thr68 phosphorylation was observed in A2780 cells only, it is clear that this Chk2 activation was not required for p53-Ser20 phosphorylation by oxali-Pt, which reaffirms conclusions in Chapter 4. Thus, oxali-Pt treatment in 2780CP/CI-16 produces similar temporal changes as those seen in A2780. Based on these observations, the 24 hr treatment time with oxali-Pt and cis-Pt appears appropriate for further investigations, including RPPA analysis.

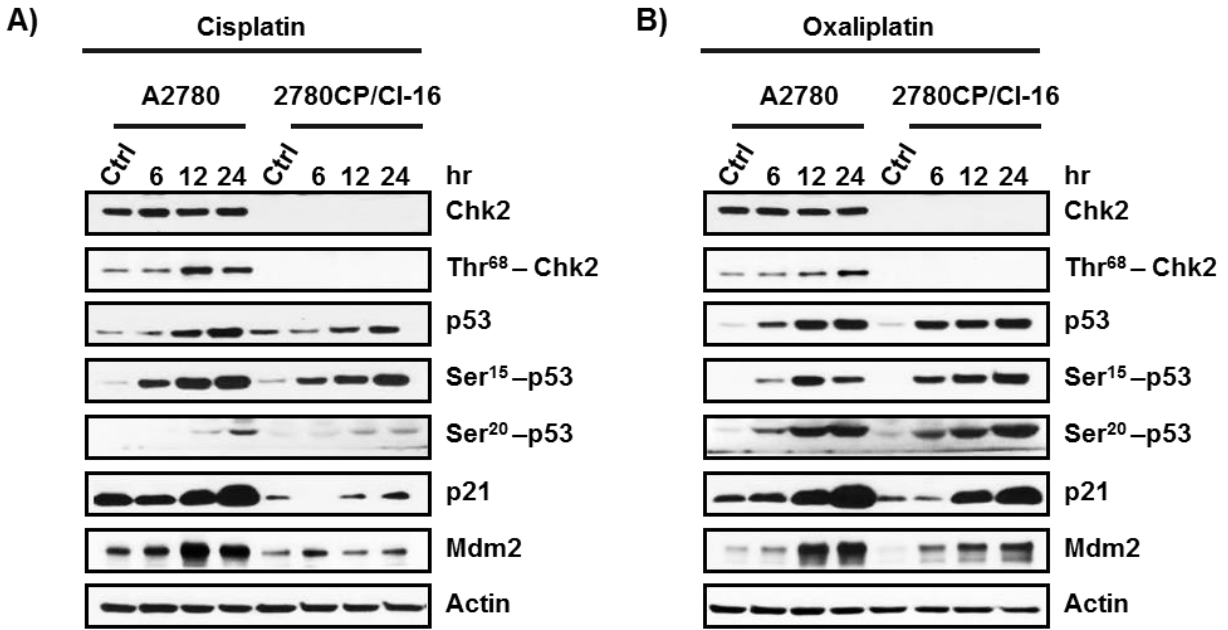


Figure 32. Time-dependent activation of p53 in A2780 and 2780CP/CI-16 by cis-Pt and oxali-Pt

A) p53 pathway response in A2780 cells treated with cis-Pt 1 μ M and in 2780CP/CI-16 cells treated with cis-Pt 5 μ M for 6 hr, 12 hr and 24 hr. **B)** p53 pathway response in A2780 cells treated with oxali-Pt 0.6 μ M and in 2780CP/CI-16 cells treated with oxali-Pt 3 μ M for 6 hr, 12 hr and 24 hr.

5.2.2. Analysis of differences in the mechanism of action of cis-Pt vs. oxali-Pt in A2780 and 2780CP/CI-16:

The drug exposure time of 24 hr was established in the preceding section for undertaking RPPA analysis. The approach taken was to treat cis-Pt sensitive A2780 and its isogenic cis-Pt resistant 2780CP/CI-16 with cis-Pt or oxali-Pt, but before submitting samples for RPPA analysis by the Core Facility, differential drug effects at the level of p53-Ser20 phosphorylation on the same immunoblots were confirmed. In essence, the data confirm that A2780, but not 2780CP/CI-16, contains p53-Ser20 phosphorylation when exposed to cis-Pt, whereas oxali-Pt induces p53-Ser20 phosphorylation to a similar level in both cell lines (**Figure 33A**). The resultant differential effects of the two Pt drugs in 2780CP/CI-16 cells were also confirmed for p21 and Mdm2 inductions and Mdm4 degradation. As observed in **Section 5.2.1**, phosphorylation of p53 at Ser15 was not drastically different between the two Pt drugs. These results demonstrate that specific responses to the two drugs in A2780 and 2780CP/CI-16 cells is reproducible and validate the samples for processing by the RPPA facility. The heat map obtained from RPPA analysis is shown in **Figure 33B**. Relative expression by RPPA of over 217 proteins are presented in the **Appendix**.

5.2.3. Analysis of RPPA data to identify the unknown kinase responsible for p53 phosphorylation at Ser20 and p53 transcriptional activation by oxali-Pt:

To identify hits of possible kinases responsible for p53-Ser20 phosphorylation and p53 transcriptional activity in cis-Pt resistant 2780CP/CI-16 cell line by oxali-Pt, the RPPA data obtained (**Section 5.2.2**) was subjected to different intersections. For these studies, the intersection of interest is the one exhibiting a significant increase in the signal obtained from A2780 treated with cis-Pt and oxali-Pt, and 2780CP/CI-16 treated with oxali-Pt only. This is depicted as A2780 cis-Pt up, A2780 oxali-Pt up and 2780CP/CI-16 oxali-Pt up (**Figure 34A**). This stipulation is based on the premise that the unknown kinase can be activated by either cis-Pt or oxali-Pt in sensitive cells, but only oxali-Pt can activate it in resistant cells. Based on this intersection, five proteins were identified: p53, BAX, MAPK pT202_Y204, Mcl-1 and Notch1 (**Figure 34B**). The only positive kinase hit was MAPK pT202_Y204, which is also known as p-ERK1/2-T202/Y204. These results provided the basis to study the involvement of the MAPK pathway; either the ERK1/2 kinase or upstream kinase MEK1/2 in mediating p53 phosphorylation at Ser20 and p53 transcriptional activation after oxali-Pt treatment. Validation of these RPPA results for the kinases by Western blot analysis was employed (**Figure 34C**). In general, total levels of MEK1/2 and ERK1/2 remain largely unchanged after cis-Pt and oxali-Pt treatment in A2780 and 2780CP/CI-16 cells. Moreover, levels of MEK1/2-S217/221 phosphorylation increased in A2780 and 2780CP/CI-16 after cis-Pt and oxali-Pt treatment. Finally, it was observed that the level of ERK1/2-T202/Y204 phosphorylation is lower in 2780CP/CI-16 cells compared to A2780 cells after cis-Pt treatment. In contrast, ERK1/2-T202/Y204 phosphorylation was

robust in both cell lines after oxali-Pt treatment (**Figure 34C**). These results positively validate the RPPA data.

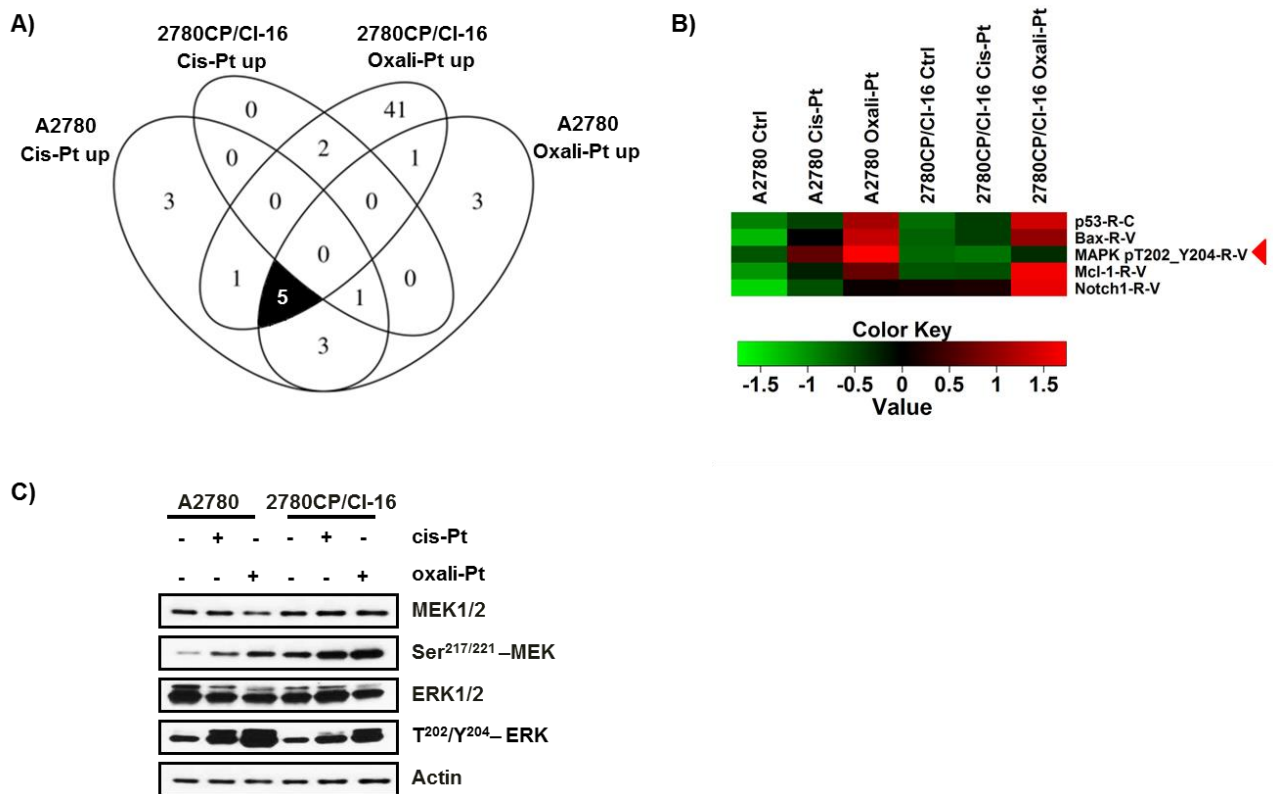


Figure 34. Analysis of RPPA data to identify the unknown kinase responsible for p53 phosphorylation at Ser20 and p53 transcriptional activation by oxali-Pt

A) Diagram for RPPA analysis from A2780 treated with cis-Pt 1 μ M or oxali-Pt 0.6 μ M and 2780CP/CI-16 treated with cis-Pt 5 μ M or oxali-Pt 3 μ M for 24 hr. Only proteins significantly upregulated (up) by Pt treatment were included in the analysis. **B)** Output obtained from the intersection A2780 cis-Pt up, A2780 oxali-Pt up and 2780CP/CI-16 oxali-Pt up. **C)** RPPA data validation through Western blot analysis in A2780 treated with cis-Pt 1 μ M or oxali-Pt 0.6 μ M and 2780CP/CI-16 treated with cis-Pt 5 μ M or oxali-Pt 3 μ M for 24 hr.

5.2.4. Involvement of ERK1/2 in mediating p53 phosphorylation at Ser20 and p53 transcriptional activation by oxali-Pt:

To further explore the involvement of ERK1/2 as the novel kinase required by oxali-Pt to exert its mechanism of action, the ERK1/2 SCH772984 inhibitor was used. SCH772984 is a novel, specific inhibitor of ERK1/2 with IC₅₀ of 4 nM and 1 nM, respectively, which has been shown to inhibit ERK1/2 phosphorylation at T202/Y204 [163;164]. The capacity of SCH772984 to inhibit ERK1/2-T202/Y204 phosphorylation was examined at 0.5 µM, 1.5 µM and 5 µM for 1 hr and 24 hr in 2780CP/CI-16 (**Figure 35A**). The data show 1.5 µM of SCH772984 as the optimal concentration to inhibit ERK1/2 phosphorylation at T202/Y204; thus, this concentration was selected for further experiments involving SCH772984. The capacity of oxali-Pt to induce p53-Ser20 phosphorylation and p53 transcriptional activation in cis-Pt resistant 2780CP/CI-16 cell line through an ERK1/2 dependent manner was then evaluated. Thus, 2780CP/CI-16 cells were treated with the ERK1/2 inhibitor SCH772984 or DMSO for 1 hr followed by cis-Pt or oxali-Pt treatment for 24 hr (**Figure 35B**). The data shows that SCH772984 was able to inhibit ERK1/2-T202/Y204 phosphorylation. Moreover, 2780CP/CI-16 cells treated with cis-Pt treatment in combination with SCH772984 for 24 hr exhibited a reduction in p53 and p53-Ser15 phosphorylation levels. In addition, induction of p53-Ser20 phosphorylation and p21 were not observed after cis-Pt treatment in 2780CP/CI-16 cells treated with DMSO or SCH772984. Finally, SCH772984 did not impact the ability of oxali-Pt to induce p53, p53-Ser15 phosphorylation, p53-S20 phosphorylation and p21 expression in 2780CP/CI-16 cells since high levels of these proteins were obtained after oxali-Pt treatment in DMSO and SCH772984 treated cells. As a

conclusion, these results demonstrate that ERK1/2 is not the kinase activated by oxali-Pt to restore p53-Ser20 phosphorylation and p53 transcriptional activity in the cis-Pt resistant 2780CP/CI-16 cell line.

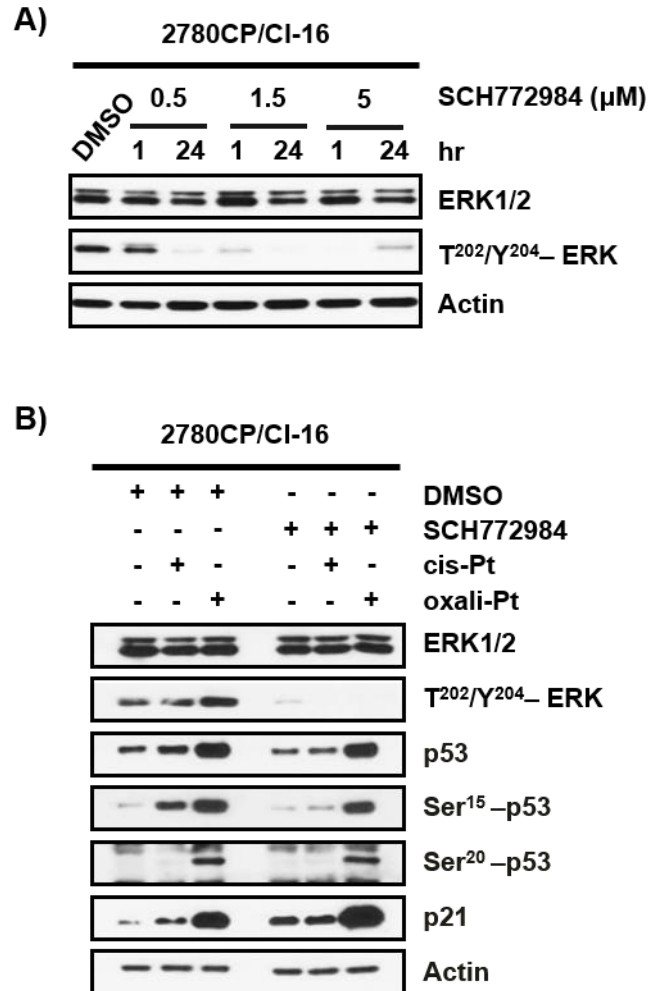


Figure 35. Involvement of ERK1/2 in p53 phosphorylation at Ser20 and p53 transcriptional activation by oxali-Pt

A) Evaluation of ERK1/2-T202/Y204 phosphorylation levels in 2780CP/CI-16 treated with 0.5 μM , 1.5 μM and 5 μM of the ERK1/2 inhibitor SCH772984 for 1 hr and 24 hr.

B) Evaluation of the p53 signaling pathway in 2780CP/CI-16 pre-treated with SCH772984 1.5 μM for 1 hr and treated with cis-Pt 5 μM or oxali-Pt 3 μM for 24 hr.

5.2.5. Involvement of MEK1/2 in p53 phosphorylation at Ser20 and p53 transcriptional activation by oxali-Pt:

Since ERK1/2 is not the kinase involved in Ser20 phosphorylation of p53 by oxali-Pt in 2780CP/CI-16 cells, but is itself phosphorylated by MEK1/2, it was rational to evaluate the involvement of MEK1/2 as the novel kinase required by oxali-Pt to exert its mechanism of action. This was assessed by using the MEK1/2 inhibitor, U0126 [165]. To determine the appropriate concentration of U0126 to be used in the study, a concentration-response relationship of U0126 was evaluated using 1 μ M, 5 μ M, 10 μ M, 25 μ M, 50 μ M, 75 μ M and 100 μ M for 24 hr in 2780CP/CI-16 cells (**Figure 36A**). The results obtained indicate 1 μ M of U0126 as the lowest concentration able to inhibit ERK1/2 phosphorylation at T202/Y204. Next, oxali-Pt induction of p53-Ser20 phosphorylation and p53 transcriptional activation in cis-Pt resistant 2780CP/CI-16 cell line through a MEK1/2 dependent manner was examined. In addition, a second MEK1/2 inhibitor, namely PD98059, at a concentration reported previously was used [129]. Inhibition of MEK1/2 by either U0126 or PD98059 was able to decrease ERK1/2-T202/Y204 phosphorylation in 2780CP/CI-16 cells after cis-Pt or oxali-Pt treatment (**Figure 36B** and **36C**). Moreover, 2780CP/CI-16 cells treated with cis-Pt treatment in combination with MEK1/2 inhibitors for 24 hr exhibited a reduction in p53 and p53-Ser15 phosphorylation levels. In addition, inductions of p53-Ser20 phosphorylation and p21 were not observed after cis-Pt treatment in 2780CP/CI-16 cells in the presence of MEK1/2 inhibitors. In terms of oxali-Pt, a slight reduction in p53 and p53-Ser15 phosphorylation levels in the presence of MEK1/2 inhibitors in 2780CP/CI-16 cells was observed. Finally, MEK1/2 inhibitors drastically impacted oxali-Pt capacity to induce

p53-Ser20 and p21 expression in 2780CP/CI-16 cis-Pt resistant cells. In summary, results show that the ability of oxali-Pt to induce p53-S20 phosphorylation and p21 expression in 2780CP/CI-16 cells is decreased in the presence of the MEK1/2 inhibitors. Therefore, these results demonstrate that the kinase activity of MEK1/2 plays an important role in mediating oxali-Pt capacity to restore p53-Ser20 phosphorylation and p53 transcriptional activity in the cis-Pt resistant 2780CP/CI-16 cell line.

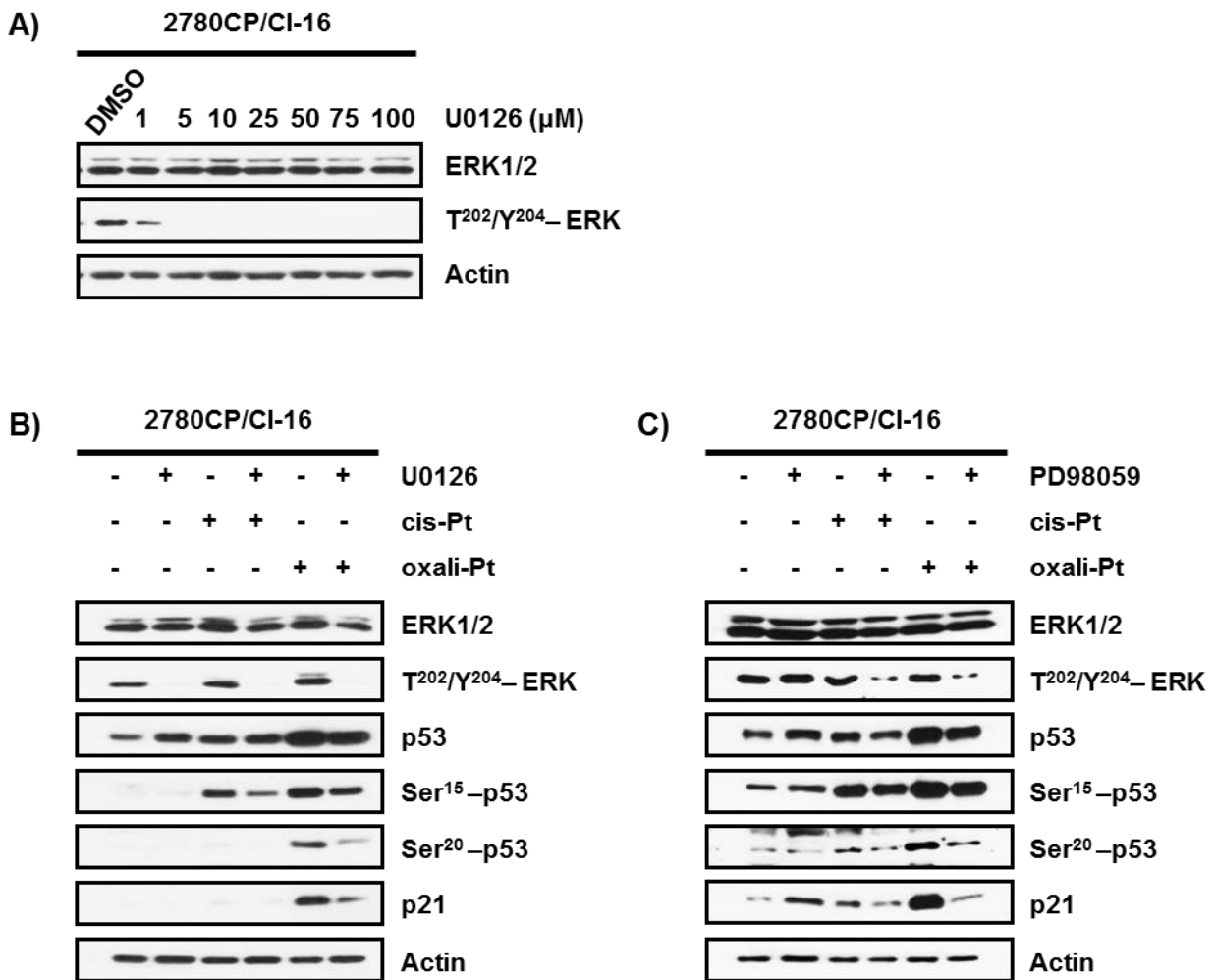


Figure 36. Involvement of MEK1/2 in mediating p53 phosphorylation at Ser20 and p53 transcriptional activation by oxali-Pt

A) Evaluation of ERK1/2-T202/Y204 phosphorylation levels in 2780CP/CI-16 cells treated with 1 μM , 5 μM , 10 μM , 25 μM , 50 μM , 75 μM and 100 μM of the MEK inhibitor U0126 for 24 hr. **B)** Evaluation of the p53 signaling pathway in 2780CP/CI-16 cells pre-treated with U0126 10 μM for 1 hr, followed by cis-Pt 5 μM or oxali-Pt 3 μM treatment for 24 hr. **C)** Evaluation of the p53 signaling pathway in 2780CP/CI-16 cells pre-treated with PD98059 100 μM for 1 hr, followed by cis-Pt 5 μM or oxali-Pt 3 μM treatment for 24 hr.

5.2.6. MEK1/2 expression positively correlates with cell survival and therapeutic response to Pt:

With the demonstration that MEK1/2 plays a role in mediating oxali-Pt mechanism of action, it was appropriate to assess whether MEK1/2 inhibition will impact Pt cytotoxic response. Therefore, the involvement of MEK1/2 in Pt resistance and therapeutic response was investigated in the 2780CP/CI-16 cell line and ovarian cancer patients. Cell survival experiments were performed in 2780CP/CI-16 in the presence of the MEK1/2 inhibitor U0126 followed by cis-Pt or oxali-Pt treatment. Inhibition of MEK1/2 promotes a significant decrease in cell survival percentage after cis-Pt treatment in 2780CP/CI-16 cells. In direct contrast, MEK1/2 inhibition promotes a significant increase in cell survival after oxali-Pt treatment in 2780CP/CI-16 cells (**Figure 37A**), which supports the relevance of MEK1/2 in the mode of action of oxali-Pt. To further investigate if these observations are clinically relevant in ovarian cancer patients, the TCGA data was mined for correlation of survival and phospho-MEK1/2 levels. The analysis indicates that Pt sensitive or resistant patients having high levels of MEK1/2-S-217/221 phosphorylation in their tumors had better overall survival following Pt treatment than Pt sensitive or resistant patients expressing low levels of MEK1/2-S-217/221 phosphorylation (**Figure 37B**). These results indicate that higher expression of phospho-MEK1/2 has a prognostic value within the sensitive or resistant cohort.

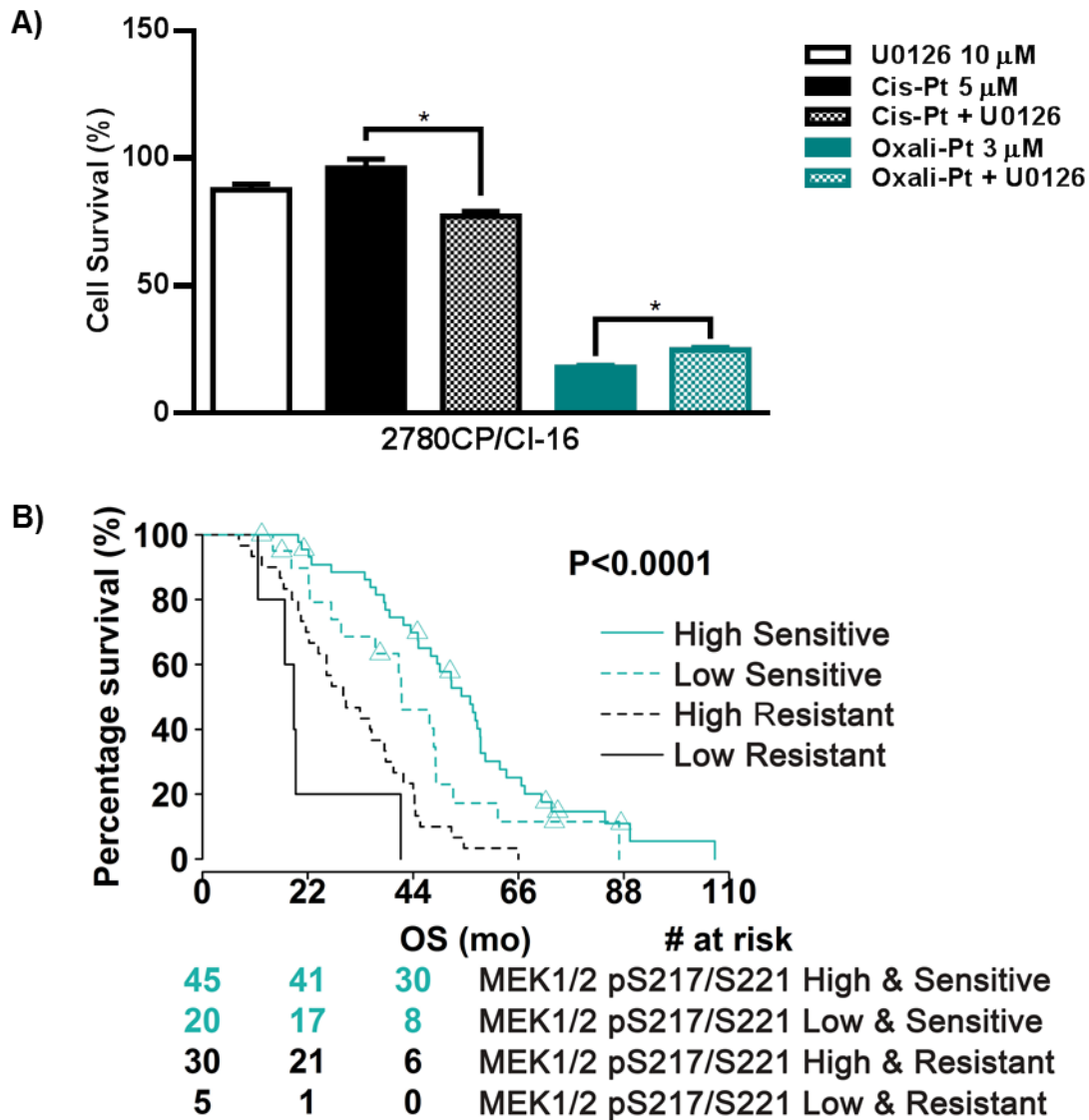


Figure 37. MEK1/2 expression positively correlates with cytotoxic and therapeutic response to Pt

A) 2780CP/CI-16 cells were treated for 1 hr with DMSO or 10 μ M of U0126 inhibitor, followed by addition of cis-Pt 5 μ M or oxali-Pt 3 μ M for 3-days at 37°C. Student's t test was used to determine statistical significance, p value ≤ 0.05 . N=3; Mean \pm SD **B)** Kaplan-Meier curves for ovarian cancer patients grouped into high and low levels of MEK1/2 pS217/S221 and further stratified according to Pt status. The analysis was carried out in R (version 3.2.2). All the tests were two-sided and considered statistically significant at p value ≤ 0.05 .

5.2.7. MEK1/2 phosphorylate p53 at Ser20 in vitro:

Finally, the capacity of MEK1/2 to phosphorylate p53 at Ser20 directly was evaluated by performing a kinase assay with recombinant MEK1, MEK2 and substrate p53. Chk2 was used as an experimental control, since it is already known that Chk2 induces p53-Ser20 phosphorylation. Indeed, it was observed that Chk2 induced p53 phosphorylation at Ser20 when incubated with recombinant p53 (**Figure 38**). Incubation of either MEK1 or MEK2 with p53 led to p53-Ser20 phosphorylation (**Figure 38**). Therefore, in a cell free system MEK1/2 is capable of phosphorylating p53 at Ser20. This demonstrates that MEK1/2 clearly has potential to phosphorylate p53 at the Ser20 site.

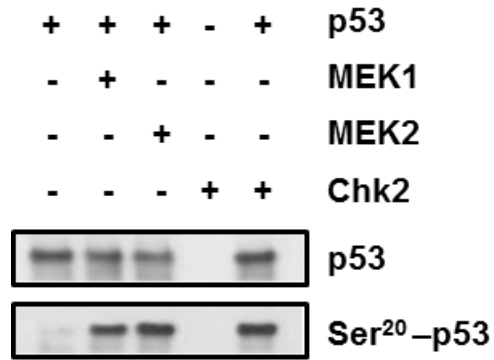


Figure 38. MEK1/2 phosphorylate p53 at Ser20 in vitro

Western blot analysis of p53 and p53-Ser20 phosphorylation in the kinase activity assay performed with 25 μ M of ATP, 12.5 ng/ μ L of recombinant p53, 20 ng/ μ L of recombinant MEK1 or MEK2 and immunoprecipitated Chk2 incubated at 30°C for 20 min.

5.3. Conclusions:

In this Chapter, the mechanism of action of oxali-Pt was investigated. Overall, similar responses seen in Chapter 4 by the A2780 Chk2^{-/-} clones treated with cis-Pt or oxali-Pt were observed in cis-Pt resistant 2780CP/CI-16 cells. In summary, Chk2 was expressed in A2780, but not in 2780CP/CI-16 cells. Furthermore, cis-Pt treatment in A2780 was able to induce p53-Ser20 phosphorylation, p21 and Mdm2. However, in 2780CP/CI-16 cells, cis-Pt failed to promote a robust increase in p53-Ser20 phosphorylation, p21 and Mdm2 levels when compared to the levels observed in A2780. On the other hand, in both A2780 and 2780CP/CI-16 cell lines, oxali-Pt treatment led to robust induction of p53-Ser20 phosphorylation, p21 and Mdm2 proteins. RPPA analysis using the restricted parameters of a significant increase in the signal obtained from A2780 treated with cis-Pt and oxali-Pt, and 2780CP/CI-16 treated with oxali-Pt led to the identification of the MAPK kinase ERK1/2 as a positive hit. Thus, the involvement of the MAPK kinase family, in specific the Ras/MEK1/2/ERK1/2 pathway, in mediating p53 phosphorylation at Ser20 and p53 transcriptional activation by oxali-Pt was investigated. Studies performed in 2780CP/CI-16 cells with selective ERK1/2 inhibitor SCH772984 demonstrated that this inhibitor did not affect oxali-Pt capacity to induce p53 phosphorylation at Ser20 and p53 transcriptional activation. Thus, these results exclude the possibility of ERK1/2 as the novel kinase utilized by oxali-Pt to exert its mechanism of action. However, inhibition of MEK1/2 by the MEK1/2 specific inhibitors, U0126 or PD98059, in cis-Pt resistant 2780CP/CI-16 cells treated with oxali-Pt led to decrease p53-S20 phosphorylation and p21 expression. Therefore, MEK1/2 plays an important role in mediating oxali-Pt capacity to restore p53-Ser20

phosphorylation and p53 transcriptional activity. In addition, MEK1/2 inhibition promotes a significant increase in cell survival after oxali-Pt treatment in 2780CP/CI-16 cells, which supports the relevance of MEK1/2 in the mode of action of oxali-Pt. In the clinic setting, Pt sensitive or resistant ovarian cancer patients with high levels of MEK1/2-S-217/221 had increased overall survival when compared to corresponding patients expressing low levels of MEK1/2-S-217/221. Finally, kinase assay with recombinant MEK1/2 and p53 as the substrate has demonstrated that MEK1/2 has potential to phosphorylate p53 at the Ser20 site. In conclusion, it was demonstrated in Chapter 4 that cis-Pt fails to activate p53 due to loss of Chk2 leading to resistance. However, oxali-Pt was able to circumvent cis-Pt resistance by rewiring the p53 response. In this Chapter, it was identified that MEK1/2 play an important role in mediating p53 response by oxali-Pt (**Figure 39**). These studies are the first to uncover the importance of MEK1/2 in p53-Ser20 phosphorylation. Such discovery will have a great impact in the way patients undergoing Pt-chemotherapy are treated.

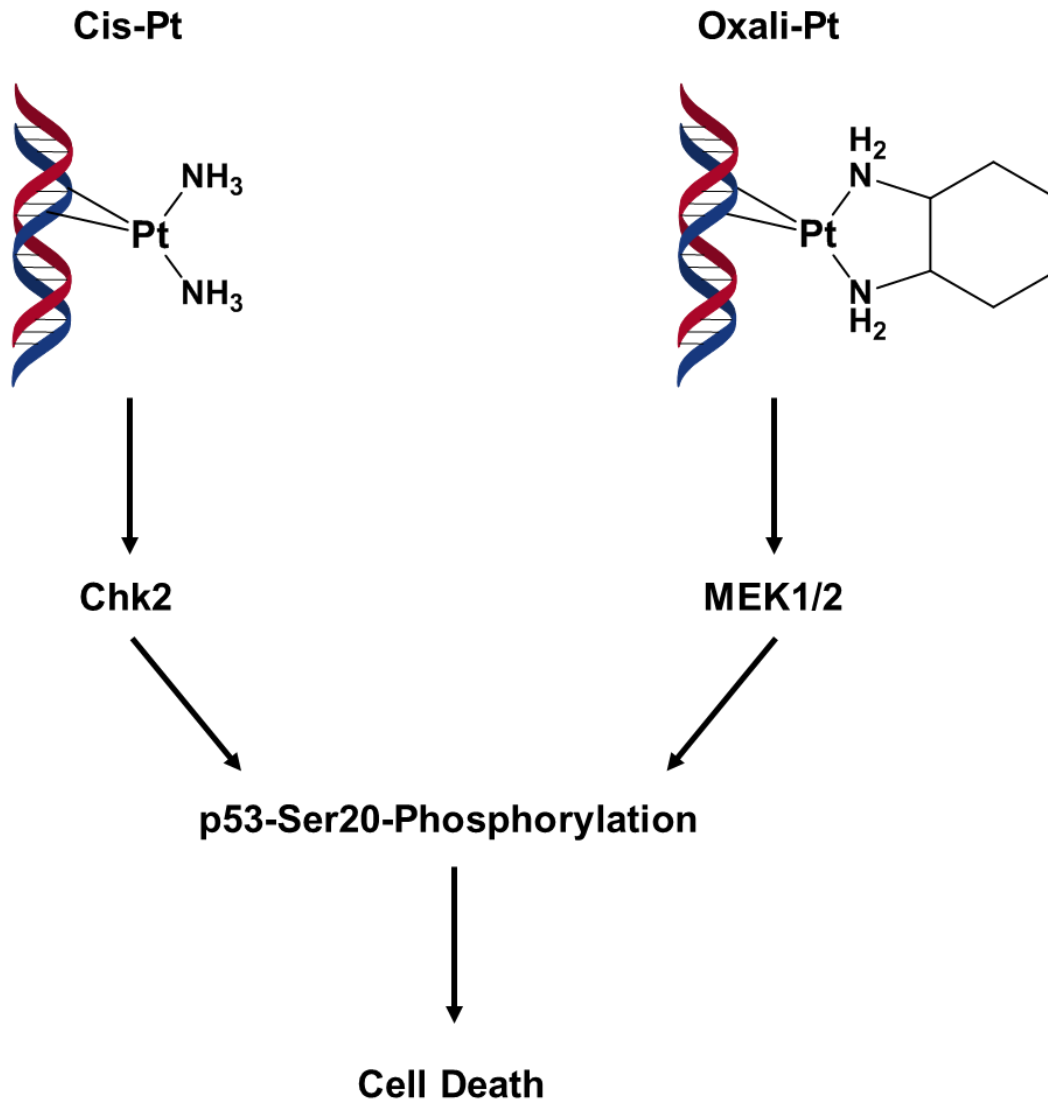


Figure 39. Conclusions Chapter 5

Cis-Pt fails to activate p53 due to loss of Chk2, leading to resistance. However, oxali-Pt was able to circumvent cis-Pt resistance by rewiring the p53 response via MEK1/2.

Chapter 6

Discussion

6.1. Overall Discussion:

Cis-Pt is currently used as the first line treatment in ovarian cancer patients. However, the clinical use of cis-Pt has many drawbacks such as irreversible toxic side effects and development of resistance [20]. Therefore, structurally-distinct Pt analogs were studied in cis-Pt-resistant ovarian tumor models with the goal of identifying Pt compounds able to overcome cis-Pt resistance that could be of clinical relevance. More specifically, Pt analogs with different ligand groups, namely 1) Amino, 2) Pyridine and 3) DACH based on Fojo et al. [137], were studied. In the beginning of the history of Pt complexes, the significance of the cis configuration to obtain anticancer activity almost became a dogma since transplatinum compounds were thought to be inactive [159;166]. Along with this concept, our studies have reported trans-Pt compound exhibiting the highest IC₅₀ values in all the cis-Pt resistant cell lines. Interestingly, newer classes of transplatinum compounds containing bulky amino planar ligands (instead of amino ligands) have been shown to retain activity against cis-Pt resistant cells from various NCI-60 cell types [137]. Moreover, trans-PyPt has been previously shown to be active in leukemia and human ovarian tumor cells resistant to cis-Pt [137;167]. Our cytotoxic studies demonstrated that trans-PyPt was able to circumvent cis-Pt resistance in all cis-Pt resistant ovarian cancer cell lines. This increase in potency was observed to be intrinsic for the trans isomer since the activity exhibited by cis-PyPt was similar to the one obtained for cis-Pt. As a consequence, cis-PyPt was found to be cross-resistant to cis-Pt. Thus, these results confer a unique characteristic for the trans compounds with bulky amino planar ligands as is the case for trans-PyPt, which is not conferred by its cis isomer, cis-PyPt, nor trans-Pt in which the carrier ligand is an amino group.

Circumvention of cis-Pt resistance by trans-PyPt was found to be driven by its high cellular concentration. In fact, from all Pt analogs, trans-PyPt exhibited the greatest Pt cellular uptake and Pt-DNA adducts concentration values. Studies performed in leukemia cells have found similar Pt cellular uptake results [168]. It was noted that trans-Pt and cis-PyPt also exhibited high Pt uptake values. Therefore, the greater Pt uptake observed for trans-PyPt compound could be a consequence of an addition from its trans configuration and the hydrophobic pyridine ligand, which in turn results in high Pt-DNA adducts. In fact, this greater cellular uptake and DNA adduct formation by trans-PyPt was shown to be due to its greater lipophilicity and reactivity. Lipophilic compounds are mostly found in the hydrophobic phase [139]; thus, it is likely that the lipophilicity of trans-PyPt favors its transport through the cell membrane allowing this compound to accumulate in high concentrations inside the cell. Reactivity studies of Pt compounds towards calf thymus DNA have reported the order of binding affinity as: trans-Pt > cis-Pt > cis-PyPt > trans-PyPt [167]. Such results suggest that trans-PyPt is a stable compound. In contrast, we found that among all Pt analogs, trans-PyPt formed greater DNA-Pt adducts in cis-Pt sensitive and resistant cell lines. Therefore, it would be expected that trans-PyPt will exhibit high binding capacity towards DNA in a cell free system. In fact, our studies show that trans-PyPt is a highly reactive compound, even more than trans-Pt. The high reactivity of trans-PyPt raises a barrier in its delivery to the tumor site since it is expected that most of the compound will become deactivated in the bloodstream. In fact, it has been shown that the inactivity of trans-Pt compound in vitro and in vivo is based on its chemical reactivity since most of the compound becomes deactivated by side reactions before targeting the DNA [15]. In addition, the reactivity of

cis-PyPt was similar to cis-Pt, thus, it appears that the high reactivity is due to the trans configuration of the compound independently of the ligand group.

The cytotoxicity observed in cis-Pt resistant ovarian cancer cell lines by trans-PyPt could be a result of its high concentrations inside the cell, which could trigger the activation of multiple mechanisms, including those that may be independent of DNA damage signaling pathway. Nevertheless, trans-PyPt compound was found to promote greater ICL index levels. The capacity of trans-PyPt to promote ICLs makes this compound very attractive since such capacity is not shared by cis-Pt. In fact, evidence shows that cis-Pt mainly produces intrastrand cross-links between neighboring purine residues, specifically 60% on dGG and 30% on dAG [18]. On the other hand, trans-Pt has been found to mainly promote ICLs and monofunctional adducts [159]. Trans-Pt compound can form high levels of ICLs because it is sterically restricted and is unable to crosslink neighboring bases in a DNA strand as with cis-Pt [159]. Our results also indicate that the pyridine ligand adds to steric restriction of the compound resulting in substantially greater ICLs levels. As a consequence, the capacity of trans-PyPt to form ICLs could also account for the toxicity obtained in cis-Pt resistant ovarian cancer cell lines. Thus trans-PyPt has been shown to differ from cis-Pt in its molecular pharmacologic capacity. These intrinsic DNA damage capacity of trans-PyPt, together with its different carrier ligand group (pyridine vs. amino) could result in important mechanistic implications. Thus, efforts by researchers in modifying and optimizing trans-PyPt chemical structure to increase its stability could enhance its clinical potential.

Along with trans-PyPt, oxali-Pt and DAP were also able to circumvent cis-Pt resistance in all cis-Pt resistant ovarian cancer cell lines. In fact, these two compounds have shown favorable cytotoxic and antitumor activity against tumor models that demonstrate cis-Pt resistance [49;137]. In addition, oxali-Pt treatment has shown positive response in Phase II and Phase III clinical trials of advanced ovarian cancer patients that do not respond to cis-Pt [133]. Furthermore, oxali-Pt is currently used in the treatment of colon cancer, a disease in which cis-Pt treatment has proven to be ineffective [169]. On the other hand, DAP has been shown to be a novel Pt compound effective against cis-Pt –sensitive and –resistant ovarian cancer cells [170]. However, the clinical potential of DAP still relies on the investigation of its mechanism of action. One difference between cis-Pt and DAP, recently reported by our lab, is that at 18 hrs cis-Pt induces G2/M arrest but DAP induces G1 arrest [171]. Hence, there are some differences between DAP and cis-Pt as regards their mechanisms of action. Taken together, oxali-Pt and DAP are attractive compounds for the treatment against ovarian cancers that have failed to respond to cis-Pt treatment.

Interestingly, the capacity of oxali-Pt and DAP to overcome cis-Pt resistance does not rely on increased Pt uptake or DNA-Pt adducts formation. In fact, oxali-Pt and DAP exhibited the lowest Pt uptake and, in turn, the lowest DNA-Pt adducts between all Pt compounds. This low Pt uptake of oxali-Pt and DAP could be due to their lipophilicity. Therefore, modification of the chemical structure of these Pt compounds to increase their lipophilicity could enhance their Pt uptake. It has been shown that conjugation of oxali-Pt linked to texaphyrin results in higher Pt uptake when compared to oxali-Pt [147].

Whether increasing oxali-Pt or DAP cellular uptake could enhance their cytotoxic capacity still needs to be addressed. However, it is worth highlighting that low concentrations of Pt uptake and DNA-Pt adducts from oxali-Pt and DAP were sufficient to result in high cytotoxic activity. In addition, oxali-Pt and DAP exhibited the lowest ICLs index values between all compounds, which correlated with their capacity to form DNA-Pt adducts. Oxali-Pt has been shown to induce 3 types of crosslinks: DNA intrastrand crosslinks, DNA interstrand crosslinks and protein crosslinks. However, oxali-Pt predominantly induces similar DNA lesions as cis-Pt in the form of dGG and dAG intrastrand crosslinks [172]. Thus, formation of ICLs seems less important in the mechanism of action of oxali-Pt and DAP for overcoming cis-Pt resistance.

The low capacity of oxali-Pt and DAP to interact with DNA suggests that the cytotoxic activity of these compounds could be driven by their capacity to form highly toxic DNA lesions, in such a way that even low DNA damage is potent enough to trigger cell death. In fact, Woynarowski et al. reported that oxali-Pt-induced DNA-Pt adducts in leukemia cells were significantly lower than the respective lesions induced by equimolar concentrations of cis-Pt, regardless of oxali-Pt increased cytotoxicity [172]. These paradoxical findings suggest that cis-Pt-induced DNA damage may differ from that of oxali-Pt and DAP. A possible explanation of the capacity of these compounds to induce different DNA damage relies in their different chemical structures. In general, Pt compounds contain a central Pt atom with oxidation state (II) and have a square planar configuration with a chemical structure of $[Pt(X)_2(L)_2]$ (X= equatorial leaving group and L= equatorial carrier amine ligand) [15]. In the case of cis-Pt L= NH_3 and X= Cl. In

contrast, oxali-Pt possess L= DACH and X= oxalate. DAP is a Pt (IV) compound with a tetrahedral chemical structure $[Pt(AL)_2(X)_2(L)_2]$ (AL= axial ligand) with L= DACH, X= Cl and AL= acetate. Thus, oxali-Pt and DAP share the same L group. The main difference between these two compounds is that DAP is a Pt (IV) compound. Pt (IV) compounds have been shown to have greater stability and lipophilicity than their Pt (II) counterparts [139]. Indeed, our studies indicate that DAP exhibited the greater half-life between all compounds, including its Pt (II) counterpart oxali-Pt. In addition, DAP exhibited greater lipophilicity than oxali-Pt. However, Pt (IV) compounds are activated by their reduction to Pt (II), and it is the Pt (II) complex which interacts with DNA [140]. Therefore, oxali-Pt and DAP are expected to produce the same DNA damage: DACH-Pt-DNA adducts. In contrast, cis-Pt will produce cis-diammine-Pt-DNA adducts. Although cis-Pt and oxali-Pt produce the same type of intrastrand crosslinks, the bulky DACH moiety may lead to different biological properties. In fact, DACH-Pt-DNA adducts have been shown to be more effective at inhibiting DNA synthesis and more cytotoxic than cis-diammine-Pt-DNA adducts formed by cis-Pt [133]. In direct contrast with cis-diammine-Pt-DNA adducts, DACH-Pt-DNA adducts formed by oxali-Pt and DAP do not depend on the recognition by HMGB and MMR proteins, resulting in greater irreversibility of the lesions [133]. As a consequence, cis-diammine-Pt-DNA adducts and DACH-Pt-DNA adducts induce the activation of independent DNA damage signaling pathways, but which converge on p53-dependent apoptosis. Such mechanism could provide insights in the circumvention of cis-Pt resistance.

The design of novel Pt compounds circumventing cis-Pt resistance should take into account three basic fundamentals: 1) proper pharmacokinetic and toxicity properties, 2) its mechanisms of action and the corresponding target biomolecules and 3) its possible mechanisms of resistance [173]. Thus, the ideal Pt compound is that exhibiting the best pharmacokinetics properties when compared to cis-Pt in terms of: 1) increased stability, 2) lower cytotoxic values in resistant cell lines, 3) higher Pt uptake and DNA damage formation and 4) different type of DNA damage. All these parameters are needed to trigger the activation of a signaling cascade pathway resulting in apoptosis. Therefore, from a mechanistic point of view, the ideal Pt compound should be able to produce a DNA damage resulting in the activation of different targets from those activated by cis-Pt since this will allow the circumvention of cis-Pt resistance. For the design of Pt (IV) compounds it is best to oxidize the already proven active Pt (II) compounds, which may improve the compound's stability, lipophilicity, thus, enhancing its ability to circumvent cis-Pt resistance. This stems from the fact that ultimately the Pt (IV) compound activity relies on its reduction to Pt (II), since it is the Pt (II) complex which confers the cytotoxic mechanism of action [141].

The p53 pathway has been proven to play a major role in mediating Pt-chemotherapy response. This is best illustrated by the significant loss in sensitivity towards cis-Pt treatment after siRNA-mediated silencing of p53 in TGCT cells [22;23]. Therefore, loss of p53 function leads to cis-Pt resistance. The most popular mechanism that directly impedes p53 function is through mutation in the p53 protein as occurs in 50% of all human cancers [161]. Thus, it would be reasonable to think that mutation in

the p53 protein will lead to a Pt resistant phenotype. In our studies, all cis-Pt resistant cell lines contained p53 missense mutations (heterozygous V172F mutation in 2780CP/CI-16, V172F and G266R heterozygous mutations in OVCAR-10 and P72R homozygous mutation in HEY and OVCA-433). Based on the transcriptional activity in a yeast functional assay (FASAY) from http://p53.fr/TP53Mutload/database_access/search.php, the P72R mutant has p53 wild-type like activity. However, V172F and G266R mutations, both were detected to have LOF. Nevertheless, it was reported that the mutant p53^{V172F} in 2780CP/CI-16 cells responds normally to ionizing radiation by becoming stabilized and then transactivating the target p21 gene [146]. Along this concept, our studies also demonstrate that these p53 mutations did not prevent p53 stabilization and transcriptional activity when challenged with cis-Pt or oxali-Pt. Therefore, mutation of p53 did not prevent its functional activity and, thus, it is not the reason for the development of cis-Pt resistance in the ovarian cancer cell lines. Similarly, a previous report has demonstrated that the mutant p53^{V172F} in 2780CP/CI-16 cells become stabilized and transactivated by ionizing radiation [146]. Moreover, a detailed study evaluating p53 transcriptional activity in 2,314 distinct p53 mutants, representing all possible p53 missense mutations, revealed that 63.9% of p53 mutants retained p53 activity comparable to that of wild-type p53 [98]. Our results clearly demonstrate that not all p53 mutants are inactivating or dysfunctional. These findings raise a concern in utilizing *TP53* status as a biological marker to predict chemotherapeutic response.

According to TCGA, *TP53* is the most commonly mutated gene in HGSOC patients, exhibiting a mutation rate of 86% [94]. However, we have found that p53 status, wild-type or mutant, did not provide any advantage capabilities in terms of survival response in HGSOC patients treated with Pt chemotherapy. In accordance with our findings, results gathered from many clinical studies that attempted to correlate mutant p53 with chemoresistance were contradictory with each other [91-93]. Such discrepancies could be due to incomplete analysis since we have shown that mutations in p53 alone cannot provide definite information regarding its functional activity. Therefore, p53 status is not a reliable marker to predict chemotherapeutic outcome in ovarian cancer patients and classification of p53 status goes beyond the typical and simplistic categories of wild-type vs. mutant. In fact, we found in HGSOC patients using the TCGA data bank that 21% of p53 missense mutations were predicted by FASAY to have either completely or partial p53 functional activity (**Appendix 4**). In addition, as demonstrated by our data, the G266R p53 mutation in OVCAR-10 was predicted by FASAY to be functionally inactive, however, after Pt treatment transcriptional activity of p53 was obtained. Hence, there could be a possibility that the p53 transcriptional activity could be restored for the other 79% of p53 missense mutations in patients after Pt treatment. These results denote that even from a clinical level p53 mutation does not equal inactivation. As a consequence, we propose that each p53 molecule should be classified by their functional activity (functional, LOF or GOF) in order to better understand and predict its biological role and response to Pt treatment.

We further study the role of p53 in mediating Pt response in p53^{-/-} ovarian cancer clones generated by the noble CRISPR/Cas9 technique. Interestingly, we found that p53 had a dual role in mediating response to Pt treatment. In the case of cis-Pt, p53 mediated sensitivity in A2780 and 2780CP/CI-16 clones but resistance in OVCAR-10 and HEY clones. However, p53 was found to be essential to mediate sensitivity to oxali-Pt treatment in all cell lines. These results are the first to show that the same p53 molecule (in the case of OVCAR-10 and HEY cell lines) can exert different cytotoxic responses depending on the Pt compound used. Thus, these Pt compounds appeared to be regulating the transcriptional activity of a given p53 molecule differently and such regulation dictates the way in which p53 mediates Pt response. In fact, we found that even though cis-Pt and oxali-Pt treatment led to p53 expression and transcriptional activity, oxali-Pt was able to trigger a more robust p53 response, which led to greater transcriptional activity (as indicated by p21 levels) compared to cis-Pt in resistant cell lines. These findings show that different chemotherapeutic agents, such as oxali-Pt, can reactivate a given p53 molecule, wild-type or mutant, as long as it can exhibit wild-type p53-like activity.

It has been shown that p53 transcriptional activity is highly dependent on p53 post-translational modifications, mainly through phosphorylation events [31]. Phosphorylation of p53 at Ser15 and Ser20 has been reported as most critical for its anti-proliferative and apoptotic functions [81;82]. We have found that oxali-Pt triggered a better p53-Ser20 phosphorylation response than cis-Pt in all cell lines. However, there was no specific pattern observed in differences of Ser15 induction between the two Pt

compounds. Furthermore, the capacity of cis-Pt and oxali-Pt to induce Ser20, but not Ser15, correlated with their capacity to induce p53 transcriptional activity. A study performed in cell lines from UV-induced murine tumors showed that mutant p53 is constitutively phosphorylated at Ser15, but not Ser20, and such phosphorylation contributed mainly to mutant p53 stabilization [156]. Therefore, Ser15 phosphorylation is a good marker to determine p53 stabilization. In addition, we showed in A2780 p53^{-/-} cells transfected with wild-type p53, mutant p53-S20A (constitutively dephosphorylated mimic) or mutant p53-S20D (constitutively phosphorylated mimic) that Ser20 phosphorylation significantly enhanced p53 transcriptional activity. These results corroborate that Ser20 phosphorylation is a good marker to determine p53 transcriptional activity. There are different ways in which Ser20 phosphorylation enhances p53 transcriptional activity. For instance, Ser20 phosphorylation is important to disrupt the Mdm2-p53 binding complex, which allows the free p53 to interact with coactivators, such as p300 [174]. In fact, Ser20 phosphorylation has been shown to play a critical role in promoting p53 activation by stabilizing the binding of p300 to p53. The p53-p300 complex is essential for sequence-specific DNA-dependent acetylation of p53, which allows the complex to clamp at a specific DNA site [175;176]. Finally, an inverse correlation between Mdm4 levels and p53-Ser20 phosphorylation was observed in our studies. Thus, it would be interesting to study the role of Ser-20 phosphorylation in mediating p53-Mdm4 interaction.

Pt-induced DNA damage triggers p53 phosphorylation via the activation of specific kinases [31]. Studies have shown that downregulation of Chk2, a kinase

reported to phosphorylate p53 at Ser20 after cis-Pt treatment, leads to resistance [99;177]. In our studies, we found that Chk2 protein levels were substantially lower in all cis-Pt resistant cell lines (2780CP/CI-16, OVCAR-10, HEY, and OVCA-433) relative to cis-Pt sensitive cell line (A2780). Furthermore, downregulation of Chk2 in cis-Pt resistant cells occurred at the transcriptional level. MicroRNAs have been shown to play an important role in regulation of cell cycle checkpoint and apoptotic proteins [178]. Expression of microRNAs -340 and -425, which were predicted to interact with *CHEK2* transcripts, were detected in A2780, 2780CP/CI-16, OVCAR-10, HEY and OVCA-433 by RT-PCR. However, miR-340 and miR-425 were not implicated in the mechanism responsible for decreased levels of *CHEK2* transcripts since knock-in of these microRNAs did not lead to decrease levels of Chk2 in A2780 cells. It has been previously reported in gliomas and non-small cell lung cancer that Chk2 downregulation is due to promoter methylation [152;153]. However, our bisulfite pyrosequencing and MSP studies indicated that decrease in levels of *CHEK2* transcripts is not due to promoter methylation since no differences in *CHEK2* methylation between cis-Pt sensitive and resistant cells were observed. Specifically, no cell line exhibited methylation of *CHEK2* at exon 1. In contrast, all cell lines exhibited methylation of *CHEK2* at exon 2, including cis-Pt sensitive cell line A2780. The ideal scenario would have been to observe high *CHEK2* exon methylation in cis-Pt resistant cells since low levels of Chk2 were found in these cells. The results gathered for A2780 cells were found to contradict the data published by Zhang et al {Zhang, 2004 1771 /id}. In fact, the MSP studies for *CHEK2* performed in non-small cell lung cancer by this lab included A2780 cells as control and it was reported that *CHEK2* exon 2 was not methylated in

this cell line. However, in their studies a very light band for *CHEK2* methylation at exon 2 was observed in A2780 cells. It could be possible that methylation levels of *CHEK2* at exon 2 in A2780 are substantially lower in comparison with non-small cell lung cancer cell lines but not with cis-Pt resistant ovarian cancer cell lines, thus, leading to different results. Nevertheless, it has been reported that expression of Chk2 in lymphoid malignancies was restored following treatment with histone deacetylase inhibitors or with DNA methyltransferase inhibitors [179]. Therefore, the epigenetic changes in the form of histone modifications should be considered as a valuable mechanism leading to decreased levels of Chk2 in cis-Pt resistant cell lines.

Our lab has previously reported that knock-down of Chk2 in A2780 cells reduced cis-Pt ability to induce p53 and p21 [171]. However, whether Chk2 is involved in cis-Pt sensitivity via p53 Ser20 phosphorylation and activation has not been investigated. Cis-Pt treatment of A2780 control and Chk2^{-/-} clones revealed that Chk2 knock-out resulted in a dramatic decrease in p53-Ser20 phosphorylation and p21 levels. Remarkably, loss of Chk2 did not affect the ability of oxali-Pt to induce p53-Ser20 phosphorylation and p21 expression. Moreover, loss of Chk2 in A2780 led to significantly decreased cis-Pt and oxali-Pt sensitivities (i.e. increased IC₅₀) when compared to controls, thus indicating that loss of Chk2 leads to dual Pt resistance. Such results were expected since both Pt compounds were able to induce Chk2-Thr68 phosphorylation. In fact, cis-Pt was found to induce higher levels of Chk2-Thr68 phosphorylation compared to oxali-Pt, and therefore cis-Pt mechanism of action is more dependent on Chk2. We have shown that a mechanism contributing to cis-Pt resistance in A2780 Chk2^{-/-} clones is the inability of

cis-Pt to activate p53 due to loss of Chk2. However, since oxali-Pt capacity to induce p53 activity is not dependent on Chk2, the resistance observed in A2780 Chk2^{-/-} clones is mediated through p53 independent mechanisms. In fact, Chk2 has been shown to regulate apoptosis through different proteins, such as PML and E2F-1 [180]. Furthermore, exogenous re-expression of Chk2 in A2780 Chk2^{-/-} clones restored cis-Pt and oxali-Pt sensitivity and the ability of cis-Pt to induce p53 transcriptional activity. A greater sensitivity was observed with cis-Pt treatment, which supports that cis-Pt is more dependent on Chk2. Analysis from the TCGA data bank of HGSOC Pt sensitive or resistant patients clustered into two groups according to their Chk2 expression (high versus low), showed that Pt-sensitive patients with high levels of Chk2 had greater overall survival. In agreement with our findings, it has been reported that ovarian cancer cell lines expressing low levels of Chk2 have reduced Pt sensitivity [177]. In addition, Chk2 has been reported as a good biomarker for Pt chemotherapy in advanced stage HGSOC patients [181]. Taken together, we have shown that Chk2 is essential for cis-Pt-induced p53-Ser20 phosphorylation and p53 transcriptional activity, and is an important mediator of cis-Pt chemotherapy sensitivity. Oxali-Pt, however, retained the capacity to induce p53-Ser20 phosphorylation and p53 transcriptional activity independently of Chk2.

Finally, we investigated the involvement of the Ras-MEK1/2-ERK1/2 pathway as a possible mechanism mediating oxali-Pt-induced p53-Ser20 phosphorylation and p53 transcriptional activity since the intersections made to the RPPA data gathered for 217 proteins from A2780 and its isogenic 2780CP/CI-16 cells treated with cis-Pt or oxali-Pt

identified ERK1/2 kinase as the only positive hit. ERK1/2 has been previously shown to induce p53-Ser15 phosphorylation in UV-induced mouse skin tumors [156]. However, there is no evidence indicating that ERK1/2 is capable of inducing p53-Ser20 phosphorylation. Our data demonstrated that ERK1/2 is not directly involved in oxali-Pt mechanism of action since treatment of 2780CP/CI-16 cells with the ERK1/2 inhibitor SCH772984 did not impact the ability of oxali-Pt to induce p53-Ser20 phosphorylation or p21 expression. In accordance with published data [156], inhibition of ERK1/2 promoted a reduction in the capacity of cis-Pt, but not oxali-Pt, to induce p53-Ser15 phosphorylation.

Moving upstream in the MAPK signaling pathway, we discovered that the ability of oxali-Pt to induce p53-Ser20 phosphorylation and p21 expression in 2780CP/CI-16 cells drastically decreased in the presence of MEK1/2 inhibitors U0126 and PD98059. Previous studies performed in A2780 cells reported that PD98059 decreased cis-Pt capacity to induce p53-Ser15 phosphorylation and p21 levels and mistakenly addressed this effect to ERK1/2 [129]. As discussed, PD98059 is a selective MEK1/2 inhibitor; therefore, any effect should have been ascribed to MEK1/2. However, effective inhibition of MEK1/2 is assessed by probing for ERK1/2-T202/Y204 phosphorylation, which could have led to the wrong interpretation. We have provided solid evidence to demonstrate, by using multiple MAPK inhibitors, that MEK1/2, but not ERK1/2, is the key player in mediating oxali-Pt-induced p53 activation. Another gap in their study is the absence of p53-Ser20 phosphorylation data. In our studies, we have shown that p53-Ser20, but not Ser15, plays a major role in p53 transcriptional activity. In addition, we

have shown that both MEK1/2 inhibitors U0126 and PD98059 decreased the ability of oxali-Pt to induce p53-Ser20 phosphorylation. Therefore, the decreased capacity of cis-Pt to induce p21 levels in A2780 cells in the presence of MEK1/2 inhibitor PD98059 reported by Persons et al. {Persons, 2000 2004 /id} could be due to p53-Ser20 phosphorylation. Up to date there is no literature evidence that shows that MEK1/2 induces p53-Ser20 phosphorylation. For the first time, to our knowledge, we have demonstrated by performing a kinase activity assay that MEK1/2 has the potential to directly phosphorylate p53 at the Ser20 site.

Furthermore, MEK1/2 inhibition promoted a significant increase in cell survival in 2780CP/CI-16 cells after oxali-Pt treatment, but not cis-Pt treatment, which strongly supports the crucial role of MEK1/2 in the mode of action of oxali-Pt-induced cytotoxicity. Along with our findings, there are many studies showing that inhibition of MEK1/2 increases tumor response to cis-Pt [182;183]. In such case MEK1/2 leads to resistance possibly by activating transcription factors implicated in the induction of genes that increase thiol-containing molecules and/or upregulate DNA adduct repair pathways [20]. One major limitation in our studies was having performed the MEK1/2 studies in a single resistant cell line. Therefore, to further strengthen our MEK1/2 findings it will be necessary to perform similar experiments in the other cis-Pt resistant cell lines: OVCAR-10, HEY and OVCA-433. Additionally, for these studies results from the cis-Pt sensitive A2780 cell line were not included since this cell line contains high levels of Chk2, which could have affected the signaling pathway under study. Nevertheless, MEK1/2 was found to have a significant prognostic value in HGSOC

patients. Survival analysis on HGSOc Pt-sensitive or -resistant patients with high versus low MEK1/2-Ser217/Ser221 phosphorylation revealed that both Pt-sensitive and -resistant patients had overall increased survival if tumors expressed high levels of MEK1/2-Ser217/Ser221 phosphorylation following Pt chemotherapy. Our studies are the first one to identify MEK1/2 as a novel biomarker for oxali-Pt-induced p53-Ser20 phosphorylation, p53 transcriptional activity and chemotherapy sensitivity.

The different signaling pathway triggered by cis-Pt or oxali-Pt via Chk2 or MEK1/2, respectively could be due to the different DNA damage produced by these two Pt compounds. Although cis-Pt and oxali-Pt mainly produce DNA damage in the form of intrastrand crosslinks, mainly the 1,2-GG intrastrand form, the different carrier ligand groups from these compounds can affect differently the degree of the DNA bending and unwinding angles [19]. In fact, it has been reported that in a 1,2-GG intrastrand adduct, cis-Pt promotes in the DNA a bending of 34° and unwinding of 20°, whereas oxali-Pt promotes a bending of 31° or 23° in the [Pt(R,R-DACH)]²⁺ enantiomer and unwinding of 19° or 16° depending in the in the [Pt(S,S-DACH)]²⁺ enantiomer [184]. Therefore, their capacity to distort the DNA differently results in the recognition by different DNA damage sensor proteins. For instance, cis-Pt-DNA adducts, but not oxali-Pt, are highly recognized by HMGB and MMR proteins [19]. Therefore, if the signaling pathway that recognized cis-Pt DNA damage has been shut down for whatever reason, the capacity of oxali-Pt to form different DNA distortion could result in circumvention of cis-Pt resistance by using an alternate signaling pathway.

It could be possible that eventually ovarian tumors could give rise to oxali-Pt resistance. However, other Pt compounds with different carrier ligands groups that could promote different DNA distortions could circumvent oxali-Pt resistance. In fact, a study by Tito Fojo et al. [137] classified 107 Pt compounds into 12 groups based on their chemical structures and distinctive activity profiles against 60 diverse NCI human cancer cell lines including cis-Pt and oxali-Pt ovarian cancer cell lines. In this study, they reported that Pt compounds from the same group were cross-resistant with each other as was the case for cis-Pt and carboplatin. However, Pt compounds from a different group were non-cross-resistant with each other as was the case for cis-Pt and oxali-Pt. Interestingly, further structure-activity studies of 38 Pt compounds from 4 groups using A2780 (1A9) E-80 cells (highly resistant to cis-Pt (150-fold) and much less resistant to oxali-Pt (9-fold)) and A2780 (1A9) OX60 cells (highly resistant to oxali-Pt (733-fold) and considerably less resistant to cis-Pt (112-fold)) showed that the compounds in the Pyridine and Mixed Groups retained activity against these resistant cell lines [137]. Moreover, correlation studies suggest that Pt compounds in different groups act through the activation of distinct principal targets.

In conclusion, these novel findings provide a better understanding of how Pt chemotherapy works in relation with p53 status, and thus, establish a foundation for personalized therapy and combinational treatment depending on the tumor gene expression profile. Specifically, this study identified Chk2 and MEK1/2 as important biomarkers mediating differential Pt responses by cis-Pt and oxali-Pt, respectively, which also uncovers connection between ubiquitously studied cellular pathways.

Specifically, patients treated with cis-Pt will be expected to rely on Chk2 activity to promote p53-Ser20 phosphorylation and transcriptional activity. Alternatively, oxali-Pt induces p53-Ser20 phosphorylation and transcriptional activity through MEK1/2. The fact that cis-Pt and oxali-Pt work through different kinases to activate p53 will help determine which patients will benefit from either treatment and will offer alternative treatment options to HGSOC patients (**Figure 40**). These discoveries will ultimately impact the way in which HGSOC patients and perhaps other patients undergo Pt chemotherapy treatment, ultimately enhancing survival of patients.

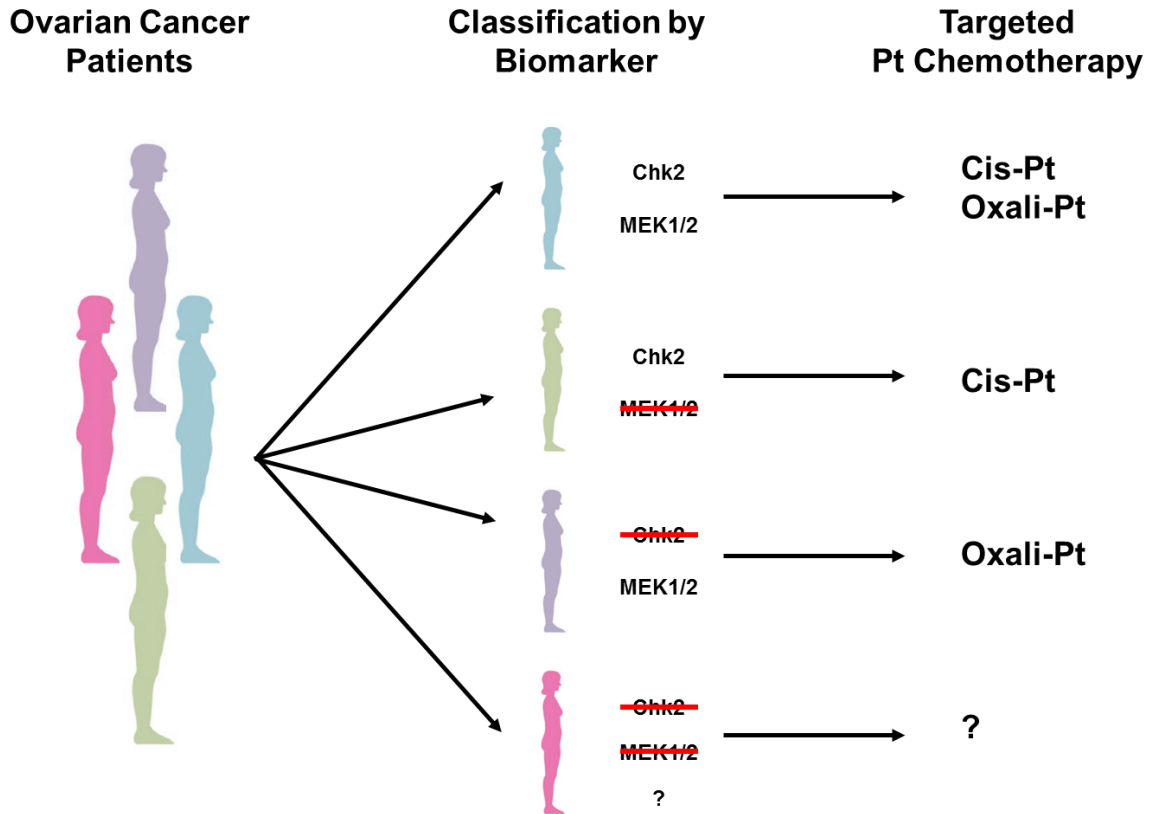


Figure 40. Targeted Pt chemotherapy in ovarian cancer patients

Cis-Pt and oxali-Pt work through different kinases to activate p53, Chk2 or MEK1/2, respectively. Patients exhibiting differences in expression of Chk2 or MEK1/2 can be clustered in order to determine the predicted beneficial Pt targeted chemotherapy. These alternative treatment options will enhance the survival of HGSOc patients.

Chapter 7

Future Directions

7.1. Future Directions:

1. *Enhance the stability of trans-PyPt:*

Trans-PyPt exhibited intrinsic molecular pharmacologic characteristics when compared to the other Pt analogs (cis-Pt, trans-Pt, cis-PyPt, oxali-Pt and DAP). However, trans-PyPt was found to be the most reactive compound within this group, which is an obstacle for its delivery to the tumor site since most of the compound will become inactivated in the bloodstream by aquation reactions before reaching its DNA target. Therefore, it would be interesting to further modify and optimize the chemical structure of trans-PyPt through synthesis to increase its stability. Our studies showed that DAP, a Pt (IV) compound, was the most stable among all Pt compounds. In fact, axial ligands in Pt (IV) compounds have been shown to enhance the compound's stability and lipophilicity [96;140]. With the goal to make a more stable compound, we oxidized trans-PyPt by adding hydroxyl groups, as axial ligands, giving rise to trans-Pt[(Py)₂Cl₂](OH)₂ (IV). However, the stability of this compound slightly increased when compared to trans-PyPt but not with the rest of the Pt analogs. Therefore, substitution with other chemical groups should be considered for further optimization of trans-PyPt. Some of the axial ligand groups that could be considered to develop a more stable trans-PyPt (IV) compound are: acetate, propionate, butyrate, valerate, hexanoate, heptanoate and carboxylic acids [140;170].

2. Evaluation of p53 GOF capacity in OVCAR-10 and HEY cell lines:

It was shown that p53 knock-out in OVCAR-10 and HEY clones led to a significant decrease in cis-Pt IC₅₀ values, indicating that the presence of potentially functional p53 in these cell lines is associated with cis-Pt resistance. Therefore, the capacity of p53 to exert GOF through inactivation of transcriptional factors that have an important role in the cell death pathway (i.e. p63 and p73) and/or transcriptional activation or repression of genes whose expression is not normally regulated by wild-type p53 (*BFGF*, *EGFR*, *HSP70* and *C-Myc*) [68] should be evaluated through Western blot and/or RT-PCR in OVCAR-10 and HEY cell lines after cis-Pt treatment. BFGF and EGFR have been shown to play a fundamental role in enhancing tumor growth, invasion and metastasis [185;186]. In specific, BFGF and EGFR lead to resistance by activating pathways involve in cell survival, such as RAS–RAF–MAPK, PI3K–AKT, STAT and PLC γ [187;188]. Similarly, C-Myc has been identified as an oncogene. C-Myc expression is obtained from many growth promoting signal transduction pathways (i.e. MAPK) and it acts as a transcription factor regulating the expression of genes involved in cell proliferation [189]. In addition, oxali-Pt should be included in parallel studies to compare it with cis-Pt results, since a significant increase in oxali-Pt IC₅₀ values in all p53 knock-out cell lines was obtained (including OVCAR-10 and HEY), indicating that the p53 in these cells is functional and leads to sensitivity. Thus, it would be expected that only cis-Pt, but not oxali-Pt, will be capable to exert p53 GOF in OVCAR-10 and HEY.

3. *Characterization of p53-Thr18 phosphorylation in Pt mode of action:*

We showed that Chk2 is essential for cis-Pt induced p53-Ser20 phosphorylation and p53 transcriptional activity, and is an important mediator of cis-Pt chemotherapy sensitivity. Chk2 has been shown to also induce p53 phosphorylation at multiple sites, such as Thr18 [31]. In addition, p53-Thr18 phosphorylation has been shown to play an important role in inducing p53 transcriptional activity [81]. Therefore, it would be interesting to investigate the role of p53-Thr18 phosphorylation in mediating cis-Pt and oxali-Pt response in sensitive and resistant ovarian cancer cell lines. Levels of p53-Thr18 phosphorylation should be evaluated in the studies performed for p53-Ser15 and p53-Ser20 phosphorylation. It is expected that p53-Thr18 phosphorylation exhibit a similar response as the one obtained for p53-Ser20 phosphorylation. Therefore, cis-Pt is expected to induce p53-Thr18 phosphorylation in a Chk2 dependent manner, thus, it is highly expected that cis-Pt capacity to induce levels of p53-Thr18 are low in cis-Pt resistant cell lines, which were shown to have low levels of Chk2. It is important to mention that it is possible that cis-Pt mechanism of action could be inducing compensatory pathways through activation of different kinases specific to induce p53-Thr18 phosphorylation, in which case different results could be obtained. In addition, it would be interesting to study if oxali-Pt induces p53-Thr18 phosphorylation through MEK1/2. Overall these studies will help define the role of p53 phosphorylation in relation with Pt chemotherapy.

4. Role of MEK1/2 in oxali-Pt-induced Mdm4 degradation:

In normal cells, p53 levels are kept low due to its negative interaction with Mdm2 and Mdm4 [68]. Mdm2 and Mdm4 can bind independently to the N-terminus domain of p53 and can also bind to each other to form heterodimers through the C-terminal RING domain. Such interaction is required for the E3 ligase activity of Mdm2, culminating in p53 proteosomal degradation [190]. Therefore, the transcriptional activity of p53 is negatively regulated by Mdm2 and Mdm4 levels. DNA damage signals after treatment with Pt compounds can inhibit interaction between p53 and Mdm2 or Mdm4, and accelerate Mdm4 degradation by Mdm2, to stabilize and transcriptionally activate p53 [190]. Furthermore, Chk2 has been shown to phosphorylate Mdm4 at Ser342 and Ser367, leading to Mdm2-mediated ubiquitination and degradation of Mdm4 [191-193]. Therefore, in accordance with the literature, it was observed that Mdm4 control levels increased in A2780 Chk2^{-/-} clones when compared to A2780 clones (see **Figure 24**), thus, Chk2 reduced levels of Mdm4. Furthermore, oxali-Pt treatment, but not cis-Pt, was able to reduce Mdm4 levels in A2780 Chk2^{-/-}. Therefore, cis-Pt, but not oxali-Pt, relies on Chk2 to decrease levels of Mdm4. Since we showed that MEK1/2 is implicated in oxali-Pt mechanism of action, it would be interesting to investigate whether MEK1/2 is involved in oxali-Pt-induced Mdm4 degradation.

5. *Identification of kinases inducing p53 activity after Pt treatment:*

We were able to identify Chk2 and MEK1/2 as important biomarkers mediating differential Pt responses by cis-Pt and oxali-Pt, respectively, thus, proving that Pt compounds work through different mechanisms of action. It has been shown that an individual phosphorylation site can be targeted by multiple kinases [31]. Therefore, a high-throughput screening [194] using a universal luminescent kinase assay should be performed in order to identify the involvement of other possible kinases in cis-Pt or oxali-Pt-induced p53 activity. For this experiment, specific kinases will be knocked-down using a validated siRNA library, followed by Pt treatment and measurement of p53 activity by using a luciferase reporter. Knock-down of essential kinases are expected to decrease the signal obtained for p53 activity after cis-Pt or oxali-Pt treatment.

6. *Study the role of Chk2-Thr68 expression in Pt therapy outcomes in HGSOc patients:*

Ovarian cancer patients stratified as sensitive or resistant to Pt-therapy and grouped according to Chk2 expression (high vs. low) showed that high levels of Chk2 led to increased overall survival, whereas low levels of Chk2 was associated with reduced overall survival (see **Figure 25B**). Phosphorylation of Chk2 at Thr-68 has been shown to be a biomarker for Chk2 kinase activity [195]. Therefore, it would be interesting to investigate the role of Chk2-Thr68 phosphorylation expression in the survival of HGSOc

patients treated with Pt therapy. It would be expected that Pt sensitive and resistant patients have overall increased survival if tumors express high levels of Chk2-Thr68 phosphorylation following Pt chemotherapy.

7. *Epigenetic regulation of CHEK2 transcripts:*

Our data showed that cis-Pt resistant ovarian tumor cell lines exhibit substantial downregulation of Chk2 as a common feature at the transcriptional level (see **Figure 23 and 27A**). Therefore, the mechanism by which *CHEK2* levels are decreased in cis-Pt resistant cell lines should be investigated. Recently, it has been reported that Hodgkin's lymphoma (HL) cell lines had drastically decreased expression of Chk2 due to altered epigenetic regulation [179]. In specific, treatment of HL cell lines with the histone deacetylase inhibitors trichostatin A (TsA) and sodium butyrate (SB), or with the DNA methyltransferase inhibitor 5-aza-20-deoxycytidine (5Aza-dC) restored Chk2 expression and chromatin-immunoprecipitation (ChIP) assays revealed that this was obtained through increased levels of acetylated histones H3 and H4, and decreased levels of dimethylated H3 lysine 9 at the Chk2 promoter [179]. Therefore, *CHEK2* levels should be evaluated in cis-Pt resistant cell lines after treatment with TsA, SB or 5Aza-dC. In addition, a ChIP assay would be able to determine specific histone modifications at the *CHEK2* promoter after TsA, SB or 5Aza-dC treatment. It is expected that cis-Pt resistant cells (containing low levels of Chk2) will have decreased levels of acetylated histones

H3 and H4, and increased levels of dimethylated H3 lysine 9 at the *CHEK2* promoter when compared to cis-Pt sensitive cell lines (containing high levels of Chk2).

8. Characterization of p53 and MEK1/2 interaction:

Oxali-Pt was found to induce p53-Ser20 phosphorylation via MEK1/2. In addition, MEK1/2 was found to be able to induce p53-Ser20 phosphorylation *in vitro*. However, there is no evidence to ascribe that MEK1/2 phosphorylates p53 via a direct interaction. Therefore, to further define the mechanism by which MEK1/2 mediates oxali-Pt-induced p53-Ser20 phosphorylation; immunoprecipitation studies should be performed in order to assess if MEK1/2 and p53 are able to interact after oxali-Pt treatment in 2780CP/CI-16 cells. For this experiment similar procedure as the one reported in [156] could be followed. Briefly, 2780CP/CI-16 cells should be treated with cis-Pt 5 μ M or oxali-Pt 3 μ M for 6 hr or 12 hr. After each time point, cells should be collected. Lysates from pellets should be incubated overnight at 4°C under mechanical rotation with p53-FL antibody. Samples should be added Protein A-Agarose beads and should be further incubated for 1 hr at 4°C under mechanical rotation. Beads should be pulled down and washed with ice-cold extraction buffer three times. Samples should be processed for western blot analysis. If MEK1/2 induces p53-Ser20 phosphorylation via direct interaction after oxali-Pt treatment, then interaction between p53 and MEK1/2 should be detected.

9. *Role of Raf in mediating MEK1/2-oxali-Pt-induced p53-Ser20 phosphorylation:*

As previously stated oxali-Pt was able to induce p53-Ser20 phosphorylation via MEK1/2. As discussed in **Section 1.6** MEK1/2 is itself phosphorylated by Raf [123]. Raf is widely recognized as an oncogene and mutations in these protein promoting its activity leads to tumor progression [196-198]. Therefore, studies determining if oxali-Pt activates MEK1/2 through the conventional Raf pathway will uncover a new role of the Raf protein in cancer. To answer this question, knocked-down or knock-out of Ras should be accomplished in 2780CP/CI-16 by siRNA or CRISPR techniques, respectively. After knock-down or knock-out of Raf is achieved, cells should be treated with Pt compounds for 24 hrs. Finally, the effect of decreased levels of Raf in the p53-Ser20 phosphorylation and p53 transcriptional activation as well as cytotoxicity should be evaluated.

10. *Evaluation of RPPA intersections:*

The RPPA data obtained in this project for 217 proteins from A2780 and 2780CP/CI-16 cell lines treated with cis-Pt or oxali-Pt was subjected to multiple intersections. To better define the mechanisms of action of cis-Pt and oxali-Pt, these intersections should be carefully evaluated. In **Appendix 2**, evaluations of significant upregulation or downregulation of proteins were made to A2780 or 2780CP/CI-16 independently. These evaluations may enable the identification of common as well as different targets in

response to Pt therapy. In addition, in **Appendix 3**, several intersections between A2780 and 2780CP/CI-16 cell lines treated with cis-Pt or oxali-Pt were made. These intersections may identify novel targets utilized by either cis-Pt or oxali-Pt for Pt therapy sensitivity. These intersections may also enable the identification of targets involved in Pt therapy resistance.

Appendix I. RPPA values for heatmap for A2780 and 2780CP/CI-16 treated with cis-Pt and oxali-Pt										
SAMPLE	ACVRL1-R-C	ADAR1-M-V	Akt-R-V	Akt_pS473-R-V	Akt_pT308-R-V	AMPK-alpha-R-C	AMPK-alpha_pT172-R-V	Annexin-I-M-V	Annexin-VII-M-V	AR-R-V
A2780 Control_A	0.001	0.035	-0.049	-1.275	-0.784	-0.166	-0.235	-0.232	-0.436	0.084
A2780 Control_B	0.069	0.115	-0.108	-1.091	-0.687	-0.140	0.011	-0.167	-0.380	0.094
A2780 Control_C	-0.034	0.092	-0.072	-1.148	-0.854	-0.182	-0.234	-0.141	-0.312	0.131
A2780 Cis-Pt_A	-0.017	-0.039	-0.001	-1.360	-0.743	-0.055	-0.147	-0.196	-0.484	0.058
A2780 Cis-Pt_B	-0.161	0.003	0.001	-1.094	-0.624	-0.016	-0.202	-0.162	-0.325	0.119
A2780 Cisp-Pt_C	-0.097	-0.003	0.043	-1.202	-0.730	-0.004	-0.057	-0.186	-0.399	0.139
A2780 Oxali-Pt_A	-0.009	0.051	0.027	-0.582	-0.337	0.004	-0.025	-0.018	-0.349	0.090
Oxali-Pt_B A2780	-0.0003	0.685	-0.069	-0.520	-0.285	-0.008	-0.144	-0.115	-0.426	0.073
A2780 Oxali-Pt_C	0.021	-0.034	0.065	-0.692	-0.351	0.034	-0.011	-0.054	-0.313	0.017
2780CP/CI16 Control_A	0.016	-0.330	0.125	1.361	1.140	-0.033	0.106	0.125	0.335	-0.237
2780CP/CI16 Control_B	-0.023	-0.392	0.117	1.570	1.250	-0.027	-0.051	0.272	0.312	-0.288
2780CP/CI16 Control_C	0.059	-0.289	0.042	1.302	0.926	0.160	0.021	0.068	0.363	-0.158
2780CP/CI16 Cis-Pt_A	-0.003	-0.262	-0.067	1.115	0.606	0.183	0.029	0.200	0.464	-0.153
2780CP/CI16 Cis-Pt_B	0.000	-0.322	0.120	1.278	1.011	0.177	0.131	0.080	0.355	-0.161
2780CP/CI16 Cis-Pt_C	-0.060	-0.268	0.056	1.097	0.865	0.419	0.074	0.018	0.319	-0.133
2780CP/CI16 Oxali-Pt_A	0.172	0.285	-0.473	0.520	0.285	0.169	0.519	0.491	0.933	-0.017
2780CP/CI16 Oxali-Pt_B	0.181	0.068	-0.432	0.691	0.393	0.516	0.368	0.440	0.769	-0.089
2780CP/CI16 Oxali-Pt_C	0.046	0.165	-0.533	0.545	0.373	0.278	0.395	0.291	0.806	-0.160

Appendix I. RPPA values for heatmap for A2780 and 2780CP/CI-16 treated with cis-Pt and oxali-Pt										
SAMPLE	ARHI-M-C	ATM-R-V	ATM_pS1981-R-V	ATP5H-M-C	ATR-R-C	b-Catenin-R-V	b-Catenin_pT41_S45-R-V	B-Raf-M-C	B-Raf_pS445-R-V	Bad_pS112-R-V
A2780 Control_A	-0.261	0.250	-0.201	0.185	0.117	-0.842	-0.059	-0.079	0.001	-0.019
A2780 Control_B	-0.063	0.527	-0.100	0.377	0.222	-0.846	-0.083	0.081	0.085	-0.077
A2780 Control_C	-0.054	0.471	-0.186	0.125	0.215	-0.955	-0.120	0.072	0.040	-0.037
A2780 Cis-Pt_A	-0.004	0.511	0.548	0.184	-0.003	-0.518	-0.004	-0.019	0.012	-0.089
A2780 Cis-Pt_B	-0.044	0.575	0.201	0.085	0.103	-0.777	-0.119	-0.037	0.069	-0.017
A2780 Cisp-Pt_C	0.002	0.478	0.282	-0.032	0.063	-0.740	-0.140	0.051	0.085	-0.054
A2780 Oxali-Pt_A	0.038	0.507	0.039	0.014	-0.093	-0.733	-0.149	0.019	0.141	0.053
A2780 Oxali-Pt_B	0.009	0.304	0.394	-0.046	-0.163	-0.451	-0.059	-0.166	0.078	0.031
A2780 Oxali-Pt_C	-0.002	0.453	0.236	-0.014	-0.065	-0.573	-0.184	-0.182	0.172	0.017
2780CP/CI16 Control_A	-0.156	-0.347	-0.322	-0.165	0.075	0.568	0.004	0.040	-0.041	0.094
2780CP/CI16 Control_B	-0.127	-0.468	-0.139	-0.259	0.119	0.762	0.042	0.112	-0.020	0.026
2780CP/CI16 Control_C	-0.026	-0.295	-0.167	-0.106	0.003	0.653	0.140	0.111	-0.021	0.107
2780CP/CI16 Cis-Pt_A	0.065	-0.250	-0.009	-0.157	0.014	0.451	0.158	-0.077	-0.051	0.031
2780CP/CI16 Cis-Pt_B	0.103	-0.412	0.022	-0.204	-0.054	0.796	0.183	0.332	-0.001	0.037
2780CP/CI16 Cis-Pt_C	0.110	-0.381	-0.074	-0.294	-0.108	0.555	0.095	0.336	-0.014	0.038
2780CP/CI16 Oxali-Pt_A	0.294	-0.833	0.009	0.565	-0.303	1.324	0.285	-0.513	-0.424	-0.067
2780CP/CI16 Oxali-Pt_B	0.321	-0.787	0.010	0.458	-0.232	1.441	0.271	-0.666	-0.413	-0.081
2780CP/CI16 Oxali-Pt_C	0.132	-0.863	-0.038	0.454	-0.192	1.436	0.226	-0.640	-0.554	-0.142

Appendix I. RPPA values for heatmap for A2780 and 2780CP/CI-16 treated with cis-Pt and oxali-Pt										
SAMPLE	Bak-R-C	BAP1-M-V	Bax-R-V	Bcl-xL-R-V	Bcl2-M-V	Beclin-G-C	Bid-R-C	Bim-R-V	BRCA2-R-C	C-Jun_pS73-R-V
A2780 Control_A	0.009	-0.044	-0.465	-0.011	-0.132	0.237	0.061	0.210	0.168	-0.445
A2780 Control_B	-0.033	0.033	-0.419	-0.160	-0.075	0.091	-0.022	0.180	0.067	-0.479
A2780 Control_C	-0.062	-0.009	-0.395	-0.197	-0.240	-0.016	-0.010	0.034	0.000	-0.467
A2780 Cis-Pt_A	0.038	-0.060	0.086	0.419	-0.334	-0.062	0.063	-0.163	-0.026	-0.452
A2780 Cis-Pt_B	0.050	-0.066	0.075	0.093	-0.277	-0.091	-0.019	-0.182	-0.063	-0.390
A2780 Cisp-Pt_C	-0.004	-0.091	0.014	0.006	-0.394	0.061	-0.010	-0.158	-0.091	-0.496
A2780 Oxali-Pt_A	-0.052	0.004	0.426	-0.006	-0.285	0.045	-0.050	-0.467	-0.231	-0.472
A2780 Oxali-Pt_B	0.101	-0.151	0.729	0.237	-0.300	0.065	0.105	-0.328	-0.346	-0.081
A2780 Oxali-Pt_C	-0.022	-0.053	0.342	0.133	-0.259	0.003	-0.001	-0.536	-0.303	-0.440
2780CP/CI16 Control_A	-0.219	0.091	-0.158	-0.226	0.303	0.036	0.001	0.069	-0.012	0.178
2780CP/CI16 Control_B	-0.100	0.084	-0.233	-0.022	0.232	-0.076	0.032	0.048	0.040	0.154
2780CP/CI16 Control_C	-0.063	0.063	-0.187	-0.203	0.075	-0.077	-0.004	-0.142	0.177	0.231
2780CP/CI16 Cis-Pt_A	-0.187	0.101	-0.206	-0.318	0.281	-0.045	-0.006	0.212	0.253	0.365
2780CP/CI16 Cis-Pt_B	0.053	0.018	-0.014	0.116	0.102	-0.115	0.016	-0.198	0.265	0.081
2780CP/CI16 Cis-Pt_C	0.004	-0.004	-0.094	0.019	0.184	0.041	-0.017	-0.034	0.167	0.253
2780CP/CI16 Oxali-Pt_A	0.036	0.081	0.469	-0.085	0.728	-0.003	0.132	0.498	0.026	0.781
2780CP/CI16 Oxali-Pt_B	0.027	-0.053	0.362	0.011	0.681	-0.007	0.133	0.506	-0.007	0.646
2780CP/CI16 Oxali-Pt_C	0.058	0.006	0.352	0.101	0.675	0.018	0.139	0.554	0.000	0.747

Appendix I. RPPA values for heatmap for A2780 and 2780CP/CI-16 treated with cis-Pt and oxali-Pt										
SAMPLE	c-Kit-R-V	c-Met-M-QC	c-Met_pY1234_Y1235-R-V	c-Myc-R-C	C-Raf-R-V	C-Raf_pS338-R-V	Caspase-7-cleaved-R-C	Caspase-8-M-QC	Caveolin-1-R-V	CD29-M-V
A2780 Control_A	-0.063	-0.032	0.086	0.040	-0.170	-0.162	0.050	0.083	0.062	-0.104
A2780 Control_B	-0.077	-0.078	0.031	-0.016	-0.035	-0.062	-0.246	0.077	0.003	-0.030
A2780 Control_C	0.004	0.007	0.030	-0.065	-0.004	-0.165	-0.437	0.039	-0.173	0.065
A2780 Cis-Pt_A	0.023	-0.081	-0.026	-0.382	-0.138	-0.169	0.279	0.080	-0.122	-0.012
A2780 Cis-Pt_B	-0.028	-0.092	0.013	-0.309	-0.114	-0.156	0.528	0.051	-0.146	0.012
A2780 Cisp-Pt_C	-0.031	-0.034	-0.007	-0.504	-0.150	-0.161	0.357	0.016	0.009	-0.081
A2780 Oxali-Pt_A	-0.034	-0.110	-0.066	-0.390	-0.082	0.088	0.197	-0.041	-0.003	-0.036
A2780 Oxali-Pt_B	0.070	0.050	0.026	0.182	-0.259	-0.012	0.258	-0.059	0.213	-0.114
A2780 Oxali-Pt_C	0.002	-0.092	-0.037	-0.305	-0.061	0.062	0.207	-0.022	0.054	-0.078
2780CP/CI16 Control_A	-0.093	0.044	0.004	-0.013	0.632	0.286	-0.579	-0.016	-0.120	-0.021
2780CP/CI16 Control_B	-0.032	-0.038	0.055	0.013	0.650	0.157	-0.497	-0.023	-0.081	-0.122
2780CP/CI16 Control_C	0.048	0.055	-0.070	0.154	0.735	0.246	-0.500	-0.035	-0.124	0.150
2780CP/CI16 Cis-Pt_A	-0.002	0.032	0.005	0.683	0.501	0.160	-0.300	0.074	-0.314	0.115
2780CP/CI16 Cis-Pt_B	0.170	0.021	-0.090	-0.030	0.678	0.062	-0.335	0.020	-0.148	0.075
2780CP/CI16 Cis-Pt_C	0.163	-0.007	-0.140	1.188	0.662	0.250	-0.056	0.069	0.044	0.016
2780CP/CI16 Oxali-Pt_A	0.085	0.366	-0.027	0.530	0.062	0.012	0.001	-0.086	0.265	0.639
2780CP/CI16 Oxali-Pt_B	0.036	0.263	-0.004	1.357	0.008	-0.092	0.179	-0.342	0.200	0.475
2780CP/CI16 Oxali-Pt_C	-0.035	0.286	0.037	0.658	0.004	-0.048	-0.001	-0.299	0.159	0.460

Appendix I. RPPA values for heatmap for A2780 and 2780CP/CI-16 treated with cis-Pt and oxali-Pt										
SAMPLE	CD31-M-V	CD49b-M-V	CDK1-R-V	Chk1-M-C	Chk1_pS345-R-C	Chk2-M-V	Chk2_pT68-R-C	Claudin-7-R-V	Collagen-VI-R-V	Complex-II-Subunit-M-V
A2780 Control_A	-0.237	-0.060	0.012	-0.157	-0.167	1.429	0.001	-0.010	-0.582	-0.077
A2780 Control_B	-0.498	0.241	-0.034	0.006	-0.280	1.453	-0.001	-0.015	-0.266	-0.089
A2780 Control_C	-0.034	0.097	0.010	0.017	-0.144	1.240	0.028	0.051	0.120	-0.113
A2780 Cis-Pt_A	0.016	0.188	0.314	-0.025	0.040	1.583	0.093	0.035	-0.243	-0.088
A2780 Cis-Pt_B	-0.021	0.022	0.309	-0.006	0.073	1.433	0.233	0.029	0.175	0.010
A2780 Cisp-Pt_C	-0.046	0.014	0.327	0.117	0.026	1.445	0.178	-0.018	0.060	-0.016
A2780 Oxali-Pt_A	0.084	-0.005	-0.032	-0.405	-0.105	1.349	0.088	0.010	0.020	0.113
A2780 Oxali-Pt_B	-0.050	0.005	-0.010	-0.610	-0.009	1.454	0.067	0.011	-0.020	-0.109
A2780 Oxali-Pt_C	-0.109	0.074	-0.082	-0.496	-0.058	1.512	0.197	0.109	0.079	0.015
2780CP/CI16 Control_A	-0.016	-0.239	-0.146	0.329	0.009	-1.260	-0.066	-0.104	-0.210	0.081
2780CP/CI16 Control_B	-0.129	-0.202	-0.184	0.299	0.061	-1.633	-0.181	-0.148	0.045	0.111
2780CP/CI16 Control_C	0.046	-0.080	-0.092	0.390	0.028	-1.825	-0.106	-0.124	-0.025	0.092
2780CP/CI16 Cis-Pt_A	0.096	-0.088	0.377	0.232	0.250	-2.346	-0.067	-0.051	-0.196	-0.012
2780CP/CI16 Cis-Pt_B	0.137	-0.183	0.056	0.488	0.435	-1.584	-0.137	-0.212	-0.049	-0.049
2780CP/CI16 Cis-Pt_C	0.125	-0.196	0.317	0.510	0.350	-1.249	-0.047	-0.086	-0.048	-0.010
2780CP/CI16 Oxali-Pt_A	0.554	0.139	-0.148	-0.462	-0.138	-1.473	0.142	0.216	0.385	0.903
2780CP/CI16 Oxali-Pt_B	0.479	-0.086	0.539	-0.566	-0.055	-1.520	-0.124	0.269	0.340	0.836
2780CP/CI16 Oxali-Pt_C	0.290	0.099	-0.060	-0.565	-0.176	-1.240	-0.078	0.287	0.470	0.914

Appendix I. RPPA values for heatmap for A2780 and 2780CP/CI-16 treated with cis-Pt and oxali-Pt										
SAMPLE	Cox-IV-M-C	Cox2-R-C	Cyclin-B1-R-V	Cyclin-D1-R-V	Cyclin-E1-M-V	Cyclophilin-F-M-V	DJ1-R-V	Dvl3-R-V	E-Cadherin-R-V	E2F1-M-V
A2780 Control_A	-0.180	0.193	-0.457	-0.054	0.006	-0.075	-0.113	0.062	-0.028	-0.011
A2780 Control_B	-0.065	0.056	-0.139	-0.038	0.075	-0.046	-0.075	0.015	0.038	0.251
A2780 Control_C	0.126	0.081	-0.376	-0.004	-0.006	-0.166	0.029	0.038	-0.111	-0.127
A2780 Cis-Pt_A	-0.070	0.536	0.982	-0.086	-0.182	-0.217	-0.015	0.110	-0.062	-0.142
A2780 Cis-Pt_B	-0.076	0.284	1.146	-0.092	-0.235	-0.175	0.037	0.036	-0.102	-0.143
A2780 Cisp-Pt_C	-0.101	0.272	1.110	-0.046	-0.233	-0.185	0.003	-0.006	-0.022	-0.084
A2780 Oxali-Pt_A	-0.086	0.342	-0.039	0.135	0.463	-0.264	0.143	0.148	-0.002	-0.119
A2780 Oxali-Pt_B	-0.017	0.500	-0.170	0.167	0.222	-0.209	-0.002	0.058	-0.048	-0.136
A2780 Oxali-Pt_C	0.060	0.372	-0.235	0.064	0.406	-0.250	0.054	0.189	-0.105	-0.056
2780CP/CI16 Control_A	-0.057	-0.271	0.039	0.004	0.159	0.220	-0.045	0.006	0.207	0.085
2780CP/CI16 Control_B	-0.118	-0.263	0.086	-0.045	0.110	0.213	-0.027	-0.033	0.232	0.092
2780CP/CI16 Control_C	0.538	-0.229	0.053	0.108	0.135	0.085	0.040	-0.058	0.002	0.011
2780CP/CI16 Cis-Pt_A	0.051	-0.229	0.609	0.127	0.062	0.090	0.195	-0.124	0.026	0.089
2780CP/CI16 Cis-Pt_B	0.032	-0.056	0.760	0.079	-0.015	0.046	0.002	-0.101	0.011	-0.071
2780CP/CI16 Cis-Pt_C	0.017	-0.326	0.826	-0.013	-0.039	0.077	0.037	-0.231	-0.070	0.101
2780CP/CI16 Oxali-Pt_A	0.400	-0.349	-0.082	0.145	-0.112	0.886	-0.390	-0.261	0.304	0.186
2780CP/CI16 Oxali-Pt_B	0.377	-0.157	-0.203	0.040	-0.216	0.825	-0.542	-0.280	0.304	0.154
2780CP/CI16 Oxali-Pt_C	0.430	-0.198	-0.207	-0.004	-0.192	0.786	-0.578	-0.299	0.047	0.194

Appendix I. RPPA values for heatmap for A2780 and 2780CP/CI-16 treated with cis-Pt and oxali-Pt										
SAMPLE	eEF2-R-C	eEF2K-R-V	EGFR-R-V	EGFR_pY1068-R-C	EGFR_pY1173-R-V	eIF4E-R-V	eIF4G-R-C	ER-alpha-R-V	ER-alpha_pS118-R-V	ERCC1-M-V
A2780 Control_A	0.747	0.067	0.193	0.344	0.091	0.091	0.153	-0.458	0.091	0.235
A2780 Control_B	0.136	0.106	-0.279	0.512	0.082	0.151	0.163	-0.110	-0.003	0.099
A2780 Control_C	0.107	0.168	-0.594	0.101	0.009	0.024	0.098	-0.223	0.028	-0.056
A2780 Cis-Pt_A	0.829	0.202	-0.237	-0.184	0.000	0.044	-0.098	-0.090	0.222	0.162
A2780 Cis-Pt_B	0.176	0.071	-0.453	-0.080	0.000	0.092	-0.122	-0.052	0.100	-0.134
A2780 Cisp-Pt_C	0.158	0.135	-0.317	-0.045	0.005	0.122	-0.138	0.041	0.004	-0.143
A2780 Oxali-Pt_A	0.012	-0.183	-0.392	-0.320	-0.068	0.146	-0.220	-0.035	-0.079	-0.166
A2780 Oxali-Pt_B	0.374	-0.280	0.024	-0.189	0.030	0.105	-0.333	-0.077	0.069	-0.070
A2780 Oxali-Pt_C	0.168	-0.278	-0.479	-0.313	-0.011	0.157	-0.254	-0.101	-0.051	-0.110
2780CP/CI16 Control_A	-0.124	-0.061	0.042	-0.014	-0.119	-0.024	0.421	0.035	-0.141	0.423
2780CP/CI16 Control_B	-0.012	-0.028	-0.017	0.086	-0.054	-0.052	0.202	-0.161	-0.129	0.441
2780CP/CI16 Control_C	-0.214	0.016	0.034	0.029	0.053	-0.102	0.338	0.046	-0.051	0.197
2780CP/CI16 Cis-Pt_A	-0.358	-0.016	-0.043	-0.016	-0.046	-0.128	0.229	0.086	-0.099	0.343
2780CP/CI16 Cis-Pt_B	-0.108	0.131	0.075	0.039	0.017	-0.096	0.280	0.077	0.064	0.170
2780CP/CI16 Cis-Pt_C	-0.271	0.070	0.017	-0.013	-0.007	-0.062	0.304	0.090	0.234	0.056
2780CP/CI16 Oxali-Pt_A	-0.742	-0.996	0.590	0.111	-0.009	-0.351	-0.190	0.464	-0.148	-0.182
2780CP/CI16 Oxali-Pt_B	-0.696	-1.015	0.608	0.181	0.010	-0.329	-0.194	0.360	-0.139	-0.076
2780CP/CI16 Oxali-Pt_C	-0.742	-1.132	0.513	0.013	-0.081	-0.362	-0.174	0.230	0.003	-0.144

Appendix I. RPPA values for heatmap for A2780 and 2780CP/CI-16 treated with cis-Pt and oxali-Pt										
SAMPLE	Ets-1-R-V	FAK-R-E	FAK_pY397-R-V	FASN-R-V	Fibronectin-R-V	FoxM1-R-V	FoxO3a-R-C	FoxO3a_pS318_S321-R-C	G6PD-M-V	Gab2-R-V
A2780 Control_A	0.337	0.056	0.380	0.283	-0.373	-0.842	-0.006	0.064	0.041	-0.269
A2780 Control_B	0.103	0.038	0.633	0.584	0.025	-0.771	0.117	-0.182	-0.167	-0.053
A2780 Control_C	-0.081	0.033	0.353	0.493	-0.018	-0.721	0.168	-0.123	-0.155	-0.026
A2780 Cis-Pt_A	0.207	-0.045	0.147	0.254	0.200	-0.081	-0.109	-0.078	0.030	-0.351
A2780 Cis-Pt_B	-0.051	-0.016	-0.041	0.276	-0.129	-0.018	-0.071	-0.138	-0.071	-0.604
A2780 Cisp-Pt_C	0.009	-0.002	0.038	0.379	0.030	-0.022	-0.108	-0.101	-0.100	-0.413
A2780 Oxali-Pt_A	-0.149	0.026	-0.128	0.347	0.043	-0.519	-0.137	-0.041	-0.152	-0.791
A2780 Oxali-Pt_B	0.187	-0.042	-0.097	0.172	0.018	-0.658	-0.215	0.079	-0.015	-0.799
A2780 Oxali-Pt_C	0.005	0.029	0.000	0.280	-0.150	-0.589	-0.156	-0.001	-0.055	-0.695
2780CP/CI16 Control_A	0.075	0.114	-0.151	-0.247	-0.363	0.129	0.047	0.147	0.122	0.768
2780CP/CI16 Control_B	0.269	0.109	-0.337	-0.310	-0.387	0.018	0.040	0.114	0.230	0.797
2780CP/CI16 Control_C	-0.077	0.021	0.067	-0.172	-0.158	0.064	0.060	0.001	-0.014	0.856
2780CP/CI16 Cis-Pt_A	-0.024	0.002	-0.020	-0.212	-0.090	0.439	0.075	0.069	0.067	0.895
2780CP/CI16 Cis-Pt_B	-0.051	-0.108	0.000	-0.250	-0.037	0.505	0.006	-0.039	0.014	0.728
2780CP/CI16 Cis-Pt_C	-0.075	-0.096	-0.108	-0.181	0.603	0.572	0.024	-0.079	-0.102	0.674
2780CP/CI16 Oxali-Pt_A	-0.075	-0.308	-0.038	-0.993	0.236	0.278	0.006	0.378	0.067	0.388
2780CP/CI16 Oxali-Pt_B	0.096	-0.304	0.068	-1.022	0.139	0.136	-0.150	0.526	0.107	0.349
2780CP/CI16 Oxali-Pt_C	-0.005	-0.382	0.016	-1.122	0.598	0.148	-0.132	0.558	0.051	0.026

Appendix I. RPPA values for heatmap for A2780 and 2780CP/CI-16 treated with cis-Pt and oxali-Pt										
SAMPLE	GAPDH-M-C	GATA3-M-V	GCN5L2-R-V	GPBB-R-V	GSK-3ab-M-V	GSK-3ab_pS21_S9-R-V	GSK-3b_pS9-R-V	Gys-R-V	Gys_pS641-R-V	HER2-M-V
A2780 Control_A	0.278	0.431	-0.018	0.153	-0.012	-0.201	-0.103	-0.486	-0.058	-0.177
A2780 Control_B	0.571	0.123	0.161	-0.003	-0.012	-0.161	-0.207	-0.139	-0.175	1.176
A2780 Control_C	-0.041	-0.135	0.162	-0.374	-0.029	-0.324	-0.264	-0.274	-0.229	-0.028
A2780 Cis-Pt_A	0.112	0.446	0.001	-0.146	0.000	-0.006	-0.017	-0.440	-0.138	1.233
A2780 Cis-Pt_B	0.003	0.108	0.148	-0.440	0.029	0.037	-0.042	-0.292	-0.132	0.060
A2780 Cisp-Pt_C	-0.003	0.109	0.160	-0.200	0.003	0.086	-0.036	-0.277	-0.096	-0.015
A2780 Oxali-Pt_A	-0.118	-0.119	0.211	-0.413	0.000	0.326	0.203	-0.295	-0.201	0.017
A2780 Oxali-Pt_B	0.107	0.366	-0.119	-0.100	-0.088	0.381	0.238	-0.389	-0.119	0.008
A2780 Oxali-Pt_C	0.033	-0.061	0.055	-0.393	0.007	0.318	0.220	-0.239	-0.078	0.030
2780CP/CI16 Control_A	0.327	-0.081	-0.133	0.674	0.071	0.087	0.342	0.688	0.593	-0.120
2780CP/CI16 Control_B	0.496	0.307	-0.151	0.581	0.046	0.027	0.303	0.638	0.671	-0.008
2780CP/CI16 Control_C	0.047	-0.202	-0.058	0.559	0.010	0.006	0.236	0.843	0.404	-0.124
2780CP/CI16 Cis-Pt_A	-0.015	-0.183	-0.160	0.534	-0.114	-0.119	0.017	0.688	0.179	-0.083
2780CP/CI16 Cis-Pt_B	-0.120	0.121	-0.037	0.464	0.116	0.011	0.199	0.645	0.627	-0.271
2780CP/CI16 Cis-Pt_C	-0.243	-0.055	-0.035	0.502	0.084	-0.055	0.078	0.882	0.393	-0.207
2780CP/CI16 Oxali-Pt_A	-0.632	-0.095	0.131	0.003	-0.384	-0.705	-0.379	0.240	0.058	0.383
2780CP/CI16 Oxali-Pt_B	-0.470	0.002	-0.001	0.038	-0.445	-0.703	-0.400	0.139	0.165	0.476
2780CP/CI16 Oxali-Pt_C	-0.900	-0.002	0.030	-0.071	-0.383	-0.718	-0.472	0.164	0.127	0.475

Appendix I. RPPA values for heatmap for A2780 and 2780CP/CI-16 treated with cis-Pt and oxali-Pt										
SAMPLE	HER2_pY1248-R-C	HER3-R-V	HER3_pY1289-R-C	Heregulin-R-V	HIAP-R-C	Histone-H3-R-V	IGF1R-beta-R-V	IGFBP2-R-V	INPP4b-R-V	IRS1-R-V
A2780 Control_A	0.140	0.001	0.358	-0.003	-0.089	-0.262	0.145	-0.167	-0.065	0.251
A2780 Control_B	0.646	-0.174	0.199	-0.048	-0.099	-0.448	0.220	-0.063	0.000	0.207
A2780 Control_C	0.152	-0.119	0.157	0.055	-0.029	-0.254	0.267	-0.074	0.091	0.192
A2780 Cis-Pt_A	-0.002	-0.117	0.281	0.025	-0.070	-0.016	0.239	-0.011	-0.022	0.246
A2780 Cis-Pt_B	-0.129	-0.214	0.188	0.007	-0.164	0.079	0.223	0.011	-0.063	0.153
A2780 Cisp-Pt_C	0.013	-0.182	0.190	-0.021	-0.183	0.053	0.152	-0.063	-0.091	0.189
A2780 Oxali-Pt_A	-0.010	-0.344	0.048	-0.029	-0.023	0.016	0.202	0.038	0.004	0.053
A2780 Oxali-Pt_B	-0.042	-0.221	0.239	0.080	-0.102	0.216	0.046	-0.139	-0.105	0.172
A2780 Oxali-Pt_C	-0.083	-0.276	0.036	0.003	-0.060	0.146	0.210	-0.057	0.000	0.120
2780CP/CI16 Control_A	-0.008	0.092	-0.085	-0.234	0.047	-0.143	-0.683	-0.157	0.348	-0.206
2780CP/CI16 Control_B	-0.117	0.154	-0.036	-0.156	0.023	-0.106	-0.767	-0.200	0.371	-0.104
2780CP/CI16 Control_C	-0.017	0.014	-0.208	-0.053	0.141	-0.249	-0.700	0.049	0.507	-0.215
2780CP/CI16 Cis-Pt_A	0.083	0.043	-0.870	0.035	0.067	0.446	-0.707	0.105	0.431	-0.190
2780CP/CI16 Cis-Pt_B	0.002	0.085	-0.036	-0.047	0.055	-0.164	-0.706	0.132	0.296	-0.242
2780CP/CI16 Cis-Pt_C	-0.037	-0.001	-0.085	0.562	0.083	1.791	-0.796	0.270	0.304	-0.148
2780CP/CI16 Oxali-Pt_A	0.383	0.373	-1.083	0.075	0.061	-0.122	-0.046	0.403	-0.132	-0.062
2780CP/CI16 Oxali-Pt_B	0.282	0.371	-0.576	-0.017	0.091	0.320	-0.095	0.239	-0.169	-0.053
2780CP/CI16 Oxali-Pt_C	0.250	0.305	-0.410	0.525	0.110	1.339	-0.053	0.281	-0.296	-0.056

Appendix I. RPPA values for heatmap for A2780 and 2780CP/CI-16 treated with cis-Pt and oxali-Pt										
SAMPLE	JAB1-M-C	JNK_pT183_Y185-R-V	JNK2-R-C	Lck-R-V	MAPK_pT202_Y204-R-V	Mcl-1-R-V	MDM2_pS166-R-V	MEK1-R-V	MEK1_pS217_S221-R-V	MEK2-R-V
A2780 Control_A	-0.106	0.663	0.086	0.028	-0.136	-0.237	0.101	-0.008	-0.636	0.045
A2780 Control_B	-0.039	0.186	-0.163	0.003	-0.100	-0.211	-1.059	-0.066	-0.735	-0.001
A2780 Control_C	-0.011	0.237	-0.176	0.104	-0.079	-0.187	-0.965	0.036	-0.610	0.028
A2780 Cis-Pt_A	0.142	0.067	0.221	0.173	0.945	-0.009	0.410	0.012	-0.028	0.014
A2780 Cis-Pt_B	-0.049	0.071	0.028	0.073	1.084	0.065	-0.225	0.006	0.028	-0.040
A2780 Cisp-Pt_C	0.022	-0.041	-0.018	0.029	1.068	0.009	-0.098	-0.025	-0.023	-0.089
A2780 Oxali-Pt_A	-0.120	-0.033	-0.057	0.132	1.534	0.282	0.182	-0.077	0.294	-0.090
A2780 Oxali-Pt_B	0.096	0.017	0.126	0.427	1.831	0.193	0.949	-0.120	0.302	-0.058
A2780 Oxali-Pt_C	-0.065	0.047	0.063	0.063	1.701	0.292	0.557	0.016	0.266	-0.095
2780CP/CI16 Control_A	-0.173	-0.100	0.143	-0.642	-0.157	-0.045	-0.151	0.060	0.104	0.106
2780CP/CI16 Control_B	-0.034	-0.091	0.351	-0.600	-0.240	-0.159	0.557	-0.006	0.165	0.167
2780CP/CI16 Control_C	0.028	-0.027	0.018	-0.520	-0.415	-0.055	-0.814	0.056	0.023	0.109
2780CP/CI16 Cis-Pt_A	0.104	0.022	-0.154	-0.508	-0.401	0.013	-0.860	0.153	-0.104	0.267
2780CP/CI16 Cis-Pt_B	-0.039	-0.017	0.286	-0.383	-0.438	-0.058	0.269	0.048	0.123	0.029
2780CP/CI16 Cis-Pt_C	0.013	-0.113	-0.035	-0.353	-0.297	-0.176	-0.741	0.056	0.117	0.001
2780CP/CI16 Oxali-Pt_A	0.076	0.027	-0.577	-0.003	0.304	0.557	-0.411	-0.480	-0.198	-0.121
2780CP/CI16 Oxali-Pt_B	0.011	-0.089	-0.381	-0.097	0.267	0.426	0.124	-0.529	-0.255	-0.122
2780CP/CI16 Oxali-Pt_C	0.104	-0.087	-0.424	-0.163	0.079	0.435	0.098	-0.522	-0.304	-0.078

Appendix I. RPPA values for heatmap for A2780 and 2780CP/CI-16 treated with cis-Pt and oxali-Pt										
SAMPLE	Merlin-R-C	MIG6-M-V	MSH2-M-V	MSH6-R-C	mTOR-R-V	mTOR_pS2448-R-C	Myosin-11-R-V	Myosin-IIa_pS1943-R-V	N-Cadherin-R-V	N-Ras-M-V
A2780 Control_A	-0.383	-0.090	-0.018	0.153	0.066	0.095	0.091	0.230	-0.085	-0.173
A2780 Control_B	-0.545	-0.196	0.274	0.213	0.115	0.153	0.111	-0.077	-0.296	0.016
A2780 Control_C	-0.664	-0.101	0.413	0.113	0.166	0.086	0.034	-0.184	-0.099	0.037
A2780 Cis-Pt_A	-0.395	-0.011	-0.020	0.225	0.178	0.011	0.056	0.140	-0.090	-0.210
A2780 Cis-Pt_B	-0.419	-0.146	0.496	0.285	0.106	-0.081	0.061	-0.200	0.094	-0.016
A2780 Cisp-Pt_C	-0.531	-0.196	0.348	0.238	0.083	-0.079	-0.070	-0.007	-0.104	-0.179
A2780 Oxali-Pt_A	-0.567	-0.175	0.389	0.043	0.074	-0.116	-0.018	-0.181	-0.141	0.079
A2780 Oxali-Pt_B	-0.502	-0.156	0.018	0.155	0.126	-0.073	0.036	0.044	0.043	-0.067
A2780 Oxali-Pt_C	-0.571	-0.254	0.159	0.058	0.228	0.077	-0.001	-0.059	-0.187	-0.028
2780CP/CI16 Control_A	0.694	0.167	-0.193	-0.307	-0.150	0.131	0.034	0.442	-0.101	0.028
2780CP/CI16 Control_B	1.085	0.151	-0.311	-0.234	-0.126	0.082	0.056	0.405	-0.043	-0.093
2780CP/CI16 Control_C	0.603	0.132	-0.075	-0.418	-0.066	0.071	0.001	0.519	0.148	0.102
2780CP/CI16 Cis-Pt_A	0.383	0.176	-0.270	-0.582	-0.315	-0.073	-0.034	0.007	0.086	0.100
2780CP/CI16 Cis-Pt_B	1.164	0.059	0.236	-0.043	-0.103	-0.008	-0.072	0.574	0.519	-0.100
2780CP/CI16 Cis-Pt_C	0.828	0.034	0.261	-0.209	-0.073	0.008	-0.170	0.492	0.133	-0.052
2780CP/CI16 Oxali-Pt_A	0.708	0.091	-0.345	-0.791	-0.398	-0.118	-0.098	-0.105	0.480	0.377
2780CP/CI16 Oxali-Pt_B	0.818	0.043	-0.578	-0.709	-0.356	-0.043	-0.033	-0.131	0.585	0.270
2780CP/CI16 Oxali-Pt_C	0.815	0.011	-0.534	-0.689	-0.279	-0.075	-0.192	-0.286	0.486	0.312

Appendix I. RPPA values for heatmap for A2780 and 2780CP/CI-16 treated with cis-Pt and oxali-Pt										
SAMPLE	NAPSIN-A-R-C	NDRG1_pT346-R-V	NF-kB-p65_pS536-R-C	Notch1-R-V	p16INK4a-R-V	p21-R-V	p27-Kip-1-R-V	p27_pT157-R-C	p27_pT198-R-V	p38-alpha-M-V
A2780 Control_A	0.064	-0.270	-0.698	-0.614	0.223	-0.111	-0.063	-0.029	0.016	0.000
A2780 Control_B	0.115	0.102	-0.735	-0.551	0.378	0.031	-0.083	-0.008	-0.040	0.000
A2780 Control_C	0.063	-0.159	-0.543	-0.568	-0.048	-0.094	0.041	0.132	0.077	-0.036
A2780 Cis-Pt_A	0.141	0.555	-0.221	-0.264	0.235	0.543	0.026	-0.177	-0.166	-0.006
A2780 Cis-Pt_B	-0.097	0.241	-0.021	-0.214	-0.057	0.387	-0.012	-0.157	-0.074	-0.047
A2780 Cisp-Pt_C	-0.115	0.357	0.025	-0.190	0.023	0.541	-0.017	-0.163	-0.133	-0.006
A2780 Oxali-Pt_A	-0.126	-0.065	0.118	0.126	-0.041	1.651	0.448	-0.050	-0.106	0.003
A2780 Oxali-Pt_B	-0.048	-0.074	-0.093	-0.096	0.127	1.612	0.357	0.008	0.107	-0.040
A2780 Oxali-Pt_C	-0.077	-0.167	0.021	-0.032	-0.113	1.528	0.367	-0.044	-0.158	0.077
2780CP/CI16 Control_A	-0.114	0.428	0.433	0.056	0.001	-0.100	0.072	0.097	-0.075	0.275
2780CP/CI16 Control_B	0.063	0.329	0.432	0.011	-0.047	-0.155	-0.004	0.090	-0.122	0.209
2780CP/CI16 Control_C	0.021	0.566	0.726	0.008	-0.041	-0.176	0.132	0.049	0.068	0.289
2780CP/CI16 Cis-Pt_A	0.060	-0.077	0.543	-0.008	-0.001	-0.282	-0.045	0.011	0.277	0.300
2780CP/CI16 Cis-Pt_B	-0.006	0.163	0.719	0.066	-0.092	-0.227	-0.036	-0.099	-0.016	0.247
2780CP/CI16 Cis-Pt_C	0.006	0.065	0.592	0.061	0.111	-0.229	-0.042	-0.021	0.370	0.217
2780CP/CI16 Oxali-Pt_A	-0.028	-0.137	-0.239	0.580	-0.019	0.321	0.024	0.062	0.202	-0.081
2780CP/CI16 Oxali-Pt_B	-0.034	-0.296	-0.298	0.477	0.015	-0.031	0.004	0.034	0.587	-0.137
2780CP/CI16 Oxali-Pt_C	0.103	-0.670	-0.536	0.416	0.006	0.143	-0.089	0.015	0.231	-0.055

Appendix I. RPPA values for heatmap for A2780 and 2780CP/CI-16 treated with cis-Pt and oxali-Pt										
SAMPLE	p38-R-V	p38_pT180_Y182-R-V	p53-R-C	p70-S6K_pT389-R-V	p70-S6K1-R-V	PAI-1-M-V	PARP-cleaved-M-QC	PARP1-R-V	Paxillin-R-C	PCNA-M-C
A2780 Control_A	-0.103	0.964	-0.264	-0.096	0.059	-0.424	-0.038	0.086	-0.307	-0.032
A2780 Control_B	0.049	0.978	-0.265	0.359	0.267	-0.171	0.028	0.163	-0.610	0.228
A2780 Control_C	0.000	0.840	-0.179	0.239	0.331	-0.211	0.105	0.350	-0.520	0.011
A2780 Cis-Pt_A	-0.090	0.447	-0.109	-0.370	0.279	-0.415	0.300	0.258	0.012	-0.011
A2780 Cis-Pt_B	0.000	0.564	-0.012	-0.254	0.291	-0.311	0.217	0.425	-0.381	0.102
A2780 Cisp-Pt_C	-0.003	0.387	0.012	-0.384	0.217	-0.375	0.175	0.410	-0.361	0.014
A2780 Oxali-Pt_A	0.034	0.279	0.659	-1.020	0.202	-0.085	0.135	0.370	-0.390	0.056
A2780 Oxali-Pt_B	-0.113	0.284	0.583	-0.906	0.127	-0.238	0.063	0.334	-0.099	-0.044
A2780 Oxali-Pt_C	-0.014	0.333	0.464	-0.791	0.242	-0.257	0.086	0.230	-0.305	0.113
2780CP/CI16 Control_A	0.428	-0.439	-0.144	1.188	-0.254	0.085	-0.368	-0.771	0.577	0.012
2780CP/CI16 Control_B	0.479	-0.520	-0.305	1.227	-0.229	0.155	-0.312	-0.852	0.595	0.086
2780CP/CI16 Control_C	0.459	-0.279	-0.078	1.045	-0.059	0.316	-0.040	-0.283	0.620	-0.114
2780CP/CI16 Cis-Pt_A	0.266	-0.518	-0.121	0.627	-0.075	0.517	-0.188	-0.514	0.464	0.028
2780CP/CI16 Cis-Pt_B	0.490	-0.403	0.040	0.831	-0.174	0.265	-0.189	-0.139	0.587	-0.286
2780CP/CI16 Cis-Pt_C	0.505	-0.472	0.017	0.938	-0.202	0.295	-0.147	-0.086	0.515	-0.249
2780CP/CI16 Oxali-Pt_A	-0.350	-1.033	0.725	0.038	-0.676	2.014	0.242	-0.280	0.052	-0.476
2780CP/CI16 Oxali-Pt_B	-0.380	-1.261	0.632	-0.038	-0.757	1.876	-0.028	-0.284	0.035	-0.379
2780CP/CI16 Oxali-Pt_C	-0.352	-1.307	0.612	-0.172	-0.833	1.794	-0.120	-0.562	-0.012	-0.395

Appendix I. RPPA values for heatmap for A2780 and 2780CP/CI-16 treated with cis-Pt and oxali-Pt										
SAMPLE	Pdcd-1L1-G-C	Pdcd4-R-C	PDGFR-beta-R-V	PDK1-R-V	PDK1_pS241-R-V	PEA-15-R-V	PEA-15_pS116-R-V	PI3K-p110-alpha-R-C	PI3K-p85-R-V	PKC-alpha-M-V
A2780 Control_A	0.246	0.965	1.179	-0.022	-0.111	0.341	0.472	0.000	-0.103	-0.585
A2780 Control_B	0.097	1.030	1.490	-0.118	-0.118	-0.007	0.266	0.068	-0.088	-0.400
A2780 Control_C	-0.147	1.098	1.409	-0.004	-0.002	-0.030	0.152	0.159	-0.014	-0.749
A2780 Cis-Pt_A	-0.190	1.427	1.296	0.066	-0.163	0.318	0.194	-0.019	-0.023	-0.419
A2780 Cis-Pt_B	-0.021	1.485	1.268	0.099	0.002	0.021	0.000	0.088	-0.004	-0.653
A2780 Cisp-Pt_C	0.017	1.499	1.260	0.055	0.008	0.007	-0.019	0.070	0.011	-0.616
A2780 Oxali-Pt_A	-0.010	2.007	1.175	0.000	0.092	-0.008	-0.055	0.091	0.044	-0.699
A2780 Oxali-Pt_B	0.011	1.964	0.980	0.028	-0.101	0.146	0.248	0.039	-0.030	-0.513
A2780 Oxali-Pt_C	-0.077	2.100	1.222	0.062	0.013	0.117	0.078	0.069	0.030	-0.814
2780CP/CI16 Control_A	-0.121	-1.062	-1.443	-0.067	0.023	0.062	0.211	-0.027	0.004	0.506
2780CP/CI16 Control_B	-0.067	-1.209	-0.980	0.000	-0.042	0.160	0.236	-0.023	0.041	0.479
2780CP/CI16 Control_C	-0.089	-1.022	-1.434	0.042	0.082	-0.027	0.000	0.000	0.097	0.408
2780CP/CI16 Cis-Pt_A	-0.078	-0.965	-1.448	0.054	0.115	-0.041	-0.244	0.094	0.259	0.400
2780CP/CI16 Cis-Pt_B	0.010	-1.102	-1.436	0.016	0.029	0.010	-0.084	-0.090	0.065	0.413
2780CP/CI16 Cis-Pt_C	0.185	-0.999	-1.173	-0.012	0.046	-0.076	-0.099	-0.058	0.129	0.436
2780CP/CI16 Oxali-Pt_A	0.371	-1.280	-1.207	-0.307	-0.342	-0.527	-0.269	-0.171	-0.421	0.988
2780CP/CI16 Oxali-Pt_B	0.142	-1.330	-1.240	-0.178	-0.419	-0.349	-0.125	-0.171	-0.224	1.066
2780CP/CI16 Oxali-Pt_C	0.178	-1.458	-1.155	-0.158	-0.439	-0.432	-0.255	-0.216	-0.367	1.023

Appendix I. RPPA values for heatmap for A2780 and 2780CP/CI-16 treated with cis-Pt and oxali-Pt										
SAMPLE	PKC-alpha_pS657-R-C	PKC-beta-II_pS660-R-V	PKC-delta_pS664-R-V	PMS2-R-V	Porin-M-V	PR-R-V	PRAS40_pT246-R-V	PREX1-R-V	PTEN-R-V	Rab11-R-E
A2780 Control_A	-0.755	-0.109	-0.101	0.205	-0.171	0.097	0.058	0.019	-0.100	0.134
A2780 Control_B	-0.442	0.113	-0.177	0.108	0.109	-0.027	0.257	-0.128	-0.176	0.076
A2780 Control_C	-0.578	0.059	-0.052	-0.002	-0.179	-0.029	0.148	-0.104	-0.043	-0.033
A2780 Cis-Pt_A	-0.825	0.139	-0.006	0.091	-0.003	0.248	-0.101	-0.163	0.009	-0.067
A2780 Cis-Pt_B	-0.650	0.332	-0.008	-0.082	-0.093	-0.011	-0.058	-0.115	-0.006	-0.207
A2780 Cisp-Pt_C	-0.720	0.393	-0.053	-0.004	-0.126	0.051	-0.074	-0.159	-0.072	-0.123
A2780 Oxali-Pt_A	-0.678	0.959	0.006	0.057	0.029	0.009	-0.259	-0.062	-0.002	-0.027
A2780 Oxali-Pt_B	-0.833	0.965	0.328	0.014	0.796	0.213	-0.144	-0.069	0.002	-0.016
A2780 Oxali-Pt_C	-0.829	0.870	0.013	-0.057	0.141	-0.009	-0.192	-0.331	0.021	-0.090
2780CP/CI16 Control_A	0.538	0.002	-0.053	0.083	0.003	-0.197	0.834	0.053	0.050	0.092
2780CP/CI16 Control_B	0.463	-0.097	0.015	0.002	0.053	-0.070	0.783	-0.012	0.051	-0.064
2780CP/CI16 Control_C	0.635	-0.033	0.088	-0.124	-0.249	-0.093	0.714	0.118	0.068	0.016
2780CP/CI16 Cis-Pt_A	0.454	-0.071	-0.023	0.020	-0.237	-0.205	0.464	0.069	0.037	0.027
2780CP/CI16 Cis-Pt_B	0.500	-0.048	0.123	0.005	-0.203	0.024	0.590	0.084	0.092	-0.079
2780CP/CI16 Cis-Pt_C	0.442	-0.002	-0.100	-0.004	-0.272	-0.145	0.590	0.174	0.030	0.934
2780CP/CI16 Oxali-Pt_A	1.216	-0.162	1.047	-0.354	0.848	0.062	-0.125	0.239	-0.407	0.302
2780CP/CI16 Oxali-Pt_B	1.223	-0.254	0.820	-0.450	0.740	0.056	-0.084	0.245	-0.357	0.210
2780CP/CI16 Oxali-Pt_C	1.241	-0.268	0.826	-0.454	0.742	0.065	-0.134	0.012	-0.366	0.861

Appendix I. RPPA values for heatmap for A2780 and 2780CP/CI-16 treated with cis-Pt and oxali-Pt										
SAMPLE	Rab25-R-V	Rad50-M-V	Rad51-R-V	Raptor-R-V	Rb-M-QC	Rb_pS807_S811-R-V	RBM15-R-V	Rictor-R-C	Rictor_pT1135-R-V	RSK-R-C
A2780 Control_A	0.149	0.143	0.313	0.308	0.099	-0.253	0.278	-0.004	-0.032	0.249
A2780 Control_B	-0.002	0.012	0.273	0.289	0.093	-0.165	0.005	0.141	0.072	0.138
A2780 Control_C	-0.053	0.047	0.065	0.188	0.061	-0.337	0.003	0.109	0.040	0.151
A2780 Cis-Pt_A	-0.152	0.267	0.335	0.358	0.039	0.455	-0.003	-0.063	-0.094	0.532
A2780 Cis-Pt_B	-0.134	0.035	0.213	0.227	0.010	0.429	-0.017	-0.008	-0.080	0.531
A2780 Cisp-Pt_C	-0.087	0.004	0.195	0.249	-0.010	0.498	-0.049	-0.086	-0.160	0.541
A2780 Oxali-Pt_A	0.005	-0.004	-0.230	0.164	0.036	-0.319	0.116	-0.075	-0.122	0.662
A2780 Oxali-Pt_B	-0.062	0.137	-0.067	0.148	0.079	-0.409	1.271	-0.149	-0.112	0.583
A2780 Oxali-Pt_C	0.073	0.073	-0.215	0.221	0.056	-0.397	0.160	-0.066	-0.077	0.730
2780CP/CI16 Control_A	-0.012	-0.113	0.067	-0.225	-0.024	0.165	-0.014	0.321	0.666	-0.219
2780CP/CI16 Control_B	-0.117	0.019	0.126	-0.148	0.014	0.240	-0.077	0.327	0.591	-0.200
2780CP/CI16 Control_C	0.099	-0.048	-0.055	-0.230	-0.097	0.293	-0.161	0.418	0.502	-0.314
2780CP/CI16 Cis-Pt_A	0.002	-0.042	0.016	-0.420	-0.058	0.244	-0.044	0.282	0.399	-0.336
2780CP/CI16 Cis-Pt_B	0.062	-0.084	-0.016	-0.303	-0.111	0.622	-0.153	0.249	0.367	-0.165
2780CP/CI16 Cis-Pt_C	-0.016	-0.092	-0.170	-0.334	-0.140	0.551	-0.202	0.251	0.381	-0.318
2780CP/CI16 Oxali-Pt_A	0.425	-0.143	-0.556	-0.553	-0.118	-0.982	0.858	0.004	0.032	-0.605
2780CP/CI16 Oxali-Pt_B	0.350	-0.146	-0.483	-0.487	-0.204	-0.993	0.554	-0.075	-0.079	-0.197
2780CP/CI16 Oxali-Pt_C	0.362	-0.056	-0.446	-0.429	-0.189	-0.931	0.767	-0.269	-0.195	-0.138

Appendix I. RPPA values for heatmap for A2780 and 2780CP/CI-16 treated with cis-Pt and oxali-Pt										
SAMPLE	S6_pS235_S236-R-V	S6_pS240_S244-R-V	SCD-M-V	SETD2-R-QC	SF2-M-V	Shc_pY317-R-V	Smac-M-QC	Smad1-R-V	Smad3-R-V	Smad4-M-V
A2780 Control_A	-0.926	-0.366	0.124	0.180	-0.071	0.157	0.084	-0.060	0.173	0.514
A2780 Control_B	-0.529	-0.332	0.206	0.327	-0.013	0.074	-0.049	-0.140	0.006	0.506
A2780 Control_C	-0.858	-0.523	0.009	0.269	0.013	0.033	-0.012	-0.066	0.082	0.418
A2780 Cis-Pt_A	-1.370	-0.721	-0.081	0.169	0.016	-0.126	0.263	-0.061	0.098	0.459
A2780 Cis-Pt_B	-1.059	-0.695	-0.220	0.148	-0.054	-0.110	0.012	-0.120	0.006	0.382
A2780 Cisp-Pt_C	-1.059	-0.747	-0.044	0.134	0.068	-0.155	-0.017	-0.181	0.010	0.475
A2780 Oxali-Pt_A	-0.903	-1.017	0.033	-0.026	0.027	-0.097	0.101	-0.224	-0.072	0.347
A2780 Oxali-Pt_B	-1.109	-1.001	0.066	-0.033	0.098	-0.143	0.164	-0.149	0.104	0.369
A2780 Oxali-Pt_C	-0.987	-0.902	-0.006	-0.077	-0.024	-0.140	0.157	-0.173	-0.014	0.287
2780CP/CI16 Control_A	2.065	1.378	0.006	0.010	-0.127	-0.006	-0.461	0.101	-0.017	-0.526
2780CP/CI16 Control_B	1.956	1.641	-0.062	-0.010	-0.205	0.093	-0.219	0.145	-0.006	-0.568
2780CP/CI16 Control_C	1.980	1.149	-0.061	0.064	0.035	0.036	-0.324	0.110	-0.083	-0.464
2780CP/CI16 Cis-Pt_A	1.527	0.896	-0.161	0.041	-0.034	0.088	-0.360	0.060	-0.153	-0.440
2780CP/CI16 Cis-Pt_B	1.921	1.608	-0.143	-0.010	-0.063	-0.084	-0.263	0.067	-0.061	-0.520
2780CP/CI16 Cis-Pt_C	1.899	1.414	-0.138	-0.020	-0.017	-0.091	-0.324	0.072	-0.060	-0.344
2780CP/CI16 Oxali-Pt_A	0.739	0.354	0.151	-0.117	0.207	0.084	0.375	0.088	-0.023	-0.287
2780CP/CI16 Oxali-Pt_B	0.545	0.332	0.092	-0.146	0.104	0.006	0.362	0.133	0.010	-0.410
2780CP/CI16 Oxali-Pt_C	0.529	0.363	0.081	-0.065	0.064	0.058	0.336	0.124	0.050	-0.384

Appendix I. RPPA values for heatmap for A2780 and 2780CP/CI-16 treated with cis-Pt and oxali-Pt										
SAMPLE	Snail-M-QC	Src-M-V	Src_pY416-R-C	Src_pY527-R-V	Stat3_pY705-R-V	Stat5a-R-V	Stathmin-1-R-V	Syk-M-V	TAZ-R-V	TFRC-R-V
A2780 Control_A	-0.139	-0.315	0.745	0.221	-0.164	-0.075	-0.062	0.116	-0.173	0.288
A2780 Control_B	-0.068	-0.117	1.202	0.183	0.034	-0.077	0.014	-0.023	-0.211	-0.071
A2780 Control_C	-0.032	-0.015	1.371	0.077	-0.026	-0.014	0.010	-0.229	-0.204	-0.003
A2780 Cis-Pt_A	-0.117	-0.065	0.937	-0.077	-0.084	0.201	-0.022	0.102	-0.269	0.395
A2780 Cis-Pt_B	-0.043	-0.112	0.955	-0.180	-0.002	0.012	-0.005	-0.171	-0.230	0.104
A2780 Cisp-Pt_C	-0.047	-0.085	1.147	-0.131	-0.083	0.002	0.029	-0.025	-0.313	0.083
A2780 Oxali-Pt_A	-0.049	0.084	0.744	0.262	-0.060	-0.072	0.023	-0.055	-0.271	0.003
A2780 Oxali-Pt_B	-0.041	0.015	1.051	0.718	0.037	0.063	0.030	0.005	-0.041	0.178
A2780 Oxali-Pt_C	-0.063	-0.093	0.291	0.265	0.015	-0.035	0.045	-0.069	-0.242	0.164
2780CP/CI16 Control_A	0.032	-0.025	-0.596	-0.369	-0.044	0.077	0.027	0.204	0.268	-0.316
2780CP/CI16 Control_B	0.138	-0.197	-0.529	-0.410	-0.074	0.074	-0.039	-0.074	0.286	-0.140
2780CP/CI16 Control_C	0.287	0.160	-0.372	-0.441	0.113	0.128	0.089	-0.063	0.260	-0.463
2780CP/CI16 Cis-Pt_A	0.321	0.378	-0.291	-0.479	0.072	0.058	-0.079	0.075	0.191	-0.662
2780CP/CI16 Cis-Pt_B	0.285	0.028	-0.325	-0.576	-0.020	0.062	-0.009	0.072	0.159	-0.153
2780CP/CI16 Cis-Pt_C	0.358	0.217	-0.610	-0.678	0.002	-0.002	0.005	0.077	0.158	-0.512
2780CP/CI16 Oxali-Pt_A	0.549	1.023	-0.618	0.383	0.194	-0.380	-0.072	0.282	0.102	-0.177
2780CP/CI16 Oxali-Pt_B	0.487	0.638	-0.608	0.335	0.051	-0.280	-0.140	0.252	0.041	0.335
2780CP/CI16 Oxali-Pt_C	0.462	0.504	-1.025	0.416	0.118	-0.258	-0.263	-0.005	0.105	0.409

Appendix I. RPPA values for heatmap for A2780 and 2780CP/CI-16 treated with cis-Pt and oxali-Pt										
SAMPLE	TIGAR-R-V	Transglutaminase-M-V	TSC1-R-C	TTF1-R-V	Tuberin-R-V	Tuberin_pT1462-R-V	TWIST-M-C	Tyro3-R-V	UBAC1-R-V	UGT1A-M-V
A2780 Control_A	0.090	-0.025	0.240	0.176	-0.042	-0.059	1.069	-0.657	0.174	0.020
A2780 Control_B	0.153	0.065	0.464	0.116	0.295	-0.205	0.850	-0.551	0.122	0.452
A2780 Control_C	0.042	0.027	0.424	0.126	0.087	-0.152	0.644	-0.379	-0.004	0.005
A2780 Cis-Pt_A	0.285	-0.036	0.177	0.343	0.050	-0.018	0.954	-0.665	0.109	-0.052
A2780 Cis-Pt_B	0.306	-0.066	0.270	0.374	0.148	0.017	0.708	-0.722	0.089	-0.069
A2780 Cisp-Pt_C	0.333	-0.087	0.273	0.315	0.145	0.026	0.752	-0.675	0.031	-0.001
A2780 Oxali-Pt_A	0.503	-0.049	0.389	0.117	0.183	0.041	1.117	-1.130	-0.017	-0.070
A2780 Oxali-Pt_B	0.402	0.064	0.061	0.001	0.006	0.112	1.991	-1.180	0.073	0.120
A2780 Oxali-Pt_C	0.529	0.070	0.327	0.060	0.141	0.102	1.102	-1.087	0.017	0.001
2780CP/CI16 Control_A	-0.049	-0.037	-0.081	-0.001	-0.104	0.075	-1.327	0.379	-0.022	-0.031
2780CP/CI16 Control_B	-0.042	0.012	-0.162	-0.102	-0.131	0.091	-1.401	0.398	0.030	0.096
2780CP/CI16 Control_C	-0.126	0.030	-0.061	-0.109	0.009	0.017	-1.101	0.602	-0.041	-0.033
2780CP/CI16 Cis-Pt_A	-0.053	0.147	-0.134	-0.188	-0.130	-0.061	-1.136	0.433	-0.153	-0.082
2780CP/CI16 Cis-Pt_B	-0.113	-0.012	-0.122	-0.052	-0.006	0.037	-1.113	0.552	0.004	-0.058
2780CP/CI16 Cis-Pt_C	-0.065	-0.043	-0.064	-0.015	-0.063	-0.017	-0.986	0.511	-0.090	-0.067
2780CP/CI16 Oxali-Pt_A	-0.191	0.181	-0.546	-0.510	-1.257	-0.048	-0.644	1.118	-0.658	0.145
2780CP/CI16 Oxali-Pt_B	-0.205	0.029	-0.592	-0.733	-1.439	-0.119	-0.787	1.012	-0.476	0.216
2780CP/CI16 Oxali-Pt_C	-0.199	-0.041	-0.640	-0.569	-1.419	-0.113	-0.822	1.009	-0.594	0.255

Appendix I. RPPA values for heatmap for A2780 and 2780CP/CI-16 treated with cis-Pt and oxali-Pt							
SAMPLE	UQCRC2-M-C	VEGFR-2-R-V	XRCC1-R-C	YAP-R-E	YAP_pS127-R-E	YB1-R-V	YB1_pS102-R-V
A2780 Control_A	0.488	-0.080	0.158	0.085	-0.014	0.103	-0.511
A2780 Control_B	0.351	0.138	0.182	0.102	-0.013	-0.204	-0.465
A2780 Control_C	-0.073	0.152	0.088	0.064	-0.116	-0.180	-0.449
A2780 Cis-Pt_A	0.370	-0.012	0.038	0.003	-0.006	0.016	-0.328
A2780 Cis-Pt_B	-0.085	0.084	0.024	-0.003	-0.039	0.049	-0.252
A2780 Cisp-Pt_C	-0.049	0.073	0.136	0.027	0.006	-0.160	-0.290
A2780 Oxali-Pt_A	-0.154	0.109	0.153	0.034	0.224	-0.177	-0.103
A2780 Oxali-Pt_B	0.151	0.012	0.362	0.220	-0.079	-0.073	-0.131
A2780 Oxali-Pt_C	-0.145	-0.111	0.115	0.087	0.099	-0.179	-0.044
2780CP/CI16 Control_A	0.049	-0.048	-0.078	-0.104	0.264	0.026	0.144
2780CP/CI16 Control_B	0.268	-0.025	-0.163	-0.137	0.247	-0.048	0.145
2780CP/CI16 Control_C	-0.296	0.152	-0.210	-0.069	0.265	-0.144	0.192
2780CP/CI16 Cis-Pt_A	-0.248	-0.149	-0.184	0.036	0.379	-0.016	0.102
2780CP/CI16 Cis-Pt_B	-0.255	0.033	-0.202	-0.126	0.197	0.188	0.044
2780CP/CI16 Cis-Pt_C	-0.441	0.053	-0.172	-0.032	0.214	0.150	0.094
2780CP/CI16 Oxali-Pt_A	0.304	-0.255	-0.024	-0.151	-0.407	0.287	0.389
2780CP/CI16 Oxali-Pt_B	0.350	-0.322	-0.168	-0.129	-0.378	0.219	0.318
2780CP/CI16 Oxali-Pt_C	0.201	-0.420	-0.055	-0.123	-0.427	0.331	0.311

Appendix 2: Analysis of protein changes from RPPA data generated for A2780 and 2780CP/CI-16 treated with cis-Pt and oxali-Pt

Proteins significantly downregulated in A2780 after cis-Pt treatment	
Protein Name	Fold Change
MAPK14_p38_pT180_Y182-R-V	-1.19
EIF4EBP1_4E-BP1_pS65-R-V	-1.18
ACACA ACACB_ACC_pS79-R-V	-1.15
EIF4G1_eIF4G-R-C	-1.13
SRC YES1 FYN FGR_Src_pY527-R-V	-1.13
MYC_c-Myc-R-C	-1.13
EIF4EBP1_4E-BP1_pT37_T46-R-V	-1.11
RPS6_S6_pS240_S244-R-V	-1.11
BCL2L11_Bim-R-V	-1.09
MTOR_mTOR_pS2448-R-C	-1.06
CCNE1_Cyclin-E1-M-V	-1.06
SHC1_Shc_pY317-R-V	-1.06
GAB2_Gab2-R-V	-1.05
CDKN1B_p27_pT198-R-V	-1.04
RICTOR_Rictor_pT1135-R-V	-1.04
ATR_ATR-R-C	-1.04
PTK2_FAK_pY397-R-V	-1.03
ARAF_A-Raf-R-V	-1.03
SCD_SCD-M-V	-1.02
YAP1_YAP-R-E	-1.02
PTK2_FAK-R-E	-1.02
RAB11A RAB11B_Rab11-R-E	-1.02
RB1_Rb-M-QC	-1.02
BCL2_Bcl2-M-V	-1.02
ADAR_ADAR1-M-V	-1.01

Proteins significantly upregulated in A2780 after cis-Pt treatment	
Protein Name	Fold Change
CCNB1_Cyclin-B1-R-V	2.20
RB1_Rb_pS807_S811-R-V	1.40
CDKN1A_p21-R-V	1.24
MAPK1 MAPK3_MAPK_pT202_Y204-R-V	1.23

MAP2K1 MAP2K2_MEK1_pS217_S221-R-V	1.21
FOXO1_FoxO1-R-V	1.21
BAX_Bax-R-V	1.20
PDCD4_Pdcd4-R-C	1.19
RELA_NF-kB-p65_pS536-R-C	1.15
RPS6KA1 RPS6KA2 RPS6KA3_RSK-R-C	1.14
NOTCH1_Notch1-R-V	1.14
GSK3A GSK3B_GSK-3ab_pS21_S9-R-V	1.11
CDC2-CDK1_CDK1-R-V	1.10
NKX2-1_TTF1-R-V	1.10
C12ORF5_TIGAR-R-V	1.09
CASP7_Caspase-7-cleaved-R-C	1.07
H3F3A H3F3B_Histone-H3-R-V	1.06
ATM_ATM_pS1981-R-V	1.06
PRKAA1_AMPK-alpha-R-C	1.06
NDRG1_NDRG1_pT346-R-V	1.06
CHEK1_Chk1_pS345-R-C	1.05
YBX1_YB1_pS102-R-V	1.05
MCL1_Mcl-1-R-V	1.05
AKT1 AKT2 AKT3_Akt-R-V	1.04
PARP1_PARP-cleaved-M-QC	1.02
TP53_p53-R-C	1.02

Proteins significantly downregulated in A2780 after oxali-Pt treatment	
Protein Name	Fold Change
ACACA ACACB_ACC_pS79-R-V	-1.31
RPS6KB1_p70-S6K_pT389-R-V	-1.28
EIF4EBP1_4E-BP1_pS65-R-V	-1.27
MAPK14_p38_pT180_Y182-R-V	-1.27
EIF4EBP1_4E-BP1_pT37_T46-R-V	-1.24
EIF4G1_eIF4G-R-C	-1.21
RPS6_S6_pS240_S244-R-V	-1.21
EEF2K_eEF2K-R-V	-1.17
BCL2L11_Bim-R-V	-1.17
AKT1S1_PRAS40_pT246-R-V	-1.17
CHEK1_Chk1-M-C	-1.15
TYRO3_Tyro3-R-V	-1.11
RAD51_Rad51-R-V	-1.10

GAB2_Gab2-R-V	-1.08
ATR_ATR-R-C	-1.08
PPIF_Cyclophilin-F-M-V	-1.06
BRCA2_BRCA2-R-C	-1.06
SETD2_SETD2-R-QC	-1.06
RICTOR_Rictor-R-C	-1.06
SHC1_Shc_pY317-R-V	-1.06
SMAD4_Smad4-M-V	-1.04
PTK2_FAK_pY397-R-V	-1.04
FOXO3_FoxO3a-R-C	-1.04
RICTOR_Rictor_pT1135-R-V	-1.04
NAPSA_NAPSIN-A-R-C	-1.03
EGFR_EGFR_pY1068-R-C	-1.03
MAP2K2_MEK2-R-V	-1.03
CASP8_Caspase-8-M-QC	-1.03

Proteins significantly upregulated in A2780 after oxali-Pt treatment	
Protein Name	Fold Change
CDKN1A_p21-R-V	2.13
PRKCA PRKCB PRKCD PRKCE PRKCH PRKCQ_PKC-beta-II_pS660-R-V	1.54
PDCD4_Pdcd4-R-C	1.52
MAPK1 MAPK3_MAPK_pT202_Y204-R-V	1.47
BAX_Bax-R-V	1.44
MAP2K1 MAP2K2_MEK1_pS217_S221-R-V	1.35
GSK3A GSK3B_GSK-3ab_pS21_S9-R-V	1.26
NOTCH1_Notch1-R-V	1.24
RPS6KA1 RPS6KA2 RPS6KA3_RSK-R-C	1.20
RELA_NF-kB-p65_pS536-R-C	1.18
C12ORF5_TIGAR-R-V	1.18
GSK3B_GSK-3b_pS9-R-V	1.16
AKT1 AKT2 AKT3_Akt_pT308-R-V	1.14
YBX1_YB1_pS102-R-V	1.11
MCL1_Mcl-1-R-V	1.10
CCNE1_Cyclin-E1-M-V	1.10
AKT1 AKT2 AKT3_Akt_pS473-R-V	1.09

TP53_p53-R-C	1.08
H3F3A H3F3B_Histone-H3-R-V	1.08
PRKAA1_AMPK-alpha-R-C	1.08
CDKN1B_p27-Kip-1-R-V	1.07
RAF1_C-Raf_pS338-R-V	1.06
PTGS2_Cox2-R-C	1.06
CCND1_Cyclin-D1-R-V	1.05
FOXM1_FoxM1-R-V	1.04
TSC2_Tuberlin_pT1462-R-V	1.04
BAD_Bad_pS112-R-V	1.02
ANXA1_Annexin-I-M-V	1.00

Proteins significantly downregulated in 2780CP/CI-16 after cis-Pt treatment	
Protein Name	Fold Change
RPS6KB1_p70-S6K_pT389-R-V	-1.15
AKT1S1_PRAS40_pT246-R-V	-1.12
PEA15_PEA-15_pS116-R-V	-1.11
GSK3B_GSK-3b_pS9-R-V	-1.08
RICTOR_Rictor_pT1135-R-V	-1.07
RPTOR_Raptor-R-V	-1.07
NDRG1_NDRG1_pT346-R-V	-1.05
PTK2_FAK-R-E	-1.05
SDHA_Complex-II-Subunit-M-V	-1.05
MTOR_mTOR_pS2448-R-C	-1.05
CDKN1A_p21-R-V	-1.04
WWTR1_TAZ-R-V	-1.04
CCNE1_Cyclin-E1-M-V	-1.04
YBX1_YB1_pS102-R-V	-1.03
SCD_SCD-M-V	-1.01

Proteins significantly upregulated in 2780CP/CI-16 after cis-Pt treatment	
Protein Name	Fold Change
CCNB1_Cyclin-B1-R-V	1.46
FOXM1_FoxM1-R-V	1.16
CHEK1_Chk1_pS345-R-C	1.08
IGFBP2_IGFBP2-R-V	1.03
CASP8_Caspase-8-M-QC	1.02
DIRAS3_ARHI-M-C	1.01

Proteins significantly downregulated in 2780CP/CI-16 after oxali-Pt treatment	
Protein Name	Fold Change
RPS6_S6_pS235_S236-R-V	-2.07
TSC2_Tuberin-R-V	-1.75
RPS6_S6_pS240_S244-R-V	-1.69
RB1_Rb_pS807_S811-R-V	-1.66
AKT1S1_PRAS40_pT246-R-V	-1.53
RPS6KB1_p70-S6K_pT389-R-V	-1.50
EEF2K_eEF2K-R-V	-1.47
MAPK14_p38-R-V	-1.46
EIF4EBP1_4E-BP1_pS65-R-V	-1.42
AKT1 AKT2 AKT3_Akt_pT308-R-V	-1.40
BRAF_B-Raf-M-C	-1.39
GAPDH_GAPDH-M-C	-1.37
FASN_FASN-R-V	-1.35
CHEK1_Chk1-M-C	-1.33
AKT1 AKT2 AKT3_Akt_pS473-R-V	-1.33
GSK3A GSK3B_GSK-3ab_pS21_S9-R-V	-1.31
RELA_NF-kB-p65_pS536-R-C	-1.30
GSK3B_GSK-3b_pS9-R-V	-1.28
EIF4G1_eIF4G-R-C	-1.28
MAPK9_JNK2-R-C	-1.26
YAP1_YAP_pS127-R-E	-1.25
MYH9_Myosin-IIa_pS1943-R-V	-1.25
GYS1_Gys-R-V	-1.25
EIF4EBP1_4E-BP1_pT37_T46-R-V	-1.24
AKT1 AKT2 AKT3_Akt-R-V	-1.24
RAF1_C-Raf-R-V	-1.24
ACACA_ACC1-R-E	-1.24
RICTOR_Rictor_pT1135-R-V	-1.23
NKX2-1_TTF1-R-V	-1.23
PXN_Paxillin-R-C	-1.22
EEF2_eEF2-R-C	-1.22
GSK3A GSK3B_GSK-3ab-M-V	-1.21
MSH6_MSH6-R-C	-1.21
UBAC1_UBAC1-R-V	-1.21
TSC1_TSC1-R-C	-1.19
MAPK14_p38_pT180_Y182-R-V	-1.18
RICTOR_Rictor-R-C	-1.17

GYS1_Gys_pS641-R-V	-1.17
PEA15_PEA-15-R-V	-1.17
MAP2K1_MEK1-R-V	-1.16
PARK7_DJ1-R-V	-1.16
YWHAZ_14-3-3-zeta-R-V	-1.16
RPS6KB1_p70-S6K1-R-V	-1.16
EIF4EBP1_4E-BP1-R-V	-1.16
INPP4B_INPP4b-R-V	-1.16
PDPK1_PDK1_pS241-R-V	-1.15
EIF4E_eIF4E-R-V	-1.15
ERCC1_ERCC1-M-V	-1.14
PEA15_PEA-15_pS116-R-V	-1.14
PTK2_FAK-R-E	-1.13
RPTOR_Raptor-R-V	-1.13
MSH2_MSH2-M-V	-1.13
CCNB1_Cyclin-B1-R-V	-1.13
RAD51_Rad51-R-V	-1.12
MAP2K1 MAP2K2_MEK1_pS217_S221-R-V	-1.12
GAB2_Gab2-R-V	-1.12
PYGB_GPBB-R-V	-1.12
MAPK14_p38-alpha-M-V	-1.11
PCNA_PCNA-M-C	-1.11
STAT5A_Stat5a-R-V	-1.11
MTOR_mTOR-R-V	-1.11
PMS2_PMS2-R-V	-1.10
RAF1_C-Raf_pS338-R-V	-1.10
PTEN_PTEN-R-V	-1.10
PIK3R1_PI3K-p85-R-V	-1.10
BRAF_B-Raf_pS445-R-V	-1.09
NDRG1_NDRG1_pT346-R-V	-1.09
ATM_ATM-R-V	-1.09
CCNE1_Cyclin-E1-M-V	-1.08
ATR_ATR-R-C	-1.08
PRKCA PRKCB PRKCD PRKCE PRKCH PRKCQ_PKC-beta-II_pS660-R-V	-1.08
DVL3_Dvl3-R-V	-1.07
KDR_VEGFR-2-R-V	-1.07
ARAF_A-Raf-R-V	-1.07
MTOR_mTOR_pS2448-R-C	-1.07

WWTR1_TAZ-R-V	-1.07
MAP2K2_MEK2-R-V	-1.06
BAD_Bad_pS112-R-V	-1.05
C12ORF5_TIGAR-R-V	-1.05
PIK3CA_PI3K-p110-alpha-R-C	-1.05
PDPK1_PDK1-R-V	-1.05
CHEK1_Chk1_pS345-R-C	-1.04
PDCD4_Pdcd4-R-C	-1.03
RB1_Rb-M-QC	-1.03
ERRFI1_MIG6-M-V	-1.03
TSC2_Tuberin_pT1462-R-V	-1.03
SETD2_SETD2-R-QC	-1.02

Proteins significantly upregulated in 2780CP/CI-16 after oxali-Pt treatment	
Protein Name	Fold Change
SERPINE1_PA1-1-M-V	1.62
SDHA_Complex-II-Subunit-M-V	1.42
PPIF_Cyclophilin-F-M-V	1.39
SRC YES1 FYN FGR_Src_pY527-R-V	1.39
PRKCD_PKC-delta_pS664-R-V	1.34
CTNNB1_b-Catenin-R-V	1.32
RBM15_RBM15-R-V	1.30
COL6A1_Collagen-VI-R-V	1.28
DIABLO_Smac-M-QC	1.28
BAX_Bax-R-V	1.27
NOTCH1_Notch1-R-V	1.23
TYRO3_Tyro3-R-V	1.23
PRKCA_PKC-alpha-M-V	1.19
SRC_Src-M-V	1.19
BCL2L11_Bim-R-V	1.18
IGF1R_IGF1R-beta-R-V	1.18
FOXO3_FoxO3a_pS318_S321-R-C	1.16
PRKCA_PKC-alpha_pS657-R-C	1.16
ANXA7_Annexin-VII-M-V	1.15
TP53BP1_53BP1-R-V	1.14
PRKAA1_AMPK-alpha_pT172-R-V	1.13
MCL1_Mcl-1-R-V	1.13
JUN_c-Jun_pS73-R-V	1.13

YBX1_YB1-R-V	1.12
VDAC1_Porin-M-V	1.11
EGFR_EGFR-R-V	1.10
TP53_p53-R-C	1.09
ATP5H_ATP5H-M-C	1.09
CDH2_N-Cadherin-R-V	1.08
ERBB3_HER3-R-V	1.07
ADAR_ADAR1-M-V	1.07
MAPK1_MAPK3_MAPK_pT202_Y204-R-V	1.07
BCL2_Bcl2-M-V	1.07
YBX1_YB1_pS102-R-V	1.06
KAT2A_GCN5L2-R-V	1.06
LCK_Lck-R-V	1.06
CASP7_Caspase-7-cleaved-R-C	1.06
CD274_Pdcd-1L1-G-C	1.05
TWIST2_TWIST-M-C	1.05
SNAI1_Snail-M-QC	1.05
MET_c-Met-M-QC	1.05
IGFBP2_IGFBP2-R-V	1.04
CLDN7_Claudin-7-R-V	1.04
RAB25_Rab25-R-V	1.03
ERBB2_HER2-M-V	1.03
BID_Bid-R-C	1.03
SMAD4_Smad4-M-V	1.03
CTNNB1_b-Catenin_pT41_S45-R-V	1.03
DIRAS3_ARHI-M-C	1.03
PGR_PR-R-V	1.03
ITGB1_CD29-M-V	1.03
ANXA1_Annexin-I-M-V	1.02
PECAM1_CD31-M-V	1.02
CAV1_Caveolin-1-R-V	1.02
ESR1_ER-alpha-R-V	1.02
ERBB2_HER2_pY1248-R-C	1.02
NRAS_N-Ras-M-V	1.02
UGT1A1_UGT1A-M-V	1.02
SCD_SCD-M-V	1.02
E2F1_E2F1-M-V	1.01

Appendix 3: RPPA data intersections

A2780 RPPA Intersections		
A) Proteins significantly dowregulated by cis-Pt and oxali-Pt		
Protein Name	Cis-Pt Fold Change	Oxali-Pt Fold Change
ACACA ACACB_ACC_pS79-R-V	-1.15	-1.31
ATR_ATR-R-C	-1.04	-1.08
BCL2L11_Bim-R-V	-1.09	-1.17
EIF4EBP1_4E-BP1_pS65-R-V	-1.18	-1.27
EIF4EBP1_4E-BP1_pT37_T46-R-V	-1.12	-1.24
EIF4G1_eIF4G-R-C	-1.13	-1.21
GAB2_Gab2-R-V	-1.05	-1.08
MAPK14_p38_pT180_Y182-R-V	-1.19	-1.26
PTK2_FAK_pY397-R-V	-1.03	-1.04
RICTOR_Rictor_pT1135-R-V	-1.04	-1.04
RPS6_S6_pS240_S244-R-V	-1.11	-1.20
SHC1_Shc_pY317-R-V	-1.06	-1.06
B) Proteins significantly dowregulated by cis-Pt and significantly upregulated oxali-Pt		
Protein Name	Cis-Pt Fold Change	Oxali-Pt Fold Change
CCNE1_Cyclin-E1-M-V	-1.06	1.10
C) Proteins significantly upregulated by oxali-Pt but not cis-Pt		
Protein Name	Cis-Pt Fold Change	Oxali-Pt Fold Change
PRKCA PRKCB PRKCD PRKCE PRKCH PRKCQ_PKC-beta-II_pS660-R-V		1.54
GSK3B_GSK-3b_pS9-R-V		1.16
AKT1 AKT2 AKT3_Akt_pT308-R-V		1.14
AKT1 AKT2 AKT3_Akt_pS473-R-V		1.09
CDKN1B_p27-Kip-1-R-V		1.07
RAF1_C-Raf_pS338-R-V		1.06
PTGS2_Cox2-R-C		1.06
CCND1_Cyclin-D1-R-V		1.05
TSC2_Tuberin_pT1462-R-V		1.04

BAD_Bad_pS112-R-V		1.02
ANXA1_Annexin-I-M-V		1.01
D) Proteins significantly upregulated by cis-Pt but not oxali-Pt		
Protein Name	Cis-Pt Fold Change	Oxali-Pt Fold Change
CCNB1_Cyclin-B1-R-V	2.20	
RB1_Rb_pS807_S811-R-V	1.40	
CDC2-CDK1_CDK1-R-V	1.10	
NKX2-1_TTF1-R-V	1.10	
CASP7_Caspase-7-cleaved-R-C	1.07	
ATM_ATM_pS1981-R-V	1.06	
NDRG1_NDRG1_pT346-R-V	1.06	
CHEK1_Chk1_pS345-R-C	1.05	
AKT1 AKT2 AKT3_Akt-R-V	1.04	
PARP1_PARP-cleaved-M-QC	1.02	
E) Proteins significantly upregulated by cis-Pt and oxali-Pt		
Protein Name	Cis-Pt Fold Change	Oxali-Pt Fold Change
BAX_Bax-R-V	1.20	1.44
C12ORF5_TIGAR-R-V	1.10	1.18
CDKN1A_p21-R-V	1.24	2.13
FOXM1_FoxM1-R-V	1.21	1.04
GSK3A GSK3B_GSK-3ab_pS21_S9-R-V	1.11	1.26
H3F3A H3F3B_Histone-H3-R-V	1.06	1.08
MAP2K1 MAP2K2_MEK1_pS217_S221-R-V	1.21	1.35
MAPK1 MAPK3_MAPK_pT202_Y204-R-V	1.23	1.47
MCL1_Mcl-1-R-V	1.05	1.10
NOTCH1_Notch1-R-V	1.14	1.24
PDCD4_Pdcd4-R-C	1.19	1.52
PRKAA1_AMPK-alpha-R-C	1.06	1.08
RELA_NF-kB-p65_pS536-R-C	1.15	1.18
RPS6KA1 RPS6KA2 RPS6KA3_RSK-R-C	1.14	1.20
TP53_p53-R-C	1.02	1.08
YBX1_YB1_pS102-R-V	1.05	1.11

2780CP/CI-16 RPPA Intersections

A) Proteins significantly downregulated by cis-Pt and oxali-Pt

Protein Name	Cis-Pt Fold Change	Oxali-Pt Fold Change
AKT1S1_PRAS40_pT246-R-V	-1.12	-1.53
CCNE1_Cyclin-E1-M-V	-1.04	-1.08
GSK3B_GSK-3b_pS9-R-V	-1.08	-1.28
MTOR_mTOR_pS2448-R-C	-1.05	-1.07
NDRG1_NDRG1_pT346-R-V	-1.05	-1.09
PEA15_PEA-15_pS116-R-V	-1.11	-1.14
PTK2_FAK-R-E	-1.05	-1.13
RICTOR_Rictor_pT1135-R-V	-1.07	-1.23
RPS6KB1_p70-S6K_pT389-R-V	-1.15	-1.50
RPTOR_Raptor-R-V	-1.07	-1.13
WWTR1_TAZ-R-V	-1.04	-1.07

B) Proteins significantly downregulated by cis-Pt and significantly upregulated oxali-Pt

Protein Name	Cis-Pt Fold Change	Oxali-Pt Fold Change
SCD_SCD-M-V	-1.01	1.02
SDHA_Complex-II-Subunit-M-V	-1.05	1.42
YBX1_YB1_pS102-R-V	-1.03	1.06

C) Proteins significantly upregulated by oxali-Pt but not cis-Pt

Protein Name	Cis-Pt Fold Change	Oxali-Pt Fold Change
SERPINE1_PAI-1-M-V		1.62
PPIF_Cyclophilin-F-M-V		1.39
SRC YES1 FYN FGR_Src_pY527-R-V		1.39
PRKCD_PKC-delta_pS664-R-V		1.34
CTNNB1_b-Catenin-R-V		1.32
RBM15_RBM15-R-V		1.30
COL6A1_Collagen-VI-R-V		1.28
DIABLO_Smac-M-QC		1.28
BAX_Bax-R-V		1.27
NOTCH1_Notch1-R-V		1.23
TYRO3_Tyro3-R-V		1.23
PRKCA_PKC-alpha-M-V		1.19
SRC_Src-M-V		1.19
BCL2L11_Bim-R-V		1.18

IGF1R_IGF1R-beta-R-V		1.18
FOXO3_FoxO3a_pS318_S321-R-C		1.16
PRKCA_PKC-alpha_pS657-R-C		1.16
ANXA7_Annexin-VII-M-V		1.15
TP53BP1_53BP1-R-V		1.14
PRKAA1_AMPK-alpha_pT172-R-V		1.13
MCL1_Mcl-1-R-V		1.13
JUN_c-Jun_pS73-R-V		1.13
YBX1_YB1-R-V		1.12
VDAC1_Porin-M-V		1.11
EGFR_EGFR-R-V		1.10
TP53_p53-R-C		1.09
ATP5H_ATP5H-M-C		1.09
CDH2_N-Cadherin-R-V		1.08
ERBB3_HER3-R-V		1.07
ADAR_ADAR1-M-V		1.07
MAPK1_MAPK3_MAPK_pT202_Y204-R-V		1.07
BCL2_Bcl2-M-V		1.07
KAT2A_GCN5L2-R-V		1.06
LCK_Lck-R-V		1.06
CASP7_Caspase-7-cleaved-R-C		1.06
CD274_Pdcd-1L1-G-C		1.05
TWIST2_TWIST-M-C		1.05
SNAI1_Snail-M-QC		1.05
MET_c-Met-M-QC		1.05
CLDN7_Claudin-7-R-V		1.04
RAB25_Rab25-R-V		1.03
ERBB2_HER2-M-V		1.03
BID_Bid-R-C		1.03
SMAD4_Smad4-M-V		1.03
CTNNB1_b-Catenin_pT41_S45-R-V		1.03
PGR_PR-R-V		1.03
ITGB1_CD29-M-V		1.03
ANXA1_Annexin-I-M-V		1.02
PECAM1_CD31-M-V		1.02
CAV1_Caveolin-1-R-V		1.02
ESR1_ER-alpha-R-V		1.02
ERBB2_HER2_pY1248-R-C		1.02
NRAS_N-Ras-M-V		1.02

UGT1A1_UGT1A-M-V		1.02
E2F1_E2F1-M-V		1.01
D) Proteins significantly upregulated by cis-Pt and significantly downregulated by oxali-Pt		
Protein Name	Cis-Pt Fold Change	Oxali-Pt Fold Change
CCNB1_Cyclin-B1-R-V	1.46	-1.13
CHEK1_Chk1_pS345-R-C	1.08	-1.04
E) Proteins significantly upregulated by cis-Pt but not oxali-Pt		
Protein Name	Cis-Pt Fold Change	Oxali-Pt Fold Change
FOXM1_FoxM1-R-V	1.16	
CASP8_Caspase-8-M-QC	1.02	
F) Proteins significantly upregulated by oxali-Pt and cis-Pt		
Protein Name	Cis-Pt Fold Change	Oxali-Pt Fold Change
DIRAS3_ARHI-M-C	1.01	1.03
IGFBP2_IGFBP2-R-V	1.03	1.04

A2780 and 2780CP/CI-16 RPPA Intersections

A) Proteins significantly downregulated in A2780 and 2780CP/CI-16 by cis-Pt and oxali-Pt

Protein Name	A2780		2780CP/CI-16	
	Cis-Pt Fold Change	Oxali-Pt Fold Change	Cis-Pt Fold Change	Oxali-Pt Fold Change
RICTOR_Rictor_pT1135-R-V	-1.039	-1.037	-1.072	-1.23

B) Proteins significantly downregulated in A2780 by cis-Pt and oxali-Pt but not in 2780CP/CI-16

Protein Name	A2780		2780CP/CI-16	
	Cis-Pt Fold Change	Oxali-Pt Fold Change	Cis-Pt Fold Change	Oxali-Pt Fold Change
ACACA ACACB_ACC_pS79-R-V	-1.153	-1.31		
PTK2_FAK_pY397-R-V	-1.032	-1.041		
SHC1_Shc_pY317-R-V	-1.059	-1.058		

C) Proteins significantly downregulated by cis-Pt and upregulated by oxali-Pt in A2780 and significantly downregulated by cis-Pt and oxali-Pt in 2780CP/CI-16

Protein Name	A2780		2780CP/CI-16	
	Cis-Pt Fold Change	Oxali-Pt Fold Change	Cis-Pt Fold Change	Oxali-Pt Fold Change
CCNE1_Cyclin-E1-M-V	-1.061	1.0996	-1.035	-1.081

D) Proteins significantly upregulated by oxali-Pt in 2780CP/CI-16

Protein Name	A2780		2780CP/CI-16	
	Cis-Pt Fold Change	Oxali-Pt Fold Change	Cis-Pt Fold Change	Oxali-Pt Fold Change
SERPINE1_PA1-1-M-V				1.6204
PRKCD_PKC-delta_pS664-R-V				1.3388
CTNNB1_b-Catenin-R-V				1.3239
RBM15_RBM15-R-V				1.300

COL6A1_Collagen-VI-R-V				1.2757
DIABLO_Smac-M-QC				1.2752
PRKCA_PKC-alpha-M-V				1.1919
SRC_Src-M-V				1.1856
IGF1R_IGF1R-beta-R-V				1.1756
FOXO3_FoxO3a_pS318_S321-R-C				1.1634
PRKCA_PKC-alpha_pS657-R-C				1.1591
ANXA7_Annexin-VII-M-V				1.146
TP53BP1_53BP1-R-V				1.1424
PRKAA1_AMPK-alpha_pT172-R-V				1.1337
JUN_c-Jun_pS73-R-V				1.1257
YBX1_YB1-R-V				1.1205
VDAC1_Porin-M-V				1.1124
EGFR_EGFR-R-V				1.102
ATP5H_ATP5H-M-C				1.0863
CDH2_N-Cadherin-R-V				1.075
ERBB3_HER3-R-V				1.0741
KAT2A_GCN5L2-R-V				1.0634
LCK_Lck-R-V				1.0583
CD274_Pdcd-1L1-G-C				1.0543
TWIST2_TWIST-M-C				1.0509
SNAI1_Snail-M-QC				1.0493
MET_c-Met-M-QC				1.0465
CLDN7_Claudin-7-R-V				1.035
RAB25_Rab25-R-V				1.0339
ERBB2_HER2-M-V				1.0311
BID_Bid-R-C				1.0309
CTNNB1_b-Catenin_pT41_S45-R-V				1.0289

PGR_PR-R-V				1.0272
ITGB1_CD29-M-V				1.0256
PECAM1_CD31-M-V				1.0207
CAV1_Caveolin-1-R-V				1.0197
ESR1_ER-alpha-R-V				1.0188
ERBB2_HER2_pY1248-R-C				1.0179
NRAS_N-Ras-M-V				1.0176
UGT1A1_UGT1A-M-V				1.0175
E2F1_E2F1-M-V				1.0084

E) Proteins significantly upregulated by oxali-Pt in A2780

Protein Name	A2780		2780CP/CI-16	
	Cis-Pt Fold Change	Oxali-Pt Fold Change	Cis-Pt Fold Change	Oxali-Pt Fold Change
CDKN1B_p27-Kip-1-R-V		1.0734		
PTGS2_Cox2-R-C		1.0597		
CCND1_Cyclin-D1-R-V		1.0496		

F) Proteins significantly upregulated by oxali-Pt in A2780 and in 2780CP/CI-16

Protein Name	A2780		2780CP/CI-16	
	Cis-Pt Fold Change	Oxali-Pt Fold Change	Cis-Pt Fold Change	Oxali-Pt Fold Change
ANXA1_Annexin-I-M-V		1.0076		1.021

G) Proteins significantly upregulated by cis-Pt in A2780

Protein Name	A2780		2780CP/CI-16	
	Cis-Pt Fold Change	Oxali-Pt Fold Change	Cis-Pt Fold Change	Oxali-Pt Fold Change
CDC2-CDK1_CDK1-R-V	1.0992			

ATM_ATM_pS1981-R-V	1.0619			
PARP1_PARP-cleaved-M-QC	1.0193			
H) Proteins significantly upregulated by cis-Pt and upregulated by oxali-Pt in A2780 and significantly downregulated by cis-Pt and significantly upregulated by oxali-Pt in 2780CP/CI-16				
	A2780		2780CP/CI-16	
Protein Name	Cis-Pt Fold Change	Oxali-Pt Fold Change	Cis-Pt Fold Change	Oxali-Pt Fold Change
YBX1_YB1_pS102-R-V	1.0517	1.1148	-1.027	1.0643
I) Proteins significantly upregulated by cis-Pt and upregulated by oxali-Pt in A2780				
	A2780		2780CP/CI-16	
Protein Name	Cis-Pt Fold Change	Oxali-Pt Fold Change	Cis-Pt Fold Change	Oxali-Pt Fold Change
H3F3A H3F3B_Histone-H3-R-V	1.0643	1.0829		
PRKAA1_AMPK-alpha-R-C	1.0617	1.0783		
RPS6KA1 RPS6KA2 RPS6KA3_RSK-R-C	1.1392	1.1962		
J) Proteins significantly upregulated by cis-Pt and upregulated by oxali-Pt in A2780 and significantly upregulated by oxali-Pt in 2780CP/CI-16				
	A2780		2780CP/CI-16	
Protein Name	Cis-Pt Fold Change	Oxali-Pt Fold Change	Cis-Pt Fold Change	Oxali-Pt Fold Change
BAX_Bax-R-V	1.1958	1.4433		1.2667
MAPK1 MAPK3_MAPK_pT202_Y204-R	1.2282	1.47		1.0695
MCL1_Mcl-1-R-V	1.0462	1.1006		1.1326
NOTCH1_Notch1-R-V	1.1376	1.2428		1.2274
TP53_p53-R-C	1.0167	1.0841		1.0908

K) Proteins significantly upregulated by cis-Pt and upregulated by oxali-Pt in A2780 and significantly upregulated by cis-Pt in 2780CP/CI-16				
Protein Name	A2780		2780CP/CI-16	
	Cis-Pt Fold Change	Oxali-Pt Fold Change	Cis-Pt Fold Change	Oxali-Pt Fold Change
FOXM1_FoxM1-R-V	1.2065	1.0434	1.1573	

Appendix 4: Analysis of the functionality of p53 missense mutations in ovarian cancer patients and cell lines

A) Analysis of p53 functionality for HGSOc Patients (Data for p53 mutation was extracted from TCGA, FASAY was used to assess p53 functionality for a given mutation and a value ≥ 20 (in green) was considered indicative of p53 functionality)

AA change	Freq	#cases/mut	Promoters							
			WAF1	MDM2	BAX	AIP	GADD45	NOXA	p53R2	14-3-3-s
S127Y	0.57	1	13.79	18.9	14.21	4.14	6.9	7	7.98	11.53
S127F	0.57	1	12.47	20.1	14.35	8.15	8.38	5.61	8.99	12.02
L130V	0.57	1	8.89	18.26	18.34	14.3	24.79	24.71	20.77	16.93
K132M	0.57	1	14.93	23.99	16.47	7.32	4.57	6.97	7.69	8.98
K132E	0.57	1	0.56	0	0	0	0	0	0	0
K132N	1.14	2	10.49	17.8	12.87	6.13	3.16	4.58	4.95	8.41
F134V	0.57	1	10.89	18.79	12.4	6.43	2.64	3.88	5.09	8.74
C135Y	0.57	1	10.88	16.63	12.63	5.66	3.45	4.59	5.35	7.4
C135R	0.57	1	0.86	8.34	3.98	7.57	12	11.13	10	1.99
L145Q	0.57	1	12.41	16.96	13.1	5.9	3.99	6.37	8.32	12.93
L145R	0.57	1	12.61	16.92	13.34	5.54	3.8	5.76	7.14	10.13
P151S	0.57	1	0.85	8.9	0.02	8.78	3.58	15.81	6.82	0

T155A	0.57	1	40.74	51.26	74.1	76.3	67.55	188.57	118.13	100.18
R156P	0.57	1	8.22	13	13.41	6.6	2.57	7.83	6.39	6.44
V157F	2.86	5	9.06	17.5	15.64	6.98	3.4	10.67	11.24	6.51
A159V	1.14	2	6.91	23.42	26.41	16.68	10.76	18.48	15.82	9.98
Y163N	0.57	1	11.38	14.95	11.29	5.56	2.97	8.13	6.15	6.83
Y163H	0.57	1	11.22	16.67	12.64	6.51	3.26	8.06	12.31	5.59
Y163C	1.14	2	18.3	17.51	12.62	4.04	2.19	5.83	5.4	3.85
K164E	0.57	1	12.39	19.27	12.37	8.95	4.35	8.1	34.67	8
V173L	0.57	1	3.61	0	0	0	0	0	3.52	0
R175H	4.57	8	12.41	17.56	10.52	2.63	4.08	7.29	7.83	10.52
C176F	0.57	1	22.88	15.7	14.96	19.49	27.85	95.79	100.91	5
C176Y	2.86	5	14.82	12.89	13.51	7.43	11.24	29.28	73.51	3.64
P177R	0.57	1	17.88	17.68	14.74	8.32	2.69	9.23	84.58	5.9
H178N	0.57	1	28.34	18.3	11.97	24.33	27.95	41.2	47.73	6.69
H179R	2.29	4	13.02	18.04	14	15.33	20.49	44.88	67.55	8.55
H179Q	0.57	1	17.51	19.45	11.25	7.17	14.2	37.87	80.28	6.83
R181P	0.57	1	14.12	22.86	16.66	8.71	4.96	11.72	23.08	7.24
H193R	1.71	3	10.15	19.32	13.69	6.11	4.62	4.21	10.14	7.17
L194R	1.14	2	10.61	22.57	14.48	7.09	4.77	3.9	9.66	10.2
I195T	4.00	7	11.24	22.29	13.79	8.91	6.16	8.18	16.47	8.37
I195N	0.57	1	10.54	23.64	15.7	8.2	4.9	4.55	10.95	9.07
I195F	0.57	1	10.47	21.24	14.57	7.91	4.7	5.87	11.91	8.27
Y205C	1.14	2	8.94	20.66	9.66	5.82	4	6.32	12.91	6.83
D208V	0.57	1	4.74	6.36	3.52	12.76	12.55	7.83	7.09	3.64
H214R	0.57	1	3.12	4.07	3.39	20.95	14.94	10.83	13.09	5.72
S215R	1.14	2	1.17	2.77	2.41	0.11	1.22	0	1.23	0
V216G	0.57	1	2.05	1.16	0	0	0.97	0	0	0
V216M	1.14	2	0.16	13.23	0.1	3.15	1.3	0.97	2.57	0
Y220C	4.57	8	1.21	8.6	2.55	1.39	2.97	0.24	5.11	0
I232N	0.57	1	0.72	0	3.96	0.78	1.17	0	3.04	0
Y234C	1.14	2	2.14	0.46	14.55	10.28	14.08	10.76	14.85	9.83

Y234N	0.57	1	0.36	0	3.25	0	0	0	0.48	0
Y236C	1.14	2	0.7	23.65	3.33	0	0	0	1.84	0
M237I	0.57	1	0.43	11.46	2.63	0	0	0	2.2	0
M237K	0.57	1	14.24	17.35	23.93	12.51	10.57	17.53	25.4	14.23
C238Y	0.57	1	14.58	20.39	25.25	11.07	6.01	13.13	15.79	13.07
C238F	0.57	1	0.82	0	4.64	0	0	0	1.73	0
N239S	0.57	1	14.86	21.81	17.98	7.64	4.2	14.97	17.17	10.2
S241Y	0.57	1	6.57	0.04	0	0	0	0	1.84	0
S241F	2.29	4	0	0	0.31	0	0	0	0.84	0
G244D	0.57	1	0.52	0	0.32	0	1.61	0	131.35	0
G244C	1.14	2	0	0	0	0	0	0	4.71	0
G245V	1.14	2	0	0	0	0	0	0	0	0
G245R	0.57	1	7.9	0	0	0	2.89	1.53	10.92	0
G245D	1.14	2	1.95	8.82	11.86	2.94	0.24	3.29	2.64	2.07
G245S	1.71	3	0	1.64	0.72	0	0	0	31.35	0
G245C	0.57	1	0	0.34	0	0	0	0	0	0
R248W	2.86	5	0	0	0.68	0	0	0	0	0
R248G	0.57	1	0	0.64	0	0	0	0	0	0
R248Q	4.57	8	0	1.75	0	0	0	0	0	0
R249G	0.57	1	0.17	4.26	0	0	0	0	0.57	0
P250L	1.14	2	0	2.92	1.46	5.35	14.52	10.19	11.65	0.48
I251S	0.57	1	0	2.96	7.16	0.14	2.63	2.17	4.95	0
L257Q	0.57	1	10.96	22.82	12.77	8.43	4.89	9.14	14.04	7.96
D259Y	1.14	2	9.92	15.66	10.68	6.4	2.06	7.68	4.79	6.66
G262V	0.57	1	11.71	20.21	15.24	8.17	4.44	9.42	13.09	9.29
L265P	0.57	1	0	0	0.4	0	0	0	0.1	0
G266R	1.14	2	10.77	19.28	16.72	8.41	5.14	8.5	13.97	10.47
G266V	1.14	2	0	0	1.74	0	0	0	0	0
F270L	0.57	1	8.14	24.52	24.27	12.42	13.91	20.02	23.99	16.95
V272M	1.14	2	8.79	24.82	16.4	13.19	17.96	23.18	21.73	10.79
R273H	5.71	10	1.01	0	2.42	0	0	0	15.97	0

R273C	4.00	7	0.91	0	2.69	0	0.4	0	1.21	0.26
R273P	0.57	1	0.58	0	1.52	0	0.05	0	0	0
R273L	1.14	2	0.86	0	0	0	0	0	0.03	0
V274G	0.57	1	5.25	9.05	7.62	2.28	3.11	0	3.82	1.24
V274D	0.57	1	1.32	0	0	0	0	0	0.48	0
C275Y	1.14	2	0.42	0	0	0	0	0	0	0
A276P	0.57	1	0.62	0	0	0	0	0	0.13	0
C277F	0.57	1	0.31	0	0	0	0	0	1.43	0
P278R	0.57	1	0.72	4.04	5.33	0	1.01	1.73	1.52	0
P278H	0.57	1	0.28	0	0	0	0	0	0	0
G279E	0.57	1	0.27	0	1.24	0	6.75	0	0.78	0
R280I	0.57	1	0.18	0	0.66	0	0.07	0	0.38	0
R282W	2.86	5	0.55	0	0.49	0	0	0	0	0
R337C	0.57	1	11.86	32.19	14.66	12.85	7.92	8.86	26.16	15.64
Total	100	175								

B) Analysis of p53 functionality for Ovarian Cancer Cell Lines

AA change	Promoters							14-3-3- s
	WAF1	MDM2	BAX	AIP	GADD45	NOXA	p53R2	
V172F	8.17	19.81	12.64	4.62	17.58	22	24.28	19.63
G266R	10.77	19.28	16.72	8.41	5.14	8.5	13.97	10.47
P72R	67.23	75.09	85.95	50.18	64.13	127.33	102.27	101.3

References

1. Elzek MA and Rodland KD, Proteomics of ovarian cancer: functional insights and clinical applications. *Cancer and Metastasis Reviews* 34: 83-96, 2015.
2. Kalachand R, Hennessy BT, and Markman M, Molecular Targeted Therapy in Ovarian Cancer What is on the Horizon? *Drugs* 71: 947-967, 2011.
3. Hennessy BT, Coleman RL, and Markman M, Ovarian cancer. *Lancet* 374: 1371-1382, 2009.
4. Bukowski RM, Ozols RF, and Markman M, The management of recurrent ovarian cancer. *Seminars in Oncology* 34: S1-S15, 2007.
5. Siegel R, Ma JM, Zou ZH, and Jemal A, Cancer Statistics, 2014. *Ca-A Cancer Journal for Clinicians* 64: 9-29, 2014.
6. Bast RC, Hennessy B, and Mills GB, The biology of ovarian cancer: new opportunities for translation. *Nature Reviews Cancer* 9: 415-428, 2009.
7. Ozols RF, Challenges for chemotherapy in ovarian cancer. *Annals of Oncology* 17: V181-V187, 2006.

8. Vaughan S, Coward JI, Bast RC, Berchuck A, Berek JS, Brenton JD, Coukos G, Crum CC, Drapkin R, Etemadmoghadam D, Friedlander M, Gabra H, Kaye SB, Lord CJ, Lengyel E, Levine DA, McNeish IA, Menon U, Mills GB, Nephew KP, Oza AM, Sood AK, Stronach EA, Walczak H, Bowtell DD, and Balkwill FR, Rethinking ovarian cancer: recommendations for improving outcomes. *Nature Reviews Cancer* 11: 719-725, 2011.
9. ROSENBER.B, Vancamp L, and Krigas T, Inhibition of Cell Division in *Escherichia Coli* by Electrolysis Products from A Platinum Electrode. *Nature* 205: 698-&, 1965.
10. ROSENBER.B, Renshaw E, Vancamp L, Hartwick J, and Drobnik J, Platinum-Induced Filamentous Growth in *Escherichia Coli*. *Journal of Bacteriology* 93: 716-&, 1967.
11. ROSENBER.B, Vancamp L, Grimley EB, and Thomson AJ, Inhibition of Growth Or Cell Division in *Escherichia Coli* by Different Ionic Species of Platinum(4) Complexes. *Journal of Biological Chemistry* 242: 1347-&, 1967.
12. ROSENBER.B, Vancamp L, Trosko JE, and Mansour VH, Platinum Compounds - A New Class of Potent Antitumour Agents. *Nature* 222: 385-&, 1969.
13. ROSENBER.B and Vancamp L, Successful Regression of Large Solid Sarcoma 180-Tumors by Platinum Compounds. *Cancer Research* 30: 1799-&, 1970.

14. Kelland L, The resurgence of platinum-based cancer chemotherapy. *Nature Reviews Cancer* 7: 573-584, 2007.
15. Alderden RA, Hall MD, and Hambley TW, The discovery and development of cisplatin. *Journal of Chemical Education* 83: 728-734, 2006.
16. Ivanov AI, Christodoulou J, Parkinson JA, Barnham KJ, Tucker A, Woodrow J, and Sadler PJ, Cisplatin binding sites on human albumin. *Journal of Biological Chemistry* 273: 14721-14730, 1998.
17. Deconti RC, Toftness BR, Lange RC, and Creasey WA, Clinical and Pharmacological Studies with Cis-Diamminedichloroplatinum(II). *Cancer Research* 33: 1310-1315, 1973.
18. Jamieson ER and Lippard SJ, Structure, recognition, and processing of cisplatin-DNA adducts. *Chemical Reviews* 99: 2467-2498, 1999.
19. Ahmad S, Platinum-DNA Interactions and Subsequent Cellular Processes Controlling Sensitivity to Anticancer Platinum Complexes. *Chemistry & Biodiversity* 7: 543-566, 2010.
20. Siddik ZH, Cisplatin: mode of cytotoxic action and molecular basis of resistance. *Oncogene* 22: 7265-7279, 2003.

21. Cavallo F, Feldman DR, and Barchi M, Revisiting DNA damage repair, p53-mediated apoptosis and cisplatin sensitivity in germ cell tumors. *International Journal of Developmental Biology* 57: 273-280, 2013.
22. Gutekunst M, Oren M, Weilbacher A, Dengler MA, Markwardt C, Thomale J, Aulitzky WE, and van der Kuip H, p53 Hypersensitivity Is the Predominant Mechanism of the Unique Responsiveness of Testicular Germ Cell Tumor (TGCT) Cells to Cisplatin. *Plos One* 6: 2011.
23. Kerley-Hamilton JS, Pike AM, Li N, DiRenzo J, and Spinella MJ, A p53-dominant transcriptional response to cisplatin in testicular germ cell tumor-derived human embryonal carcinoma. *Oncogene* 24: 6090-6100, 2005.
24. Smith ND, Rubenstein JN, Eggener SE, and Kozlowski JM, The p53 tumor suppressor gene and nuclear protein: basic science review and relevance in the management of bladder cancer. *J.Urol.* 169: 1219-1228, 2003.
25. Varna M, Bousquet G, Plassa LF, Bertheau P, and Janin A, TP53 status and response to treatment in breast cancers. *J.Biomed.Biotechnol.* 2011: 284584, 2011.
26. Zilfou JT and Lowe SW, Tumor suppressive functions of p53. *Cold Spring Harb.Perspect.Biol.* 1: a001883, 2009.

27. Wang W, Rastinejad F, and El Deiry WS, Restoring p53-dependent tumor suppression. *Cancer Biol.Ther.* 2: S55-S63, 2003.
28. Lain S, Protecting p53 from degradation. *Biochem.Soc.Trans.* 31: 482-485, 2003.
29. Mandinova A and Lee SW, The p53 pathway as a target in cancer therapeutics: obstacles and promise. *Sci.Transl.Med.* 3: 64rv1, 2011.
30. Meek DW, Mechanisms of switching on p53: a role for covalent modification? *Oncogene* 18: 7666-7675, 1999.
31. Toledo F and Wahl GM, Regulating the p53 pathway: in vitro hypotheses, in vivo veritas. *Nat.Rev.Cancer* 6: 909-923, 2006.
32. Lain S and Lane D, Improving cancer therapy by non-genotoxic activation of p53. *Eur.J.Cancer* 39: 1053-1060, 2003.
33. Al Ejuh F, Kumar R, Wiegmans A, Lakhani SR, Brown MP, and Khanna KK, Harnessing the complexity of DNA-damage response pathways to improve cancer treatment outcomes. *Oncogene* 29: 6085-6098, 2010.
34. Efeyan A and Serrano M, p53: guardian of the genome and policeman of the oncogenes. *Cell Cycle* 6: 1006-1010, 2007.

35. Lane DP and Lain S, Therapeutic exploitation of the p53 pathway. *Trends Mol.Med.* 8: S38-S42, 2002.
36. Schuler M and Green DR, Mechanisms of p53-dependent apoptosis. *Biochem.Soc.Trans.* 29: 684-688, 2001.
37. Haupt S, Berger M, Goldberg Z, and Haupt Y, Apoptosis - the p53 network. *J.Cell Sci.* 116: 4077-4085, 2003.
38. Yu J and Zhang L, No PUMA, no death: implications for p53-dependent apoptosis. *Cancer Cell* 4: 248-249, 2003.
39. Henry H, Thomas A, Shen Y, and White E, Regulation of the mitochondrial checkpoint in p53-mediated apoptosis confers resistance to cell death. *Oncogene* 21: 748-760, 2002.
40. Erster S and Moll UM, Stress-induced p53 runs a direct mitochondrial death program: its role in physiologic and pathophysiologic stress responses in vivo. *Cell Cycle* 3: 1492-1495, 2004.
41. Galluzzi L, Morselli E, Kepp O, Tajeddine N, and Kroemer G, Targeting p53 to mitochondria for cancer therapy. *Cell Cycle* 7: 1949-1955, 2008.

42. Erster S and Moll UM, Stress-induced p53 runs a transcription-independent death program. *Biochem.Biophys.Res.Commun.* 331: 843-850, 2005.
43. Kaina B, DNA damage-triggered apoptosis: critical role of DNA repair, double-strand breaks, cell proliferation and signaling. *Biochem.Pharmacol.* 66: 1547-1554, 2003.
44. Brown JM and Attardi LD, The role of apoptosis in cancer development and treatment response. *Nat.Rev.Cancer* 5: 231-237, 2005.
45. Iliakis G, Wang Y, Guan J, and Wang H, DNA damage checkpoint control in cells exposed to ionizing radiation. *Oncogene* 22: 5834-5847, 2003.
46. Samuel T, Weber HO, and Funk JO, Linking DNA damage to cell cycle checkpoints. *Cell Cycle* 1: 162-168, 2002.
47. Pietenpol JA and Stewart ZA, Cell cycle checkpoint signaling: cell cycle arrest versus apoptosis. *Toxicology* 181-182: 475-481, 2002.
48. Gartel AL and Tyner AL, Transcriptional regulation of the p21((WAF1/CIP1)) gene. *Exp.Cell Res.* 246: 280-289, 1999.
49. Hagopian GS, Mills GB, Khokhar AR, Bast RC, Jr., and Siddik ZH, Expression of p53 in cisplatin-resistant ovarian cancer cell lines: modulation with the novel

platinum analogue (1R, 2R- diaminocyclohexane)(trans-diacetato)(dichloro)-platinum(IV). Clin Cancer Res 5: 655-663, 1999.

50. O'Connor PM and Kohn KW, A fundamental role for cell cycle regulation in the chemosensitivity of cancer cells? Semin Cancer Biol 3: 409-416, 1992.
51. O'Connor PM and Fan S, DNA damage checkpoints: implications for cancer therapy. Prog.Cell Cycle Res. 2: 165-173, 1996.
52. Vekris A, Meynard D, Haaz MC, Bayssas M, Bonnet J, and Robert J, Molecular determinants of the cytotoxicity of platinum compounds: the contribution of in silico research. Cancer Res. 64: 356-362, 2004.
53. Lincet H, Poulain L, Remy JS, Deslandes E, Duigou F, Gauduchon P, and Staedel C, The p21(cip1/waf1) cyclin-dependent kinase inhibitor enhances the cytotoxic effect of cisplatin in human ovarian carcinoma cells. Cancer Lett. 161: 17-26, 2000.
54. Wu Q, Kirschmeier P, Hockenberry T, Yang TY, Brassard DL, Wang L, McClanahan T, Black S, Rizzi G, Musco ML, Mirza A, and Liu S, Transcriptional regulation during p21WAF1/CIP1-induced apoptosis in human ovarian cancer cells. J.Biol.Chem. 277: 36329-36337, 2002.

55. Fry DW, Harvey PJ, Keller PR, Elliott WL, Meade M, Trachet E, Albassam M, Zheng X, Leopold WR, Pryer NK, and Toogood PL, Specific inhibition of cyclin-dependent kinase 4/6 by PD 0332991 and associated antitumor activity in human tumor xenografts. *Mol.Cancer Ther.* 3: 1427-1438, 2004.
56. Soni R, O'Reilly T, Furet P, Muller L, Stephan C, Zumstein-Mecker S, Fretz H, Fabbro D, and Chaudhuri B, Selective in vivo and in vitro effects of a small molecule inhibitor of cyclin-dependent kinase 4. *J.Natl.Cancer Inst.* 93: 436-446, 2001.
57. Deng C, Zhang P, Harper JW, Elledge SJ, and Leder P, Mice lacking p21CIP1/WAF1 undergo normal development, but are defective in G1 checkpoint control. *Cell* 82: 675-684, 1995.
58. Martin-Caballero J, Flores JM, Garcia-Palencia P, and Serrano M, Tumor susceptibility of p21(Waf1/Cip1)-deficient mice. *Cancer Res.* 61: 6234-6238, 2001.
59. Itahana K, Dimri G, and Campisi J, Regulation of cellular senescence by p53. *Eur.J.Biochem.* 268: 2784-2791, 2001.
60. Stuhmer T and Bargou RC, Selective pharmacologic activation of the p53-dependent pathway as a therapeutic strategy for hematologic malignancies. *Cell Cycle* 5: 39-42, 2006.

61. Schmitt CA, Cellular senescence and cancer treatment. *Biochim.Biophys.Acta* 1775: 5-20, 2007.
62. Zuckerman V, Wolyniec K, Sionov RV, Haupt S, and Haupt Y, Tumour suppression by p53: the importance of apoptosis and cellular senescence. *J.Pathol.* 219: 3-15, 2009.
63. Gewirtz DA, Holt SE, and Elmore LW, Accelerated senescence: an emerging role in tumor cell response to chemotherapy and radiation. *Biochem.Pharmacol.* 76: 947-957, 2008.
64. Wang X, Wong SC, Pan J, Tsao SW, Fung KH, Kwong DL, Sham JS, and Nicholls JM, Evidence of cisplatin-induced senescent-like growth arrest in nasopharyngeal carcinoma cells. *Cancer Res.* 58: 5019-5022, 1998.
65. Gewirtz DA, Growth arrest and cell death in the breast tumor cell in response to ionizing radiation and chemotherapeutic agents which induce DNA damage. *Breast Cancer Res.Treat.* 62: 223-235, 2000.
66. Chang BD, Broude EV, Dokmanovic M, Zhu H, Ruth A, Xuan Y, Kandel ES, Lausch E, Christov K, and Roninson IB, A senescence-like phenotype distinguishes tumor cells that undergo terminal proliferation arrest after exposure to anticancer agents. *Cancer Res.* 59: 3761-3767, 1999.

67. Chang BD, Swift ME, Shen M, Fang J, Broude EV, and Roninson IB, Molecular determinants of terminal growth arrest induced in tumor cells by a chemotherapeutic agent. *Proc.Natl.Acad.Sci.U.S.A* 99: 389-394, 2002.
68. Martinez-Rivera M and Siddik ZH, Resistance and gain-of-resistance phenotypes in cancers harboring wild-type p53. *Biochem.Pharmacol.* 83: 1049-1062, 2012.
69. Dai C and Gu W, p53 post-translational modification: deregulated in tumorigenesis. *Trends Mol.Med.* 16: 528-536, 2010.
70. Horn HF and Vousden KH, Coping with stress: multiple ways to activate p53. *Oncogene* 26: 1306-1316, 2007.
71. Meek DW and Anderson CW, Posttranslational modification of p53: cooperative integrators of function. *Cold Spring Harb.Perspect.Biol.* 1: a000950, 2009.
72. Colman MS, Afshari CA, and Barrett JC, Regulation of p53 stability and activity in response to genotoxic stress. *Mutat.Res.* 462: 179-188, 2000.
73. Appella E and Anderson CW, Post-translational modifications and activation of p53 by genotoxic stresses. *Eur.J.Biochem.* 268: 2764-2772, 2001.

74. MacLaine NJ and Hupp TR, The regulation of p53 by phosphorylation: a model for how distinct signals integrate into the p53 pathway. *Aging (Albany.NY)* 1: 490-502, 2009.
75. MacLaine NJ and Hupp TR, How phosphorylation controls p53. *Cell Cycle* 10: 916-921, 2011.
76. Dornan D and Hupp TR, Inhibition of p53-dependent transcription by BOX-I phospho-peptide mimetics that bind to p300. *EMBO Rep.* 2: 139-144, 2001.
77. Craig AL, Burch L, Vojtesek B, Mikutowska J, Thompson A, and Hupp TR, Novel phosphorylation sites of human tumour suppressor protein p53 at Ser20 and Thr18 that disrupt the binding of mdm2 (mouse double minute 2) protein are modified in human cancers. *Biochem.J.* 342 (Pt 1): 133-141, 1999.
78. Meek DW, The p53 response to DNA damage. *DNA Repair (Amst)* 3: 1049-1056, 2004.
79. Teufel DP, Bycroft M, and Fersht AR, Regulation by phosphorylation of the relative affinities of the N-terminal transactivation domains of p53 for p300 domains and Mdm2. *Oncogene* 28: 2112-2118, 2009.

80. Ferreon JC, Lee CW, Arai M, Martinez-Yamout MA, Dyson HJ, and Wright PE, Cooperative regulation of p53 by modulation of ternary complex formation with CBP/p300 and HDM2. *Proc.Natl.Acad.Sci.U.S.A* 106: 6591-6596, 2009.
81. Nakamizo A, Amano T, Zhang W, Zhang XQ, Ramdas L, Liu TJ, Bekele BN, Shono T, Sasaki T, Benedict WF, Sawaya R, and Lang FF, Phosphorylation of Thr18 and Ser20 of p53 in Ad-p53-induced apoptosis. *Neuro.Oncol.* 10: 275-291, 2008.
82. Amano T, Nakamizo A, Mishra SK, Gumin J, Shinojima N, Sawaya R, and Lang FF, Simultaneous phosphorylation of p53 at serine 15 and 20 induces apoptosis in human glioma cells by increasing expression of pro-apoptotic genes. *J.Neurooncol.* 92: 357-371, 2009.
83. Brachova P, Thiel KW, and Leslie KK, The consequence of oncomorphic TP53 mutations in ovarian cancer. *Int.J.Mol.Sci.* 14: 19257-19275, 2013.
84. Donzelli S, Biagioni F, Fausti F, Strano S, Fontemaggi G, and Blandino G, Oncogenomic Approaches in Exploring Gain of Function of Mutant p53. *Curr.Genomics* 9: 200-207, 2008.
85. Brosh R and Rotter V, When mutants gain new powers: news from the mutant p53 field. *Nat.Rev.Cancer* 9: 701-713, 2009.

86. Goldstein I, Marcel V, Olivier M, Oren M, Rotter V, and Hainaut P, Understanding wild-type and mutant p53 activities in human cancer: new landmarks on the way to targeted therapies. *Cancer Gene Ther.* 18: 2-11, 2011.
87. Song S, Wientjes MG, Gan Y, and Au JL, Fibroblast growth factors: an epigenetic mechanism of broad spectrum resistance to anticancer drugs. *Proc.Natl.Acad.Sci.U.S.A* 97: 8658-8663, 2000.
88. Jackman D, Pao W, Riely GJ, Engelman JA, Kris MG, Janne PA, Lynch T, Johnson BE, and Miller VA, Clinical definition of acquired resistance to epidermal growth factor receptor tyrosine kinase inhibitors in non-small-cell lung cancer. *J.Clin.Oncol.* 28: 357-360, 2010.
89. Vargas-Roig LM, Gago FE, Tello O, Aznar JC, and Ciocca DR, Heat shock protein expression and drug resistance in breast cancer patients treated with induction chemotherapy. *Int.J.Cancer* 79: 468-475, 1998.
90. Leonetti C, Biroccio A, Candiloro A, Citro G, Fornari C, Mottolese M, Del Bufalo D, and Zupi G, Increase of cisplatin sensitivity by c-myc antisense oligodeoxynucleotides in a human metastatic melanoma inherently resistant to cisplatin. *Clin.Cancer Res.* 5: 2588-2595, 1999.
91. Righetti SC, Della TG, Pilotti S, Menard S, Ottone F, Colnaghi MI, Pierotti MA, Lavarino C, Cornarotti M, Oriana S, Bohm S, Bresciani GL, Spatti G, and Zunino

- F, A comparative study of p53 gene mutations, protein accumulation, and response to cisplatin-based chemotherapy in advanced ovarian carcinoma. *Cancer Res* 56: 689-693, 1996.
92. Lavarino C, Pilotti S, Oggionni M, Gatti L, Perego P, Bresciani G, Pierotti MA, Scambia G, Ferrandina G, Fagotti A, Mangioni C, Lucchini V, Vecchione F, Bolis G, Scarfone G, and Zunino F, p53 gene status and response to platinum/paclitaxel-based chemotherapy in advanced ovarian carcinoma. *J.Clin.Oncol.* 18: 3936-3945, 2000.
93. Gadducci A, Di Cristofano C, Zavaglia M, Giusti L, Menicagli M, Cosio S, Naccarato AG, Genazzani AR, Bevilacqua G, and Cavazzana AO, P53 gene status in patients with advanced serous epithelial ovarian cancer in relation to response to paclitaxel- plus platinum-based chemotherapy and long-term clinical outcome. *Anticancer Res.* 26: 687-693, 2006.
94. Weinstein JN, Collisson EA, Mills GB, Shaw KR, Ozenberger BA, Ellrott K, Shmulevich I, Sander C, and Stuart JM, The Cancer Genome Atlas Pan-Cancer analysis project. *Nat.Genet.* 45: 1113-1120, 2013.
95. Correa I, Cerbon MA, Salazar AM, Solano JD, Garcia-Carranca A, and Quintero A, Differential p53 protein expression level in human cancer-derived cell lines after estradiol treatment. *Arch.Med.Res.* 33: 455-459, 2002.

96. Hall J, Paul J, and Brown R, Critical evaluation of p53 as a prognostic marker in ovarian cancer. *Expert Rev.Mol.Med.* 6: 1-20, 2004.
97. Hall PA and Lane DP, p53 in tumour pathology: can we trust immunohistochemistry?--Revisited! *J.Pathol.* 172: 1-4, 1994.
98. Kato S, Han SY, Liu W, Otsuka K, Shibata H, Kanamaru R, and Ishioka C, Understanding the function-structure and function-mutation relationships of p53 tumor suppressor protein by high-resolution missense mutation analysis. *Proc.Natl.Acad.Sci.U.S.A* 100: 8424-8429, 2003.
99. Antoni L, Sodha N, Collins I, and Garrett MD, CHK2 kinase: cancer susceptibility and cancer therapy - two sides of the same coin? *Nat.Rev.Cancer* 7: 925-936, 2007.
100. Takai H, Naka K, Okada Y, Watanabe M, Harada N, Saito S, Anderson CW, Appella E, Nakanishi M, Suzuki H, Nagashima K, Sawa H, Ikeda K, and Motoyama N, Chk2-deficient mice exhibit radioresistance and defective p53-mediated transcription. *EMBO J* 21: 5195-5205, 2002.
101. MacLaren A, Slavin D, and McGowan CH, Chk2 protects against radiation-induced genomic instability. *Radiat.Res.* 172: 463-472, 2009.

102. Basu A and Krishnamurthy S, Cellular responses to Cisplatin-induced DNA damage. *J.Nucleic Acids* 2010: 2010.
103. Andrews PA, Mann SC, Huynh HH, and Albright KD, Role of the Na⁺, K⁽⁺⁾-adenosine triphosphatase in the accumulation of cis-diamminedichloroplatinum(II) in human ovarian carcinoma cells. *Cancer Res.* 51: 3677-3681, 1991.
104. Hall MD, Okabe M, Shen DW, Liang XJ, and Gottesman MM, The role of cellular accumulation in determining sensitivity to platinum-based chemotherapy. *Annu.Rev.Pharmacol.Toxicol.* 48: 495-535, 2008.
105. Safaei R, Holzer AK, Katano K, Samimi G, and Howell SB, The role of copper transporters in the development of resistance to Pt drugs. *J.Inorg.Biochem.* 98: 1607-1613, 2004.
106. Komatsu M, Sumizawa T, Mutoh M, Chen ZS, Terada K, Furukawa T, Yang XL, Gao H, Miura N, Sugiyama T, and Akiyama S, Copper-transporting P-type adenosine triphosphatase (ATP7B) is associated with cisplatin resistance. *Cancer Res.* 60: 1312-1316, 2000.
107. Katano K, Safaei R, Samimi G, Holzer A, Rochdi M, and Howell SB, The copper export pump ATP7B modulates the cellular pharmacology of carboplatin in ovarian carcinoma cells. *Mol.Pharmacol.* 64: 466-473, 2003.

108. Kuo MT, Chen HH, Song IS, Savaraj N, and Ishikawa T, The roles of copper transporters in cisplatin resistance. *Cancer Metastasis Rev.* 26: 71-83, 2007.
109. Safaei R, Otani S, Larson BJ, Rasmussen ML, and Howell SB, Transport of cisplatin by the copper efflux transporter ATP7B. *Mol.Pharmacol.* 73: 461-468, 2008.
110. Mangala LS, Zuzel V, Schmandt R, Leshane ES, Halder JB, Armaiz-Pena GN, Spannuth WA, Tanaka T, Shahzad MM, Lin YG, Nick AM, Danes CG, Lee JW, Jennings NB, Vivas-Mejia PE, Wolf JK, Coleman RL, Siddik ZH, Lopez-Berestein G, Lutsenko S, and Sood AK, Therapeutic Targeting of ATP7B in Ovarian Carcinoma. *Clin.Cancer Res.* 15: 3770-3780, 2009.
111. Moreno-Smith M, Halder JB, Meltzer PS, Gonda TA, Mangala LS, Rupaimoole R, Lu C, Nagaraja AS, Gharpure KM, Kang Y, Rodriguez-Aguayo C, Vivas-Mejia PE, Zand B, Schmandt R, Wang H, Langley RR, Jennings NB, Ivan C, Coffin JE, Armaiz GN, Bottsford-Miller J, Kim SB, Halleck MS, Hendrix MJ, Bornman W, Bar-Eli M, Lee JS, Siddik ZH, Lopez-Berestein G, and Sood AK, ATP11B mediates platinum resistance in ovarian cancer. *J.Clin.Invest* 123: 2119-2130, 2013.
112. Halleck MS, Schlegel RA, and Williamson PL, Reanalysis of ATP11B, a type IV P-type ATPase. *J.Biol.Chem.* 277: 9736-9740, 2002.

113. Kelley SL, Basu A, Teicher BA, Hacker MP, Hamer DH, and Lazo JS, Overexpression of metallothionein confers resistance to anticancer drugs. *Science* 241: 1813-1815, 1988.
114. Zhao H and Piwnicka-Worms H, ATR-mediated checkpoint pathways regulate phosphorylation and activation of human Chk1. *Mol.Cell Biol.* 21: 4129-4139, 2001.
115. Mayo LD and Donner DB, The PTEN, Mdm2, p53 tumor suppressor-oncoprotein network. *Trends Biochem.Sci.* 27: 462-467, 2002.
116. Oren M, Damalas A, Gottlieb T, Michael D, Taplick J, Leal JF, Maya R, Moas M, Seger R, Taya Y, and Ben Ze'Ev A, Regulation of p53: intricate loops and delicate balances. *Ann.N.Y.Acad.Sci.* 973: 374-383, 2002.
117. Hayakawa J, Ohmichi M, Kurachi H, Kanda Y, Hisamoto K, Nishio Y, Adachi K, Tasaka K, Kanzaki T, and Murata Y, Inhibition of BAD phosphorylation either at serine 112 via extracellular signal-regulated protein kinase cascade or at serine 136 via Akt cascade sensitizes human ovarian cancer cells to cisplatin. *Cancer Res.* 60: 5988-5994, 2000.
118. Cardone MH, Roy N, Stennicke HR, Salvesen GS, Franke TF, Stanbridge E, Frisch S, and Reed JC, Regulation of cell death protease caspase-9 by phosphorylation. *Science* 282: 1318-1321, 1998.

119. Dhillon AS, Hagan S, Rath O, and Kolch W, MAP kinase signalling pathways in cancer. *Oncogene* 26: 3279-3290, 2007.
120. Roberts PJ and Der CJ, Targeting the Raf-MEK-ERK mitogen-activated protein kinase cascade for the treatment of cancer. *Oncogene* 26: 3291-3310, 2007.
121. Burotto M, Chiou VL, Lee JM, and Kohn EC, The MAPK pathway across different malignancies: a new perspective. *Cancer* 120: 3446-3456, 2014.
122. McCubrey JA, Steelman LS, Abrams SL, Lee JT, Chang F, Bertrand FE, Navolanic PM, Terrian DM, Franklin RA, D'Assoro AB, Salisbury JL, Mazzarino MC, Stivala F, and Libra M, Roles of the RAF/MEK/ERK and PI3K/PTEN/AKT pathways in malignant transformation and drug resistance. *Adv.Enzyme Regul.* 46: 249-279, 2006.
123. Shaul YD and Seger R, The MEK/ERK cascade: from signaling specificity to diverse functions. *Biochim.Biophys.Acta* 1773: 1213-1226, 2007.
124. Persons DL, Yazlovitskaya EM, Cui W, and Pelling JC, Cisplatin-induced activation of mitogen-activated protein kinases in ovarian carcinoma cells: inhibition of extracellular signal-regulated kinase activity increases sensitivity to cisplatin. *Clin.Cancer Res.* 5: 1007-1014, 1999.

125. Robinson MJ and Cobb MH, Mitogen-activated protein kinase pathways. *Curr.Opin.Cell Biol.* 9: 180-186, 1997.
126. Fuchs SY, Adler V, Pincus MR, and Ronai Z, MEKK1/JNK signaling stabilizes and activates p53. *Proc.Natl.Acad.Sci.U.S.A* 95: 10541-10546, 1998.
127. Cagnol S and Chambard JC, ERK and cell death: mechanisms of ERK-induced cell death--apoptosis, autophagy and senescence. *FEBS J.* 277: 2-21, 2010.
128. Li DW, Liu JP, Mao YW, Xiang H, Wang J, Ma WY, Dong Z, Pike HM, Brown RE, and Reed JC, Calcium-activated RAF/MEK/ERK signaling pathway mediates p53-dependent apoptosis and is abrogated by alpha B-crystallin through inhibition of RAS activation. *Mol.Biol.Cell* 16: 4437-4453, 2005.
129. Persons DL, Yazlovitskaya EM, and Pelling JC, Effect of extracellular signal-regulated kinase on p53 accumulation in response to cisplatin. *J.Biol.Chem.* 275: 35778-35785, 2000.
130. Yeh PY, Chuang SE, Yeh KH, Song YC, Ea CK, and Cheng AL, Increase of the resistance of human cervical carcinoma cells to cisplatin by inhibition of the MEK to ERK signaling pathway partly via enhancement of anticancer drug-induced NF kappa B activation. *Biochem.Pharmacol.* 63: 1423-1430, 2002.

131. Capdevila J, Elez E, Peralta S, Macarulla T, Ramos FJ, and Tabernero J, Oxaliplatin-based chemotherapy in the management of colorectal cancer. *Expert Rev.Anticancer Ther.* 8: 1223-1236, 2008.
132. Kelland LR, Sharp SY, O'Neill CF, Raynaud FI, Beale PJ, and Judson IR, Mini-review: discovery and development of platinum complexes designed to circumvent cisplatin resistance. *J.Inorg.Biochem.* 77: 111-115, 1999.
133. Fu S, Kavanagh JJ, Hu W, and Bast RC, Jr., Clinical application of oxaliplatin in epithelial ovarian cancer. *Int.J.Gynecol.Cancer* 16: 1717-1732, 2006.
134. Raymond E, Chaney SG, Taamma A, and Cvitkovic E, Oxaliplatin: a review of preclinical and clinical studies. *Ann.Oncol.* 9: 1053-1071, 1998.
135. Rosenberg B, Van Camp L, Grimley EB, and Thomson AJ, The inhibition of growth or cell division in *Escherichia coli* by different ionic species of platinum(IV) complexes. *J.Biol.Chem.* 242: 1347-1352, 1967.
136. Berners-Price SJ and Kuchel PW, Reaction of cis- and trans-[PtCl₂(NH₃)₂] with reduced glutathione inside human red blood cells, studied by ¹H and ¹⁵N-[¹H] DEPT NMR. *J.Inorg.Biochem.* 38: 327-345, 1990.
137. Fojo T, Farrell N, Ortuzar W, Tanimura H, Weinstein J, and Myers TG, Identification of non-cross-resistant platinum compounds with novel cytotoxicity

profiles using the NCI anticancer drug screen and clustered image map visualizations. *Crit Rev.Oncol.Hematol.* 53: 25-34, 2005.

138. Aris SM and Farrell NP, Towards Antitumor Active trans-Platinum Compounds. *Eur.J.Inorg.Chem.* 2009: 1293, 2009.
139. Hall MD, Amjadi S, Zhang M, Beale PJ, and Hambley TW, The mechanism of action of platinum(IV) complexes in ovarian cancer cell lines. *J.Inorg.Biochem.* 98: 1614-1624, 2004.
140. Choi S, Vastag L, Leung CH, Beard AM, Knowles DE, and Larrabee JA, Kinetics and mechanism of the oxidation of guanosine derivatives by Pt(IV) complexes. *Inorg.Chem.* 45: 10108-10114, 2006.
141. Chaney SG, Wyrick S, and Till GK, In vitro biotransformations of tetrachloro(d,l-trans)-1,2-diaminocyclohexaneplatinum(IV) (tetraplatin) in rat plasma. *Cancer Res.* 50: 4539-4545, 1990.
142. He G, Kuang J, Huang Z, Koomen J, Kobayashi R, Khokhar AR, and Siddik ZH, Upregulation of p27 and its inhibition of CDK2/cyclin E activity following DNA damage by a novel platinum agent are dependent on the expression of p21. *Br.J.Cancer* 95: 1514-1524, 2006.

143. Pazderski L, Szlyk E, Sitkowski J, Kamienski B, Kozerski L, Tousek J, and Marek R, Experimental and quantum-chemical studies of ¹⁵N NMR coordination shifts in palladium and platinum chloride complexes with pyridine, 2,2'-bipyridine and 1,10-phenanthroline. *Magn Reson.Chem.* 44: 163-170, 2006.
144. Kido Y, Khokhar AR, al Baker S, and Siddik ZH, Modulation of cytotoxicity and cellular pharmacology of 1,2-diaminocyclohexane platinum (IV) complexes mediated by axial and equatorial ligands. *Cancer Res.* 53: 4567-4572, 1993.
145. Godwin AK, Meister A, O'Dwyer PJ, Huang CS, Hamilton TC, and Anderson ME, High resistance to cisplatin in human ovarian cancer cell lines is associated with marked increase of glutathione synthesis. *Proc.Natl.Acad.Sci.U.S.A* 89: 3070-3074, 1992.
146. Siddik ZH, Mims B, Lozano G, and Thai G, Independent pathways of p53 induction by cisplatin and X-rays in a cisplatin-resistant ovarian tumor cell line. *Cancer Res.* 58: 698-703, 1998.
147. Arambula JF, Sessler JL, and Siddik ZH, Overcoming biochemical pharmacologic mechanisms of platinum resistance with a texaphyrin-platinum conjugate. *Bioorg.Med.Chem.Lett.* 21: 1701-1705, 2011.
148. Yoshida M, Khokhar AR, and Siddik ZH, Axial ligands and alicyclic ring size modulate the activity and biochemical pharmacology of ammine/cycloalkylamine-

- platinum(IV) complexes in tumor cells resistant to cis-diamminedichloroplatinum(II) or trans-1R,2R-1S,2S-diaminocyclohexanetetrachloroplatinum(IV). *Cancer Res.* 54: 4691-4697, 1994.
149. Yoshida M, Khokhar AR, Kido Y, Ali-Osman F, and Siddik ZH, Correlation of total and interstrand DNA adducts in tumor and kidney with antitumor efficacies and differential nephrotoxicities of cis-ammine/cyclohexylamine-dichloroplatinum(II) and cisplatin. *Biochem.Pharmacol.* 48: 793-799, 1994.
150. Chung YM, Park SH, Tsai WB, Wang SY, Ikeda MA, Berek JS, Chen DJ, and Hu MC, FOXO3 signalling links ATM to the p53 apoptotic pathway following DNA damage. *Nat.Comm.* 3: 1000, 2012.
151. Colella S, Shen L, Baggerly KA, Issa JP, and Krahe R, Sensitive and quantitative universal Pyrosequencing methylation analysis of CpG sites. *Biotechniques* 35: 146-150, 2003.
152. Zhang P, Wang J, Gao W, Yuan BZ, Rogers J, and Reed E, CHK2 kinase expression is down-regulated due to promoter methylation in non-small cell lung cancer. *Mol.Cancer* 3: 14, 2004.
153. Wang H, Wang S, Shen L, Chen Y, Zhang X, Zhou J, Wang Z, Hu C, Yue W, and Wang H, Chk2 down-regulation by promoter hypermethylation in human bulk gliomas. *Life Sci.* 86: 185-191, 2010.

154. Rakitina TV, Vasilevskaya IA, and O'Dwyer PJ, Additive interaction of oxaliplatin and 17-allylamino-17-demethoxygeldanamycin in colon cancer cell lines results from inhibition of nuclear factor kappaB signaling. *Cancer Res.* 63: 8600-8605, 2003.
155. Wang J, Pabla N, Wang CY, Wang W, Schoenlein PV, and Dong Z, Caspase-mediated cleavage of ATM during cisplatin-induced tubular cell apoptosis: inactivation of its kinase activity toward p53. *Am.J.Physiol Renal Physiol* 291: F1300-F1307, 2006.
156. Melnikova VO, Santamaria AB, Bolshakov SV, and Ananthaswamy HN, Mutant p53 is constitutively phosphorylated at Serine 15 in UV-induced mouse skin tumors: involvement of ERK1/2 MAP kinase. *Oncogene* 22: 5958-5966, 2003.
157. Malinge JM, Giraud-Panis MJ, and Leng M, Interstrand cross-links of cisplatin induce striking distortions in DNA. *J.Inorg.Biochem.* 77: 23-29, 1999.
158. Wozniak K and Blasiak J, Recognition and repair of DNA-cisplatin adducts. *Acta Biochim.Pol.* 49: 583-596, 2002.
159. Kasparikova J, Marini V, Bursova V, and Brabec V, Biophysical studies on the stability of DNA intrastrand cross-links of transplatin. *Biophys.J.* 95: 4361-4371, 2008.

160. Kojima K, Konopleva M, McQueen T, O'Brien S, Plunkett W, and Andreeff M, Mdm2 inhibitor Nutlin-3a induces p53-mediated apoptosis by transcription-dependent and transcription-independent mechanisms and may overcome Atm-mediated resistance to fludarabine in chronic lymphocytic leukemia. *Blood* 108: 993-1000, 2006.
161. Olivier M, Hollstein M, and Hainaut P, TP53 mutations in human cancers: origins, consequences, and clinical use. *Cold Spring Harb. Perspect. Biol.* 2: a001008, 2010.
162. Schildkraut JM, Goode EL, Clyde MA, Iversen ES, Moorman PG, Berchuck A, Marks JR, Lissowska J, Brinton L, Peplonska B, Cunningham JM, Vierkant RA, Rider DN, Chenevix-Trench G, Webb PM, Beesley J, Chen X, Phelan C, Sutphen R, Sellers TA, Pearce L, Wu AH, Van Den BD, Conti D, Elund CK, Anderson R, Goodman MT, Lurie G, Carney ME, Thompson PJ, Gayther SA, Ramus SJ, Jacobs I, Kruger KS, Hogdall E, Blaakaer J, Hogdall C, Easton DF, Song H, Pharoah PD, Whittemore AS, McGuire V, Quaye L, Anton-Culver H, Ziogas A, Terry KL, Cramer DW, Hankinson SE, Tworoger SS, Calingaert B, Chanock S, Sherman M, and Garcia-Closas M, Single nucleotide polymorphisms in the TP53 region and susceptibility to invasive epithelial ovarian cancer. *Cancer Res.* 69: 2349-2357, 2009.
163. Wong DJ, Robert L, Atefi MS, Lassen A, Avarappatt G, Cerniglia M, Avramis E, Tsoi J, Foulad D, Graeber TG, Comin-Anduix B, Samatar A, Lo RS, and Ribas A,

Antitumor activity of the ERK inhibitor SCH772984 [corrected] against BRAF mutant, NRAS mutant and wild-type melanoma. *Mol.Cancer* 13: 194, 2014.

164. Chaikuad A, Tacconi EM, Zimmer J, Liang Y, Gray NS, Tarsounas M, and Knapp S, A unique inhibitor binding site in ERK1/2 is associated with slow binding kinetics. *Nat.Chem.Biol.* 10: 853-860, 2014.
165. Fukazawa H, Noguchi K, Murakami Y, and Uehara Y, Mitogen-activated protein/extracellular signal-regulated kinase kinase (MEK) inhibitors restore anoikis sensitivity in human breast cancer cell lines with a constitutively activated extracellular-regulated kinase (ERK) pathway. *Mol.Cancer Ther.* 1: 303-309, 2002.
166. Boudvillain M, Dalbies R, Aussourd C, and Leng M, Intrastrand cross-links are not formed in the reaction between transplatin and native DNA: relation with the clinical inefficiency of transplatin. *Nucleic Acids Res.* 23: 2381-2388, 1995.
167. Farrell N, Kelland LR, Roberts JD, and Van Beusichem M, Activation of the trans geometry in platinum antitumor complexes: a survey of the cytotoxicity of trans complexes containing planar ligands in murine L1210 and human tumor panels and studies on their mechanism of action. *Cancer Res.* 52: 5065-5072, 1992.
168. Murphy RF, Komlodi-Pasztor E, Robey R, Balis FM, Farrell NP, and Fojo T, Retained platinum uptake and indifference to p53 status make novel

- transplatinum agents active in platinum-resistant cells compared to cisplatin and oxaliplatin. *Cell Cycle* 11: 963-973, 2012.
169. Alcindor T and Beauger N, Oxaliplatin: a review in the era of molecularly targeted therapy. *Curr.Oncol.* 18: 18-25, 2011.
170. Ali K, Sr., Huang S, Shamsuddin S, Inutsuka S, Whitmire KH, Siddik ZH, and Khokhar AR, Synthesis, characterization and cytotoxicity of new platinum(IV) axial carboxylate complexes: crystal structure of potential antitumor agent [PtIV(trans-1R,2R-diaminocyclohexane)trans(acetate)2Cl₂]. *Bioorg.Med.Chem.* 8: 515-521, 2000.
171. He G, Kuang J, Khokhar AR, and Siddik ZH, The impact of S- and G2-checkpoint response on the fidelity of G1-arrest by cisplatin and its comparison to a non-cross-resistant platinum(IV) analog. *Gynecol.Oncol.* 122: 402-409, 2011.
172. Woynarowski JM, Faivre S, Herzig MC, Arnett B, Chapman WG, Trevino AV, Raymond E, Chaney SG, Vaisman A, Varchenko M, and Juniewicz PE, Oxaliplatin-induced damage of cellular DNA. *Mol.Pharmacol.* 58: 920-927, 2000.
173. Montana AM and Batalla C, The rational design of anticancer platinum complexes: the importance of the structure-activity relationship. *Curr.Med.Chem.* 16: 2235-2260, 2009.

174. Unger T, Juven-Gershon T, Moallem E, Berger M, Vogt SR, Lozano G, Oren M, and Haupt Y, Critical role for Ser20 of human p53 in the negative regulation of p53 by Mdm2. *EMBO J.* 18: 1805-1814, 1999.
175. Dornan D, Shimizu H, Perkins ND, and Hupp TR, DNA-dependent acetylation of p53 by the transcription coactivator p300. *J.Biol.Chem.* 278: 13431-13441, 2003.
176. Dornan D, Shimizu H, Burch L, Smith AJ, and Hupp TR, The proline repeat domain of p53 binds directly to the transcriptional coactivator p300 and allosterically controls DNA-dependent acetylation of p53. *Mol.Cell Biol.* 23: 8846-8861, 2003.
177. Pabla N, Huang S, Mi QS, Daniel R, and Dong Z, ATR-Chk2 signaling in p53 activation and DNA damage response during cisplatin-induced apoptosis. *J.Biol.Chem.* 283: 6572-6583, 2008.
178. Zhao L, Bode AM, Cao Y, and Dong Z, Regulatory mechanisms and clinical perspectives of miRNA in tumor radiosensitivity. *Carcinogenesis* 33: 2220-2227, 2012.
179. Kato N, Fujimoto H, Yoda A, Oishi I, Matsumura N, Kondo T, Tsukada J, Tanaka Y, Imamura M, and Minami Y, Regulation of Chk2 gene expression in lymphoid malignancies: involvement of epigenetic mechanisms in Hodgkin's lymphoma cell lines. *Cell Death Differ.* 11 Suppl 2: S153-S161, 2004.

180. Ahn J, Urist M, and Prives C, The Chk2 protein kinase. *DNA Repair (Amst)* 3: 1039-1047, 2004.
181. Alkema NG, Tomar T, van der Zee AG, Everts M, Meersma GJ, Hollema H, de Jong S, van Vugt MA, and Wisman GB, Checkpoint kinase 2 (Chk2) supports sensitivity to platinum-based treatment in high grade serous ovarian cancer. *Gynecol.Oncol.* 133: 591-598, 2014.
182. Jo SK, Cho WY, Sung SA, Kim HK, and Won NH, MEK inhibitor, U0126, attenuates cisplatin-induced renal injury by decreasing inflammation and apoptosis. *Kidney Int.* 67: 458-466, 2005.
183. Fung MK, Cheung HW, Ling MT, Cheung AL, Wong YC, and Wang X, Role of MEK/ERK pathway in the MAD2-mediated cisplatin sensitivity in testicular germ cell tumour cells. *Br.J.Cancer* 95: 475-484, 2006.
184. Malina J, Novakova O, Vojtiskova M, Natile G, and Brabec V, Conformation of DNA GG intrastrand cross-link of antitumor oxaliplatin and its enantiomeric analog. *Biophys.J.* 93: 3950-3962, 2007.
185. Sasaki T, Hiroki K, and Yamashita Y, The role of epidermal growth factor receptor in cancer metastasis and microenvironment. *Biomed.Res.Int.* 2013: 546318, 2013.

186. Larrieu-Lahargue F, Welm AL, Bouche-careilh M, Alitalo K, Li DY, Bikfalvi A, and Auguste P, Blocking Fibroblast Growth Factor receptor signaling inhibits tumor growth, lymphangiogenesis, and metastasis. *Plos One* 7: e39540, 2012.
187. Turner N and Grose R, Fibroblast growth factor signalling: from development to cancer. *Nat.Rev.Cancer* 10: 116-129, 2010.
188. Normanno N, De Luca A, Bianco C, Strizzi L, Mancino M, Maiello MR, Carotenuto A, De Feo G, Caponigro F, and Salomon DS, Epidermal growth factor receptor (EGFR) signaling in cancer. *Gene* 366: 2-16, 2006.
189. Dang CV, MYC on the path to cancer. *Cell* 149: 22-35, 2012.
190. Xie X, Lozano G, and Siddik ZH, Heterozygous p53V172F mutation in cisplatin-resistant human tumor cells promotes MDM4 recruitment and decreases stability and transactivity of p53. *Oncogene*, 2016.
191. LeBron C, Chen L, Gilkes DM, and Chen J, Regulation of MDMX nuclear import and degradation by Chk2 and 14-3-3. *EMBO J.* 25: 1196-1206, 2006.
192. Chen L, Gilkes DM, Pan Y, Lane WS, and Chen J, ATM and Chk2-dependent phosphorylation of MDMX contribute to p53 activation after DNA damage. *EMBO J.* 24: 3411-3422, 2005.

193. Okamoto K, Kashima K, Pereg Y, Ishida M, Yamazaki S, Nota A, Teunisse A, Migliorini D, Kitabayashi I, Marine JC, Prives C, Shiloh Y, Jochemsen AG, and Taya Y, DNA damage-induced phosphorylation of MdmX at serine 367 activates p53 by targeting MdmX for Mdm2-dependent degradation. *Mol.Cell Biol.* 25: 9608-9620, 2005.
194. Inglese J, Shamu CE, and Guy RK, Reporting data from high-throughput screening of small-molecule libraries. *Nat.Chem.Biol.* 3: 438-441, 2007.
195. Schwarz JK, Lovly CM, and Piwnica-Worms H, Regulation of the Chk2 protein kinase by oligomerization-mediated cis- and trans-phosphorylation. *Mol.Cancer Res.* 1: 598-609, 2003.
196. Gollob JA, Wilhelm S, Carter C, and Kelley SL, Role of Raf kinase in cancer: therapeutic potential of targeting the Raf/MEK/ERK signal transduction pathway. *Semin.Oncol.* 33: 392-406, 2006.
197. Matallanas D, Birtwistle M, Romano D, Zebisch A, Rauch J, von Kriegsheim A, and Kolch W, Raf family kinases: old dogs have learned new tricks. *Genes Cancer* 2: 232-260, 2011.
198. Leicht DT, Balan V, Kaplun A, Singh-Gupta V, Kaplun L, Dobson M, and Tzivion G, Raf kinases: function, regulation and role in human cancer. *Biochim.Biophys.Acta* 1773: 1196-1212, 2007.

Vita

Michelle Martinez-Rivera was born in San Juan, Puerto Rico on April 25, 1988, the daughter of Damaris Rivera-Ortiz and José Martinez-Rivera. After completing her work at St. Vincent de Paul School, Santurce, Puerto Rico in 2006, she entered The University of Puerto Rico-Rio Piedras Campus in San Juan, Puerto Rico. She received the degree of Bachelor of Sciences with a major in Chemistry from The University of Puerto Rico-Rio Piedras Campus in June, 2010. In August 2010 she entered The University of Texas Graduate School of Biomedical Science at Houston.

Permanent Address:

1885 El Paseo St. 33207

Houston, Texas 77054